TECHNICAL UNIVERSITY OF CRETE

STATISTICAL QUANTITATIVE EEG ANALYSIS BASED ON TIME-FREQUENCY AND NONLINEAR SYNCHRONIZATION METHODS DURING ALTERED STATES OF CONSCIOUSNESS

VANGELIS D. SAKKALIS

December 2006

STATISTICAL QUANTITATIVE EEG ANALYSIS BASED ON TIME-FREQUENCY AND NONLINEAR SYNCHRONIZATION METHODS DURING ALTERED STATES OF CONSCIOUSNESS.

by

Vangelis D. Sakkalis

A thesis submitted in partial fulfillment of the

requirements for the degree of

Doctor of Philosophy, PhD

TECHNICAL UNIVERSITY OF CRETE

DEPARTMENT OF ELECTRONIC AND COMPUTER ENGINEERING

Chairperson of the Supervisory Committee: Professor Michalis Zervakis

Chania, Greece, 2006

To my beloved family: Dimitris, Stella and Sissy

ABSTRACT

Neuronal dynamics and synchronization phenomena have been increasingly recognized to be an important mechanism by which specialized cortical and sub-cortical regions integrate their activity to form distributed neuronal assemblies that function in a cooperative manner. Synchronous oscillations of certain types of such assemblies in different frequency bands relate to different perceptual, motor or cognitive states and may be indicative of a wider range of cognitive functions or brain pathologies.

The traditionally formulated but still the most common way of analyzing both the neuronal dynamics and the functional coupling of cortical assemblies has been the *Fourier power spectrum* (FPS) and the *magnitude squared coherence* (MSC) or *coherence*. PS is a linear method of identifying localized brain activity, whereas MSC is a normalized measure of linear dependence between two signals which is capable of identifying linear synchrony on certain frequency bands. Since all the measures mentioned above are linear and imply signal stationarity, I extend our investigations by considering also nonlinear measures, while non-stationarity requirement is negated with the use of the Wavelet transform (WT). Phase Synchronization (PS) presents a different approach in analyzing the possible nonlinear interdependencies of the EEG signal and focuses on the phases of the signals. The idea of studying the phase relationships of two neurophysiological signals is not new, but later studies have shown that even if the amplitudes of two coupled chaotic oscillators remain uncorrelated, their phases may synchronize. Another group of synchronization measures are based on the assumption that neurons are highly nonlinear devices, which in some cases show chaotic behavior. Hence, the use of nonlinear measures derived from studying chaotic dynamical systems may be of interest in neurophysiology applications. Such measures belong to the Generalized Synchronization concept and are based on analyzing the interdependence between the amplitudes of the signals in a state-space reconstructed domain. In this study, I use two different variants of this idea. The results presented in this thesis show ways to improve and broaden the currently clinically used methodologies.

In particular, this thesis is the first work where a novel methodology based on wavelet and statistical measures in the time-scale domain makes use of electroencephalographic (EEG) signals to evaluate cortex reactions during different cognitive tasks (mathematical reasoning, working memory) and certain pathologies (epilepsy and schizophrenia). My purpose is to extract more precise information from the cortex reactions during each cognitive engagement. Statistical significance-based criteria for comparing wavelet power spectra between the task and the rest condition are considered. The results obtained from a mathematical reasoning task between normals are in accordance with similar previous studies, showing activations of frontal and central regions. Compared with the alternative spectral-based techniques, this method achieves higher task discrimination, provides additional detail-signal information to evaluate cortical reactivity during local cortical activation.

Hopefully, the ideas extracted throughout this thesis will elucidate the longstanding "obscured" brain dynamics and possibly help in every day clinical practice to early diagnose and improve the quality of life for several diseased people.

PREFACE

In this thesis I mainly focus my interest on analyzing various established approaches in time series analysis, as well as new extensions on these. The application of these, even if not strictly restricted to physiological signals, is applied on Electroencephalographic signals. In general terms two major domains are discussed: i) time frequency methods and ii) nonlinear methods based on chaos theory. Comparisons and extensions are thoroughly investigated spotting their advantages over traditional and conventional techniques. The application domain includes cognitive awareness assessment and pathological cases, such as Schizophrenia and Epilepsy. In particular, this work is the first one to apply the novel "significant wavelet transform" to the characterization and analysis of pathoneurophysiological cases. Nonlinear synchronization measures as applied to EEGs are also investigated. Finally, graph theory and specific theoretic measures are successfully incorporated in a similar framework to better describe and understand the functional characteristics of brain networks.

An overview of the thesis structure is given below:

- The first part of the thesis is intended to give a brief introduction to some basic concepts in neurophysiology and EEG specifics (**chapter 2**), which will help the reader to get acquainted with the underlying theory discussed in the remaining thesis. This chapter covers the physiology of the brain, EEG internals (montages and artifacts) and adaptations to study the oscillatory behavior of the brain. Finally, a brief presentation of the epilepsy and schizophrenia syndrome is attempted.

- **Chapter 3** is the main part of the thesis with each section referring to an alternative analysis method. The internal structure is kept roughly the same; initially the theoretical basis of each method is introduced, followed by a comparison stressing the strong points of each versus the alternative ones.

- More specifically, classical Fourier based techniques and application considerations in extracting the power spectrum and interdependence measures (by means of the coherence) are described in **section 3.1**.

- The advanced short time Fourier transform is given in **section 3.2.1** together with other time-frequency alternatives including the wavelet transforms (**§3.2.2**) and their counterparts, the short time Fourier coherence (**§3.2.4**) and the wavelet coherence (**§3.2.5**). Advances of the wavelet methods, namely the significant wavelet transform and the significant wavelet coherence that take into account population statistics to add confidence in the acquired results, are proposed next in **sections 3.2.3** and **§3.2.6**, respectively.

- **Chapter 3.3** presents Phase Locking Value, an alternative to the coherence method, which focuses only on phase differences to quantify possible interdependence between couple of channels.

- **Chapter 3.4** focuses on the nonlinear dynamics or chaos theory as adapted to encounter interdependencies in the EEG domain. Mainly, two approaches applied on state-space delayed vectors are discussed (**§3.4.4**). Surrogate time series analysis (**§3.4.5**) provides the valuable tool to assist the decision on whether one should depend mostly on linear or nonlinear methods.

- The application of these tools on disease diagnosis is described in **chapter 3.5**. One way to focus only on those features (channels or brain lobes) that have the most prominent functional impact on different cognitive tasks or pathological cases.

- Furthermore, **chapter 3.6** presents an alternative approach to the characterization of complex brain networks using graph theoretic measures.

- **Chapter 4** presents the major application domains of the previously reported methods. Mathematical reasoning, along with working memory and visual stimuli (fractal observation) tasks comprise the cognitive applications, whereas schizophrenia and epilepsy are the pathological cases studied. This chapter actually forms one piece which fits into a wider context of published work attached in the Publications appendix.

- Finally, in **chapter 5** general remarks and conclusive considerations of which method performs best under certain assumptions, is presented.

Acknowledgments

First, I would like to thank my advisor, Michalis Zervakis, for his continuing support and guidance over the years. Perhaps the most notable thing I inherited was his patience, planning and adhesion. Thank you for the time, the trust and support on me even during most of my difficult moments at TUC. I would also like to thank my co-supervisor, Sifis Micheloyannis whose emphasis on understanding brain and mind has been a consistent inspiration since the beginning of this project. His acerbity and dedication will always be remembered. Thanks also to Yannis Tollis for the time I was allowed to work on these matters and the additional members of my defense committee, for their time and interest.

Special thanks to Akis Simos for much help in specific statistical modeling topics; somehow I began to enjoy statistical inference in psychology! I would also like to thank Sophia Erimaki for the invigorating discussions –even off the EEG topic– and the rest of the L. Widen clinical Neurophysiology lab students.

Special thanks to my fellow TUC students Petros, Kostas and George. Petro, I hope Florida will turn out to be a challenging experience. Kosta, I enjoyed working with you and wish the best of luck in everything! Special thanks are due to the rest of the DISPLAY research group members which over the years have listened to my talks and have offered me valuable advice. To the CSD graduates Fanis and Vassilis. Fani I am glad you got through it all! Vassili I really appreciate your dedication as much as your excellent and accurate code scripts!

Klio, I actually started writing this while you are sitting in front of me on the sofa working and reading on your multi-criteria UTASTAR algorithm! As always it is good to have you around, even if I do not have the answers to all your questions.

Nullum enim offcium referenda gratia magis necessarium est.

.– Cicero

Chania, December 2006

Vangelis Sakkalis

Table of Contents

List of Author publications

A) Journal papers

[P1] *V. Sakkalis*, M. Zervakis, and S. Micheloyannis, "Significant EEG Feature Selection for the Evaluation of Cognitive Task Complexity Functions", Brain Topography, Vol. 19, No.1-2, pp.53-60, 2006.

[P2] S. Micheloyannis, *V. Sakkalis*, M. Vourkas, C.J. Stam, and P.G. Simos, "Cortical networks involved in mathematical thinking: Evidence from linear and non-linear cortico-cortical synchronization of electrical activity", Neuroscience Letters, Vol. 373, pp. 212-217, 2005.

[P3] P. G. Simos, E. Papanikolaou, *E. Sakkalis*, and S. Micheloyannis, "Modulation of Gamma-Band Spectral Power by Cognitive Task Complexity", Brain Topography, Vol. 14, No. 3, pp. 191-196, Spring 2002.

[P4] *V. Sakkalis*, P. Xanthopoulos, M. Zervakis, and S. Micheloyannis, "Assessment of linear and nonlinear EEG synchronization measures for evaluating mild epileptic signal patterns", invited publication IEEE Trans. Inf. Tech. (under preparation).

[P5] *V. Sakkalis*, M. Zervakis, E. Karakonstantaki, and S. Micheloyannis, "Linear and Nonlinear evidence of epileptic signatures in otherwise clinically healthy evaluated children ", Clin. Neurophys. (under preparation).

B) Conference proceedings

[P6] T. Oikonomou, *V. Sakkalis*, I. Tollis, S. Micheloyannis, "Searching and Visualizing Brain Networks in Schizophrenia", Lecture Notes in Computer Science, Biological and Medical Data Analysis, 7th International Symposium, (ISBMDA 2006), Thessaloniki, Greece, Vol. 4345, pp. 172-182, December 7-8, 2006.

[P7] *V. Sakkalis*, M. Zervakis, C. Bigan, T. Cassar, K.P. Camilleri, S.G. Fabri, and Sifis Micheloyannis, "Validation of time-frequency and ARMA feature extraction methods in classification of mild epileptic signal patterns", Information Technology Applications in Biomedicine (IEEE-ITAB 2006), Ioannina - Epirus, Greece, October 26-28, 2006.

[P8] *V. Sakkalis*, C.D.Giurcăneanu, P. Xanthopoulos, M. Zervakis, Y. Yang, and S. Micheloyannis, "Assessment of linear and non-linear EEG synchronization measures for evaluating mild epileptic signal patterns", Information Technology Applications in Biomedicine (ITAB 2006), Ioannina - Epirus, Greece, October 26-28, 2006.

[P9] P. Xanthopoulos, S. Golemati, *V. Sakkalis*, P.Y. Ktonas, M.D. Ortigueira, M. Zervakis, T. Paparrigopoulos, X.Tsekou, and C.R. Soldatos, "Comparative analysis of time-frequency methods estimating the time-varying microstructure of sleep EEG spindles", Information Technology Applications in Biomedicine (ITAB 2006), Ioannina - Epirus, Greece, October 26-28, 2006.

[P10] *V. Sakkalis*, T. Oikonomou, E. Pachou, I. Tollis, S. Micheloyannis, and M. Zervakis, "Time-significant Wavelet Coherence for the Evaluation of Schizophrenic Brain Activity using a Graph theory approach", Engineering in Medicine and Biology Society (EMBC 2006), New York, USA, August 30-Sept. 3, 2006.

[P11] P. Xanthopoulos, S. Golemati, *V. Sakkalis*, P.Y. Ktonas, M. Zervakis, and and C.R. Soldatos, "Modeling the time-varying microstructure of simulated sleep EEG spindles using time-frequency analysis methods", Engineering in Medicine and Biology Society (EMBC 2006), New York, USA, August 30-Sept. 3, 2006.

[P12] C. Bigan, M. Besleaga, M. Zervakis, *V. Sakkalis*, K. Michalopoulos, M. Woolfson, M. Ortigueira, A. Batista, R. Rato, M. Righi, U. Barcaro, A. Starita, K.P. Camilleri, S.G. Fabri, J. Muscat, R. Grech, and T. Cassar, " EEG signal pre-processing for segmentation into significant regions, major artefacts removal, and uncertainty reduction in epileptic seizure characterization", Joint Workshop On BIOPATTERN Analysis In Brain Diseases, Goteborg, Sweden, May 18-19, 2006.

[P13] P. Xanthopoulos, S. Golemati, *V. Sakkalis*, P.Y. Ktonas, M.D. Ortigueira, M. Zervakis, T. Paparrigopoulos, X. Tsekou, and C.R. Soldatos, "Modeling the time-varying microstructure of sleep EEG spindles using time-frequency analysis methods", Joint Workshop On BIOPATTERN Analysis In Brain Diseases, Goteborg, Sweden, May 18-19, 2006.

[P14] *V. Sakkalis*, M. Zervakis, C. Bigan, T. Cassar, K.P. Camilleri, S.G. Fabri, and S. Micheloyannis, "EEG feature extraction and selection methods using wavelets and ARMA model for classifying mild epileptic signal patterns", Joint Workshop On BIOPATTERN Analysis In Brain Diseases, Goteborg, Sweden, May 18-19, 2006.

[P15] S. Erimaki, K. Kanatsouli, E. Karakonstandaki, M. Vourkas, *V. Sakkalis*, and S. Micheloyannis, "EEG Responses To Complex Fractal Stimuli", 2nd International Nonlinear Science Conference, Heraklion, Crete, Greece March 10-12, 2006.

[P16] *V. Sakkalis*, M. Zervakis, S. Erimaki, and S. Micheloyannis, "Evaluation of Electroencephalographic Activity involved in Mathematical thinking using Wavelet Analysis and Significance-Based Features", 2nd International Conference on Computational Intelligence in Medicine and Healthcare (CIMED), Lisbon, PORTUGAL, June 2005.

[P17] *V. Sakkalis*, M. Zervakis, and S. Micheloyannis, "Biopattern Initiative: towards the Development and Integration of Next-Generation Information Fusion Approaches", 26th IEEE-EMBS - Annual International Conference of the IEEE Engineering in Medicine and Biology Society, San Fransisco, CA, USA, September 2004.

[P18] *V. Sakkalis*, M. Zervakis, and S. Micheloyannis, "Evaluation of EEG Power Spectrum Measures using Fourier and Wavelet based Transformation Techniques as a Function of Task Complexity ", EWADB 2004 - 1st European Workshop on the Assessment of Diagnostic Performance, Milan, ITALY, July 2004.

Abbreviations

CM	Coherence Matrix
CNS	Central Nervous System
CWT	Continuous Wavelet Transform
DAC	Analog to Digital Converter
DFT	Discrete-time Fourier Transform
DOF	Degrees Of Freedom
DWT	Discrete Wavelet Transform
ECG	Electrocardiogram
EEG	Electroencephalogram
EMG	Electromyogram
ERP	Event-Related Potential
FFT	Fast Fourier Transform
FPS	Fourier Power Spectrum
HT	Hilbert Transform
MSC	Magnitude Squared Coherence
PS	Phase Synchronization
PSD	Power Spectral Density
S.E.	Standard Error of the mean
SL	Synchronization Likelihood
SMR	Sensory Motor Rhythm
STFT	Short-Time Fourier Transform
TPS	Thin Plate Spline
WC	Wavelet Coherence
WT	Wavelet Transform
XWT	Cross Wavelet Transform

1

INTRODUCTION

Whereas a giant leap is realized both in the medical domain and neuroinformatics over the last two decades, brain understanding in general and certain brain pathologies remain hardly resolved. More specifically, numerous sources of medical and clinical information could become particularly meaningful if integrated in a consistent and logical manner.

The work and speculation presented in this thesis is heading towards a better understanding of brain dynamics. In this sense, one should pay attention in those modalities used for diagnosis, like the MRI (Magnetic Resonance Imaging), CT (Computed Tomography), PET (Positron Emission Tomography) and fMRI (functional MRI), EEG (Electroencephalogram)/ MEG (Magneto encephalogram) triplets. The first ones pose high spatial resolution images of the brain structures; thus provide structural information (MRI provides better soft tissue visualization, whereas CT performs better in viewing hard tissues). The second triplet is able to convey functional information (PET and fMRI can provide localization information that resembles brain activity, (but both rely on measures of cerebral

blood flow or metabolism) whereas EEG and MEG can be of particular value due to their ultra high temporal resolution). In actual medical practice, it is also critical to consider issues, such as limited availability due to high cost of owning and utilizing some of these modalities, as well as ethical issues. Hence, inferring as much significant clinical info as possible out of the MRI and EEG modalities, which are widely available and routinely used, is a highly desired prospect. This thesis is focused on EEG itself.

Except from visual inspection, which is and will remain the main diagnostic tool for radiologists and neurologists, neuroinformatics have provided several knowledge-discovery algorithms. In the study of lower and higher cognitive functions of the brain, Power Spectrum approaches based on linear Windowed Fourier Transform (WFT) and Coherence measures are commonly used. Wavelets and nonlinear Synchronization interdependence methods are proposed as the latest substitutes of the WFT and Coherence, respectively, and seem to override certain limitations of earlier techniques and provide greater control of their properties. Finally, visualization maybe significantly aided by adapting specialized EEG graphs.

However, despite all technological advances, the rationalization and intellectual processes that a physician may employ to address a clinical problem is incredibly diverse. Towards this direction this thesis attempts to reduce neurophysiologist's subjectivity by providing more objective quantitative EEG analysis tools and methods. These have been the motivation and scope of the thesis.

More specifically, there are currently several algorithms available that may be used in most biological sciences as a quantifying tool. Although there have been a very wide use of mathematical methodologies, less effort has been made to formulate an integrative scenario capable of revealing brain function internals. This thesis concentrates on both recent and traditionally used techniques that are being applied in brain research and wherever possible proposes significant extensions or just validate their ability to unravel the global, collective dynamics of brain activity. A successful neurophysiologist should comprehend the theoretical concepts of each analysis method and critically inspect the accuracy of the proposed interpretations of the results based on established neurophysiological

ground. It is hoped that this work will help clarify the current trends in brain science and may provoke further reflections on how confident one should be in conceptualizing brain and cognitive functions based on certain physiological and methodological constraints intrinsic on various theoretical frameworks.

1.1 Contributions

This thesis describes theoretical foundations as well as practical applications of various proposed methodologies in EEG analysis. The theoretical outcome consists of the following:

- An analytic comparison of available algorithms to calculate both power spectral-based brain activity, as well as interdependence estimation methods. Evaluation of each method is based on the theoretical basis itself and on model simulations.

- The development of "significant wavelet transform" and coherence methodology that take into account population statistics to form a reference background signal. Time segments of significant EEG activity may be identified with increased confidence.

- The presentation of an alternative approach to characterization of complex brain networks using graphotheoretic properties and coupling visualization.

- Insights in higher brain functional reactivity, while complex cognitive tasks, including mathematical reasoning, working memory and visual tasks, are performed. Certain pathologies like schizophrenia and controlled epilepsy are also considered.

Practical contributions and empirical studies include the following:

- Evaluation of the previous presented and proposed methodologies on actual EEG data.

- Feature extraction and selection methods that may successfully classify abnormal versus normal EEG patterns.

- Ideal EEG methodological analysis scenario proposal.

If the doors of perception were cleansed every thing would
appear to man as it is, infinite.

—. *William Blake*

2

BACKGROUND

This chapter will give a brief introductory review of the origins and technique of performing quantitative EEG analysis. It presents certain topics necessary for better understanding and describing the electroencephalogram as applied to the study of brain oscillations and certain pathologies such as epilepsy and schizophrenia. The physiology, measuring and sources/ treatment of artifacts are presented in Appendix B.

2.1   The Origins and evolution of the EEG

Technical developments in the field of electrical measurement and recording during the last quarter of the 19th century, made possible one of the greatest triumphs of modern neuroscience; the Electroencephalogram (EEG). The EEG was discovered in the 1920's and applied in humans by a German psychiatrist named Hans Berger (Tudor et al., 2005). He managed to measure small potential differences at the scalp by using two large sheets of tinfoil, which served as

electrodes. The first was placed on the forehead and the other on the back of the head. Currents inside the brain generate these potential differences.

The field was evolved as likely to give the psychiatric professionals an insight into the brain's function. Since the times of Berger, it was known that the characteristics of EEG activity change in many different situations, particularly with the level of vigilance (alertness, rest, sleep and dreaming). In the 1930's, the electrical patterns were found to have neurological correlates for some disorders, such as epilepsy and tumors, in work by Frederick Gibbs, MD, and Charles Yeager, MD as well as others. The 1940's and 50's found the instrumentation advancing, with commercially available equipment, fostering establishment of laboratories throughout the world.

EEG can be roughly described as the measurement of the mean electrical activity of the brain in different sites of the head. It is the sum of *extracellular* current flows of a large group of neurons, as described in the next section. EEG recording became possible by placing high conductivity electrodes (impedance < 5000Ω) in a fixed head mesh.

Electric potentials may be acquired either between pairs of active electrodes, using the so called *bipolar montage* or with respect to a passive electrode known as the reference, using the *monopolar montage*. The placement of the electrodes can be either non-invasive superficial on the head (*scalp EEG*) or introduced into the brain after surgical intervention (*intracranial EEG*). To perform *scalp EEG* there are established standards of *electrode placement* since 1949, when Rasmussen convened an international committee and designed the international *10-20-electrode placement* system[*]. Such system consists of 20 electrodes uniformly distributed along the head generally referenced to two earlobe (A1, A2) electrodes (Reilly, 1999). Normal scalp EEG are routinely taken with the subject at relaxed (i) with eyes closed, (ii) with eyes open or (iii) while the subject performs predefined cognitive tasks. The major difficulty one encounters while performing scalp EEG recordings are the artifacts (Reilly, 1999). A variety of different in morphology artifacts arise mainly due to head movements, eye blinking, muscle activity, electrocardiogram (ECG) recording and so on. Due to the increased importance of

---

[*] Appendix A

this topic appendix B.3 is dedicated to possible artifact sources and treatment. On the other hand, intracranial recordings using implanted electrodes achieve a significantly higher resolution since possible deviations or alterations of the source EEG signal in its way from the originating neurons towards the scalp are overcome and artifacts are diminished. Mainly two types of intracranial electrodes are used: i) the *subdural electrodes* typically arranged in grids or strips placed on the brain and ii) the *deep electrodes* arranged on a needle entering deep brain structures (Niedermeyer, 1999a). The latter involve a major surgery and their use is restricted to pathological cases like the epileptic patients who undergo surgical resection.

2.2   The digital EEG processing era

In the 1960's and the 1970's the digitizing of the EEG was first attempted and the computer was a valuable tool for data analysis. At that moment the original aspiration of Berger and the whole psychiatric community began to see the correlation of the EEG with psychiatric conditions, as well as the brain's detailed response to medication intended to treat these disorders. Even though such medication effects where reported in the previous years, they were often misleadingly interpreted as artifacts; but at this time EEG begins to be systematically studied.

In order to take advantage of the superior analyzing power and flexibility of computers, a fundamentally crucial step was missing; the so-called analog to digital converter (DAC). This electronic device takes the input of the continuous variable wave and transforms it to a list of discrete values with respect to the time and amplitude of the input wave. This process is of particular importance and is described as the sampling operation. Sampling is performed in real time and each EEG channel is processed in parallel. The sampling rate can vary according to specific measurement needs. Once the discrete signal is stored, one can perform any mathematical operation like filtering, frequency and amplitude analysis, as well as color mapping. This digital EEG analysis is known as quantitative EEG and it differs from any previous analysis attempts to assess the overall appearance of the waves in a qualitative manner.
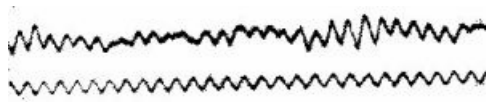
Figure 2.1: a) One of the first EEGs, appearing in Berger's first publication on EEG (Berger, 1929). The first frequency he encountered was the 10-hertz range, (8 to 12 Hz) which at first was called the Berger rhythm, currently called Alpha rhythm brain wave. His findings were published after five years of investigation and re-examination of his results. **b)** Other examples of Berger initial recordings.
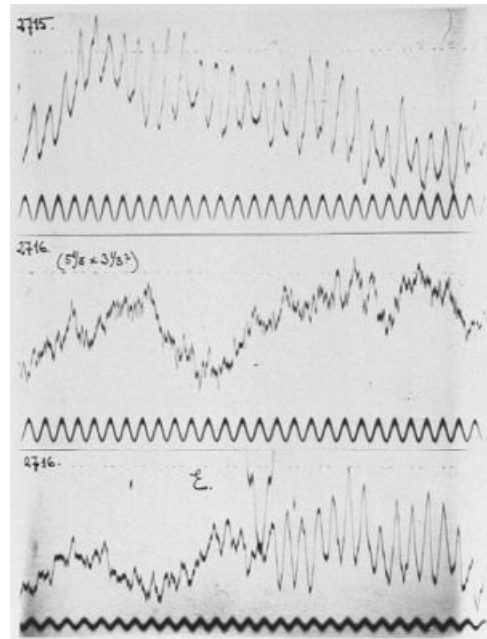
2.3   Oscillatory Brain Activity (EEG signal patterns)

Even from his first publication on EEG, Berger (1929) mentioned the presence of certain signal patterns (rhythms) that he called alpha and beta oscillations (Fig. 2.1). The patterns seen in the EEG, initiating from changes in the frequency amplitude with respect to time, have been divided into the standard bands of delta, theta, alpha and beta, which are somewhat empirical frequency limits. These rhythms are classified according to their location, frequency, amplitude, morphology, periodicity, and behavioral and functional correlates. Since the beginnings of electroencephalography these patterns have been related with different brain arousal states, functions or pathologies (Niedermeyer, 1999b; Steriade, 1999). Although these patterns may found to vary across different individuals, the frequency was shown to remain similar. This remarkable note was the spark that led to the definition of frequency bands. The frequency bands are centered around the alpha range and it can be said that are logarithmically scaled. However, these bands are to this day still not set as a standard, resulting in noting the detailed frequency limits together with the band names, in order to avoid any confusion.

- **_Delta (δ) band_ (< 4 Hz)**: Commonly, the delta band starts as low as the bandpass filter will allow, with the upper limit set at 3.5 or 4 Hz. It was described in 1936 by W. Gray Walter, while a patient was undergoing

neurosurgery for a malignant tumor. Electrodes placed over the related area recorded very slow, high voltage potentials. Since that time, focal delta activity was a reliable indicator of localized disease of the brain. In general, delta waves are not present in the normal adult waking, resting EEG. However, it may occur in elderly subjects in relatively limited amounts, particularly in the temporal regions. On the contrary, delta is considered a normal component in infants and young children. It is also characteristic of deep sleep stages, while as noted before, specific delta morphologies and localizations are correlated with different pathologies.

- *Theta (θ) band* (**4-8 Hz**): starts at 4 and goes to 7 Hz or 8 Hz and is enhanced during sleep. It is of paramount importance during infancy while diffused theta is usual during childhood. In the vigilant adult high theta activity is found in only one location or is predominant over one hemisphere. It is considered abnormal and is related to underlying brain structural disease. The lesion in this case usually is less malignant or extensive than in the case of delta band focal activity. However symmetrically distributed theta is sometimes considered a normal non-pathological variant, especially when it appears as a rhythmic activity in mid-temporal regions.

- *Alpha (α) band* (**8-13 Hz**): starts at 7-8 Hz and goes to 12-13 Hz. Neurologists commonly refer to Alpha as the background activity, since it constitutes the principal background feature of the normal adult brain. Its frequency limits are not determined in detail; rather it is defined as the rhythmic posterior activity that attenuates with sensory stimulation. It appears spontaneously during wakefulness, under relaxation and mental idle conditions. It is mostly located in occipital locations while subject remains at rest with eyes closed, but often distributes to the adjacent parietal and posterior temporal areas. Usually, alpha is more or less symmetrical but often is of higher amplitude (may reach 2:1 ratio) over the non-dominant hemisphere. If the subject is tensed alpha may not even be recorded. Alpha asymmetry is always pathological, meaning possible remote infraction in older subjects or brain damage such as congenital hemiatrophy in younger subjects.

- **_Beta (β) band_ (13-30 Hz)**: being the desynchronized faster activity above alpha, occasionally divided into beta subtypes (Beta 1-β_1 and Beta 2-β_2). It is mostly located in central and frontal lobes and has less amplitude compared to alpha waves but is enhanced upon expectancy states or tension. If completely absent it may represent an abnormality. Inter-hemispheric asymmetry and in particular the side of reduced amplitude usually points to the pathological hemisphere, but should always be considered in concert with other background frequency asymmetries.

- **_Gamma (γ) band_ (> 30 Hz)**: initially was not regarded to play an important role in interpreting EEG, but became of interest after the cellular level experiments of Gray and Singer (1989) and Gray et al. (1989) showing the link of stimulus features to a common perceptual information known as the _binding theory_. Gamma band is often divided into Gamma-1 (γ_1) and Gamma-2 (γ_2) subtypes.

A typical morphology of the most popular rhythms is depicted in Figure 2.2. Other frequency bands are also seen in the literature, including **_Mu (μ)_** and **_Lambda (λ)_**. Mu is a motor rhythm seen focally at C3 and C4[†] at 9-11 Hz, which is monomorphic or wicket shaped and is eliminated with the movement of a contra-lateral limb. Lambda is the posterior waveform elicited by visual scanning.

Another frequency pattern that can be seen in the sensory motor strip only, is the sensory motor rhythm (SMR). This particular pattern was studied by Sterman in the 1970's, and was found to correlate with a focused non-movement state. It turned out to be efficacious in the treatment of epileptics, especially in those cases where medications were unable to control the epileptic seizures for tonic-clonic or motor expressions of epilepsy.

The following table attempts, where possible, to summarize the established phenotypical characteristics, as well as the frequency range of the bands. However, one should keep in mind that the band classification does not in any way assume beforehand a necessarily distinct dissociation, but is rather a historically emerged nomenclature.

[†] Refer to the international 10-20-electrode placement system, in appendix A.

TABLE 2.I
PHENOTYPICAL CHARACTERISTICS RELATED TO EACH FREQUENCY BANDS

| Band	Freq. (Hz)	Location	Reactivity	Pathophysiology
Delta (δ)	<4	Derived from the limbic system. Are seen from the hypothalamus in the slow waves of sleep.	Normal in neonates and deep stages of adult sleep. Focal in pathologies.	Seen in white matter in case of severe, acute or ongoing injury to cortical neurons or comprehensive changes from adjacent structures.
Theta (θ)	4-8	Produced in the limbic system (septal nucleus, amygdala and hippocampus). Found in drowsy normal adult, in frontal and temporal regions.	Rarely seen in awake adults, but of paramount importance during infancy and childhood.	Focal or lateral theta indicates focal pathology. Diffused theta indicates more generalized neurological syndrome.
Alpha (α)	8-13	The most prominent rhythm in the normal adult brain (thalamus). Mostly located at occipital and parietal electrodes. About 25% stronger over the right hemisphere.	Fully present when a subject is mentally inactive, alert, with eyes closed. Disrupted by visual attentiveness. Almost totally disappears when eyes are opened.	Slowing is considered as non-specific abnormality in metabolic, toxic and infectious conditions.
Beta (β)	14-30	Three basic types: i) Frontal beta, ii) Widespread, iii) Posterior.	i) Frontal beta blocked by movement, ii) Widespread beta often non-reactive, iii) Posterior beta shows reactivity to eye opening.	Enhanced upon expectancy states or tension.
Mu (μ)	9-11	Central electrodes. Generated in the thalamo-cortical system.	Does not react to opening of eyes, shows blocking before movement of the contra lateral hand.	Not clinically useful.
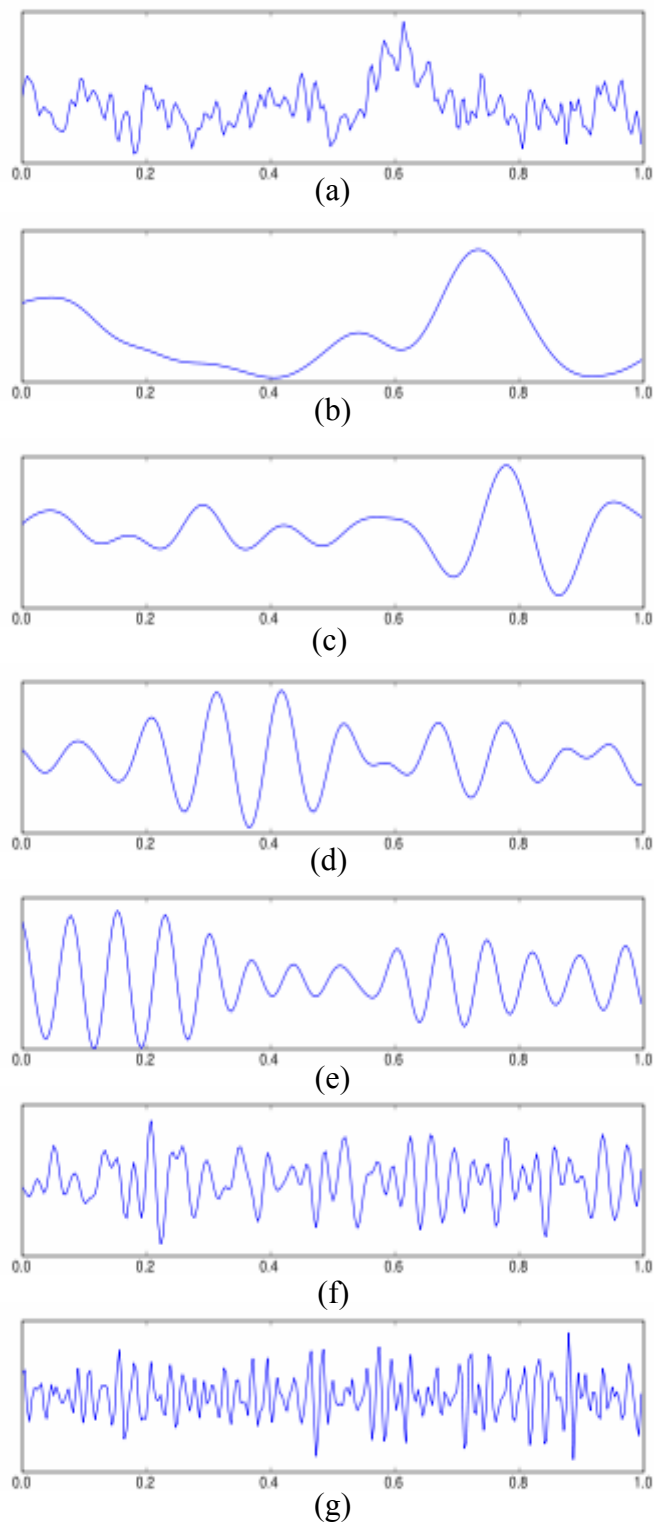
Figure 2.2: a) *A typical one second EEG signal example. Such a signal may be analyzed in* **(b)** *delta,* **(c)** *theta,* **(d)** *alpha,* **(e)** *SMR,* **(f)** *beta and* **(g)** *gamma activity waves.*

2.4 The cognitive EEG

Electroencephalographic measures have been used successfully in the past as indices of cerebral engagement in cognitive[‡] tasks. The majority of investigations have searched for systematic, task-related changes in the energy in the alpha band (8-13 Hz). Briefly, EEG studies have shown alpha suppression (Makino, 1986) and/or beta enhancement over the left hemisphere during verbal tasks (Bizas et al., 1999; Papanicolaou et al., 1986; Pulvermuller et al., 1996).

Mathematics and in general complex computations involve considerable mental effort and rely to a great extent on general verbal activities, rote learning and fact retrieval procedures (Dehaene et al., 1999). Some aspects of number processing such as reading, writing, and mentally manipulating numerical symbols rely heavily on general verbal abilities. More complex computations require, in addition to math fact retrieval, knowledge and fluent use of mathematical procedures. Human brain neuroimaging studies have demonstrated that regions of the parietal lobe, including the intraparietal sulcus (IPS) and the inferior parietal lobule (IPL) are activated when subjects are asked to perform calculation tasks. It has been suggested that these two parietal structures play complementary roles, with the IPS thought to house the circuitry that is fundamentally involved in numerical estimation (Piazza et al., 2004), number comparison (Dehaene et al., 2003; Pinel et al., 2001) and on-line calculation (often tested with subtraction), while the IPL is thought to be involved in overlearned tasks, such as multiplication (Dehaene, 1997). In addition to these parietal regions, regions of the frontal lobe are also active in calculation tasks. These activations overlap with regions involved in language processing such as Broca's[§] area and regions involved in working memory and attention. Temporal lobe activity is typically found in tasks that require fact retrieval (Dehaene et al., 1999).

[‡] Cognitive psychology is the school of psychology that examines internal mental processes such as problem solving, memory, and language.

[§] Broca's area is the section of the human brain (in the opercular and triangular sections of the inferior frontal gyrus of the frontal lobe of the cortex) that is involved in language processing, speech production and comprehension. Broca's and Wernicke's areas are found unilaterally in the brain.

Working memory[**] and general intelligence is also evident while performing mathematical reasoning tasks. Each higher brain function typically require the integrated, coordinated activity of multiple specialized neural systems that generate EEG signals at various brain regions (Breakspear et al., 2003; Bressler and Kelso, 2001; Micheloyannis et al., 2005; Sporns et al., 2002). Even if much of our understanding of working memory has come from lesion experiments in animals and imaging experiments in humans, EEG has been also found to be successful in differentiating working memory versus control (while at rest) tasks (Bizas et al., 1999).

2.5 The abnormal EEG

An EEG is characterized as abnormal not because it does not contain any normal activity patterns, but because it does include abnormal EEG patterns. Such EEG abnormal patterns are usually considered to be: (i) epileptiform activity, (ii) slow waves, (iii) amplitude abnormalities or (iv) specific deviations from normal motifs. Note that the basic abnormal EEG patterns even though they correspond fairly well with a few anatomical and pathophysiological kinds of cerebral lesions, they do not correlate directly with specific neurological diseases. This is true for the reason that similar EEG patterns may be produced by an extensive variety of neurophysiological diseases. Furthermore, many diseases may produce more than one abnormal pattern. Hopefully, there are a few specific patterns that considerably narrow the possible diagnosis. However, etiological diagnosis should not be drawn by the EEG alone, but should be used in combination with supporting examinations. The EEG only helps to establish the presence, severity and cerebral distribution of any present neurological disorders. In the next sections only two syndromes correlated with atypical EEG are briefly described since such phenomena were addressed and analyzed in this thesis. For extensive information and findings related to numerous EEG abnormalities the reader may refer to

---

[**] Working memory is a theoretical framework within cognitive psychology that refers to the structures and processes used for temporarily storing and manipulating information.

clinically oriented references and atlases (Fisch et al., 1999; Rowan and Tolunsky, 2003).

2.5.1 Epilepsy Syndrome

Epilepsy is a brain disorder that affects about 1% of the population characterized by seizures. A seizure is an episode of sudden, relatively brief disturbances (lasting one or a few minutes) of mental, motor, sensory or autonomic activity caused by an abnormal paroxysmal cerebral activity. Chronic recurrent seizures characterize an epileptic patient. The cause of epilepsy may be known (i.e., symptomatic epilepsy) or unknown (i.e., idiopathic or cryptogenic epilepsy). EEG analysis has been historically the most useful tool for evaluating the nature of this disorder. The analysis is mostly focused on interictal findings since ictal recordings (during the seizure) are rarely recorded. In the clinical environment seizures may be provoked using different methods, such as photostimulation, hyperventilation and so on, but they do not necessarily share the same properties with the spontaneous ones. However, proper counseling and selection of therapeutic plans is facilitated by making the correct epilepsy syndrome diagnosis among different epilepsy classifications.

Many classifications have been proposed comprising a debatable topic. The most widely used is the one proposed by the Commission on Classification and Terminology of the International League against Epilepsy (1981), which is based on the study of videotape recordings of simultaneously recorded EEG together with the epileptic seizures. The classification is divided into the following major categories.

- *Partial seizures*: are those in which the first clinical and electrographic changes indicate the initial involvement of a group of neurons limited to part of one cerebral hemisphere.

    o *Simple partial seizure*: is noted when consciousness is not impaired during the attack i.e., amnesia for some or all of the events happened during the attack.

    o *Complex partial seizure*: is noted when consciousness is impaired during the attack.

- ***Generalized seizures***: are those in which the first clinical and electrographic changes indicate initial involvement of both cerebral hemispheres. Loss of consciousness, bilateral motor activity or both is usually produced. Generalized seizures may be further divided into: i) absence, (ii) myoclonic, (iii) clonic, (iv) tonic, (v) tonic-clonic and (vi) atonic seizures (Commission on Classification and Terminology, 1981).

- ***Unclassified epileptic seizures***: include all kinds of seizures that cannot be classified because of inadequate or incomplete data, or due to lack of a consensus of opinion among investigators.

2.5.2 Schizophrenia Syndrome

Schizophrenia is a mental disorder characterized by impairments in the perception or expression of reality based on physic iatric diagnosis. The term *schizophrenia*, coined from Eugene Bleuler in 1908 (Berrios and Porter, 1999) comes from the Greek words "σχίζω" and "φρήν" that translate to split or divide and mind, respectively. However, schizophrenia does not necessarily correlate with dissociative identity disorder (multiple personality illusion) and there is no predisposition toward aggressive behavior.

An untreated schizophrenic demonstrates disorganized thinking and experience dilutions or auditory hallucinations. Positive and negative symptoms are possible. As *positive symptoms* are characterized those diagnosed additional to the normal experience and behavior, such as dilutions, auditory hallucinations, thought disorder and other psychosis manifestations. As *negative symptoms* are characterized those diagnosed to decline in normal experience or behavior, such as flat or constricted affect and emotion and lack of motivation.

Diagnosis is mostly based on the self-reported experiences of the patient, in combination with signs observed by a psychiatrist or a clinical physiologist. Differences in brain structure have been found between schizophrenics and their healthy counterparts, but these tend only to be reliable on the group level and due to the significant variability between each individual, may not reliably represent a particular subject. However, the lack of objective laboratory test makes the possibility of EEG a prospective diagnostic test at least for stabilized patients.

Schizophrenics often face social or occupational isolation and typically live 10 to 12 years less than the healthy subjects due to high suicide rate and increased physical health problems.

Bibliography

Berger H. Über das Elektrenkephalogramm des Menchen. Archives für Psychiatrie 1929; 87: 527-70.

Berrios GE, Porter R. A history of clinical psychiatry : the origin and history of psychiatric disorders. London ; New Brunswick, NJ; Somerset, N.J.: Athlone Press ; Distributed in the U.S., Canada, and South America by Transaction Publishers, 1999.

Bizas E, Simos PG, Stam CJ, Arvanitis S, Terzakis D, Micheloyannis S. EEG correlates of cerebral engagement in reading tasks. Brain Topogr 1999; 12: 99-105.

Breakspear M, Terry JR, Friston KJ, Harris AW, Williams LM, Brown K, et al. A disturbance of nonlinear interdependence in scalp EEG of subjects with first episode schizophrenia. Neuroimage 2003; 20: 466-78.

Bressler SL, Kelso JA. Cortical coordination dynamics and cognition. Trends Cogn Sci 2001; 5: 26-36.

Commission on Classification and Terminology ILAE. Proposal for Revised Clinical and Electroencephalographic Classification of Epileptic Seizures. Epilepsia 1981; 22: 489-501.

Dehaene S. The number sense : how the mind creates mathematics. New York: Oxford University Press, 1997.

Dehaene S, Piazza M, Pinel P, Cohen L. Three parietal circuits for number processing. Cogn. Neuropsychology 2003; 20: 487-506.

Dehaene S, Spelke E, Pinel P, Stanescu R, Tsivkin S. Sources of mathematical thinking: behavioral and brain-imaging evidence. Science 1999; 284: 970-4.

Fisch BJ, Fisch BJ, Spehlman R. Fisch and Spehlmann's EEG primer : basic principles of digital and analog EEG. Amsterdam ; New York: Elsevier, 1999.

Gray CM, Konig P, Engel AK, Singer W. Oscillatory responses in cat visual cortex exhibit inter-columnar synchronization which reflects global stimulus properties. Nature 1989; 338: 334-7.

Gray CM, Singer W. Stimulus-specific neuronal oscillations in orientation columns of cat visual cortex. Proc Natl Acad Sci U S A 1989; 86: 1698-702.

Makino A. Topographic EEG analysis in relation to higher brain function. Tokushima J Exp Med 1986; 33: 59-68.

Micheloyannis S, Sakkalis V, Vourkas M, Stam CJ, Simos PG. Neural networks involved in mathematical thinking: evidence from linear and non-linear analysis of electroencephalographic activity. Neurosci Lett 2005; 373: 212-7.

Niedermeyer E. Depth Electroencephalography. In: Niedermeyer E and Lopes da Silva FH, editors. Electroencephalography : basic principles, clinical applications, and related fields. Baltimore: Williams & Wilkins, 1999a: xi, 1258 p.

Niedermeyer E. The normal EEG of the walking adult. In: Niedermeyer E and Lopes da Silva FH, editors. Electroencephalography : basic principles, clinical applications, and related fields. Baltimore: Williams & Wilkins, 1999b.

Papanicolaou AC, Loring DW, Deutsch G, Eisenberg HM. Task-related EEG asymmetries: a comparison of alpha blocking and beta enhancement. Int J Neurosci 1986; 30: 81-5.

Piazza M, Izard V, Pinel P, Le Bihan D, Dehaene S. Tuning curves for approximate numerosity in the human intraparietal sulcus. Neuron 2004; 44: 547-55.

Pinel P, Dehaene S, Riviere D, LeBihan D. Modulation of parietal activation by semantic distance in a number comparison task. Neuroimage 2001; 14: 1013-26.

Pulvermuller F, Eulitz C, Pantev C, Mohr B, Feige B, Lutzenberger W, et al. High-frequency cortical responses reflect lexical processing: an MEG study. Electroencephalogr Clin Neurophysiol 1996; 98: 76-85.

Reilly E. EEG Recording and Operation of the Apparatus. In: Niedermeyer E and Lopes da Silva FH, editors. Electroencephalography : basic principles, clinical applications, and related fields. Baltimore: Williams & Wilkins, 1999: xi, 1258 p.

Rowan AJ, Tolunsky E. A primer of EEG : with a mini-atlas. Philadelphia, PA: Butterworth-Heinemann, 2003.

Sporns O, Tononi G, Edelman GM. Theoretical neuroanatomy and the connectivity of the cerebral cortex. Behav Brain Res 2002; 135: 69-74.

Steriade M. Cellular substrates of brain rhythms. In: Niedermeyer E and Lopes da Silva FH, editors. Electroencephalography : basic principles, clinical applications, and related fields. Baltimore: Williams & Wilkins, 1999.

Tudor M, Tudor L, Tudor KI. [Hans Berger (1873-1941)--the history of electroencephalography]. Acta Med Croatica 2005; 59: 307-13.

When we try to pick out anything by itself,

we find it hitched to everything else in the Universe.

—. [John Muir](#)

3

EEG ANALYSIS METHODS

This chapter provides a brief overview of the basic theoretical background related to various processing steps and methods involved in the course of this thesis. Certain implementation aspects will be discussed.

3.1 Fourier Transform in EEG analysis

The revolutionary discoveries of Jean Baptiste Fourier (1768-1830), have had a major impact on the development of mathematics and are of great importance in an extremely wide range of scientific and engineering disciplines.

Although, the original work of Fourier was focused on problems of mathematical Physics, which happen in the continuous time domain, there is also a rich variety of applications of the tools of Fourier analysis for discrete-time signals and systems. In particular, discrete-time concepts and methods are fundamental to the discipline of numerical analysis. Formulas for the processing of discrete sets of data points to produce numerical approximations for interpolation, integration, and

differentiation were investigated in the early 1600's. This section starts with the mathematical foundation of the Fourier Transform and related matters. Some basic and widely used applications of Fourier analysis in EEG are described next, namely Topographical Brain Mapping and Coherence.

The Fourier transform is a generalization of the *Fourier Series*. The latter is a representation of periodic signals, while Fourier transform only applies to non-periodic functions. A large class of signals, including all signals with finite energy, can also be represented through a linear combination of complex exponentials. For periodic signals the complex exponential building blocks are harmonically related, whereas for non-periodic signals, which are infinitesimally close in frequency, the representation in terms of linear combination takes the form of an integral rather than a sum.

Fourier Series

Representation of a <u>continuous-time</u> Periodic Signal

Supposing that $x(t)$ has a Fourier series representation, meaning that it can be expressed as a linear combination of harmonically related complex exponentials (equation 3.1a), then the coefficients are given by equation 3.1b. This pair of equations defines the Fourier series of a periodic continuous-time signal:

$$x(t) = \sum_{k=-\infty}^{+\infty} a_k e^{jk\omega_0 t} = \sum_{k=-\infty}^{+\infty} a_k e^{jk(2\pi/T)t},$$

$$a_k = \frac{1}{T}\int_T x(t)e^{-jk\omega_0 t}dt = \frac{1}{T}\int_T x(t)e^{-jk(2\pi/T)t}dt \qquad (3.1)$$

The above expressions for the Fourier series are equivalent in terms of a fundamental period T. Equations 3.1a and 3.1b are referred to as the *synthesis* and analysis equations, respectively. The set of coefficients α_k are often called the Fourier series coefficients or the spectral coefficients of $x(t)$. These complex coefficients measure the portion of the signal $x(t)$ that consists each harmonic of the fundamental component. The coefficient α_0 is the constant component of $x(t)$ and is given by equation 3.1b with $k=0$, and is given by:

$$a_0 = \frac{1}{T}\int_T x(t)dt \qquad (3.2)$$

which is simply the average value of $x(t)$ over one period.

Representation of a <u>discrete-time</u> periodic signal

The Fourier Series representation of a discrete-time periodic signal, consisting of N discrete values $x[n]=\{x_0,x_1,\ldots,x_{N-1}\}$, is a finite series, as opposed to the infinite series representation required for continuous-time periodic signals.

If given the sequence $x[n]$ that is periodic with fundamental period N, the discrete-time Fourier series pairs are:

$$x[n] = \sum_{k=\langle N \rangle} a_k e^{jk\omega_0 n} = \sum_{k=\langle N \rangle} a_k e^{jk(2\pi/N)n}$$

$$a_k = \frac{1}{N} \sum_{n=\langle N \rangle} x[n]e^{-jk\omega_0 n} = \frac{1}{N} \sum_{n=\langle N \rangle} x[n]e^{-jk(2\pi/N)n}$$

(3.3)

These equations are again the synthesis (equation 3.3a) and analysis (equation 3.3b) equations, similarly with equations 3.1a and 3.1b, but in the discrete-time domain, this time. As in continuous-time, the discrete-time Fourier series coefficients are often referred as the spectral coefficients of $x[n]$. These coefficients specify a decomposition of $x[n]$ into a sum of N harmonically related complex exponentials.

Fourier Transform

Representation of a <u>continuous-time</u> non-periodic signal

The development of the representation for non-periodical signals in continuous time is one of Fourier's most important contributions. In particular, Fourier reasoned that a non-periodical signal could be viewed as a periodic signal with infinite period. More precisely, in the Fourier series representation of a periodic signal, as the period increases the fundamental frequency decreases and the harmonically related components become closer in frequency. As the period becomes infinite, the frequency components form a continuum and the Fourier series sum becomes an integral.

Consider a non-periodic function $x(t)$. The continuous-time Fourier transform pair is:

$$x(t) = \frac{1}{2\pi} \int_{-\infty}^{+\infty} X(j\omega)e^{j\omega t} d\omega$$

$$X(j\omega) = \int_{-\infty}^{+\infty} x(t)e^{-j\omega t} dt$$

(3.4)

The function $X(j\omega)$ is the Fourier transform or Fourier integral of $x(t)$ and equation 3.4a is the inverse Fourier transform equation. The synthesis equation (equation 3.4a) plays a similar role for non-periodic signals to that of equation 3.1b for periodic signals, since both represent a signal as a linear combination of complex exponentials. In the case of periodic signals, these complex exponentials have amplitude α_k, as given by equation 3.1b, and occur at a discrete set of harmonically related frequencies $k\omega_0$, k=0, ±1, ±2,... . For non-periodic signals, the complex exponentials occur at a continuum of frequencies and according to the synthesis equation (equation 3.4a), have amplitude equal to $X(j\omega)(d\omega/2\pi)$. In analogy with the terminology used for the Fourier series coefficients of a periodic signal, the transform $X(j\omega)$ of a non-periodic signal $x(t)$ is commonly referred to as the spectrum of $x(t)$, as it provides us with the information needed for describing $x(t)$ as a linear combination (specifically, an integral) of sinusoidal signals at different frequencies.

Representation of a <u>discrete-time</u> signal with finite support

Following similar ideas as before, the discrete time counterparts are:

$$x[n] = \frac{1}{N}\sum_{k=0}^{N-1} X(f_k)e^{j2\pi kn/N}$$

$$X(f_k) = \sum_{n=0}^{N-1} x[n]e^{-j2\pi kn/N} \qquad k = 0,...,N-1 \tag{3.5}$$

The function $X(f_k)$ is referred to as the *discrete-time Fourier transform* (DFT) and the discrete frequencies are defined as:

$$f_k = \frac{k}{N\Delta} = \frac{kf_s}{N} \tag{3.6}$$

where Δ is the sampling interval, such as $t_i = t_0 + i\Delta$ and f_s is the sampling frequency.

The DFT has many similarities with the continuous time case. The major differences are the periodicity of the DFT and the finite interval of integration in the synthesis equation, which stem from the fact that discrete time complex exponentials of the frequency domain differ in frequency by a multiple of 2π are identical (Oppenheim et al., 1997). Finally, one should note that an efficient digital implementation of the DFT, referred as the *Fast Fourier Transform* (FFT), was

independently discovered by Cooly and Tukey in the mid-1960s (Heideman et al., 1984). This implementation made the Fourier Transform computationally attractive since it reduces the time consumed for computing transforms by orders of magnitude [DFT: $O(N^2)$ vs. FFT: $O(N\log N)$].

Aliasing effect

The frequency $f_N = \dfrac{1}{2\Delta}$, which corresponds to $k = \dfrac{N}{2}$ (as in eq. 3.6) is called the *Nyquist frequency* and determines the highest frequency detected with a sampling period Δ. Hence, if $x[n]$ comprises of higher frequencies than the Nyquist, these ones will be processed as they were in the range $f_k < f_N$ that results in the bogus aliasing effect (Heideman et al., 1984; Weaver, 1989).

Periodogram

The *power spectral density* (PSD) reveals the distribution (over frequency) of the power contained in an EEG signal, based on a finite set of data. Such estimation of power spectra is particularly useful in EEG, because it is capable of detecting signals buried in wide-band noise. There are many ways of estimating the PSD using non-parametric, parametric or subspace methods (Proakis and Manolakis, 1996). One simple way of non-parametric estimation of the PSD is to simply find the discrete-time Fourier transform of the samples of the process (usually done on a grid with an FFT) and take the magnitude squared of the result. This estimate $\widehat{P}_{xx}(f_k)$ is called the *periodogram* estimate of the PSD, which is calculated only at a finite number of frequency points N and is mathematically formulated as:

$$\widehat{P}_{xx}(f_k) = \frac{P_{xx}(f_k)}{f_s L}$$

$$P_{xx}(f_k) = |X(f_k)|^2 = X(f_k) \cdot X^*(f_k)$$

(3.7)

where * denotes complex conjugation, L is the length of the EEG signal, $X(f_k), f_k$ is given by equations 3.5 and 3.6, respectively. It is usual to choose $N > L$ so that N is the next power of two larger than L. In order to evaluate $X(f_k)$, the signal is simply padded with zeros to length N. $P_{xx}(f_k)$ is the periodogram estimation of the Power Spectrum and is given by eq. 3.7. An improved version of the periodogram is given

by the *Welch's method* of estimating the so called *averaged periodogram* (Welch, 1967). The latter method consists of dividing the time series data into (possibly overlapping) segments, computing a *modified periodogram* of each segment, and then averaging the PSD estimates. The periodogram of each segment is modified by the usage of a window, as discussed in the next section. The averaging of modified periodograms tends to decrease the variance of the estimate relative to a single periodogram estimate of the entire signal. Although overlap between segments tends to introduce redundant information, this effect is diminished by the use of a nonrectangular window, which reduce the importance or weight given to the end samples of segments (the samples that overlap).

3.1.1 Windowing Operation

Unfortunately, the increase in speed using FFT comes at the cost of versatility. The FFT function automatically places some restrictions on the time series to be evaluated in order to generate a meaningful, accurate frequency response. Because the FFT function uses a base 2 logarithm by definition, it requires that the range or length of the time series to be evaluated contains a total number of data points precisely equal to a 2-to-the-nth-power number (i.e., 512, 1024,..,etc.). This is where the problem develops. The FFT function also requires that the time series contain a whole number of periods in order to generate an accurate frequency response. Obviously, the chances of a waveform containing a number of points equal to a 2-to-the-nth-power number and ending on a whole number of periods are slim at best, so something must be done to ensure an accurate representation in the frequency domain. This inaccuracy ends up to the "leakage" effect of the power spectrum due to energy being artificially generated by the discontinuity at the end points of each period.

Fortunately, the way to minimize this leakage effect error and ensure accuracy in the frequency domain comes with the concept of windowing. Windowing is the operation of taking a signal $x[n]$ and multiplying it by a finite-duration window signal $w[n]$. Hence,

$$p[n] = x[n]w[n] \qquad\qquad (3.8)$$

24

where, $p[n]$ is also of finite duration. Windowing is particularly useful in spectral analysis because in numerous applications one wishes to compute the Fourier transform of a signal that has been measured. Since in practice one can measure a signal $x[n]$ only over a finite time interval (time window), the actual signal available for spectral analysis is:

$$p[n] = \begin{cases} x[n], & -M \leq n \leq M \\ 0, & otherwise \end{cases} \tag{3.9}$$

where $-M \leq n \leq M$ is the time window definition. In the case of the simpler *rectangular window*, $w[n]$ is defined as:

$$w[n] = \begin{cases} 1, & -M \leq n \leq M \\ 0, & otherwise \end{cases} \tag{3.10}$$

Clearly, such operation has an effect on the resulting spectrum. More specifically, in the case of the rectangular window, ripples are introduced in the Fourier transform. This effect is directly related to the Gibbs (or *spectral leakage*) phenomenon and windowing functions aim to reduce such leakage effects. As a remedy, a variety of other window signals are available for use. Their main characteristic is that these are tapered; which means that they go from 0 to 1 more gradually than the abrupt transition of the rectangular window. The result is a reduction in the amplitude of the ripples in the transformed signal at the expense of adding some distortion in terms of further smoothing of the original signal.

The most common windows are the *Hann* (due to Julius van Hann, often wrongly referred to as *Hanning window* (Dumermuth and Molinari, 1987; Wolberg, 1990), sometimes just cosine bell window) and the *Hamming window*, which are quite similar; they only differ in the choice of one parameter α.

$$w[n] = \begin{cases} a + (1-a)\cos\left(\pi \dfrac{n}{M}\right), & -M \leq n \leq M \\ 0, & otherwise \end{cases} \tag{3.11}$$

with $\alpha = 0.5$ being the Hann window and $\alpha = 0.54$ the Hamming Window. The Hamming window also has the disadvantage of being discontinuous (but not severely) at the edges. The surface shown below is of the above function varying the parameter α.
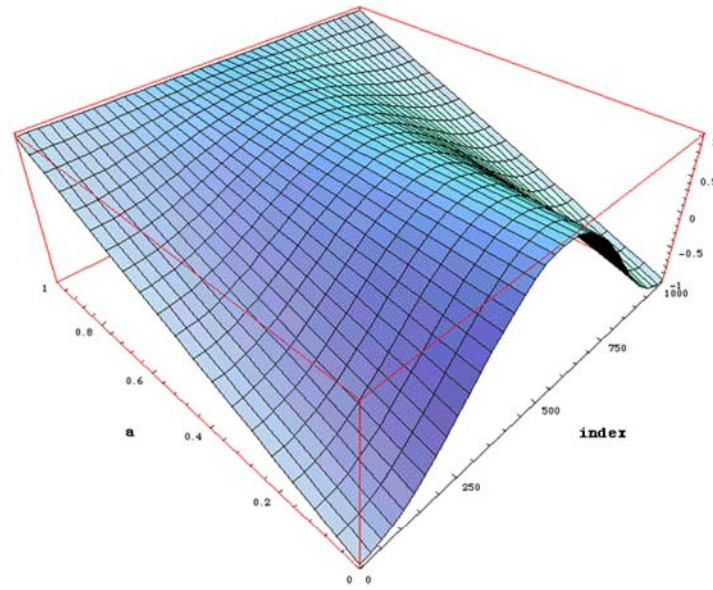
Figure 3.1: *The surface drawn is of the above function (eq. 3.11) varying the parameter **α**.*

The *Blackman window* is quite similar to Hann and Hamming window, but it has one additional cosine term to further reduce the ripple ratio and it is defined as:

$$w[n] = \begin{cases} 0.42 + \dfrac{1}{2}\cos\left(\pi\dfrac{n}{M}\right) + 0.08\cos\left(2\pi\dfrac{n}{M}\right), & -M \leq n \leq M \\ \\ 0, & otherwise \end{cases} \qquad (3.12)$$

All of the above functions will assign the greatest weight to the observation
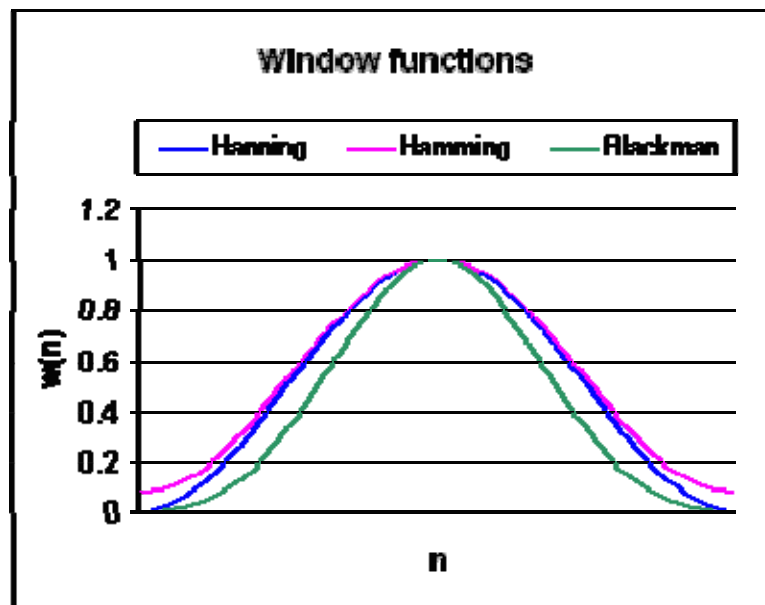
Figure 3.2: *Graph of the windowing functions discussed above.*
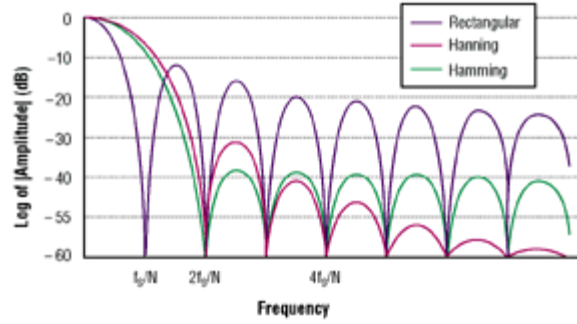
Figure 3.4: *The frequency-response plots for the rectangular, Hann, and Hamming window functions. It can be seen that the side lobes that cause the leakage are suppressed.*

being smoothed in the center of the window, and increasingly smaller weights to values that are further away from the center.

The windowing operation is graphically described in the sequence of plots in figure 3.3. Sine wave discrete values are multiplied by the corresponding values for the Hann (in this case) window. The exported signal is tapered. Figure 3.4 depicts the frequency responses for rectangular, Hann and Hamming windows, where the rectangular window provides the reference for measuring relative window performances. The plots are normalized and only positive frequencies are plotted.

The rectangular window yields the narrowest main lobe resulting in the best possible frequency resolution, but its first side lobe drops only 13 dB below the peak of the main lobe, which allows increased leakage. On the other hand the Hann and Hamming windows suppress the leakage but their main lobes are twice as wide as the main lobe of the rectangular window; thus the resolution is degraded. Fortunately, this problem can be overcome by increasing the sampling rate (Oversampling).

As a conclusion, one should point out that there is no way to avoid FFT leakage in adjacent frequencies, but by applying windowing functions prior to
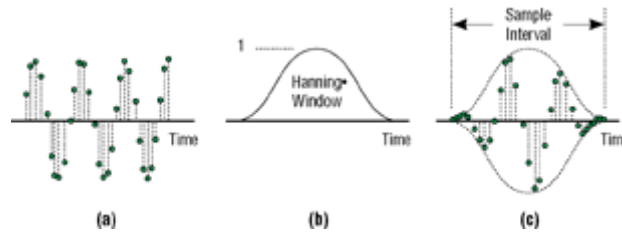

Figure 3.3: a) *Multiplying each value in a sampled signal by a corresponding Hanning window value as shown in* **(b)***, results in a signal that does not have abrupt transitions* **(c)***.*

27

performing an FFT, its effects can be substantially reduced.

3.1.2 Frequency Bands

Due to the non-stationary nature of the EEG signal one should better select representative artifact free data samples (*epochs*) prior to the FFT. Next, windowing is performed and the periodograms of the epochs are computed and averaged. Furthermore, it has been extremely useful and helpful in clinical reasoning to group adjacent frequencies as pointed out in section 2.4. The energy of these frequency bands may be evaluated separately or relatively i.e., alpha/ theta power ratio, alpha activity with eyes closed/ alpha activity with eyes open, asymmetry index (left hemisphere power − right hemisphere power/ left hemisphere power + right hemisphere power), and so on (Nuwer et al., 1994). Finally, specifically the energy contained in certain frequency bands is extensively used to establish normal ranges and significant deviations indicating several pathologies (John et al., 1987).

3.1.3 Topographic Brain Mapping

A special display of the distribution of scalp EEG activity is referred as *topographic mapping* (Brandt, 1992; Fisch et al., 1999; Lopes da Silva, 1999) and may be drawn in two or three dimensions. While spatial EEG features have often been difficult to discern in polygraph tracings, the availability of EEG color topographic maps (Duffy et al., 1979) has made appreciating them easy, even for the non-EEG specialist. The use of mapping techniques is frequently allied to different brain pathologies, including Alzheimer disease, vascular diseases etc. where comparison against reference and quantitative analysis is important. Activity such as spikes, hemispheric
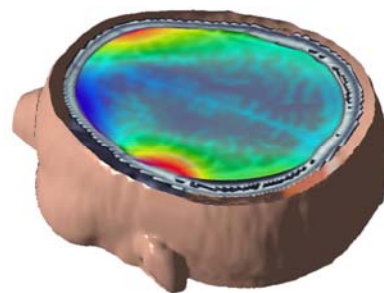

Figure 3.5: *The 3D MRI rendered model with the Brain map functional info overlaid on top, indicates the visualization process that can help the radiologist's diagnosis. It should be noted that this image illustrates only a "fusing" paradigm (Sakkalis et al., 2004).*

differences, focal finding and elevation at slow waves are also often easier to detect and recognize using a visual technique.

Such displays maybe used to illustrate:

i)   EEG voltage distributions at a particular point in time (*time domain mapping*)

ii)   EEG features derived from frequency analysis in numerous frequency bands (*frequency domain mapping*) and

iii)   Statistical comparison maps that basically illustrate significance values arising mainly from hypothesis tests (*statistical mapping*).

However, it is important to realize that the only real and valid values on topographic maps are those that represent the actual channel values. The rest values needed to create the map are estimation based on a variety of different interpolation algorithms only to turn the map into an eye pleasing image. Such, algorithms basically use linear or quadratic interpolation (Fig. 3.6) calculating the influence of the three or four neighboring channel values to the value under estimation. Another possibility, mostly used for image morphing applications, is the use of the so called *Thin Plate Spline* (TPS) interpolation method. The latter was used in the remaining of the thesis and the underlying its theoretical aspects are described next.

A thin-plate spline $f(x,y)$ (Bookstein, 1989) is a smooth function, which interpolates a surface that is fixed at the landmark points P_i at a specific height h_i. One can imagine this surface as a thin metal plate, where its shape tends to be the least bent one, by minimizing the quantity:

$$\iint_{R^2} \left(\frac{\partial^2 f}{\partial x^2} \right)^2 + 2 \left(\frac{\partial^2 f}{\partial x \partial y} \right)^2 + \left(\frac{\partial^2 f}{\partial y^2} \right)^2 \, dxdy \qquad (3.13)$$

the so-called "bending energy" of the thin-plate spline function. Instead of assuming that f corresponds to a displacement orthogonal to the image plane at the landmarks, one can assume a displacement in the image plane. By using two separate thin-plate spline functions f_x and f_y which model the displacement of the landmarks in the x and y direction we arrive at a vector-valued function F which maps each point of the image into a new point in the image plane:

$$(x,y) \rightarrow [f_x(x,y), f_y(x,y)] \qquad (3.14)$$
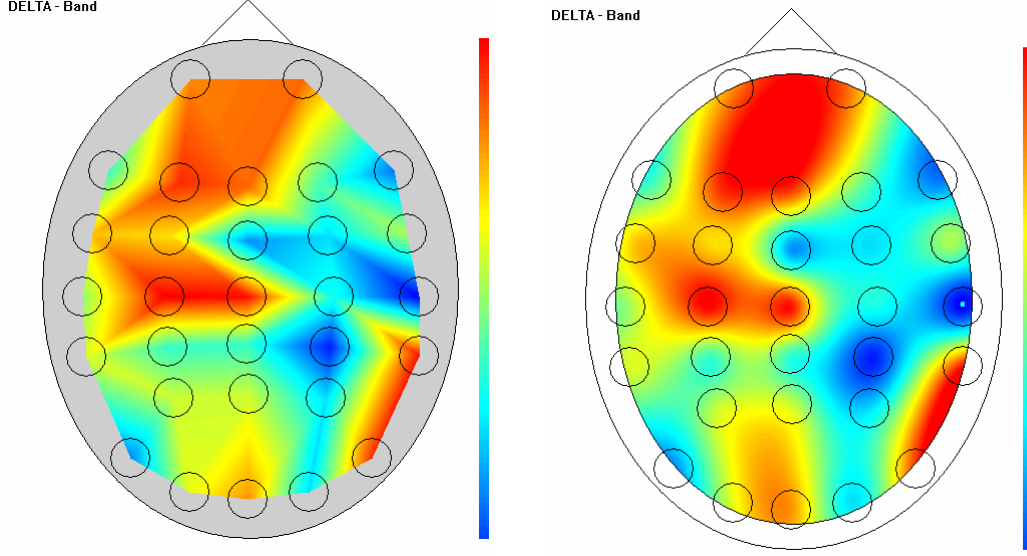
Figure 3.6: *Frequency domain mapping of delta band activity employing **(a)** Linear Interpolation and **(b)** Thin plate spline interpolation. Both images, constructed from the initial values, consist only from 28 color spots located in the center of the black circles and resembles the power recorded in each channel. Higher and lower delta activity is denoted in red and blue colorings, respectively.*

A thin-plate spline interpolation function can be written as:

$$f(x,y) = a_0 + a_x x + a_y y + \sum_{i=1}^{n} w_i U\left(\left\|(x,y) - P_i\right\|\right) \tag{3.15}$$

where:

$$z(x,y) = -U(r) = -r^2 \log(r^2) \tag{3.16}$$

is a so-called fundamental solution in the space of surfaces of the biharmonic equation :

$$\Delta^2 U = \left(\frac{\partial^2}{\partial x^2} + \frac{\partial^2}{\partial y^2}\right)^2 U = 0 \tag{3.17}$$

which must satisfy the condition of bending energy minimization. r is the spherical distance (the distance at a point (x, y) from the Cartesian origin). The biharmonic equation describes the shape of a thin steel plate lofted as a function $z(x,y)$ above the (x, y) plate. This "loft" can be color coded, as it will be described in the next section.

By appropriately choosing a $n \times 2$ matrix W of the coefficients w_i, the function F maps $F(P_i) = P_i'$ for all $i = 1,..,n$. These coefficients calculation requires the solution of n simultaneous equations and the inversion of a $n \times n$ matrix (in the
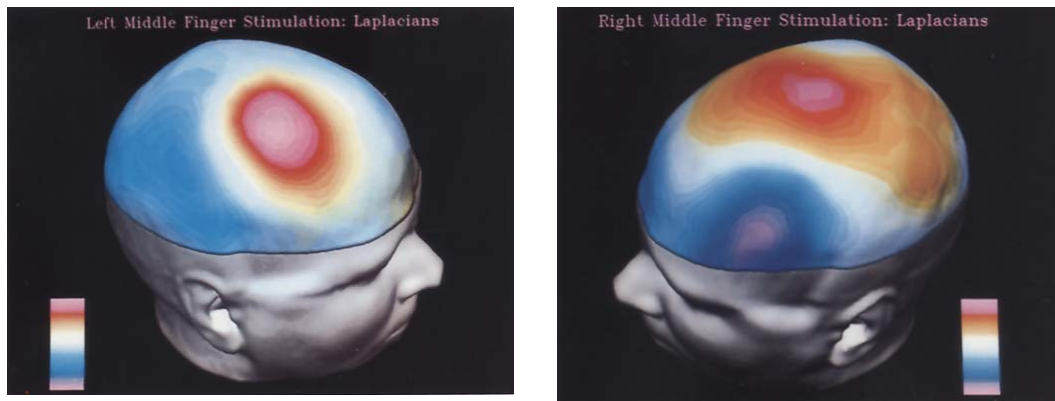
Figure 3.7: *Laplacian of 124-channel evoked potentials evoked by 15-Hz stimulation of the middle finger on left (top) and right (middle) hands of this subject mapped onto his own MRI-derived scalp surface. The map for the right index finger is shown in the bottom panel. Color scale shows zero as white and the maximum as magenta (Gevins et al., 1990).*

case of *n* fixed points). As a result, a spline fit is limited to a reasonable number of points. Points lying in more than one region are assigned a value that is a weighted average of the multiple estimates.

The past decade significant progress on three-dimensional topographic maps has been made. The focus is in increasing the spatial detail of scalp-recorded EEGs and in registering this functional information with realistic anatomical models of a person's brain using 3D structures reconstructed from MRI data. Figure 3.7 illustrates the Laplacian[*] (Hjorth, 1975) of 124-channel evoked potentials evoked by 15-Hz stimulation of the middle finger on left (top) and right (middle) hands of this subject mapped onto his own MRI-derived scalp surface (Gevins et al., 1990). Another information fusion approach is depicted in figure 3.5, illustrating the underlying brain anatomical structures fused together with a two-dimensional frequency map (Sakkalis et al., 2004).

---

[*] Electrical currents generated by sources in the brain are volume conducted through brain, cerebrospinal fluid, skull and scalp to the recording electrodes. Because of this, potentials due to a localized source are spread over a considerable area of scalp and the potential measured at a scalp site represents the summation of signals from many sources over much of the brain. The "simplest" way to reduce this distortion is to take the Laplacian in two dimensions about each electrode.

31

3.1.4 Cross-correlation & Coherence

The study of functional relationships between two brain regions has been one of the main aims of the EEG. As early as 1951, the *cross-correlation* function was used to study the similarity between two EEG signals (Brazier and Casby, 1952). Its application in the area of brain analysis is based on the assumption that the higher the correlation, the stronger the functional relationships between the related brain regions (Shaw, 1981; Shaw, 1984). It has been extensively used in studying the interrelationships between different cortical regions in relation to sensory stimulation, voluntary movements, effect of drugs and a wide range of clinical and cognitive problems and tasks.

However, since the development of FFT, correlation has been replaced by an alternative mathematical method, the *coherence spectrum*. The latter, in addition to the correlation information, has the advantage of showing the co-variation between two signals as a function of frequency, thus allowing the study of spatial correlations between different bands (Gevins, 1987; Guevara et al., 1995). Coherence studies have been successfully conducted in many fields, including those dealing with cognitive functions and psychiatric disorders (French and Beaumont, 1984). To mention a few key articles that reviewed the applications of coherence to neural data the reader is referenced to (Dumermuth and Molinari, 1991; French and Beaumont, 1984; Shaw, 1984; Thatcher et al., 1986; Zaveri et al., 1999). Especially in epileptic seizures when an abnormal synchronization of neurons takes place, coherence appears to be an ideal tool for measuring it.

Both methods, correlation and coherence, may be considered as equivalent in that they evaluate the degree of similarity between two signals. However, there are important differences between them. Coherence is calculated by dividing the numerical square of the cross-spectrum by the product of the autospectra (eq. 3.20). Since, it is a complex measure; it is sensitive to both a change in power and a change in phase relationships. Consequently, if either power or phase changes in one of the signals, the coherence value is affected. Another important difference is that the value of coherence for a single epoch is always one, regardless of the true phase relationship and the differences in power between the two signals (Bendat and Piersol, 1993).

Therefore, similarly to eq. 3.7 the *sample cross spectrum S_{xy}* between two time series is defined by calculating the product of the Fourier transformed series as follows:

$$S_{xy}(f_k) = X(f_k) \cdot Y^*(f_k) \tag{3.18}$$

The latter measures the linear cross correlation between the two signals for any given frequencies (as in eq. 3.6). In general, the correlation function requires normalization to produce an accurate estimate and is given by:

$$C_{xy}(\tau) = \frac{1}{N-\tau} \sum_{k=1}^{N-\tau} x(k+\tau)y(k) \tag{3.19}$$

where N is the total number of samples and τ the time lag between the signals. Taking the square of the cross spectrum normalized by the auto spectra of each signal defines the magnitude squared coherence or simply the coherence Γ^2_{xy} as follows:

$$\Gamma^2_{xy}(f_k) = \frac{\left| \langle S_{xy}(f_k) \rangle \right|^2}{\left| \langle S_{xx}(f_k) \rangle \right| \left| \langle S_{yy}(f_k) \rangle \right|} \tag{3.20}$$

where $\langle \cdot \rangle$ indicates average over a number of equal in length signal segments or epochs, as discussed earlier in calculating the averaged modified periodogram typically using Welch's method.

Over successive epochs the coherence measure is dependent on power and phase of the two signals along the epochs. If there is no variation over time in the original relationship between the two signals, the coherence value remains unity. This means that coherence does not give direct information on the true relationship between the two signals, but only on the stability of this relationship with respect to power asymmetry and phase relationship. Correlation, on the other hand, may be calculated over a single epoch or over several epochs and it is sensitive to both, phase and polarity, independently of amplitudes. The calculation of coherence involves squaring the signal, thus producing values which go from 0 (linearly independent signals for a given frequency) to 1 (maximum linear correlation in given frequency), and a loss in polarity information. By contrast, correlation is sensitive to polarity and its values go from -1 (complete linear inverse correlation) to $+1$ (complete linear direct correlation), with $C_{xy}(\tau) = 0$ suggesting lack of linear

interdependence for a given time lag τ. However, under normal physiological conditions, no strong and abrupt power asymmetries would be expected to occur. Thus, the influence of power on coherence should be negligible and results similar to those produced by correlation also would be expected for the coherence measures.

Additionally one is able to define the phase function of the coherence as:

$$\Phi_{xy}(f_k) = \arctan\frac{-\Im S_{xy}(f_k)}{\Re S_{xy}(f_k)} \tag{3.21}$$

where $\Im$ and $\Re$ denote the imaginary and real part. Phase measure is meaningful only in the case of significant coherence, when one is interested in estimating the time delay between the two signals (Brazier, 1972) according to:

$$\tau_{xy}(f_k) = \frac{\Phi_{xy}}{2\pi f_k} \tag{3.22}$$

where Φ_{xy} is the phase difference in degrees at a frequency f_k (as defined in eq. 3.6).

Important concerns and limitations

It should be noted that EEG represents a set of continuous voltage/time values and may therefore be considered as a multivariate time series that belongs to the category of stochastic processes which may be described by probability distributions. The concept of temporal stochastic process may be extended, in the case of the EEG, to the spatial domain (Nunez, 1995). The stochastic nature (temporal and spatial) of the EEG allows the use of correlation and coherence analyses which presuppose independence between successive points in time. However, a trade-off has to be made regarding the length of the data segment for analysis, which on one hand must be short enough to satisfy the condition of stationarity (required from Fourier Transform) and on the other hand must be long enough to provide good frequency resolution. EEG on the contrary is highly non-stationary.

Another concern is that Fourier transform drops the information concerning the time evolution of the signal, which in certain cases maybe useful.

Finally, another important point to take into account is that coherence is very sensitive to fluctuations of linearity in phase, relatively less so to nonlinear fluctuations of amplitude, and completely insensitive to linear fluctuations in amplitude. This becomes obvious if one rewrites equation 3.20 in terms of polar coordinates:

$$\Gamma^2_{xy}(f_k) = \frac{\left|\left\langle X(f_k) \cdot Y^*(f_k) \right\rangle\right|^2}{\left|\left\langle X^2(f_k)\right\rangle\right|\left|\left\langle Y^2(f_k)\right\rangle\right|} = \frac{\left|\left\langle |XY| e^{i(\arg X - \arg Y)} \right\rangle\right|^2}{\left|\left\langle |X|^2\right\rangle\right|\left|\left\langle |Y|^2\right\rangle\right|} \qquad (3.23)$$

Both amplitude and phase information are evaluated with regard to their contribution to linear dependence. The relative importance of amplitude and phase covariance in this index is not altogether clear (Lachaux et al., 1999; Varela et al., 2001). Therefore, some authors have argued that amplitude should not contribute to the final measure at all. Hence, the relationship between the phases without any influence of the amplitudes is better calculated by alternative methods, i.e. Phase Locking Value (PLV) as described in section 3.3. Just to elucidate on this; PLV is essentially the square root of equation 3.23 with all the moduli set to 1.

3.2 Time-Frequency Transform

EEG signal analysis provides the advantage of high time resolution and thus it can deduce information related to both local and widespread neuronal activations in short time periods, as well as their time evolution. FFT basic idea is the decomposition of the signal into complex sinusoids that extend through the whole time domain. While, it reveals significant frequency information, there is no information concerning the time evolution of those frequencies. Stationarity is another prerequisite which is not satisfied in practice.

Such limitations turn FFT to be inconvenient in identifying time-varying signal features, i.e., the chirp[†] signal. FFT is not able to identify the instantaneous frequency of such signal and it estimates its whole evolution as a broad frequency spectrum.

A more promising methodology is based on the time-varying spectral analysis that takes into account the non-stationary dynamics of the neuronal processes (Bianchi et al., 2000). The *short-time Fourier* (STFT) and the *wavelet transforms* are the most prevalent analysis frameworks of this class. The first approach uses a sliding time window, whereas the second one forms the projection of the signal onto several oscillatory kernel-based wavelets matching different frequency bands. Currently, such time-varying methods have been widely applied in *event-related potential* (ERP) data, where distinct waveforms are associated with an event related to some brain function (Bressler, 2002).

Under certain assumptions, both time-frequency transforms are in fact mathematically equivalent, since they both use windows that under certain conditions can provide the same results (Bruns, 2004). The reason why these approaches are often regarded as different relies in the way they are used and implemented. *Wavelet transform* (WT) is typically applied with the relative bandwidth ($\Delta f/f$) held constant, whereas the Fourier approach preserves the absolute bandwidth (Δf) constant. In other words, STFT uses an unchanged window length, which leads to the dilemma of resolution; a narrow window leads to poor frequency resolution, whereas a wide window leads to poor time resolution.

[†] A chirp signal is characterized by a well defined linearly increasing frequency.

Consequently, according to the Gabor time-frequency uncertainty principle[‡] (Feichtinger and Strohmer, 2002) one cannot accurately discriminate frequencies in small time intervals. However the WT can overcome the resolution problem by providing multiresolution analysis. The signal may be analyzed at different frequencies with different resolutions achieving good time resolution but poor frequency resolution at high frequencies and good frequency resolution but poor time resolution at low frequencies. Such a setting is suitable for short duration of higher frequency and longer duration of lower frequency components of the EEG bands.

A brief presentation of both transforms and an extension that takes into account statistical background signal properties will be described next.

3.2.1 Short time Fourier Transform (Gabor)
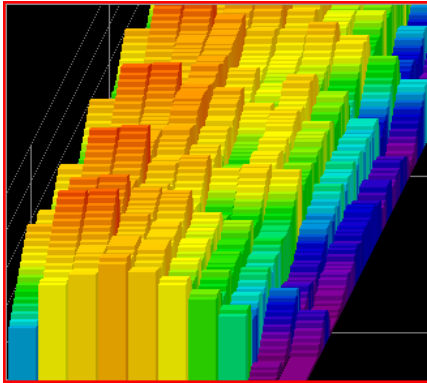
Figure 3.8: *A STFT being used to analyze a song across time. Frequency is located on the horizontal axis, with the lowest frequencies at left, and the highest at the right. The depth dimension is time, where each new bar consist a separate distinct transform. The height of each bar (augmented by color) is the amplitude of the frequencies included within that band.*

The short time Fourier transform (STFT) positions a window function $\psi(t)$ at t in the time axis, and calculates the Fourier transform of the windowed signal as:

$$G_{\psi}(f,t) = \int_{-\infty}^{\infty} x(t')\psi^{*}(t'-t)e^{-j2\pi ft'}dt' \quad (3.24)$$

where * denotes complex conjugation and $x(t)$ is the signal. When the window $\psi(t)$ is a Gaussian function (of a certain length and center t), the STFT is also called a Gabor transform. In the latter case the use of the Gaussian function $g_\alpha(t)$ emphasizes the signal values around t and suppresses them at distant times according to the length of the window, which may be defined by setting the related parameter α (Eq. 3.25).

[‡] The uncertainty principle will be discussed in the next section.
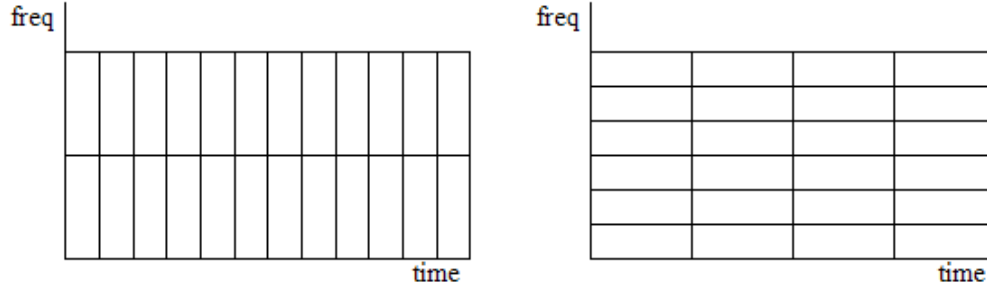
Figure 3.9: a) *A narrower window (compactly supported) gives good time resolution but poor frequency resolution.* **b)** *A wide window gives better frequency resolution but poor time resolution.*

$$g_a(t) = \left(\frac{\alpha}{\pi}\right)^{1/4} e^{\frac{-\alpha}{2}t^2} \tag{3.25}$$

The basis functions of this transform are actually generated by modulation and translation t of the window function. The fixed time window defines the time limits of the STFT and causes a fixed time-frequency resolution.

In correspondence to eq. 3.7 the spectrum may be defined as:

$$P(f,t) = \left|G_\psi(f,t)\right|^2 = G_\psi(f,t) \cdot G_\psi{}^*(f,t) \tag{3.26}$$

A time-frequency representation of the signal properties is possible by sliding the time window and plotting the energy as a function of both time and frequency (Fig. 3.8).

Uncertainty principle & resolution issues

However, one of the downfalls of the STFT is that it has a fixed resolution. The width of the windowing function relates to how the signal is represented; it determines whether there is good frequency resolution (frequency components close together can be separated) or good time resolution (the time at which frequencies change). A wide window gives better frequency resolution but poor time resolution. A narrower window (compactly supported) gives good time resolution but poor frequency resolution (Fig. 3.9). These are called narrowband and wideband transforms, respectively.

This property is related to the Gabor time-frequency uncertainty principle. It states that the product of the standard deviation in time spread Δt (time uncertainty) and frequency bandwidth Δf (frequency uncertainty) is limited. It is also known as

Heisenberg inequality and simply means that one can only trade time resolution for frequency resolution, or vice versa. Hence, for the transform pair:

$$\psi(t) \leftrightarrow \Psi(f): \quad \Delta t \Delta f \geq \frac{1}{4\pi} \qquad (3.27)$$

where Δf and Δt are the bandwidth and time spread (i.e. two pulses in time can be discriminated only if they are more than Δt apart) of $\psi(t)$, respectively, and

$$\Delta t^2 = \frac{\int t^2 |\psi(t)|^2 dt}{\int |\psi(t)|^2 dt}$$

$$\Delta f^2 = \frac{\int f^2 |\psi(f)|^2 df}{\int |\psi(f)|^2 df} \qquad (3.28)$$

When t increases, the window function translates in time. On the other hand, the increase in ψ causes a translation in frequency with a constant bandwidth (Daubechies, 1992; Sahambi et al., 1997). The boundary of the uncertainty principle (best simultaneous resolution of both) is reached with the Gaussian window function.

Finally, this time-frequency trade off is one of the reasons for the creation of the wavelet transform (or multiresolution analysis in general), which can give good time resolution for high-frequency events, and good frequency resolution for low-frequency events. The latter is considered to be the type of analysis best suited for many real signals, as well as for EEGs.

3.2.2 Continuous wavelet transform

Over the past decade the wavelet transform (WT) has been developed into an important tool for analysis of time series that contain non-stationary power at many different frequencies (such as the EEG signal), as well as a powerful feature extraction method (Daubechies, 1990; Kalayci and Ozdamar, 1995). It is capable of decomposing the signal onto a set of basic functions called wavelets.
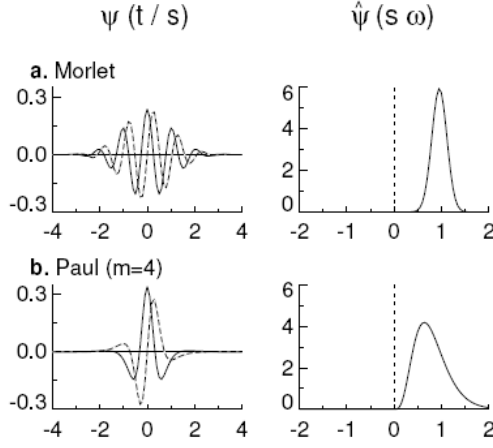
ψ (t / s) $\hat{\psi}$ (s ω)

a. Morlet

b. Paul (m=4)

Figure 3.10: *The plots on the left give the real part (solid) and imaginary part (dashed) for two different wavelet bases (namely Morlet and Paul) in the time domain. The plots on the right give the corresponding wavelets in the frequency domain. For plotting purposes, the scale was chosen to be s = 10dt. (a) Morlet, (b) Paul (m = 4).*

A set of wavelet functions is constructed from a single prototype wavelet, called the *mother wavelet*, by scaling (contraction, dilation) and shifts. By varying the so-called *wavelet scale* and translating along the time index, it is possible to identify the temporal evolution of various frequencies. There are several types of wavelet transforms, including the *discrete* (DWT) and the *continuous* (CWT), which imply the use of orthogonal basis or even a non-orthogonal wavelet function, respectively (Farge, 1992). CWT is preferred in case of a continuous signal, since the time and scale parameters can be continuous, too. In the WT the notion of scale s is introduced as an alternative to frequency, leading to the so-called time-scale representation domain.

The CWT of a discrete sequence x_n with time spacing δt and N data points ($n = 0\ldots N$-1) is defined as the convolution of x_n with consecutive scaled and translated versions of the wavelet function $\psi_0(\eta)$:

$$W_n(s) = \sum_{n'=0}^{N-1} x_n \psi^* \left[(n'-n)\delta t / s \right] \tag{3.29}$$

$$\psi_0(\eta) = \pi^{-1/4} e^{i\omega_0 \eta} e^{-\eta^2/2} \tag{3.30}$$

where η and ω_0 is a non-dimensional "time" parameter and frequency, respectively. ω_0 is usually taken to be 6 to satisfy the admissibility condition ($\int_{\mathbb{R}} \frac{|\psi(f)|^2}{|f|} df < \infty$) (Farge, 1992). $\psi_0(\eta)$ describes the most commonly used wavelet type for spectral analyses, i.e. the *normalized complex Morlet wavelet* (eq. 3.30). It consists of a plane wave modulated by a Gaussian (Fig. 3.10a). The wavelet function ψ_0 is a normalized version of ψ to have unit energy at each scale, so as each scale is directly comparable to each other. The normalization is:

$$\psi\left[(n'-n)\delta t/s\right] = \left(\delta t/s\right)^{1/2} \psi_0\left[(n'-n)\delta t/s\right] \qquad (3.31)$$

In principle a complex wavelet function is better suited for capturing oscillatory behavior because it captures both the amplitude and phase of the EEG signal. In correspondence to eq. 3.24 the CWT may be written as:

$$W_\psi(s,t) = \frac{1}{\sqrt{|s|}} \int_{-\infty}^{\infty} x(t')\psi^*\left(\frac{t'-t}{s}\right) dt' \qquad (3.32)$$

CWT suffers from high redundancy, if one varies the scale index arbitrarily, so it is more convenient to build up the scales in dyadic manner with time index remaining continuous (Burrus et al., 1998; Mallat, 1999). The scale set is given by:

$$s_j = s_0 2^{j\delta j}, \qquad j = 0 \ldots J \qquad (3.33)$$

where $s_0 = 2\delta t$ is the smallest scale chosen and δj specifies the width of the wavelet function. If $\delta j = 0.25$, means that there is a scale resolution of four sub-octaves per octave. The larger scale is determined by the value of J given by (eq. 3.34).

$$J = \delta j^{-1} \log_2(N\delta t/s_0) \qquad (3.34)$$

Finally, the *power spectrum* of the WT is defined by the square of coefficients in eq. 3.29 of the wavelet series as $\left|W_n(s)\right|^2$. By adopting the above settings a smooth wavelet power diagram is constructed as in Fig. 3.12b.

As noted beforehand, there is a relationship between each scale and an equivalent Fourier period, often known as *pseudofrequency* (Meyers et al., 1993). One way to map scale with frequency is by computing the center frequency F_c of

TABLE 3.I
FREQUENCY BANDS – SCALE SET MAPPING

Band	Frequency (Hz)	Scale
Delta (δ)	0.5-4	25, 26, 27, 28, 29
Theta (θ)	4-8	21, 22, 23, 24
Alpha1 (α1)	8-10	20
Alpha2 (α2)	10-13	18, 19
Beta (β)	13-30	14, 15, 16, 17
Gamma1 (γ1)	30-45	11, 12, 13
Gamma2 (γ2)	45-90	7, 8, 9, 10

the wavelet[§], which is the frequency maximizing the FFT of the wavelet modulus, when a purely periodic signal of frequency F_c is substituted in equation 3.29 (Abry, 1997). The pseudo-frequency F_s corresponding to the scale s is given by:

$$F_s = F_c / s \cdot \Delta \qquad (3.35)$$

where s is a scale and Δ is the sampling period. For the Morlet wavelet used throughout the thesis this relationship is $f = \dfrac{\omega_0 + \sqrt{2 + \omega_0^2}}{4\pi s}$, which in our case ($\omega_0=6$), this gives a value of $f=1/(1.03s)$. According to the former relationship the exemplar mapping tabulated in Table 3.I is possible. Note that s is calculated from eq. 3.33, by substituting $\delta j=0.25$ (four sub-octaves per octave), $J=7/\delta j$ (seven powers of two with four sub-octaves each) and $s_0 = 2\delta t$ (δt equals to a sampling period of 1/500 sec).

Resolution issues

As stated before, WT is typically applied with the relative bandwidth ($\Delta f/f$) held constant. According to the Heisenberg inequality, the time resolution becomes arbitrarily good at high frequencies, while the frequency resolution becomes arbitrarily good at low frequencies. For example, two very close short bursts can always be eventually separated by going up to higher analysis frequencies in order to increase time resolution. This kind of analysis performs best if the signal is composed of high-frequency components of short duration plus low-frequency

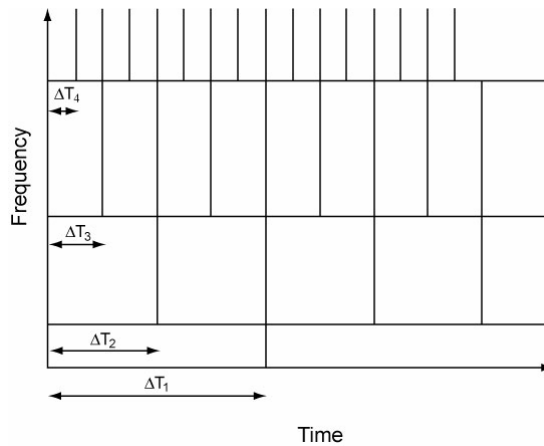**Figure 3.11:** *The time resolution becomes arbitrarily good at high frequencies, while the frequency becomes arbitrarily good at low frequencies.*

[§] The center frequency F_c is meant to be the leading dominant frequency of the wavelet.

components of long duration. This property is depicted in Figure 3.11.

Time-scale averaging – Global PS measures

Having defined the power spectrum we are able to define the *time-averaged power spectrum* $\bar{W}_t^2$ which is calculated by averaging the power spectrum $\left|W_n(s)\right|^2$ over time:

$$\bar{W}_n^2(s) = (1/N)\sum_{n=0}^{N-1}\left|W_n(s)\right|^2 \tag{3.36}$$

Further averaging in scale is also possible in order to uniquely describe each EEG frequency band. Thus, the *scale-averaged wavelet power* $\bar{W}_s^2$ is defined as the weighted sum of the wavelet power spectrum $\left|W_n(s)\right|^2$ over scales s_{j_1} to s_{j_2} within each frequency band:

$$\bar{W}_{s,n}^2 = (\delta j \delta t / C_\delta)\sum_{j=j_1}^{j_2}\left(\left|W_n(s_j)\right|^2 / s_j\right) \tag{3.37}$$

where C_δ is a constant, scale independent factor used for the exact reconstruction of a $\delta(.)$ function from its wavelet transform and for the Morlet wavelet it equals to 0.776 (Torrence and Compo, 1998).

3.2.3 Significant Wavelet Transform

Using CWT and Global PS measures one is able to extract features that describe brain activity in a certain channel or lobe subset. To further refine the features we propose to isolate only those time segments of the EEG signal where notable activity differences occur as compared to a background signal, i.e., from the control to an "active" task. The aim is to further map the EEG signal into a feature vector that best characterizes the EEG pattern of activity for the active task, in terms of significant temporal and spectral content. As we are interested in extracting information concerning ongoing EEG activity within various tasks, the temporal activity of EEG events is of interest. Notice that we focus on significant (bursty and/or sequential) activations and not on the evolution of brain operation during the task. Thus, we are mostly focused on the time-localized EEG activity

itself, without particular interest to the temporal relation of these events (as opposed to ERP analysis).

We may describe this approach as an attempt to crop up the most significantly different regions from control to the active task out of the bulk initial signal (may be either significant power increase or decrease while performing the requested task compared to the control background condition).

Significant PS measures

In fact, this thesis proposes a way to derive the so-called *significant PS activity* on significantly activated EEG time-segments, by testing for significance in the wavelet-time domain the "active" task over the control task (Significant PS).
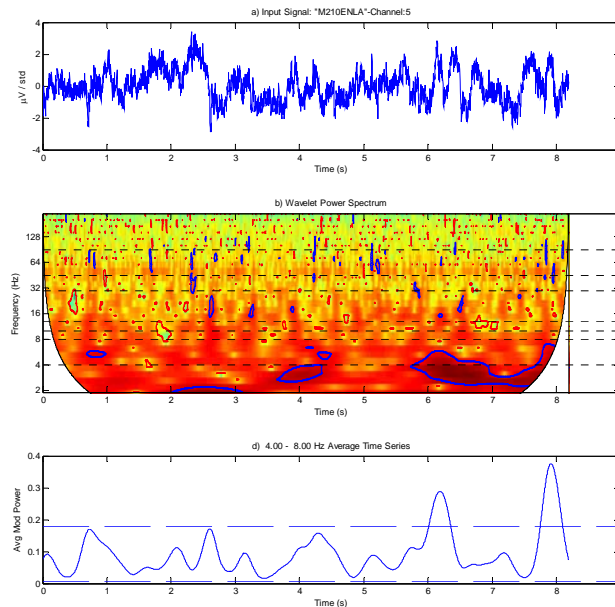
Figure 3.12: a*) A typical normalized EEG signal acquired from a single electrode.* **(b)** *The wavelet power spectrum presented as a color-coded picture. Mapped scales to frequencies are calibrated on the y-axis with the horizontal dashed lines indicating the different frequency bands. The significant regions over the time-scale transform are indicated by the closed contours. The outer elliptical region at the edges of the second graph indicates the cone of influence in which errors (edge effects) may be apparent due to the transformation of a finite-length series EEG signal (Torrence and Compo, 1998).* **(c)** *The scalogram of a selected averaged band (Theta 4-8 Hz). The significance levels are indicated by the horizontal dashed lines. PS values greater above the upper dashed-line indicate significant increase, whereas PS values below the lower dashed-line indicates significant decrease over the expected control power levels.*

The background spectrum or control-task spectra define the *mean time-averaged wavelet power spectrum*, which in the case of population based analyses could be the average PS over all subjects performing the control task (Sakkalis et al., 2006c), as:

$$\overline{W}(s) = (1/P)\sum_{p=1}^{P}\left|W_n^{\,p}(s)\right|^2 \qquad\qquad (3.38)$$

where p is the subject index and $W_n^{\,p}(s)$ is computed as in equation 3.29 for each subject. P is the total number of participants. It should be noted that all EEG signals are normalized to zero mean and identity variance. Further rescaling and comparisons are performed using each subject's actual signal variance, in order to include subject specific information.

Significant power increase on the active task is calculated using the 95% confidence level at each scale is calculated by multiplying the background control task spectrum (eq. 3.38) by the 95th percentile value for the chi-squared distributed variable χ^2 with two *degrees of freedom* (*DOF*) χ_2^2. This is justified because the wavelet power spectrum is derived from the Morlet wavelet in a complex product with the signal, so that both the squares of the real and imaginary parts of the result are being χ^2 distributed with one *DOF* each (Chatfield, 2004; Torrence and Compo, 1998). In a similar manner, significant power decrease is measured using the lower power limit of 5% confidence level at each scale, by multiplying the control task spectrum in Eq. (3.38) by the 5th percentile value for the chi-squared distributed variable χ_2^2.

In summary if the background spectrum for each scale index s is denoted as B_s the corresponding distribution for the local wavelet power spectrum is:

$$\frac{\left|W_n(s)^2\right|}{\sigma^2} \Rightarrow \frac{1}{2}B_s\chi_v^2(p) \qquad\qquad (3.39)$$

where v is equal to 1 or 2 for real or complex wavelets, and $\Rightarrow$ indicates an "is distributed as" relationship (Torrence and Compo, 1998); p in this case denotes the selected confidence level associated with probability p.

Averaging in time and scale, as mentioned in the previous paragraphs actually smoothes the power spectrum and increases the *DOF*. As a result, regions

of significant power are enhanced. For the time-averaged wavelet PS (eq. 3.36) one is actually averaging points that are correlated with correlation time appearing to be longer as the scale increases. Monte-Carlo results for the time-averaged wavelet spectra converge to:

$$DOF = 2\sqrt{1+\left(N\delta t/\gamma_s\right)^2} \qquad (3.40)$$

where γ_s is the decorrelation factor, empirically found to be *2.32* for the Morlet wavelet (Torrence and Compo, 1998). In accordance to the above, one can determine the *DOF* for the scale averaged power spectra (eq. 3.37) by:

$$DOF = \frac{2n_s}{\left(s_0 2^{0.5(j_1+j_2)\delta j}\right)\sum_{j=j_1}^{j_2}\left(1/s_j\right)}\sqrt{1+\left(N\delta t/\gamma_s\right)^2} \qquad (3.41)$$

where n_s is the number of scales that are averaged and j_1, j_2 are the initial and final scale index, respectively (Torrence and Compo, 1998).

Fig. 3.12 depicts one subject's initial normalized EEG signal (Fig. 3.12a) together with its WT (Fig. 3.12b). The significant regions over the time-scale transformed domain that differentiate the two tasks are indicated by the closed contours; red for significantly increased and blue for decreased activity. Fig. 3.12c illustrates another view of the scalogram focusing on a selected averaged band i.e., Beta 13-30 Hz. The significance levels in this case are indicated by horizontal dashed lines.

Having derived this significant information, we are now able to form the so-called *Significant Power Spectral* (Significant PS) features, which are obtained from the signal energy over those time- and band-localized regions where apparent significant differentiation is indicated (contours in Fig. 3.12b). For the computation of these features, equation 3.36 is adapted as:

$$\overline{W}_{st}^{\;2}(s) = (1/m)\sum_{m=m_i}^{m_{i+1}}\left|W_m(s)\right|^2, \qquad i=1\ldots I \qquad (3.42)$$

where m is the total number of time points delimited between the boundaries m_i and m_{i+1} of all significant regions I denoted by each contour in Fig. 3.12b and i is the index of each significant region.

46

3.2.4 Short time Fourier transform Coherence

The coherence measure, as described in section 3.1.4, assumes stationarity of the signals and is completely insensitive to the changes in coupling over time. Thus, a *short time Fourier transform* (STFT) approach is better suited and generally used to generate auto- and cross spectrograms, which are in turn utilized to produce the so called "coherogram". The coherogram is coherence calculated around a number of time instants. It results in a three dimensional matrix of time and frequency versus coherence.

However, while the assumption of wide sense stationarity is removed, stationarity is still required within each time interval for which coherence is calculated. In practice one should carefully decide on the optimal section length (over which each coherence estimate is measured), window length and overlapping (within each coherence estimate), which affects the resolution of the coupling measure. Hence, the STFT approach requires a priori information about the coupling range in time and frequency, in order to allocate the time-frequency resolution. The latter is constrained by the uncertainty principle: the wider the windows, the better the frequency resolution, at the expense of timing information, and vice versa. Lachaux et al. (2002) presents in detail this approach as applied to single-trial brain signals.

3.2.5 Wavelet Coherence

Coherence analysis, as noted before, ignores in a sense the temporal structure of the signal, thus cannot convey any information on dynamically varying or short-time dependence between the signals. To overcome this limitation and the implicit assumption that the signal is a process that remains stationary in time, *wavelet coherence* (WC) has been proposed. In contrast to the short time Fourier transform, which is just an extension of the regular Fourier transform, the wavelet transform is inherently a time frequency signal analysis. Continuous wavelet transform is preferred over the discrete counterpart in this case, as well. Since the coherence estimator is most strongly influenced by linearity in phase, the wavelet should be complex.

Here again, the conceptually simple wavelet basis used, is the Morlet wavelet, which is defined as in equation 3.30. This modulated Gaussian (Fig. 3.10) has a simple and very smooth spectrum that allows for easy interpretation of the results achieved. Initially the *cross wavelet transform* (XWT) of two time series x_n and y_n is defined as:

$$W_n^{XY}(s) = W_n^X(s)W_n^{Y*}(s) \tag{3.43}$$

where $W_n^X(s)$ and $W_n^Y(s)$ are the WT of signals X and Y, respectively and * denotes complex conjugation. Furthermore, the cross wavelet power may be defined as $\left|W_n^{XY}(s)\right|^2$. The complex argument $\arg(W_n^{XY}(s))$ may be explained as the local relative phase between the two time series in time frequency space.

If one closely follows equation 3.20, then the wavelet coherence R_n^2 of two signals comes naturally and may be defined as:

$$R_n^2(s) = \frac{\left|S(s^{-1}W_n^{XY}(s))\right|^2}{S\left(s^{-1}\left|W_n^X(s)\right|^2\right)\cdot S\left(s^{-1}\left|W_n^Y(s)\right|^2\right)} \tag{3.44}$$

where S is a smoothing operator in time S_t^{**} and scale S_s such as $S(W) = S_s(S_t(W_n(s)))$ which for the Morlet wavelet is given by a Gaussian and a boxcar filter of width equal to 0.6, (the scale-decorrelation length) respectively (Grinsted et al., 2004; Torrence and Compo, 1998):

$$S_t(W,s) = \left(W_n(s) * c_1^{-t^2/2s^2}\right) \tag{3.45}$$

$$S_s(W,n) = \left(W_n(s) * c_2 \prod (0.6s)\right) \tag{3.46}$$

where c_1 and c_2 are normalization constants and $\prod$ is the rectangle function. The squared WC time-frequency transformed scalogram is depicted in figure 3.13.

[**] The time smoothing uses a filter given by the absolute value of the wavelet function at each scale, normalized to have a total weight of unity. For the Morlet wavelet this is just a Gaussian $e^{-t^2/2s^2}$.
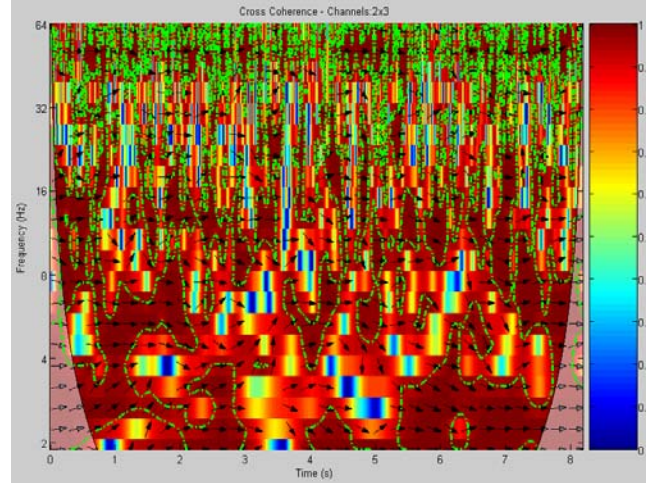
Figure 3.13: *The squared WC time-frequency transformed scalogram. The 5% significant regions over the time-scale transform are indicated by the contours (green dashed outline). The outer elliptical region at the edges of the second graph indicates the cone of influence in which errors (edge effects) may be apparent due to the transformation of a finite-length series EEG signal (Torrence and Compo, 1998). The relative phase relationship is shown as arrows (with in-phase pointing right, anti-phase pointing left).*

Note that the Schwarz inequality[††] forces the wavelet coherence to take on a value between 0 and 1. Moreover, the wavelet coherence is also a function of both time and (scale) frequency, measuring the coupling across both variables. The fact that the wavelet transform uses a shorter window for higher frequencies, and a longer one for lower frequencies makes this approach more suited to quantifying time varying coherence. This is accomplished via a frequency-adaptive tiling of the time frequency plane. In contrast, the constant size windows, and summation segments of the STFT coherence, force it to have the same resolution over all frequencies.

In summary, the XWT identifies regions with high common power and can possibly convey information about the phase relationship. For example, if two series are physically related we would expect a consistent or slowly varying phase lag. On the other hand, WTC can be thought of as the local correlation between two CWTs. In this way, locally phase locked behavior is uncovered. The more

---

[††] The Cauchy–Schwarz inequality is given using the notation of norm, as explained under norms on inner product spaces, as: $\left| \langle x, y \rangle \right| \leq \left\| x \right\| \left\| y \right\|$.

desirable features of the WTC come at the price of being slightly less localized in time frequency space.

3.2.6 Significant Wavelet Coherence

The confidence levels for the cross wavelet spectrum can be derived from the square root of the product of two chi-square distributions (Jenkins and Watts, 1968; Torrence and Compo, 1998). If the two series have theoretical Fourier spectra B_s^X and B_s^Y, then the cross wavelet distribution is:

$$\frac{W_n^X(s)W_n^{Y*}(s)}{\sigma_X \sigma_Y} \Rightarrow \frac{Z_v(p)}{v}\sqrt{B_s^X B_s^Y} \qquad (3.47)$$

where σ_X and σ_Y are the respective standard deviations and v equals to 1 ($Z_1(95\%)=2.182$) or 2 ($Z_2(95\%)=3.999$) for real and complex wavelets, respectively.

In order to apply these ideas on real EEG signals my proposal is to define population specific background spectra for each channel pair (X, Y) and scale index s. Here again the background spectra or control-task spectra are defined as the *mean time-averaged wavelet power spectrum* for each channel and scale ($\bar{W}^X(s)$ and $\bar{W}^Y(s)$), which in the case of population based analyses could be the average PS over all subjects performing the control task (Oikonomou et al., 2006; Sakkalis et al., 2006b), as defined in equation 3.38. Hence, by calculating both background spectrums ($\bar{W}^X(s)$ and $\bar{W}^Y(s)$) for a pair of channels and setting $Z_v(p)$ =$Z_2(p)$=3.999, since Morlet is complex mother wavelet, one is able to define the background spectrum using equation 3.47.

However, in order to gain confidence in causal relationships of the coherence findings one should estimate the statistical level of significance against a background spectrum using Monte Carlo methods (Grinsted et al., 2004). To adapt this idea to EEG signals I generate a large (order of 1000) ensemble of *mean time-averaged wavelet power spectrum* for each channel and scale ($\bar{W}^X(s)$ and $\bar{W}^Y(s)$)

using the bootstrap resampling procedure[‡‡]. Then, for each pair of channels and each scale the wavelet coherence is calculated. Finally, the probability distribution of the calculated coherence values is used to define the 95% confidence level. After that (similarly to the power estimation, as presented in section 3.2.3) one is able to indicate significant regions over the time-scale transform by contours (depicted in green dashed lines in Fig. 3.13).

Having derived this significant information, we are now able to form a single measure per scale which reflects the *Significant Coherence*. In complete analogy to equation 3.42 we are able to obtain the coherence values over those time- and band-localized regions where significant coherence is indicated by taking the coherence averages over certain bands and significant time points (contours in Fig. 3.13). An interesting study that successfully utilizes the latter approach in extracting the variability of neural interconnections in schizophrenia patients as compared to healthy ones is underlined in (Sakkalis et al., 2006b).

[‡‡] You actually randomize the time signatures of each coherence measure.

3.3 Phase Synchronization

Cognitive acts require the integration and constant interaction of widely distributed neuronal areas over the brain (Friston et al., 1997; Tononi and Edelman, 1998). Especially, gamma band is believed to reveal such large-scale oscillations that enter into precise phase-locking over a limited period of time, often referred as *phase-synchrony* phenomena (Lachaux et al., 1999). Another example is thought to be the genesis of epileptic phenomenon, where synchrony has long been considered as an important factor (Niedermeyer and Lopes da Silva, 1999). Hence, some method capable to obtain a statistical measure of the strength of phase synchronization in different areas of the brain has generated a lot of interest (Le Van Quyen et al., 2005; Mormann et al., 2000; Quian Quiroga et al., 2002).

One of the first experimental observations of synchronization was reported by Christiaan Huygens (1673) when two pendulum clocks hanging from the same beam got synchronized by attaining their maximal amplitudes at the same time but at opposite extremes thanks to the weakly coupling provided by the vibration of the beam in response to their movement. However, these pendulum clocks were actually harmonic linear oscillators. But, it is well known at present that even the phases of two coupled nonlinear (noisy or chaotic) oscillators may also synchronize even if their amplitudes remain uncorrelated (Pikovsky et al., 2001), as depicted in figure 3.14 (Rosenblum et al., 1996). The word *"synchronization"*
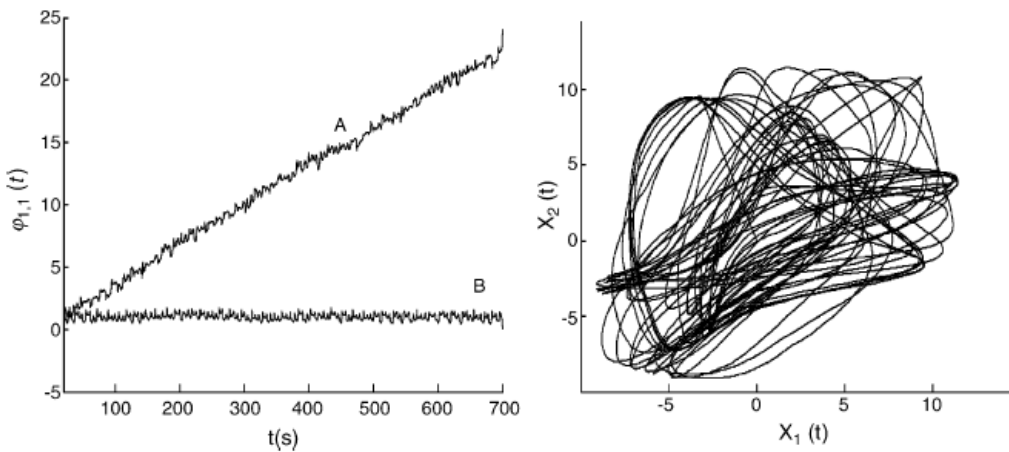

Figure 3.14: *Left: Absolute phase difference between the x variables of two typical nonlinear Rössler systems. (A) Uncoupled state: The phase difference grows and is unbounded. (B) Strong PS: The phase difference remains constant along time. Even in this latter case, the amplitudes remain completely uncorrelated (right) (Pereda et al., 2005; Rosenblum et al., 1996).*

arises from the Greek word *"σύνγχρονος"*, which consists of two parts: *συν-* (syn-=common) and *χρόνος* (chronos=time). Hence, this word is capable of describing any phenomena that "happen at the same time".

The calculation of *phase synchronization* (PS) and specifically instantaneous phase calculation can be based on both the *Hilbert* (HT) (Le Van Quyen et al., 2005; Quian Quiroga et al., 2002) or *wavelet transform* (WT) (Le Van Quyen et al., 2005). Actually both approaches are essentially equivalent (Quian Quiroga et al., 2002). The main difference is that the HT needs band-pass pre-filtering (Angelini et al., 2004; Bhattacharya and Petsche, 2001; Koskinen et al., 2001), whereas WT do not, since filtering is intrinsic in the WT. The most commonly used approach among the two utilizes the HT. Hence, HT is involved in getting the analytical signal $A(t)$:

$$A(t) = x(t) + i\tilde{x}(t) \tag{3.48}$$

where $\tilde{x}(t)$ is the HT of the signal $x(t)$, defined as:

$$\tilde{x}(t) = \frac{1}{\pi} P \int_{-\infty}^{\infty} \frac{x(\tau)}{t-\tau} d\tau \tag{3.49}$$

with P denoting the Cauchy principal value. The instantaneous phase is the "unfolded" angle of the analytic signal, which is given by:

$$\phi(t) = \arctan \frac{\tilde{x}(t)}{x(t)} \tag{3.50}$$

Synchronization of noisy signals is marked by an appearance of horizontal plateaus in the phase difference across time. The phase synchronization is defined as the locking of the phases of two oscillating systems x and y at any time t:

$$\phi_{n,m}(t) = \left| n\phi_x(t) - m\phi_y(t) \right| \le const \tag{3.51}$$

where $\phi_x(t)$ and $\phi_y(t)$ are the unwrapped phases of the signals associated to each system. In this case, as we aim to measure the synchronization between signals from within the same physiological system (i.e., the brain), we assume the phase locking ratio of $n{:}m$=1:1 as per Mormann et al. (2000).

Moreover, to quantify the strength of phase synchronization, we need to choose among a number of phase indices that have been used for intracranial and scalp EEG, such as Shannon entropy (Quian Quiroga et al., 2002) and phase

locking value (PLV) (Lachaux et al., 1999; Le Van Quyen et al., 2005; Mormann et al., 2000; Quian Quiroga et al., 2002). The latter, which is also termed as *mean phase coherence* or *synchrony factor* (Tallon-Baudry et al., 2001), has been found to be more robust than the alternatives especially when applied to low number of data samples (Quian Quiroga et al., 2002). Thus, it is an optimal choice when used for scalp EEG (Garcia Dominguez et al., 2005); thus was opted in our applications (Sakkalis et al., 2006a).

$$PLV = \left| \left\langle e^{i\phi(t)} \right\rangle \right| = \left| \frac{1}{N} \sum_{j=0}^{N-1} e^{i[\phi_x(j\Delta t) - \phi_y(j\Delta t)]} \right| \tag{3.52}$$

where $\langle \cdot \rangle$ denotes the average over time and N is the time series. This can be expanded according to Euler's formula as follows:

$$PLV = \sqrt{\left(\frac{1}{N} \sum_{j=0}^{N-1} \sin[\phi_x(j\Delta t) - \phi_y(j\Delta t)] \right)^2 + \left(\frac{1}{N} \sum_{j=0}^{N-1} \cos[\phi_x(j\Delta t) - \phi_y(j\Delta t)] \right)^2} \tag{3.53}$$

Hence, *PLV* is a normalized value which in simpler words measures how the relative phase is distributed over the unit circle. In case of perfect synchronization the relative phase will occupy a small portion of the circle and *PLV* will be close to a value of 1, whereas when *PLV* has a value close to 0 relative phases spread out over the entire unit circle and the mean phase coherence is low.

Important notes and applications

Many studies have attempted to study synchronization based on the traditionally formulated coherence. However, *PLV* is more suited mainly because of the following reasons (coherence limitations):

- *Stationarity*: Coherence may be applied only to stationary signals. In EEG the assumption of stationarity is rarely met or validated. *PLV* on the other hand does not require any stationarity.

- *Strictly phase specific measurements*: Coherence also increases with amplitude covariance and the relative importance of amplitude and phase covariance in the coherence value is not clearly justified. However, since phase-locking on its own is adequate to indicate brain lobe interactions, *PLV* is superior because it is only based on the phase and does not consider the amplitude of the signals.

A number of key works in the field demonstrate the applicability of phase synchronization method especially in combination with the gamma frequency band. Synchronization in the gamma band of the EEG is thought to reflect the appearing of an integrative mechanism bringing together widely distributed sets of neurons to effectively carry out different cognitive tasks (Bendat and Piersol, 1993; Roelfsema et al., 1997; Singer and Gray, 1995; Tallon-Baudry et al., 2001; Varela et al., 2001). Rodriguez et al. (1999) found increased PS with a latency of 260 ms after the stimulus in the frequency range between 35 and 45 Hz in a group of adult human subjects during visual perception of faces, as opposed to the no-perception situation. PS has been found also during non-visual perception but in a different frequency band (Trujillo et al., 2005). Another interesting result reported by Rodriguez et al. (1999) is the existence of a period of strong desynchronization with latency between 400 and 650 ms after the stimulus, which reflects the active uncoupling of the neural ensembles necessary to proceed from the visual perception cognitive state to the motor activation state (Rodriguez et al., 1999; Varela et al., 2001; Varela, 1995). Schnitzler and Gross (2005) have reviewed the latest findings on the concept of long-range neuronal synchronization and desynchronization in motor control and cognition, in normal as well as pathological conditions.

PS and gamma desynchronization reflects the successful formation of declarative memory, as demonstrated by the analysis of the relationship between human EEGs from the hippocampus and the rhinal cortex (Fell et al., 2001). Fell et al. (2003) concluded that, whereas rhinal-hippocampal gamma EEG PS may be closely related to actual memory processes, by enabling fast coupling and decoupling of the two structures, theta coherence might be associated with slowly modulated coupling related to an encoding state.

3.4 Nonlinear Synchronization & Interdependence analysis

In the early 1980s, the notion of synchronization was extended to the case of interacting chaotic oscillators (Afraimovich et al., 1986; Fujisaka and Yamada, 1983; Pecora and Carroll, 1990; Pikovsky, 1984). A completely different approach in analyzing the nonlinear dynamics of an EEG signal started some decades after the discovery of deterministic chaos (Lorenz, 1963).

3.4.1 Deterministic Chaos

Chaotic systems appear to have an apparently noisy behavior, which in fact is ruled by deterministic laws. In a purely deterministic system once its present state is fixed, the states of all future times are determined as well. Deterministic chaos is characterized by sensitivity to initial conditions, which means that trajectories starting from very close points may give results that diverge exponentially after some time. Hence, a first thought would sue for no synchronization between chaotic oscillators. However, extensive experimental investigations have proven its existence in a variety of application domains, i.e., electronics (Heagy et al., 1994; Parlitz et al., 1996; Pikovsky, 1985), laser dynamics (Fabiny et al., 1993; Roy and Thornburg, 1994), solid state physics (Peterman et al., 1995), plasma physics (Rosa Jr. et al., 2000), communication (Carroll and Pecora, 1993; Kocarev and Parlitz, 1995) and chaos control (Pyragas, 1992; Rulkov et al., 1995).

Non linear neural time series analysis was motivated by the fact that many crucial neural processes enclose nonlinear characteristics, i.e. the regulation of voltage-gated ion channels corresponds to a steep nonlinear step-function relating membrane potential to current flow. Neural firing is determined by a sigmoid-shaped relationship between soma membrane potential and mean firing rate (Freeman, 1975), whereas post-synaptic membrane potentials can be modeled by exponential functions (Robinson et al., 1997). Human EEG data was reported to exhibit chaotic dynamics in waking states (Accardo et al., 1997; Mayer-Kress and Layne, 1987; Pritchard and Duke, 1992) and in the alpha rhythm (Destexhe et al., 1988; Gallez and Babloyantz, 1991; Soong and Stuart, 1989). In addition, chaotic

descriptors like the *fractal dimension* of the EEG were found to change through the different sleep stages (Babloyantz et al., 1985; Fell et al., 1993; Roschke and Aldenhoff, 1991) and during the performance of various cognitive tasks (Gregson et al., 1990; Lutzenberger et al., 1992). However, even if neurons are highly nonlinear devices, further studies did not find any strong evidence of chaos in EEG (Pijn et al., 1991; Theiler et al., 1992; Theiler and Rapp, 1996). Hence, at present there is a wide consensus that EEG signal are not (low-dimensional) chaotic (Lehnertz et al., 2000). In spite of this, nonlinear measures in EEG are still used since there is evidence that even if no chaotic behavior is mathematically evident, the use of phase space representations (see next section) of the signals may reveal nonlinear structures hidden to standard linear approaches (Stam, 2005).

3.4.2 Basic concepts

Phase space

In a deterministic system it is important to establish a vector space, known as state space or phase space for the system such that specifying a point in this space specifies the state of the system, and vice versa. Even for nondeterministic systems the *state* concept is also powerful in the sense that a system maybe described by a set of states (possibly infinite) and a set of transition rules, which specify how a system proceeds from one state to the next. A phase space portrait in mechanics is extremely useful to represent the movement of a system, i.e. pendulum, by plotting the position vs. the velocity. Such a topological manifold (Fig. 3.15) represents the instantaneous state of a system and the sequence of such states over the time scale defines a curve in the phase space portrait known as trajectory.

Attractor

Typical trajectories will either ran away to infinity as time proceeds or stay in a bounded area forever. The behavior of the trajectory is strongly regulated by the initial conditions, while the bounded region to which all sufficiently close trajectories converges asymptotically is called the attractor (Schuster and Just, 2005). Geometrically, an attractor can be distinguished to:
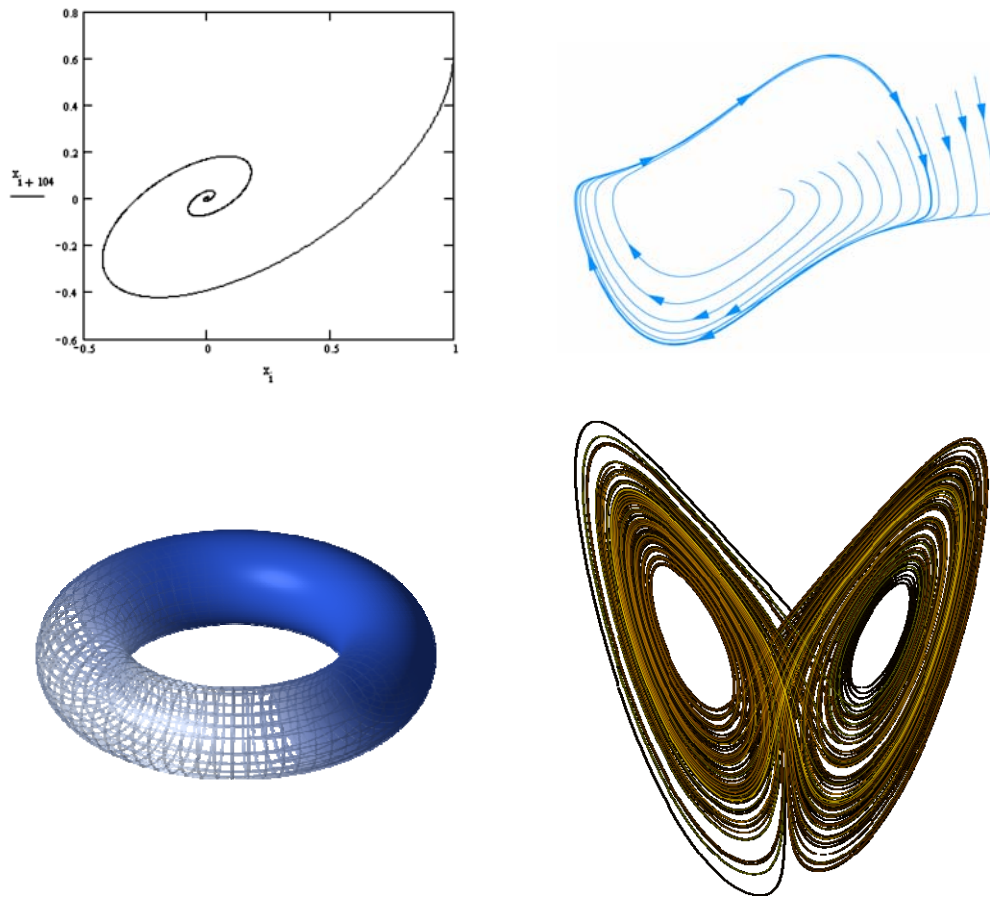
Figure 3.15: *a) Trajectories in phase space tend to a point at rest (top left), b) A limit cycle is a periodic orbit of the system that is isolated (Van de Pol phase portrait - top right), c) Toroidal surface is two dimensional where the two incommensurable frequencies correspond to the movement around and along the torus (bottom left), and d) Projection of trajectory of Lorenz system in phase space with "canonical" values of parameters r=28, σ = 10, b = 8/3. An attractor is informally described as* strange *if it has non-integer dimension or if the dynamics on the attractor are chaotic.*

- i) a ***fixed point*** (Fig. 3.15a): A fixed point is a point that a system evolves towards (tend to a point at rest), such as the final states of a falling pebble, a damped pendulum, or the water in a glass. It corresponds to a fixed point of the evolution function that is also attracting.

- ii) a ***limit cycle*** (Fig. 3.15b): A limit cycle is a periodic orbit of the system that is isolated. It is a closed (one dimensional) curve in the phase space representing a periodic motion. Examples include the swings of a pendulum clock, the tuning circuit of a radio, and the heartbeat while resting. In phase space of the ideal pendulum, near any point of a periodic orbit there is another point that belongs to a different periodic orbit.

- iii) a ***limit tori*** (Fig. 3.15c): There may be more than one frequency in the periodic trajectory of the system through the state of a limit cycle. If two of these frequencies form an irrational fraction (i.e. they are incommensurate), the trajectory will no longer be closed, and the limit cycle becomes a limit torus. Toroidal surface is two dimensional where the two incommensurable frequencies correspond to the movement around and along the torus. A time series corresponding to this attractor is a *quasiperiodic* series.

- iv) a ***strange attractor*** (Fig. 3.15d), which is a complicated set with fractal structure. Points that are initially close in the phase space become exponentially separated as the time proceeds. An attractor is informally described as *strange* if it has non-integer dimension or if the dynamics on the attractor are chaotic. The term was coined by David Ruelle (Eckman et al., 1987) and Floris Takens (Takens, 1981) to describe the attractor that resulted from a series of bifurcations of a system describing fluid flow. *Strange attractors* are often differentiable in a few directions and like a Cantor dust[§§] (Cantor, 1884) (and therefore not differentiable) in others. The Hénon attractor, Rössler attractor, and the Lorenz attractor are examples of strange attractors.

Delay reconstruction

Previous sections stress the importance of phase space for the study of the dynamic nature of a deterministic system. But in an experiment one acquires time series and not phase space portraits. We therefore need to convert the time series samples observations into state vectors. This problem of state space reconstruction is solved by the method of delays (Takens, 1980).

If we consider the time series to be x_n then a *delay reconstruction vector* in m dimensions is formed by the vectors:

$$\vec{x}_n = (x_n, x_{n-\tau}, \ldots, x_{n-(m-2)\tau}, x_{n-(m-1)\tau}) \qquad (3.54)$$

where $n=1,\ldots,N$ (N equals the signal length), m is the embedding dimension and τ denotes the *delay time* or *lag*. Note that for $\tau > 1$, only the time window covered by

---

[§§] A cantor dust is a multi-dimensional version of the Cantor set.

each vector is increased, while the number of vectors constructed from the scalar time series remains roughly the same. This is because we create a vector for every scalar observation, with $n > (m - 1)\tau$. Finding a good embedding is always a matter of great concern and is related to the proper selection of the embedding dimension m and the time lag τ. The right parameter selection depends on the underlying dynamics in the data and on the kind of the analysis intended. Generally, these parameters are optimized by either using statistics for their determination (Cao, 1997), or by starting the intended analysis right away and further increase the values of m and τ until the results are optimized. A precise knowledge of m is beneficial in order to exploit determinism with minimal computational cost and no redundancy. On the other hand a good estimate of the time lag τ is more difficult to obtain. If τ is too small compared to the internal time scales of the system under consideration, successive elements of the delay vectors are strongly correlated. On the contrary, if τ is very large, successive elements are already almost independent. However, the first zero of the autocorrelation function of the signal often yields a good trade-off between the former extreme cases.

Stationarity

The concept of stationarity has been extensively mentioned before. Technically speaking, stationarity means that the joint probability distribution function $f(x_i, x_{i+1})$ depends only on the absolute time difference $|t_i - t_{i+1}|$ and not the absolute values t_i and t_{i+1} (Jenkins and Watts, 1968). Chaotic methodologies require stationary signals, but the opposite is true for EEG signals. However, estimates of stationary epochs are possible and usually range from some seconds to a minute. In practice, whether a data segment is considered stationary or not depends on the problem being studied and the type of analysis to be performed.

Unfortunately, a large amount of data is required for the application of nonlinear analysis methods and pure stationarity is impossible to achieve. However, a more loose stationarity is sometimes possible, known as "weak stationarity" of order n; meaning that the moments up to order n are stable as time proceeds. There are some general concepts and procedures for checking stationarity (Blanco et al., 1995) and how it is related to chaos methodologies (Kantz and Schreiber, 2004; Schreiber, 1997). The most common visual
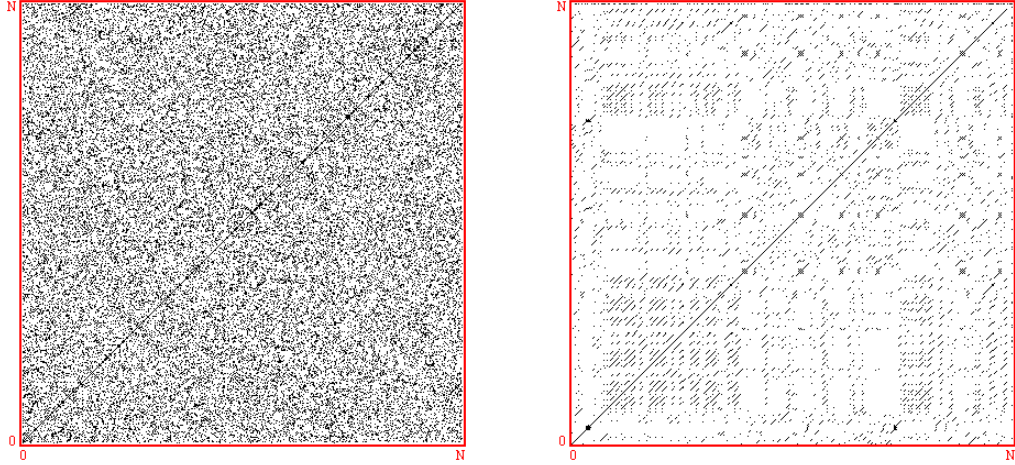
Figure 3.16: *The recurrence plot is diagonally symmetric since the distance of the ith embedded vector to the jth embedded vector is the same as the distance of the jth to the ith. Also, there is a diagonal line where $i = j$ (the distance between the vectors is 0 and hence always less than the threshold) **a)** If the recurrence plot contains points simply distributed in a homogeneous random pattern, it signifies that a random variable lacks of deterministic structures (non-stationary). For example, for a random series (white noise with mean = 0, standard deviation = 1, $\tau = 2$, $m = 1$, threshold $r = 0.05$). **b)** For a chaotic series on the right the diagram is more complicated. The set of brief periodic strips parallel to the main diagonal is the signature of determinism. The time series used is the logistic equation operating in the chaotic region, namely: $x = 4\ x_{n-1}\ (1 - x_{n-1})$ (Bourke, 1998).*

assessment topological method is given by the *recurrence plots* (Fig. 3.16) based on distance calculation in the phase space, as introduced by Eckman et al. (1987). Recurrence analysis is a graphical method designed to actually locate hidden recurring patterns and structural changes. For each pair of embedding vectors (*i,j*) a point is plotted if its Euclidean distance is less than a fixed value *r*. In practice if a plot consists of many scattered and isolated dots (Fig. 3.16a), these rather indicate coincidental closeness and hence a strong noise component. The diagonal structures (Fig. 3.16b) represent the deterministic dynamics and possible periodicity - stationarity. Such structures, however, might not be so clear (i.e., the recurrence plot could contain subtle patterns not easily ascertained by visual inspection). In this context, Zbilut and Webber (1992) propose the so called *recurrence quantification analysis* (RQA) to actually measure diagonal segments, in order to emphasize different features of the recurrence plot.

3.4.3 Main synchronization types

According to Pikovsky et al. (2001) synchronization may be understood as an "adjustment of rhythms of oscillating objects due to their weak interaction". An interaction can be realized for instance through a unidirectional or bidirectional coupling. The latter case resembles *mutual synchronization*; both systems adjust their rhythms to each other, whereas the former case refers to synchronization initiated by an external force, called a *driver*, and the driven system is called a *response*. The rhythm of the response is adjusted to the rhythms of the driver. As soon as the interaction strength gets strong (very large values of coupling) one cannot speak of two interacting systems but rather of one combined system.

The main difference of a synchronization phenomenon vs. resonance for example is the existence of own rhythms for each oscillating object, even when not driven at all. Thus, if the rhythm of a response is only induced by a driver (as it is the case with the resonance) then it is not possible to treat it as synchronization. Nevertheless, in such a large system as a human brain, with a total of 10^{14} to 10^{15} synaptic connections, one can still investigate the synchronization phenomenon between different brain regions.

In the literature three main types of synchronization are defined and distinguished, namely: *identical synchronization*, *phase synchronization*, and *generalized synchronization*[***]. Since, phase synchronization was discussed in the previous section we will now briefly discuss the other two.

Identical synchronization

The simplest form of synchronization occurs if the states of systems exactly coincide in time. This type of synchronization is usually referred to as identical synchronization. It can be observed if the coupling strength between identical systems is high enough (Pikovsky, 1984). Two systems X and Y with state vectors $\vec{x}(t)$ and $\vec{y}(t)$ are identically synchronized ($X \Leftrightarrow Y$) if:

$$\lim_{t \to \infty}[\vec{x}(t) - \vec{y}(t)] = 0 \tag{3.55}$$

[***] *Partial generalized synchronization* can also be defined when two responses are driven by the same driver but at the same time can still feedback the driver, as in Zheng Z. et al. (2002).

In order to achieve identical synchronization the parameters of the coupled systems must be identical. Otherwise, even if there is a slight mismatch the states of the systems may come close but still remain different.

Generalized synchronization

Obviously, identical synchronization is defined in a conceptual basis. In practice, even if the systems are not identical, weaker synchronization is possible when one system (response) is driven by the other (driver). This phenomenon is characterized as *generalized synchronization* (Pecora and Carroll, 1990; Rulkov et al., 1995) and is met if the state of the response $\vec{y}$ is completely defined by the state of the driver $\vec{x}$ ($X \rightarrow Y$). Hence, there exists a transformation function G such that:

$$\vec{y} = G(\vec{x}) \tag{3.56}$$

Strong or weak synchronization is realized in the case of smooth or non-smooth transformation function (Hunt et al., 1997; Pyragas, 1996). Rulkov et al. (1995) defined this function to be continuous one-to-one, meaning that not only the response orbit may be predicted by the driver's orbit, but also the neighborhoods in the driver space are mapped into the neighborhoods of the response space. The latter property is extensively utilized for experimental purposes.

Phase synchronization and generalized synchronization are not clearly related. Initially, the phase synchronization was found to appear before the generalized synchronization pops in (Parlitz et al., 1996) and as a result it was thought that generalized synchronization implies phase synchronization. However, later studies on several examples had shown the reverse order (Zheng and Hu, 2000). Another thought was to apply generalized synchronization methodologies to the phases of the systems rather than the systems themselves (Lee et al., 2003). The latter is often described as *generalized phase synchronization*.

Important notes and applications

A challenging application for measures of synchronization is the study of neuronal dynamics, since synchronization phenomena have been increasingly recognized as a key feature for establishing the communication between different regions of the brain (Fell et al., 2001; Varela et al., 2001; Varela, 1995).

Pathological cases such as Parkinson's disease or epilepsy have also profound by synchronization methods in revealing synchronization and desynchronization events. Especially, when epilepsy patients undergo pre-surgical diagnostics (Lopes da Silva, 1999), intracranial recordings are acquired in order to provide sufficient localization information for the epileptic focus in the brain. This motivated us to carry out a comprehensive comparison of different measures of synchronization, as presented in the next chapter of this thesis.

3.4.4 Nonlinear interdependence

In the experimental setting the instantaneous states of a neurophysiological process and system are not accessible. However, considering that scalp EEG is able to provide us a set of m channels equation 3.56 may be extended as:

$$y_j(t) = G(\vec{x}_s(t)) + \varepsilon_j(t), \quad j = 1, 2, \ldots, m \qquad (3.57)$$

where $\varepsilon_j(t)$ denotes extraneous noise. In the simplest case, the transformation function G may be a linear superposition of a subset (denoted as s) of the $\vec{x}_s$ (such as the oscillating membrane potentials), or may involve a more complex transformation. However, the primary aim of *interdependence* analysis is not to recover the underlying dynamics, but only to determine whether there is nonlinear interdependence between the observables y_j due to nonlinear interdependence between the local subsystems $\vec{x}_s$.

In brief, synchronization measures quantify how well the phase space trajectory can be predicted, knowing the trajectory of the other. Clearly, such an attempt makes sometimes easier or more difficult to predict the own dynamics of each system alone. Schiff et al. (1996) initially developed the first algorithm that exploited such considerations and demonstrated nonlinear interdependence in a spinal cord preparation. The idea was to first locate the k-nearest neighbors of each point along an orbit in one phase space and then project these points into the other state space. Next, the center of the resulting cloud of projected points is used to predict the state of that system. Finally, the Euclidean distance between the predicted and observed vectors yields an error, which is then normalized by

reference to a randomly chosen vector[†††]. The minimum error value of 0 or the maximum of 1 are taken when the systems experience maximum interdependence or when the systems are completely independent, respectively. Variants of this idea have been proposed in order to improve predictions (Feldmann and Bhattacharya, 2004; Terry and Breakspear, 2003).

Alternatively, another set of in principle more robust measures have been proposed, where instead of looking for predictions one quantifies how neighborhoods in one tractor maps into the other. In the following section this kind of algorithms will be discussed thoroughly.

Robust state-space generalized synchronization measure

Arnhold et al. (1999) similarly use k-nearest neighbors, but calculate the average radius of the cloudlike region formed by these neighbors. The ratio of the cloudlike radius to that of the cloud in the other system's reconstructed phase space defines a measure of system interdependence. This idea turned out to be a robust and reliable way of assessing the extent of GS (Grassberger, 1988; Sakkalis et al., 2006a; Schmitz, 2000).

First, we reconstruct delay vectors (Takens, 1980) out of our time series;

$$\boldsymbol{x}_n = (x_n, ..., x_{n-(m-1)\tau}) \text{ and } \boldsymbol{y}_n = (y_n, ..., y_{n-(m-1)\tau}) \tag{3.58}$$

where $n=1...N$, and m, τ are the embedding dimension and time lag, respectively. Let $r_{n,j}$ and $s_{n,j}$, $j=1,...,k$, denote the time indices of the k nearest neighbors of $\boldsymbol{x}_n$ and $\boldsymbol{y}_n$, respectively. For each $\boldsymbol{x}_n$ the mean squared Euclidean distance to its k neighbors is defined as:

$$R_n^{(k)}(X) = \frac{1}{k} \sum_{j=1}^{k} (\mathbf{x}_n - \mathbf{x}_{r_{n,j}})^2 \tag{3.59}$$

and the Y-conditioned squared mean Euclidean distance $R_n^{(k)}(X|Y)$ is defined by replacing the nearest neighbors by the equal time partners of the closest neighbors of $\boldsymbol{y}_n$ (Fig. 3.17):

$$R_n^{(k)}(X|Y) = \frac{1}{k} \sum_{j=1}^{k} (\mathbf{x}_n - \mathbf{x}_{s_{n,j}})^2 \tag{3.60}$$

[†††] The predicted error is, on average, no closer than random to the observed vector.

If the set of reconstructed vectors (point cloud x_n) has an average squared radius $R(X) = (1/N)\sum_{n=1}^{N} R_n^{(N-1)}(X)$, then $R_n^{(k)}(X|Y) \approx R_n^{(k)}(X) << R(X)$ if the systems are strongly correlated, while $R_n^{(k)}(X|Y) \approx R(X) >> R_n^{(k)}(X)$ if they are independent. Hence, an interdependence measure $S^{(k)}(X|Y)$ is defined as (Arnhold et al., 1999):

$$S^{(k)}(X|Y) = \frac{1}{N} \sum_{n=1}^{N} \frac{R_n^{(k)}(X)}{R_n^{(k)}(X|Y)} \qquad (3.61)$$
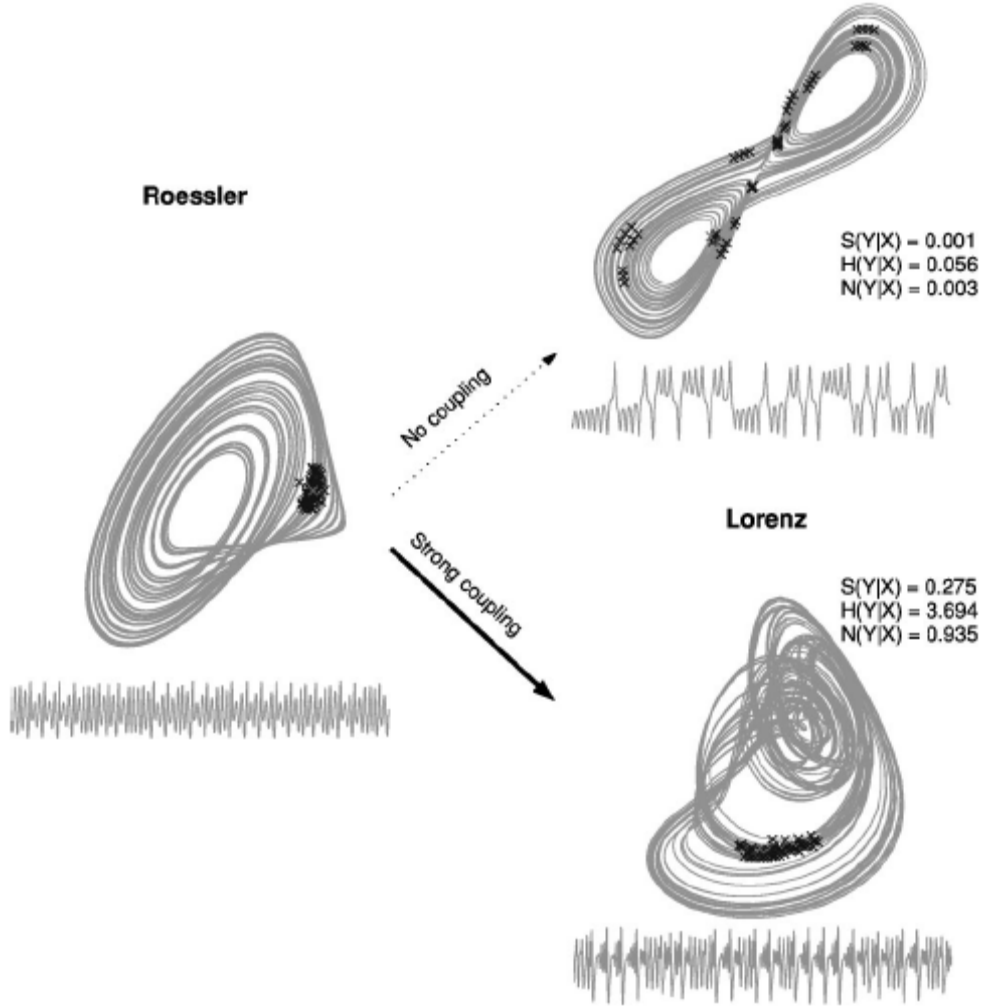
Figure 3.17: *Typically, a reliable nonlinear interdependence measure in the state space is based on the following idea: The size of the neighborhood in one of the systems (denoted as X) is compared with the size of its mapping in the other system (denoted as Y). In the case illustrated a Lorenz system is driven by a Rössler with zero and strong coupling (upper and lower case respectively). Given a cloud of points characterizing a neighborhood of a point in one of the attractors, say X, we see how this maps into the other system (Y). For synchronized systems (lower plot), the point cloud in Y will still be in a small neighborhood, whereas for independent systems (upper plot), the points in Y will most likely be spread over the attractor (upper plot) (Quian Quiroga et al., 2002).*

Figure 3.18: *Scheme representation of the basic idea of the synchronization method described by Arnhold et al. (1999).*

Since $R_n^{(k)}(X|Y) \geq R_n^{(k)}(X)$ by construction, it is clear that S ranges between 0 (indicating independence) and 1 (indicating maximum synchronization).

Following equation 3.61 another nonlinear interdependence measure $H^{(k)}(X|Y)$ is possible to be defined as (Arnhold et al., 1999; Quian Quiroga et al., 2000):

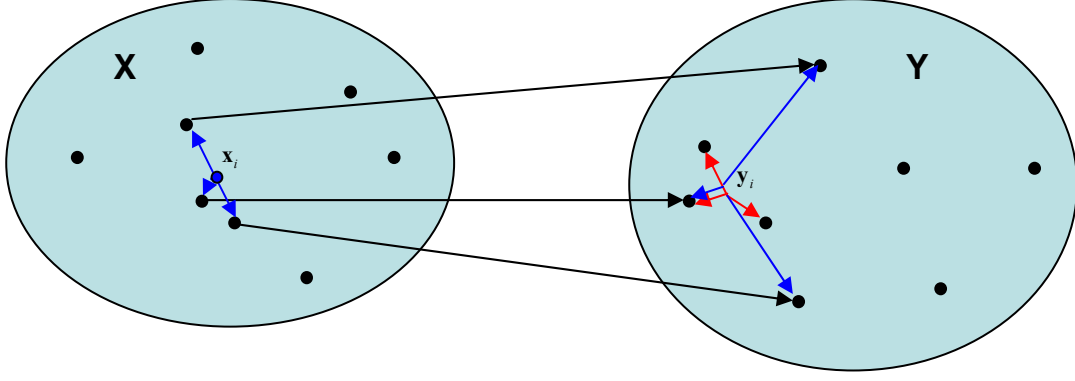$$H^{(k)}(X|Y) = \frac{1}{N} \sum_{n=1}^{N} \log \frac{R_n(X)}{R_n^{(k)}(X|Y)} \qquad (3.62)$$

This is zero if X and Y are completely independent, while it is positive if nearness in Y implies also nearness in X for equal time partners. It would be negative if close pairs in Y would correspond mainly to distant pairs in X. This measure if applied to coupled chaotic systems was found to be robust against noise (Quian Quiroga et al., 2000), but with the drawback that it is not normalized.

Hence, another normalized and more robust version of S maybe defined as in equation 2.63 (Quian Quiroga et al., 2002) and is the one actually used in our work (Sakkalis et al., 2006a):

$$N^{(k)}(X|Y) = \frac{1}{N} \sum_{n=1}^{N} \frac{R_n(X) - R_n^{(k)}(X|Y)}{R_n(X)} \qquad (3.63)$$

In fact, all three measures described are just different ways of normalizing the point cloud ratio of distances.

The opposite interdependences $S^{(k)}(Y|X)$, $H^{(k)}(Y|X)$ and $N^{(k)}(Y|X)$ are defined in complete analogy but in general are not equal to $S^{(k)}(X|Y)$, $H^{(k)}(X|Y)$ and

$N^{(k)}(X|Y)$, respectively. However, this asymmetry as opposed to other symmetrical nonlinear measures such as the phase synchronization may be advantageous, since it can give information about driver response relationships (Arnhold et al., 1999; Quian Quiroga et al., 2000; Schmitz, 2000). A schema representing the idea of this algorithm is represented in figure 3.18.

Synchronization likelihood (SL) measure

Stam & van Dijk (2002) proposed a method which, by normalizing to a reference neighborhood, yields a *synchronization likelihood* (SL) measure that is not biased by the dimension of the systems' phase spaces (which are not necessarily equal). It is closely related to the previous idea and represents a normalized version of mutual information.

Supposing that x_i, x_j and y_i, y_j be the time delay vectors, SL actually expresses the chance that if the distance between x_i and x_j is very small, the distance between the corresponding vectors y_i and y_j in the state space will also be very small. For this, we need a small critical distance ε_x, such that when the distance between x_i and x_j is smaller than ε_x, x will be considered to be in the same state at times i and j. ε_x is chosen such that the likelihood of two randomly chosen vectors from x (or y) will be closer than ε_x (or ε_y) equals a small fixed number p_{ref}. p_{ref} is the same for x and y, but ε_x need not be equal to ε_y. Now SL between x and y at time i is defined as follows:

$$SL_i = \frac{1}{N'} \sum_{\substack{j=1 \\ w_1 < |i-j| < w_2}}^{N'} \theta(\varepsilon_{y,i} - |\mathbf{y}_i - \mathbf{y}_j|)\theta(\varepsilon_{x,i} - |\mathbf{x}_i - \mathbf{x}_j|) \qquad (3.64)$$
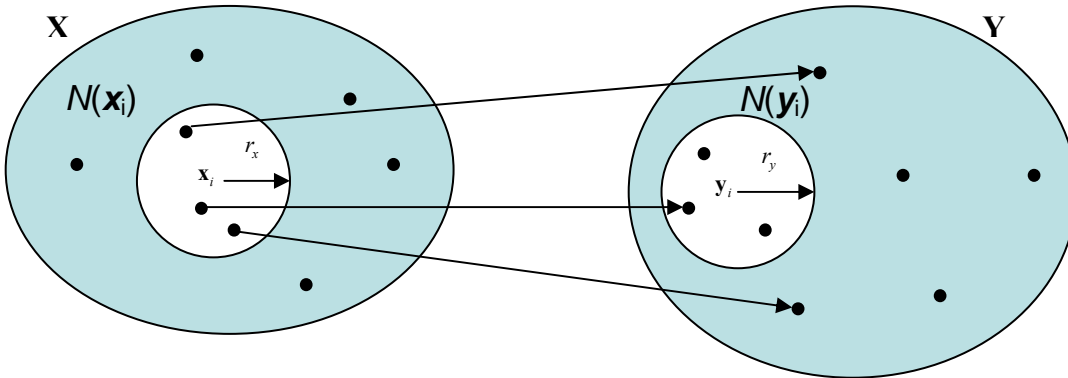

Figure 3.19: *Scheme representation of the basic idea of the synchronization method described by Stam et al. (2002).*

Here, $N'=2(w_2-w_1-1)P_{ref}$, $|\cdot|$ is the Euclidean distance and θ is the Heaviside step function, $\theta(x)=0$ if $x \leq 0$ and $\theta(x)=1$ otherwise. w_1 is the Theiler correction for autocorrelation effects and w_2 is a window that sharpens the time resolution of the synchronization measure and is chosen such that $w_1 << w_2 << N$ (Theiler, 1986). When no synchronization exists between x and y, SL_i will be equal to the likelihood that random vectors y_i and y_j are closer than ε_y; thus $SL_i = p_{ref}$. In the case of complete synchronization $SL_i=1$. Intermediate coupling is reflected by $p_{ref} < SL_i < 1$. Finally, SL is defined as the time average of the SL_i values. In this thesis's experiments (Sakkalis et al., 2006a), SL was computed with the following parameter settings: $\tau=10$; $m=10$; $w_1=100$ samples; $w_2=400$ samples; $p_{ref}=0.05$. There is no unique way to choose these parameters. However, the former choices have proven to be effective in distinguishing between experimental conditions in working memory tasks (Stam et al., 2002).

3.4.5 Surrogate time series analysis

So far we have discussed about linear and nonlinear methods for detecting synchronization in bivariate EEG signals. But how can one decide on whether a linear or nonlinear model better describes the data under study? A possible answer lies in the surrogate data testing method. In other words, to demonstrate that the synchronization methods addressed are sensitive in detecting nonlinear structures and thus reliable, *surrogate data testing* is used. The surrogate data method was introduced about a decade ago and the basic idea is to compute a nonlinear statistic Q for the original data under study, as well as for an ensemble of realizations of a linear stochastic process, which mimics "linear properties" of the studied data the surrogate data (Theiler et al., 1992). If the computed nonlinear statistic for the original dataset is significantly different from the values obtained from the surrogate set, one can infer that the data is not generated by a liner process; otherwise the null hypothesis, that a linear model fully explains the data is accepted.

The surrogating procedure preserves both the autocorrelation of the signals and their linear cross-correlation, but the nonlinear individual structure of the individual signals, as well as their nonlinear interdependence, if any, is destroyed.

This simply means that an ensemble of "surrogate data" has the same linear characteristics (power spectrum and coherence) as the experimental data, but is otherwise random.

In practice, a set of p time series (surrogates) is constructed, which share the same characteristics, but lack the property we want to test, the nonlinearity in our case. Using the newly created surrogates the same index $Q_{surrogates}$ is repeatedly calculated leading to $p+1$ estimations of this. This procedure allows testing of the null hypothesis H_0 that the original value of the statistic belongs to the distribution of the surrogates, hence H_0 is true. In other words, one has to determine whether H_0 can be rejected at the desired level of confidence. By estimating the mean and the standard deviation of the distribution of the statistic from the surrogates and then comparing them with its value from the original signals Z-$score$ is calculated:

$$Z = \frac{\left| Q - \overline{Q}_{surrogates} \right|}{\sigma_{surrogates}} \qquad (3.65)$$

Z-score reveals the number of standard deviations Q is away from the mean Qs of the surrogates. Assuming that Q is approximately normally distributed in the surrogates ensemble, H_0 is rejected at the $p<0.05$ significance level when $Z>1.96$ (one-sided test). If, in addition, no other possible causes of such a result can be accounted for, then it is reasonable to conclude that the tested measure accounts for any nonlinear phenomena.

However, it should be noted that, although the above surrogating procedure preserves both the autocorrelation of the signals and their linear cross-correlation, the nonlinear individual structure of the individual signals, if any, is also destroyed. In other words, any nonlinearity not only between but also within the signals is not present in the surrogates. Therefore, these surrogates only test the hypothesis that the data are bivariate stochastic time series with an arbitrary degree of linear auto and cross-correlation (Andrzejak et al., 2003). Nevertheless, if the two signals studied do have any nonlinear structure, it is not possible to ascribe a rejection of the hypothesis that the interdependence is nonlinear due to the nonlinearity of the interdependence, because the nonlinearity of the individual signals may also play a role. Hence, the generation of surrogate data preserving all the individual structure but destroying only the nonlinear part of the interdependence is currently one of

the most challenging tasks in the field, and it is a subject of ongoing research (Andrzejak et al., 2003; Dolan, 2004).

Pure nonlinear interdependence can contribute to linear correlations, but cannot be detected by linear methods alone. It signifies the formation of macroscopic, dynamic neural cell assemblies and transient low-dimensional interactions between them. Nonlinear interdependence informs that the underlying dynamics are governed by nonlinear processes, or that they are linear but evolving in the vicinity of a non-linear instability and driving noise. Nonlinearities generate correlations that cannot be generated by stochastic processes, such as coupling between oscillations with different frequencies (Breakspear and Terry, 2002; Friston, 1997; Schanze and Eckhorn, 1997).

The most widely used method to obtain surrogate data is to randomize the phases of the signal in the Fourier domain (Pijn et al., 1991; Prichard and Theiler, 1994; Rombouts et al., 1995; Theiler et al., 1992). Recent advances such as employing iterative loops (Schreiber and Schmitz, 1996), simulated annealing (Schreiber, 1998) and others (Schreiber and Schmitz, 2000) are all aimed to improve the goodness of the fit between the linear properties of the experimental data and surrogate ensemble. Unforunately, as noted beforehand, no surrogate technique is perfect (Schreiber and Schmitz, 2000).

To conclude the whole nonlinearity section it should be stressed that even nonlinear techniques look promising one should be cautious in practice. Many findings may have been premature in that apparent nonlinear effects were in fact caused by limitations of the data such as the sample length (Ruelle, 1990). During the previous years there was a general notion that EEG is chaotic, but nowadays there is a wide consensus and it is certainly no longer generally accepted that the healthy EEG is a chaotic signal.

3.5 Discrimination through Power and Synchronization measures

Supposing for example that we have a number of power spectrum band-averaged activity feature vectors calculated for each EEG channel, subject and possible task, we end up with a grand total of feature vectors. One way to focus only on those features (channels or brain lobes) that have the most prominent functional impact on different cognitive tasks or pathological cases; to actually select the optimum subset, given the initial large number of features, is to evaluate the recognition rate of all possible feature combinations. This extensive search is obviously impractical and time consuming. In data mining and classification applications, feature selection and reduction of dimensionality in the feature space plays a crucial role in the effective design, by regularizing and restricting the solution space. It is of practical concern that a large number of features may actually degrade the performance of the classifier, if the number of training samples is limited in comparison to the number of features (Raudys and Pikelis, 1980). Thus, numerous workarounds have been proposed, such as neural network-based selectors (Setiono and Liu, 1997), the successful and simple mutual information method (Battiti, 1994), as well as numerous variations (Torkkola, 2003).

The following sections propose a statistical method for mining the most significant channels and lobes, resembling the way many clinical neurophysiological studies evaluate the brain activation patterns (Sakkalis et al., 2006c).

3.5.1 Statistical significance of channels

The most suitable statistical method to select the most significant channels out of the whole channel set depends upon the feature-vector (channel) properties and experimental design. The actual distribution of features plays the most important role, since it is the one to judge which statistical test is the most appropriate (Fig. 3.20). One obvious feature capable of describing channel activity is the acquired power per each band. Practically speaking, for every subject
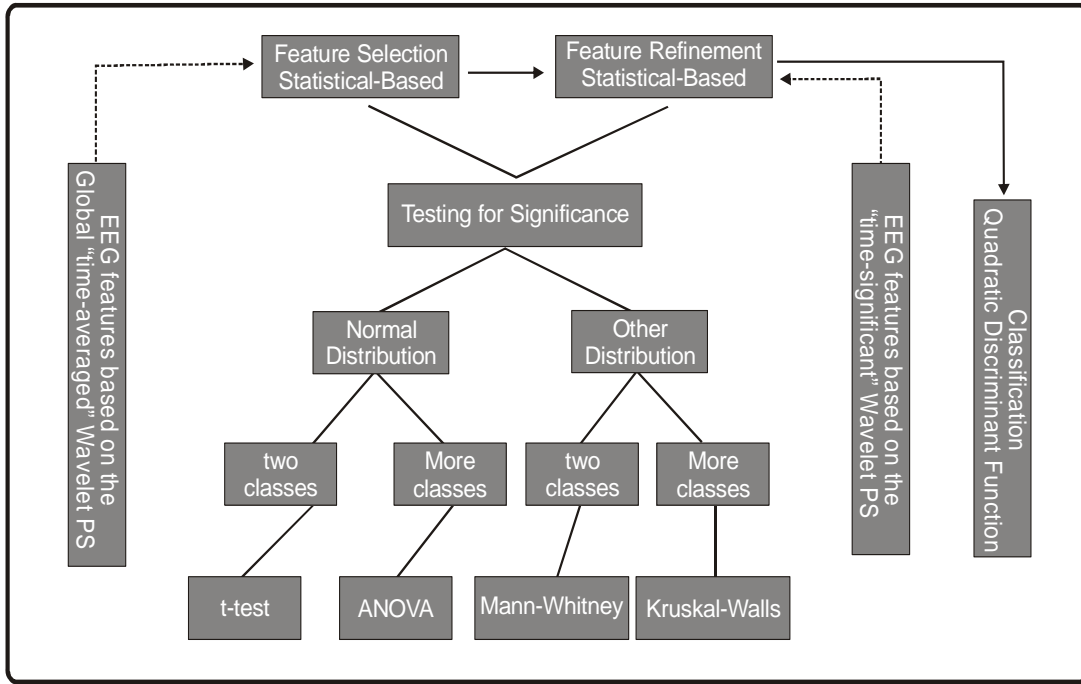
Figure 3.20: *The proposed methodology uses significance-based statistics in order to reduce the dimensionality of the classification problem and select the most salient and descriptive feature vectors. Different statistical decisions are possible according to the profile of the data under examination. If one is interested in discriminating two or more classes of normally distributed data, t-test or analysis of variance (ANOVA) tests are appropriate candidates, respectively. If the data is non-normally distributed, Mann-Whitney and Kruskal-Walls tests are the alternatives.*

participating in our study, the same power feature is extracted and then all the available features per subject, channel and frequency band are evaluated for their discrimination power.

Normality of the feature measures may be tested using the D'Agostino-Pearson test (Zar, 1999) or by visually inspecting the normal probability plot (normal Q-Q plot). For a realistic example we can assume that our clinical dataset meet the normality assumptions and two classes are being discriminated; then t-test or analysis of variance (ANOVA) is the ideal test to use (Fig. 3.20).

However, the ANOVA[‡‡‡] test is superior for complex analyses for two reasons, the first being its ability to combine complex data into one statistical procedure (more than two groups may be compared). The second benefit over a simple t-test is the ANOVA's ability to determine interaction effects. One of the

---

[‡‡‡] To be more consistent, one should not only consider the basic univariate ANOVA, but also repeated–measures and multivariate ANOVA (MANOVA) designs, with appropriate corrections to address potential problems of inhomogeneity of variance across data cells.

main assumptions underlying ANOVA is that the groups being compared are independent of each other. Statistics are usually testing for significance at the level of 0.05.

Furthermore, for those bands where the significance criterion is fulfilled, follow-up post-hoc tests for each channel or lobe are performed to accentuate the best candidates to preserve as features. The latter actually resemble the most significant brain channels in terms of activity.

3.5.2 Statistical significance of lobes

Yet, as noted before, one is interested in reducing the feature number and the degrees of freedom in the parametric statistical analyses. This is achieved by averaging together data from adjacent electrode sites (assuming that entire cortical regions function in a similar manner) to form a predefined number of *scalp regions* or *lobes* over each hemisphere. For example in the case of a four lobe selection (per hemisphere) the averaged channels may be:

- Frontal Left (FL): FP1, F3, F7, FC3, FT7;

- Frontal Right (FR): FP2, F4, F8, FC4, FT8;

- Temporal Left (TL): FT7, T3, TP7;

- Temporal Right (TR): FT8, T4, TP8;

- Central Left (CL): FC3, C3, CP3;

- Central Right (CR) FC4, C4, CP4;

- Parietal Left (PL): P3, P7, O1;

- Parietal Right (PR): P4, P8, O2.

However, lobe averaging is possible whenever power features are calculated. In the case of interdependence measures, where synchronization between channel pairs is computed, lobe averaging is performed in a pairwise manner. An estimated picture of overall synchronization in a lobe (group of channels) can be obtained by averaging the synchronization indexes between every possible pair of channels included in each lobe. For example in the case of a five lobe selection (per hemisphere) scheme the averaged interdependencies may be:

- Frontal Left: FP1-F7, FP1-F3, F7-F3;

- Frontal Right: FP2-F8, FP2-F4, F8-F4;

- Temporal Left: FT7-T3, T3-TP7, FT7-TP7;

- Temporal Right: FT8-T4, T4-TP8, FT8-TP8;

- Frontal-Temporal[§§§] Left: FP1-F7, FP1-F3, F7-F3, FT7-T3, T3-TP7, FT7-TP7;

- Frontal-Temporal Right: FP2-F8, FP2-F4, F8-F4, FT8-T4, T4-TP8, FT8-TP8;

- Central-Parietal Left: C3-CP3, CP3-P3, P3-P7;

- Central-Parietal Right: C4-CP4, CP4-P4, P4-P8;

- Occipital-Parietal Left: O1-P3, O1-P7, P7-P3;

- Occipital-Parietal Right: O2-P4, O2-P8, P4-P8.

Obviously, this averaging approach aims to obtain overall indexes of lobe synchronization and is not capable to either give topographic details or to preserve much of the information present in the initial dataset. A more detailed yet compact way of visualizing the local structure of such interdependences is possible using graph theory as will be discussed in the next section.

[§§§] Frontal-Temporal lobe may be defined as the mean of Frontal and Temporal interdependence measures.

3.6 Graph Theory in EEG analysis

An alternative approach to the characterization of complex networks is the use of graph theory (Sporns et al., 2004; Sporns and Zwi, 2004; Strogatz, 2001). A graph is a basic representation of a network, which is essentially reduced to nodes (vertices) and connections (edges) as illustrated in Fig. 3.21. Both local and long distance functional connectivity in complex networks may alternatively evaluated using measures and visualizations derived from graph theory. Special interest in using graph theory to study neural networks has been in focus recently, since it offers a unique perspective of studying local and distributed brain interactions (Fingelkurts et al., 2005; Varela et al., 2001).

Using the interdependence methods and measures analyzed in the previous sections one is able to measure (in terms of 0 to 1) the coupling between different channels. If such interdependence measures are constructed for every possible channel pair a *coherence matrix* (CM) (i.e. 30x30, if 30 channels are used) with elements ranging from 0 to 1. Next, in order to obtain a graph from a CM we need to convert it into an NxN binary adjacency matrix, A. To achieve that we define a variable called threshold T, such that $T \in [0,1]$. The value $A(i,j)$ is either 1 or 0, indicating the presence or absence of an edge between nodes i and j, respectively. Namely, $A(i,j)=1$ if $C(i,j) \geq T$, otherwise $A(i,j)=0$. Thus we define a graph for each value of T, i.e., for the purposes of our work, we defined 1000 such graphs, one for every thousandth of T (Sakkalis et al., 2006b). After constructing A, one is able to compute various properties of the resulting graph. These include the average degree K, the clustering coefficient C and the average shortest path length L of our graph, which will be presented in the next section. Figure 3.22 illustrates an example graph that resembles the brain activity of healthy versus schizophrenic populations (Sakkalis et al., 2006b).

3.6.1 Basic Concepts

Brain and other networks are conveniently described as a graph $G = (V, E)$, where the set $V = v_1; v_2; \ldots; v_n$ of nodes represents electrodes, and the set E of edges represents links between electrodes. e_{ij} denotes an edge between nodes v_i
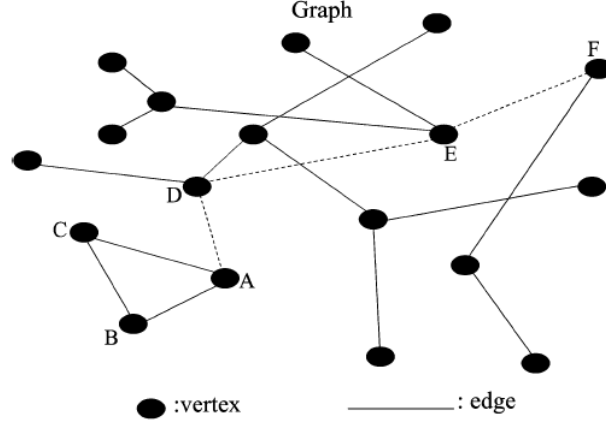
Figure 3.21: *A graph consists of elements or vertices, denoted by black dots. If two vertices are connected a line (called edge) is drawn between them. The size of a graph is equal to the total number of vertices, in this case N = 18. The degree K of a graph is the average number of edges per vertex. In a graph all vertices need to be connected. The distance between two vertices is expressed by the number of edges that have to be traveled to get from the first vertex to another. For instance, the shortest path from vertex A to vertex F has a length equal to three edges (path indicated by dotted lines). The characteristic path length L of a graph is the mean of all shortest paths connecting all pairs of vertices and is a measure of how well connected a graph is. The cluster coefficient C is a measure of local structure. For example, to compute the cluster coefficient for vertex A, we first determine the other vertices to which it is directly (with path length 1) connected. These neighbors are vertices B, C, and D. Then we determine how many edges exist in the set of neighbors. In this case, only B and C are connected. Next, we determine how many edges could have existed between the neighbors. In this case this is 3 (B-C, C-D, and B-D). The cluster coefficient of A is now the ratio of these 2 numbers: 1/3. In a similar way, the cluster coefficient can be determined for all vertices. This results in an average cluster coefficient C for the whole graph. C is a measure of the existence of local densely connected clusters within a network. Optimal networks are characterized by a high C and a low L; such networks are designated small-world networks (Watts and Strogatz, 1998).*

and v_j. We use n and m to denote the number of nodes and edges, respectively. Hereafter, we assume $v_i \in V$, where $1 \le i \le n$. We define the neighborhood for a node v_i as its immediately connected neighbors, namely $N_i = \{v_i\} : e_{ij} \in E$. The degree k_i of a node is the number of nodes in its neighborhood $|N_i|$. The mean degree of a graph is the average degree over all nodes, thus

$$K = \frac{\sum_{v_i \in V} k_i}{n} \tag{3.66}$$

The clustering coefficient C_i for a node v_i is the proportion of links between the nodes within its neighborhood divided by the number of links that could
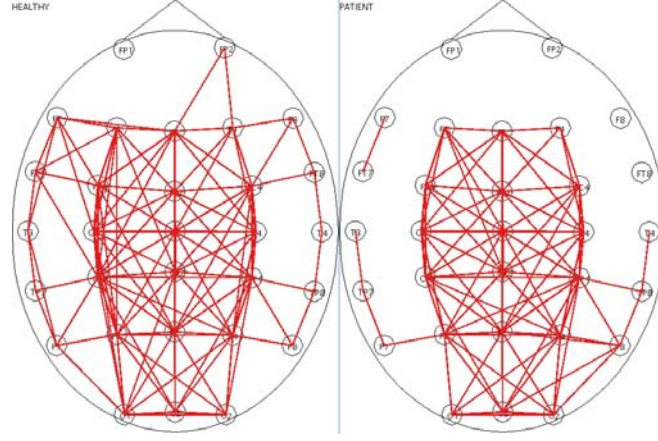
Figure 3.22: *A "healthy" network (left graph) (during a working memory task and selected threshold T) appears to have higher average degree K, clustering coefficient C and lower average shortest path length L values compared to the "schizophrenic" one (right graph). These disturbances are more prominent for the connections of the frontal lobes as well as the temporal lobes (Sakkalis et al., 2006b).*

possibly exist between them. For an undirected graph, if a node v_i has k_i neighbors, $\dfrac{k_i(k_i-1)}{2}$ edges could exist among the nodes within the neighborhood, thus

$$C_i = \frac{2\left|\{e_{jk}\}\right|}{k_i(k_i-1)} : v_j, v_k \in N_i \tag{3.67}$$

This measure is 1 if every neighbor connected to v_i is also connected to every other node within the neighborhood, and 0 if no node that is connected to v_i connects to any other node that is connected to v_i. The clustering coefficient for a graph is given by Watts and Strogatz (1998) as the average of the clustering coefficient for each node,

$$C = \frac{\sum_{i=1}^{n} C_i}{n} \tag{3.68}$$

and is a measure of the tendency of graph nodes to form local clusters.

We define a path from v_i to v_j as an alternating sequence of nodes and edges, beginning with v_i and ending with v_j, such that each edge connects its preceding with its succeeding node. The shortest path (distance or geodesic distance) d_{ij} between two nodes v_i and v_j is the minimum number of edges we need to traverse in order to go from node v_i to node v_j. By definition, $d_{ii} = 0$ for every v_i, and $d_{ij} = d_{ji}$ for v_i; v_j. There are a number of other measurements defined in terms of distance such as the eccentricity of a node and the radius and the diameter of a graph.

The eccentricity $\varepsilon(v)$ of a node v in a connected graph G is the maximum graph distance between v and any other node u of G

$$\varepsilon(v) = \left| \max\{d_{vu} : u \in V\} \right| \tag{3.69}$$

For a disconnected graph, all nodes are defined to have infinite eccentricity.

The radius and the diameter of a graph are the minimum and the maximum eccentricity of any node in the graph respectively. The diameter represents the greatest distance between any two nodes.

The average shortest path length

$$L = \frac{\sum_{i,j \in V, i \neq j} d_{ij}}{n(n-1)} \tag{3.70}$$

is the average shortest path (distance) connecting any two nodes of the graph and is a measure of the interconnectedness of the graph. Note that, in this thesis's application, the absence of a path between v_i and v_j implies $d_{ij} = 1000$.

3.6.2 Network Models

Measuring some basic properties of a complex network is the first step toward understanding its structure. The next step is to develop a mathematical model with a topology of similar (to the network) statistical properties, thereby obtaining a platform on which mathematical analysis is possible. This section refers to five of the most widely used network models, which are currently very well established and are most extensively used for modeling various real-world phenomena, possibly brain network, too. These are briefly mentioned as follows:

- ***Erdös-Rényi (random graph) model***: The earliest model of large networks was introduced by Solomonoff and Rapoport (1951) and independently Erdös and Rényi in late 50s and early 60s (Erdös and Rényi, 1959; Erdös and Rényi, 1960; Erdös and Rényi, 1961). Erdös and Rényi introduced the random graph model and initiated a large area of research, a good survey of which can be found in Bollobas's book (Bollobas, 1985).

- ***Small-World model:*** Many real world networks exhibit what is called the *small-world* property, i.e. most vertices can be reached from every other

through a small number of edges. Erdös and Rényi network have also the small-world property but a small average clustering coefficient. The most popular such model is developed by Watts and Strogatz (1998). This model is situated between an ordered finite lattice and a random graph presenting the small world property and high clustering coefficient.

- **Scale-Free model:** The *scale-free* network model, characterized by a small number of very highly connected nodes, has received a lot of attention in recent years. Barabási, Albert, and Jeong (Barabási and Albert, 1999; Barabási et al., 1999) showed that a heavy-tailed degree distribution emerges automatically from a stochastic growth model in which new nodes are added continuously and they preferentially attach to existing nodes with probability proportional to the degree of the target node. Many real world networks have power-law degree distributions, such as the Internet backbone (Faloutsos et al., 1999), metabolic reaction networks (Gray and Singer, 1989), and the World Wide Web (Broder et al., 2000).

- **Generalized Random model**: Since properties of the *random graph model* deviate from those of most real world networks, several new network models have recently been introduced. To capture the scale-free character of real-world networks, the random graph model was modified to allow for arbitrary degree distributions while keeping all other aspects of the random graph model. This model is called the generalized random graph model and finding properties of these graphs has been an active area of research (Molloy and Reed, 1995; Newman, 2002).

- **Geometric Random model:** A *geometric graph* $G(V;r)$ with radius r is a graph where points in a metric space correspond to nodes, and two nodes are adjacent if the distance between them is at most r. More details about geometric random graphs can be found in (Penrose, 2003).

Graph theory is for sure an emerging field in EEG analysis and coupling visualization. Recent articles illustrate that there may be evidence for small world networks in characterizing schizophrenia (Micheloyannis et al., 2006) and Alzheimer disease (Stam et al., 2006).

Bibliography

Abry P. Ondelettes et turbulence: Multirésolutions, algorithmes de décompositions, invariance d'échelle et signaux de pression. Paris: Diderot, Editeurs des sciences et des arts, 1997.

Accardo A, Affinito M, Carrozzi M, Bouquet F. Use of the fractal dimension for the analysis of EEG time series. Biol. Cybern. 1997; 77: 339-350.

Afraimovich VS, Verichev NN, Rabinovich MI. Stochastic synchronization of oscillations in dissipative systems. Radiophys. Quantum Electron. 1986; 29: 795.

Andrzejak RG, Kraskov A, Stogbauer H, Mormann F, Kreuz T. Bivariate surrogate techniques: necessity, strengths, and caveats. Phys. Rev. E 2003; 68: 066202.

Angelini L, de Tommaso M, Guido M, Hu K, Ivanov P, Marinazzo D, et al. Steady-state visual evoked potentials and phase synchronization in migraine patients. Phys Rev Lett 2004; 93: 038103.

Arnhold J, Lehnertz K, Grassberger P, Elger CE. A robust method for detecting interdependences: Application to intracranially recorded EEG. Physica D 1999; 134: 419.

Babloyantz A, Salazar J, Nicolis C. Evidence of chaotic dynamics of brain activity during the sleep cycle. Phys. Lett. A 1985; 111: 152-156.

Barabási AL, Albert R. Emergence of scaling in random networks. Science 1999; 286(5439): 509-512.

Barabási AL, Albert R, Jeong H. Mean-field theory for scale-free random networks. Physica A 1999; 272: 173-197.

Battiti R. Using mutual information for selecting features in supervised neural net learning. IEEE Trans. on Neural Networks 1994; 5: 537-550.

Bendat JS, Piersol AG. Engineering applications of correlation and spectral analysis. New York: J. Wiley, 1993.

Bhattacharya J, Petsche H. Musicians and the gamma band: a secret affair? Neuroreport 2001; 12: 371-4.

Bianchi AM, Mainardi LT, Cerutti S. Time-frequency analysis of biomedical signals. Trans. of the Institute of Measur. and Controls 2000; 22: 321-336.

Blanco S, Garcia H, Quian Quiroga R, Romanelli L, Rosso O. Stationarity of the EEG series. IEEE Eng Med Biol 1995; 14: 395-399.

Bollobas B. Random graphs. London ; Orlando: Academic Press, 1985.

Bookstein FL. Principal Warps: Thin-plate splines and the decomposition of deformations. IEEE Trans. On Patt. Anal. And Mach. Intell., (6), pp. 567-585 1989; 11: 567-585.

Bourke P. Recurrence plots. http://local.wasp.uwa.edu.au/~pbourke/fractals/recurrence/, 1998.

Brandt ME. Topographic mapping of brain electromagnetic signals: a review of current technology. Am J Physiol Imaging 1992; 7: 160-74.

Brazier MA. Spread of seizure discharges in epilepsy: anatomical and electrophysiological considerations. Exp Neurol 1972; 36: 263-72.

Brazier MA, Casby JU. Cross-correlation and autocorrelation studies of electroencephalographic potentials. Electroencephalogr Clin Neurophysiol Suppl 1952; 4: 201-11.

Breakspear M, Terry JR. Nonlinear interdependence in neural systems: motivation, theory, and relevance. Int J Neurosci 2002; 112: 1263-84.

Bressler SL. The Handbook of Brain Theory and Neural Networks. In: Arbib MA, editor. Cambridge MA: MIT Press, 2002: 412-415.

Broder A, Kumar R, Maghoul F, Raghavan P, Rajagopalan S, Stata R, et al. Graph structure of the web. Computer Networks 2000; 33: 309-320.

Bruns A. Fourier-, Hilbert- and wavelet-based signal analysis: are they really different approaches? J Neurosci Methods 2004; 137: 321-332.

Burrus CS, Gopinath RA, Guo H. Introduction to wavelets and wavelet transforms : a primer. Upper Saddle River, N.J.: Prentice Hall, 1998.

Cantor G. On the Power of Perfect Sets of Points (De la puissance des ensembles parfait de points). Acta Mathematica 4. English translation reprinted in Classics on Fractals, ed. Gerald A. Edgar, Addison-Wesley (1993) 1884: 381-392.

Cao L. Practical method for determining the minimum embedding dimension of a scalar time series. Physica D 1997; 110: 43-50.

Carroll TL, Pecora LM. Cascading synchronized chaotic systems. Physica D 1993; 67: 126.

Chatfield C. The analysis of time series : an introduction. Boca Raton, FL: Chapman & Hall/CRC, 2004.

Daubechies I. The Wavelet transform time-frequency localization and signal analysis. IEEE Trans. Inform. Theory 1990; 36: 961-1004.

Daubechies I. Ten lectures on wavelets. Philadelphia, Pa.: Society for Industrial and Applied Mathematics, 1992.

Destexhe A, Sepulchre J, Babloyantz A. A comparative study of the experimental quantification of deterministic chaos. Phys. Lett. A 1988; 132: 101-106.

Dolan K. Surrogate analysis of multichannel data with frequency dependant time lag. Fluct. Noise Lett. 2004; 4: L75-L81.

Duffy FH, Burchfiel JL, Lombroso CT. Brain electrical activity mapping (BEAM): a method for extending the clinical utility of EEG and evoked potential data. Ann Neurol 1979; 5: 309-21.

Dumermuth G, Molinari I. Relationships among signals: cross-spectral analysis of the EEG. In: Weitkunat R, editor. Digital Biosignal Processing. Vol 5. Amsterdam: Elsevier Science Publishers, 1991: 361-398.

Dumermuth G, Molinari L. Methods of analysis of brain electrical and magnetic signals. In: Gevins AS and Rémond A, editors. Handbook of electroencephalography and clinical neurophysiology ; rev. ser., v. 1. Vol I. NY, USA: Elsevier, 1987: 85-130.

Eckman J, Kamphorts S, Ruelle R. Recurrence plots of dynamical systems. Europhys Lett 1987; 4: 973-977.

Erdös P, Rényi A. On random graphs. Publicationes Mathematicae 1959; 6: 290-297.

Erdös P, Rényi A. On the evolution of random graphs. Publ. Math. Inst. Hung. Acad. Sci. 1960; 5: 17-61.

Erdös P, Rényi A. On the strength of connectedness of a random graph. Acta Mathematica Scientia Hungary 1961; 12: 261-267.

Fabiny L, Colet P, Roy R. Coherence and phase dynamics of spatially coupled solid-state lasers. Phys. Rev. A 1993; 47: 4287.

Faloutsos M, Faloutsos P, Faloutsos C. On power-law relationships of the internet topology. Computer Communications Review 1999; 29: 251-262.

Farge M. Wavelet transforms and their applications to turbulence. Annu. Rev. Fluid Mech. 1992; 24: 395-457.

Feichtinger HG, Strohmer T. Advances in Gabor Analysis. Boston: Birkhäuser, 2002.

Feldmann U, Bhattacharya J. Predictability improvement as an asymmetrical measure of interdependence in bivariate time series. Int. J. of Bifurcation and Chaos 2004; 14: 505-514.

Fell J, Klaver P, Elfadil H, Schaller C, Elger CE, Fernandez G. Rhinal-hippocampal theta coherence during declarative memory formation: interaction with gamma synchronization? Eur J Neurosci 2003; 17: 1082-8.

Fell J, Klaver P, Lehnertz K, Grunwald T, Schaller C, Elger CE, et al. Human memory formation is accompanied by rhinal-hippocampal coupling and decoupling. Nat Neurosci 2001; 4: 1259-64.

Fell J, Roschke J, Beckmann P. Deterministic chaos and the first positive Lyapunov exponent: a nonlinear analysis of the human electroencephalogram during sleep. Biol Cybern 1993; 69: 139-46.

Fingelkurts AA, Fingelkurts AA, Kahkonen S. Functional connectivity in the brain--is it an elusive concept? Neurosci Biobehav Rev 2005; 28: 827-36.

Fisch BJ, Fisch BJ, Spehlman R. Fisch and Spehlmann's EEG primer : basic principles of digital and analog EEG. Amsterdam ; New York: Elsevier, 1999.

Freeman WJ. Mass action in the nervous system : examination of the neurophysiological basis of adaptive behavior through the EEG. New York: Academic Press, 1975.

French CC, Beaumont JG. A critical review of EEG coherence studies of hemisphere function. Int J Psychophysiol 1984; 1: 241-54.

Friston K. Another neural code? NeuroImage 1997; 5: 213-220.

Friston KJ, Stephan KM, Frackowiak RSJ. Transient phase-locking and dynamic correlations: Are they the same thing? Human Brain Mapping 1997; 5: 48-57.

Fujisaka H, Yamada T. Stability theory of synchronized motion in coupled dynamical systems. Prog. Theor. Phys. 1983; 69: 32-47.

Gallez D, Babloyantz A. Predictability of human EEG: a dynamical approach. Biol. Cybern. 1991; 64: 381-391.

Garcia Dominguez L, Wennberg RA, Gaetz W, Cheyne D, Snead OCa, Perez Velazquez JL. Enhanced synchrony in epileptiform activity? Local versus distant phase synchronization in generalized seizures. J Neurosci 2005; 25: 8077-8084.

Gevins A, Brickett P, Costales B, Le J, Reutter B. Beyond topographic mapping: towards functional-anatomical imaging with 124-channel EEGs and 3-D MRIs. Brain Topogr 1990; 3: 53-64.

Gevins AS. Overview of computer analysis. In: Gevins AS and Rémond A, editors. Handbook of electroencephalography and clinical neurophysiology ; rev. ser., v. 1. Vol I. NY, USA: Elsevier, 1987: 31-83.

Grassberger P. Finite sample corrections to entropy and dimension estimates. Phys. Lett. A 1988; 128: 369.

Gray CM, Singer W. Stimulus-specific neuronal oscillations in orientation columns of cat visual cortex. Proc Natl Acad Sci U S A 1989; 86: 1698-702.

Gregson RA, Britton LA, Campbell EA, Gates GR. Comparisons of the nonlinear dynamics of electroencephalograms under various task loading conditions: a preliminary report. Biol Psychol 1990; 31: 173-91.

Grinsted A, Moore JC, Jevrejeva S. Application of the cross wavelet transform and wavelet coherence to geophysical time series. Nonlinear Processes in Geophysics 2004; 11: 561-566.

Guevara MA, Lorenzo I, Arce C, Ramos J, Corsi-Cabrera M. Inter- and intrahemispheric EEG correlation during sleep and wakefulness. Sleep 1995; 18: 257-65.

Heagy JF, Caroll TL, Pecora LM. Synchronous chaos in coupled oscillator systems. Phys. Rev. E 1994; 50: 1874.

Heideman MT, Johnson DH, Burrus CS. Gauss and the History of the Fast Fourier Transform. The IEEE ASSP Magazine I 1984: 14-21.

Hjorth B. An on-line transformation of EEG scalp potentials into orthogonal source derivations. Electroencephalogr Clin Neurophysiol 1975; 39: 526-30.

Hunt BR, Ott E, Yorke JA. Differentiable generalized synchronization of chaos. Phys. Rev. E 1997; 55: 4029-4034.

Huygens C. Horoloquium Oscilatorium. Paris, 1673.

Jenkins GM, Watts DG. Spectral Analysis and Its Applications. San Francisco, CA: Holden-Day, Inc., 1968.

John ER, Harmony T, Valdes-Sosa P. Methods of analysis of brain electrical and magnetic signals. In: Gevins AS and Rémond A, editors. Handbook of electroencephalography and clinical neurophysiology ; rev. ser., v. 1. Vol I. NY, USA: Elsevier, 1987: 497-540.

Kalayci T, Ozdamar O. Wavelet preprocessing for automated neural network detection of EEG spikes. IEEE Eng. Med. Biol Mag 1995; 14: 160-166.

Kantz H, Schreiber T. Nonlinear time series analysis. Cambridge, UK ; New York: Cambridge University Press, 2004.

Kocarev L, Parlitz U. General approach for chaotic synchronization with applications to communication. Phys. Rev. Lett. 1995; 74: 5028.

Koskinen M, Seppanen T, Tuukkanen J, Yli-Hankala A, Jantti V. Propofol anesthesia induces phase synchronization changes in EEG. Clin Neurophysiol 2001; 112: 386-92.

Lachaux JP, Lutz A, Rudrauf D, Cosmelli D, Le Van Quyen M, Martinerie J, et al. Estimating the time-course of coherence between single-trial brain signals: an introduction to wavelet coherence. Neurophysiol Clin 2002; 32: 157-74.

Lachaux JP, Rodriguez E, Martinerie J, Varela FJ. Measuring phase synchrony in brain signals. Hum Brain Mapp 1999; 8: 194-208.

Le Van Quyen M, Soss J, Navarro V, Robertson R, Chavez M, Baulac M, et al. Preictal state identification by synchronization changes in long-term intracranial EEG recordings. Clin Neurophysiol 2005; 116: 559-68.

Lee D-S, Kye W-H, Rim S, Kwon T-Y, Kim C-M. Generalized phase synchronization in unidirectionally coupled chaotic oscillators. Physical Review E 2003; 67: 045201.

Lehnertz K, Arnhold J, Grassberger P, Elger C. Chaos in Brain? World Scientific. Singapore, 2000.

Lopes da Silva FH. EEG Analysis: theory and practice. In: Niedermeyer E and Lopes da Silva FH, editors. Electroencephalography : basic principles, clinical applications, and related fields. Baltimore: Williams & Wilkins, 1999: 1097-1123.

Lorenz EN. Deterministic non-periodic flow. J. Atmos. Sci. 1963; 20: 130.

Lutzenberger W, Birbaumer N, Flor H, Rockstroh B, Elbert T. Dimensional analysis of the human EEG and intelligence. Neurosci Lett 1992; 143: 10-4.

Mallat SG. A wavelet tour of signal processing. San Diego, Calif.: Academic, 1999.

Mayer-Kress G, Layne S. Dimensionality of the human EEG. Annals New York Acad. Sci. 1987; 504: 62-87.

Meyers S, Kelly B, O'Brien J. An introduction to wavelet analysis in oceanography and meteorology: With application to the dispersion of Yanai waves. Mon. Wea. Rev. 1993; 121: 2858-2866.

Micheloyannis S, Pachou E, Stam CJ, Breakspear M, Bitsios P, Vourkas M, et al. Small-world networks and disturbed functional connectivity in schizophrenia. Schizophr Res 2006.

Molloy M, Reed B. A critical point of random graphs with a given degree sequence. Random Structures and Algorithms 1995; 6: 161-180.

Mormann F, Lehnertz K, David P, Elger CE. Mean phase coherence as a measure for phase synchronization and its application to the EEG of epilepsy patients. Phys. D 2000; 144: 358--369.

Newman MEJ. Random graphs as models of networks. In: Bornholdt S and Schuster HG, editors. Handbook of Graphs and Networks. Berlin: Wiley-VHC, 2002.

Niedermeyer E, Lopes da Silva FH. Electroencephalography : basic principles, clinical applications, and related fields. Baltimore: Williams & Wilkins, 1999.

Nunez PL. Quantitative states of neocortex. In: Nunez PL, editor. Neocortical Dynamics and Human EEG Rhythms. Oxford ; New York: Oxford University Press, 1995: 33-39.

Nuwer MR, Lehmann D, Lopes da Silva F, Matsuoka S, Sutherling W, Vibert JF. IFCN guidelines for topographic and frequency analysis of EEGs and EPs. Report of an IFCN committee. International Federation of Clinical Neurophysiology. Electroencephalogr Clin Neurophysiol 1994; 91: 1-5.

Oikonomou T, Sakkalis V, Tollis I, Micheloyannis S. Searching and Visualizing Brain Networks in Schizophrenia. Lecture Notes in Computer Science, Biological and Medical Data Analysis, 7th International Symposium, ISBMDA 2006, Thessaloniki, Greece, December 7-8 2006; 4345: 172-182.

Oppenheim AV, Willsky AS, Nawab SH. Signals & systems. Upper Saddle River, N.J.: Prentice Hall, 1997.

Parlitz U, Junge L, Lauterborn W, Kocarev L. Experimental observation of phase synchronization. Phys. Rev. E 1996; 54: 2115-2117.

Pecora LM, Carroll TL. Synchronization in chaotic systems. Phys. Rev. Lett. 1990; 64: 821.

Penrose M. Random geometric graphs. Oxford ; New York: Oxford University Press, 2003.

Pereda E, Quiroga RQ, Bhattacharya J. Nonlinear multivariate analysis of neurophysiological signals. Prog Neurobiol 2005; 77: 1-37.

Peterman DW, Ye M, Wigen PE. High frequency synchronization of chaos. Phys. Rev. Lett. 1995; 74: 1740.

Pijn J, Neerven J, Noest A, Silva FLd. Chaos or noise in EEG signals; dependence on state and brain site. Electroenceph. Clin. Neurophysiol. 1991; 79: 371-381.

Pikovsky A, Rosenblum M, Kurths J. Synchronization : a universal concept in nonlinear sciences. Cambridge: Cambridge University Press, 2001.

Pikovsky AS. On the interaction of strange attractors. Z. Phys. B: Condens Matter 1984; 55(2): 149.

Pikovsky AS. Phase synchronization of chaotic oscillations by a periodic external field. Sov. J. Commun. Technol. Electron. 1985; 30(10): 1970.

Prichard D, Theiler J. Generating surrogate data for time series with several simultaneously measured variables. Phys. Rev. Lett. 1994; 73: 951-954.

Pritchard W, Duke D. Dimensional analysis of no-task human EEG using the Grassberger-Procaccia method. Psychophysiol. 1992; 29: 182-192.

Proakis JG, Manolakis DG. Digital Signal Processing: Principles, Algorithms, and Applications. Englewood Cliffs, NJ: Prentice Hall, 1996.

Pyragas K. Continuous control of chaos by self-controlling feedback. Phys. Lett. A 1992; 170: 421.

Pyragas K. Weak and strong synchronization of chaos. Phys. Rev. E 1996; 54: 4508-4511.

Quian Quiroga R, Arnhold J, Grassberger P. Learning driver-response relationships from synchronization patterns. Physical Review E 2000; 61: 5142.

Quian Quiroga R, Kraskov A, Kreuz T, Grassberger P. Performance of different synchronization measures in real data: a case study on electroencephalographic signals. Phys Rev E Stat Nonlin Soft Matter Phys 2002; 65: 041903.

Raudys SJ, Pikelis V. On Dimensionality, Sample Size, Classification Error, and Complexity of Classification Algorithms in Pattern Recognition. IEEE Trans. Pattern Analysis and Machine Intelligence 1980; 2: 243-251.

Robinson P, Rennie C, Wright J. Propagation and stability of waves of electrical activity in the cerebral cortex. Phys. Rev. E 1997; 56: 826-840.

Rodriguez E, George N, Lachaux JP, Martinerie J, Renault B, Varela FJ. Perception's shadow: long-distance synchronization of human brain activity. Nature 1999; 397: 430-3.

Roelfsema PR, Engel AK, Konig P, Singer W. Visuomotor integration is associated with zero time-lag synchronization among cortical areas. Nature 1997; 385: 157-61.

Rombouts S, Keunen R, Stam C. Investigation of nonlinear structure in multichannel EEG. Physics Letters A 1995; 202: 352-358.

Rosa Jr. E, Pardo WB, Ticos CM, Walkenstein JA, Monti M. Phase synchronization of chaos in a plasma discharge tube. Int. J. Bifurc. Chaos 2000; 10: 2551.

Roschke J, Aldenhoff J. The dimensionality of human's electroencephalogram during sleep. Biol. Cybern. 1991; 64: 307-313.

Rosenblum MG, Pikovsky AS, Kurths J. Phase synchronization of chaotic oscillators. Physical Review Letters 1996; 76: 1804-1807.

Roy R, Thornburg KS. Experimental synchronization on chaotic lasers. Phys. Rev. Lett. 1994; 72: 2009.

Ruelle D. Deterministic chaos: The science and the fiction. Proc. of the Royal Society of London 1990; 427A: 241-248.

Rulkov NF, Sushchik MM, Tsimring LS, Abarbanel HDI. Generalized synchronization of chaos in directionally coupled chaotic systems. Phys. Rev. E 1995; 51(2): 980-994.

Sahambi JS, Tandon SN, Bhatt RKP. Using wavelet transform for ECG characterization. IEEE Eng. Med. Biol. 1997; 26: 77-83.

Sakkalis V, C.D.Giurcăneanu, Xanthopoulos P, Zervakis M, Yang Y, Micheloyannis S. Assessment of linear and non-linear EEG synchronization measures for evaluating mild epileptic signal patterns. Information Technology Applications in Biomedicine (ITAB 2006). Ioannina - Epirus, Greece, 2006a.

Sakkalis V, Oikonomou T, Pachou E, Tollis I, Micheloyannis S, Zervakis M. Time-significant Wavelet Coherence for the Evaluation of Schizophrenic Brain Activity using a Graph theory approach. Engineering in Medicine and Biology Society (EMBC 2006). New York, USA, 2006b.

Sakkalis V, Zervakis M, Micheloyannis S. Biopattern Initiative: towards the Development and Integration of Next-Generation Information Fusion Approaches. 26th IEEE-EMBS - Annual International Conference of the IEEE Engineering in Medicine and Biology Society. San Fransisco, CA, USA, 2004.

Sakkalis V, Zervakis M, Micheloyannis S. Significant EEG Features Involved in Mathematical Reasoning: Evidence from Wavelet Analysis. Brain Topography 2006c; 19: 53-60.

Schanze T, Eckhorn R. Phase correlation among rhythms present at different frequencies: spectral methods, application to microelectrode recordings from visual cortex and functional implications. Int. J. Psychophysiol. 1997; 26: 171-189.

Schiff SJ, So P, Chang T, Burke RE, Sauer T. Detecting dynamical interdependence and generalized synchrony through mutual prediction in a neural ensemble. Physical Review E 1996; 54: 6708.

Schmitz A. Measuring statistical dependence and coupling of subsystems. Physical Review E 2000; 62: 7508.

Schnitzler A, Gross J. Normal and pathological oscillatory communication in the brain. Nat Rev Neurosci 2005; 6: 285-96.

Schreiber T. Detecting and Analyzing Nonstationarity in a Time Series Using Nonlinear Cross Predictions. Phys. Rev. Lett. 1997; 78: 843-846.

Schreiber T. Constrained randomization of time series data. Phys. Rev. Lett. 1998; 80: 2105-2108.

Schreiber T, Schmitz A. Improved surrogate data for nonlinearity tests. Phys. Rev. Lett. 1996; 77: 635-638.

Schreiber T, Schmitz A. Surrogate time series. Physica, D 2000; 142: 346-382.

Schuster HG, Just W. Deterministic chaos : an introduction. Weinheim: Wiley-VCH, 2005.

Setiono R, Liu H. Neural-network feature selector. IEEE Trans. on Neural Networks 1997; 8: 654-662.

Shaw JC. An introduction to the coherence function and its use in EEG signal analysis. J Med Eng Technol 1981; 5: 279-88.

Shaw JC. Correlation and coherence analysis of the EEG: a selective tutorial review. Int J Psychophysiol 1984; 1: 255-66.

Singer W, Gray CM. Visual feature integration and the temporal correlation hypothesis. Annu Rev Neurosci 1995; 18: 555-86.

Solomono R, Rapoport A. Connectivity of random nets. Bulletin of Mathematical Biophysics 1951; 13: 107-117.

Soong A, Stuart C. Evidence of chaotic dynamics underlying the human alpharhythm electroencephalogram. Biol. Cybern. 1989; 42: 55-62.

Sporns O, Chialvo DR, Kaiser M, Hilgetag CC. Organization, development and function of complex brain networks. Trends Cogn Sci 2004; 8: 418-25.

Sporns O, Zwi JD. The small world of the cerebral cortex. Neuroinformatics 2004; 2: 145-62.

Stam CJ. Nonlinear dynamical analysis of EEG and MEG: review of an emerging field. Clin Neurophysiol 2005; 116: 2266-301.

Stam CJ, Jones BF, Nolte G, Breakspear M, Scheltens P. Small-World Networks and Functional Connectivity in Alzheimer's Disease. Cereb Cortex 2006.

Stam CJ, van Cappellen van Walsum AM, Micheloyannis S. Variability of EEG synchronization during a working memory task in healthy subjects. Int J Psychophysiol 2002; 46: 53-66.

Stam CJ, van Dijk BW. Synchronization likelihood: an unbiased measure of generalized synchronization in multivariate data sets. Physica D: Nonlinear Phenomena 2002; 163: 236-251.

Strogatz SH. Exploring complex networks. Nature 2001; 410: 268-76.

Takens F. Detecting strange attractors in turbulence. In: Rand D and Young L, editors. Dynamical Systems and Turbulence. Vol 898. Warwick: Springer-Verlag, 1980: 366-381.

Takens F. Detecting strange attractors in turbulence. Lecture Notes in Mathematics 1981: 366-381.

Tallon-Baudry C, Bertrand O, Fischer C. Oscillatory synchrony between human extrastriate areas during visual short-term memory maintenance. J Neurosci 2001; 21: RC177.

Terry J, Breakspear M. An improved algorithm for the detection of dynamical interdependence in bivariate time-series. Biol Cybern. 2003; 88: 129-136.

Thatcher RW, Krause PJ, Hrybyk M. Cortico-cortical associations and EEG coherence: a two-compartmental model. Electroencephalogr. Clin. Neurophysiol. 1986; 64: 123-143.

Theiler J. Spurious dimension from correlation algorithms applied to limited time-series data. Phys. Rev. A 1986; 34: 2427.

Theiler J, Eubank S, Longtin A, Galdrikian B, Farmer J. Testing for nonlinearity in time series: the method of surrogate data. Physica D 1992; 58: 77-94.

Theiler J, Rapp P. Re-examination of the evidence for low-dimensional, nonlinear structure in the human EEG. Electroenceph. Clin. Neurophysiol. 1996; 98: 213-222.

Tononi G, Edelman GM. Consciousness and complexity. Science 1998; 282: 1846-51.

Torkkola K. Feature extraction by non-parametric mutual information maximization. Journal of Machine Learning Research 2003; 3: 1415-1438.

Torrence C, Compo G. A practical Guide to Wavelet Analysis. Bull. Am. Meteorol. Soc. 1998; 79: 61-78.

Trujillo LT, Peterson MA, Kaszniak AW, Allen JJ. EEG phase synchrony differences across visual perception conditions may depend on recording and analysis methods. Clin Neurophysiol 2005; 116: 172-89.

Varela F, Lachaux JP, Rodriguez E, Martinerie J. The brainweb: phase synchronization and large-scale integration. Nat Rev Neurosci 2001; 2: 229-39.

Varela FJ. Resonant cell assemblies: a new approach to cognitive functions and neuronal synchrony. Biol Res 1995; 28: 81-95.

Watts DJ, Strogatz SH. Collective dynamics of 'small-world' networks. Nature 1998; 393: 440-2.

Weaver HJ. Theory of discrete and continuous Fourier analysis. New York: Wiley, 1989.

Welch PD. The Use of Fast Fourier Transform for the Estimation of Power Spectra: A Method Based on Time Averaging Over Short, Modified Periodograms. IEEE Trans. Audio Electroacoust. 1967; AU-15: 70-73.

Wolberg G. Digital image warping. Los Alamitos, Calif.: IEEE Computer Society Press, 1990.

Zar JH. Biostatistical analysis. Upper Saddle River, N.J.: Prentice Hall, 1999.

Zaveri HP, Williams WJ, Sackellares JC, Beydoun A, Duckrow RB, Spencer SS. Measuring the coherence of intracranial electroencephalograms. Clin. Neurophysiol. 1999; 110: 1717-1725.

Zbilut JP, Webber CL. Embeddings and Delays as Derived from Quantification of Recurrence Plots. Physics Letters A 1992; 171: 199-203.

Zheng Z, Hu G. Generalized synchronization versus phase synchronization. Phys. Rev. E 2000; 62: 7882-7885

Everything can be improved.

—. *[Clarence W. Barron](#)*

4

APPLICATION TO SCALP RECORDED EEG, RESULTS AND DISCUSSION

This chapter evaluates the performance of the algorithms and methods discussed in the previous chapter in scalp recorded EEGs and summarizes the testing procedures and results. In many cases validation of the proposed methodologies and comparisons with widely used alternative methods is performed in simulated signals and previous will. Suggestions for future work will be addressed. References to the actual published works are given, while the original published papers are included as appendices. Mainly, three different application domains are investigated:

- *Mathematical Reasoning*, which is thought to be capable of revealing the engagement of local and more spatially distributed cortical networks depending upon task specificity and complexity (Sakkalis et al., 2006d).

- *Schizophrenia*, where the hypothesis suggests that the disconnection on neuronal assemblies in patients could be visible by reduced "binding" -in

certain bands- in demanding tasks (i.e., working memory), which require considerable mental effort. The disconnection hypothesis and specifically working memory deficits are well established in the literature on schizophrenia (Sakkalis et al., 2006a).

- *Controlled epilepsy*, where children with seizures under drug control but without brain damage are evaluated during various cognitive functions (Sakkalis et al., 2006b; Sakkalis et al., 2006c).

4.1 Application to Mathematical Reasoning

Among the various frameworks in which EEG signal classification has been traditionally formulated, the most widely studied is employing Power Spectrum measures as functions of task complexity. Such measures may form signal features capable of characterizing and differentiating discrete tasks in terms of cognitive complexity. The objective of this work is to validate the use of wavelets in extracting such features in the time-scale domain and evaluate them in a mathematical reasoning test scenario, which is known as a well-accepted and informative paradigm in quantifying complex cognitive functions. The motivation for this work stems from the ability of time-frequency features to encapsulate significant power alteration of EEG in time, thus characterizing the brain response in terms of both spectral and temporal activation. Traditionally used Fourier methods are unable to detect possible temporal variations and since mathematical reasoning is a dynamic task, temporal information may prove to be of increased significance. The presented algorithmic scenario consists of three stages. Initially, the brain areas (lobes) of significant activation during the task are extracted using time-averaged wavelet power spectrum estimation. Then, a refinement step makes use of statistical significance-based criteria for comparing wavelet power spectra between the task and the rest condition. Finally, a classification procedure serves as the feature similarity evaluator to validate the cognitive task discrimination process. The results are in accordance with previous mathematical reasoning studies, showing reactivity mainly around frontal and central regions related to low and high EEG frequencies, respectively. Furthermore, the proposed method

achieved a higher classification rate against alternative traditional Fourier techniques applied on the same dataset.

4.1.1 Materials and Methods

Data Acquisition

Ongoing EEG activity was recorded from 15 right-handed volunteers (9 females and 6 males) of age range 21–26 years, at mean age 23 years, who were Medical School students in the University of Crete during performance of arithmetic tasks differing in nature and level of complexity. All participants signed an informed consent form after the nature of the procedures were explained to them, had normal or corrected-to-normal vision, and reported no history of verbal or non-verbal learning disability. Stimuli were presented on an LCD screen located in front of the participants at a distance of approximately 80 cm, subtending 2–3° of horizontal and 2–4° of vertical visual angle. The EEG signals reported here were recorded from 30 scalp locations using an electrode cap (FP1, FP2, F7, F3, FZ, F4, F8, FT7, FC3, FCZ, FC4, FT8, T3, C3, CZ, C4, T4, TP7, CP3, CPZ, CP4, TP8, P3, PZ, P4, PO7, PO8, O1, OZ and O2, referenced to linked earlobes). Vertical and horizontal eye movements and blinks were monitored through a bipolar montage from the supraorbital ridge and the lateral canthus. The signals were amplified using a set of Contact Precision Instrument amplifiers, filtered on-line with a band pass between 0.1 and 200 Hz, and digitized at 512 Hz. The datasets were visually inspected in order to identify and eliminate biogenic artifacts.

Experimental Setting and Test Description

Continuous EEG was recorded during performance of one arithmetic and one control task. The arithmetic task comprised of two-digit multiplication (e.g. 34×23, 49×32). Participants were allowed a minimum time of 8 s from the time the multiplication stimulus was presented on the screen until they indicated if they had calculated a result by raising their finger. Thus, in case a participant was able to respond in less than 8 s, then a more complex multiplication task was presented. This round was repeated until two full 8-s-long artifact-free segments (while the participant was in the thinking process) were acquired from each participant. Out of each segment, one 8-s-long epoch was used in the analysis, in accordance to

recent literature suggesting that an 8 s epoch is representative of the brain activity during each task performance (Simos et al., 2002). The first set of the epochs was used to train the classifier, while the second one formed the testing set. In this setup, each epoch is considered representative of brain activation during the specific cognitive task considered. Notice that we are interested in representing the overall activation rather than the evolution of activation during this task. Baseline EEG during the control task was recorded during a passive viewing condition when the participants simply focused at the centre of the computer screen on a small star. Such control targets have been extensively used in other published works (Micheloyannis et al., 2005; Simos et al., 2002). An 8-s-long artifact-free epoch was again selected for analysis of the control task from each participant. Thus, each epoch involves 4096 data points for each EEG channel.

Methodology Overview

Two different cognitive tasks are considered: the control and the more complex one that involves mathematical reasoning. The latter task requires considerable mental effort and is a well-known paradigm for extracting both the frequency bands and the location of brain activity, in terms of channel references or groups of channels (related to specific brain lobes) as an index of cerebral engagement in cognitive tasks. The testing hypothesis suggests that a complex mathematical reasoning task induces activity on certain brain lobes, reflected on the associated electrodes in a way significantly different compared to a control task. The WT constitutes the cornerstone of feature extraction and is used in analyzing task-related or control EEG signals by effectively capturing the power spectrum (PS) of each band and channel, particularly encoding the activation
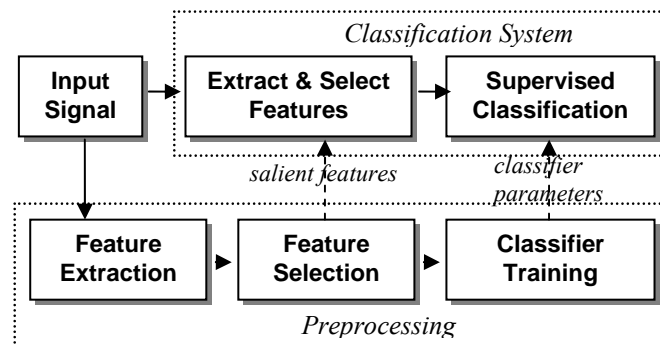

Figure 4.1: *Block diagram of a typical supervised classification system.*

93

differences between the mental states of interest. From the technical point of view, statistics is used to extract and select salient features (Fig. 4.1), testing for significance in both the time and scale domain of the signal. The feature selection steps apply test statistics on the extracted "time-averaged" PS features, but in addition our approach introduces an extra refinement step that makes further use of the time profile of the WT, as to derive and encode the temporally activated brain lobes and bands. Test statistics form appropriate means for the design of feature selection criteria strictly based on statistical significance, they are simple to implement and often perform better than other heuristic selection methods. To that respect, we base our selection on statistical tests that rely on statistical properties of the feature data under consideration. The final supervised classification step enhances the validity of any findings by elucidating and identifying neurophysiological pathways involved in higher cognitive tasks.

A generic overview of the proposed methodology emphasizing the various statistical approaches was illustrated in the previous section (Fig. 3.20). Different statistical decisions are possible according to the profile of the data under examination. The first choice is based on whether the data is normally distributed, whereas the second is based on the number of different groups under examination
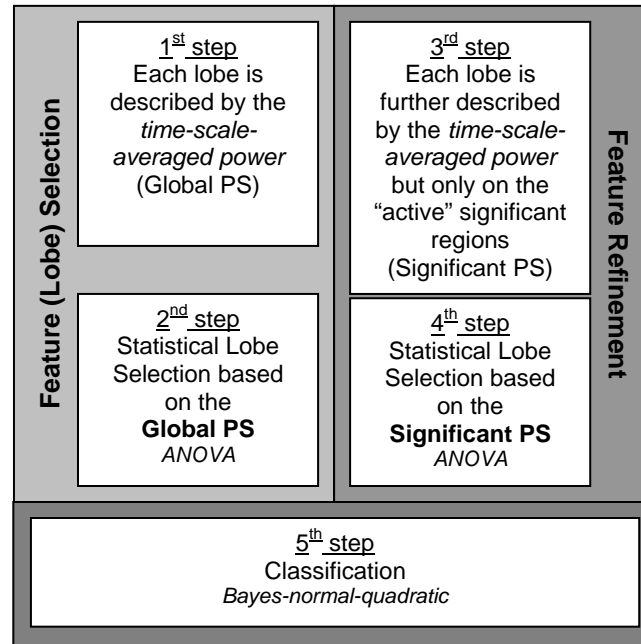

Figure 4.2: *The diagram of the proposed algorithmic transitions, heading towards (i) derivation of significant activity lobes and bands and (ii) an optimum classification rate achievement.*

i.e, whether two or more classes (tasks) are being tested. A more detailed view of feature selection and refinement blocks matching our data characteristics is presented in Fig. 4.2. The five steps involved, as well as their implementation issues are briefly described in the following sections. For a full review of the methods used the reader should refer the previous chapter.

Feature Extraction (1st step)

The continuous wavelet transform (CWT) using the Morlet wavelet was used for extracting the power spectrum of the EEG signals. In this study the power spectra is classified in six sequential frequency bands that are coarsely mapped to the scales tabulated in Table 4.I according to the relationship $f=1/(1.03s)$, where f and s denotes the frequency and scale, respectively.

TABLE 4.I
FREQUENCY BANDS – SCALE SET MAPPING

Band	Frequency (Hz)	Scale
Theta (θ)	4-8	21, 22, 23, 24
Alpha1 (α1)	8-10	20
Alpha2 (α2)	10-13	18, 19
Beta (β)	13-30	14, 15, 16, 17
Gamma1 (γ1)	30-45	11, 12, 13
Gamma2 (γ2)	45-90	7, 8, 9, 10

The first stage of our feature extraction method is based on capturing the time-averaged power spectrum for each electrode and scale. Further averaging in scale is performed, in order to map a single feature per frequency band of interest. Thus, the scale-averaged power spectrum is defined as the weighted sum of the wavelet power spectrum over the mapped scales within each frequency band, with scale correspondences defined in Table 4.I. Based on these definitions, the average power over time and frequency band is obtained.

Once the average PS for each of the six EEG bands is calculated for each EEG channel and task, we have a total of 180 (6x30) feature vectors per task (class), representing each participant (subject), which is actually the *time-scale averaged PS* (Global PS - Fig. 4.2 – 1st step) over the band of interest.

Feature Selection (2nd step)

In order to reduce the degrees of freedom in the parametric analyses of PS and since entire cortical regions are assumed to function in a similar manner, data from adjacent electrode sites are averaged together to form four right and four left brain activity lobes: Frontal left (FL): channels FP1, F3, F7, FC3, FT7; Frontal right (FR): FP2, F4, F8, FC4, FT8; Temporal left (TL): FT7, T3, TP7; Temporal right (TR): FT8, T4, TP8; Central left (CL): FC3, C3, CP3; Central right (CR) FC4, C4, CP4; and Parietal left (PL): P3, P7, O1; Parietal right (PR): P4, P8, O2. As a result of this averaging we end up with a total of 48 (6x8) feature vectors per task per subject. In this study the proposed statistical method for mining the most significant lobes (section 3.5), which actually resembles the way many clinical neurophysiological studies evaluate the brain activation patterns, is used.

Hence, the second step (Fig. 4.2 – 2nd step) of our design involves the statistical test selection of features, which depends upon the feature-vector properties and the experimental design. Normality of the log-transformed PS is tested using the D'Agostino-Pearson test (Zar, 1999). Since normality is met and two classes are being discriminated, t-test or analysis of variance (ANOVA) is the ideal test to use in our application. In our case of a related studies design (the same subjects perform each task), either matched pairs or repeated measures ANOVA are more appropriate. Hence, the best basis for the statistical analysis (best discrimination power) for our study is a repeated-measures ANOVA (Zar, 1999) with common measures factors being the two Tasks and the eight Lobes, testing for significance at the level of 0.05. Greenhouse-Geisser-corrected degrees of freedom are used on data that do not meet the sphericity assumption. For those bands where the significance criterion is fulfilled, follow-up post-hoc tests for each lobe are performed to accentuate the best candidates to preserve as features, which resemble the most significant brain lobes in terms of activity.

Feature Refinement (3rd and 4th steps)

The aforementioned steps derive a significant lobe subset, based only on task differentiation confidence intervals using *Global PS* measures (section 3.2.2). Either synchronization or de-synchronization may be detected compared to the control task. To further refine the features and optimize the classification process,

we propose to isolate only those time segments of the EEG signal where notable activity differences occur from the control to the arithmetic task as described in section 3.2.3. We focus on significantly activated EEG time-segments, by testing for significance in the wavelet-time domain the "active" task over the *mean time-averaged wavelet power spectrum* over all subjects performing the control task (Significant PS - Fig. 4.2 – 3rd step).

Figure 4.3 depicts one subject's initial normalized EEG signal (Fig. 4.3a) together with its WT (Fig. 4.3b). The significant regions over the time-scale transformed domain that differentiate the two tasks are indicated by the closed contours; red for significantly increased and blue for decreased activity. Fig. 4.3c illustrates another view of the scalogram focusing on a selected averaged band i.e., (Beta 13-30 Hz). The significance levels in this case are indicated by horizontal dashed lines.
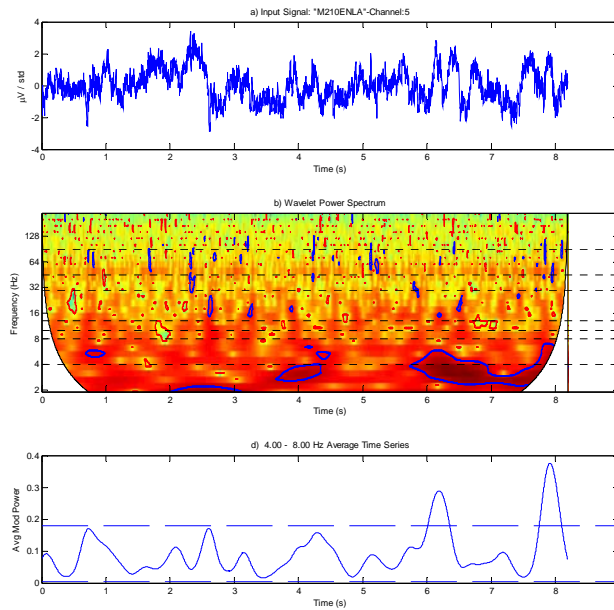
Figure 4.3: a*) A typical normalized EEG signal acquired from a single electrode.* **(b)** *The wavelet power spectrum presented as a color-coded picture. Mapped scales to frequencies are calibrated on the y-axis with the horizontal dashed lines indicating the different frequency bands. The significant regions over the time-scale transform are indicated by the closed contours. The outer elliptical region at the edges of the second graph indicates the cone of influence in which errors (edge effects) may be apparent due to the transformation of a finite-length series EEG signal (Torrence and Compo, 1998).* **(c)** *The scalogram of a selected averaged band (Theta 4-8 Hz). The significance levels are indicated by the horizontal dashed lines. PS values greater above the upper dashed-line indicate significant increase, whereas PS values below the lower dashed-line indicates significant decrease over the expected control power levels.*

Finally, the last step (Fig. 4.2 – 4th step) is actually a repetition of the statistical testing in the second step on the new feature set. ANOVA statistics (as described previously), are used to further sort out and select the best candidate features (significant energy per time, band and brain lobe), in terms of their task discriminating power.

Classification

Once the feature extraction and selection steps are accomplished, one can choose among a number of different classifier designs (Fig. 4.2 – 5th step). The concept remains the same; patterns that are similar should be assigned to the same class. In our study a probabilistic classifier with a parametric density estimator and a quadratic decision boundary is used, namely the *Bayes-normal-quadratic* classifier. This method, apart from its simplicity, assumes normal data distribution, which is justified by our data distribution, and performs fast and quite efficiently (Hastie et al., 2001). The classifier is trained using the initial 8-s data segments of each subject, whereas the second segment is used for testing.

4.1.2 Results

The proposed methodology is initially tested on simulated data, where there exist well defined spatiotemporal differences in frequency content between the target and control tasks, as discussed in the next section. After elucidating its benefits with the simulated data, the proposed approach is further applied on the actual experimental dataset.

Simulation Test

Two different tasks are simulated by two different groups of signals. The first group (control task) consists of ten simulated spatiotemporal signals, each one comprised of five channels. The idea is to reflect ten participants virtually registered with a 5-channel-EEG system, each. All the channels of the control task are randomly generated quasi-white noise signals, approximately 9-s-long (500 Hz sampling rate – 4608 samples). The second group (target task) comprises of three channels (channel 1, 3, 4) reflecting white noise and two channels (channel 2, 5) encoding frequency modulated signals mixed again with quasi-white noise.
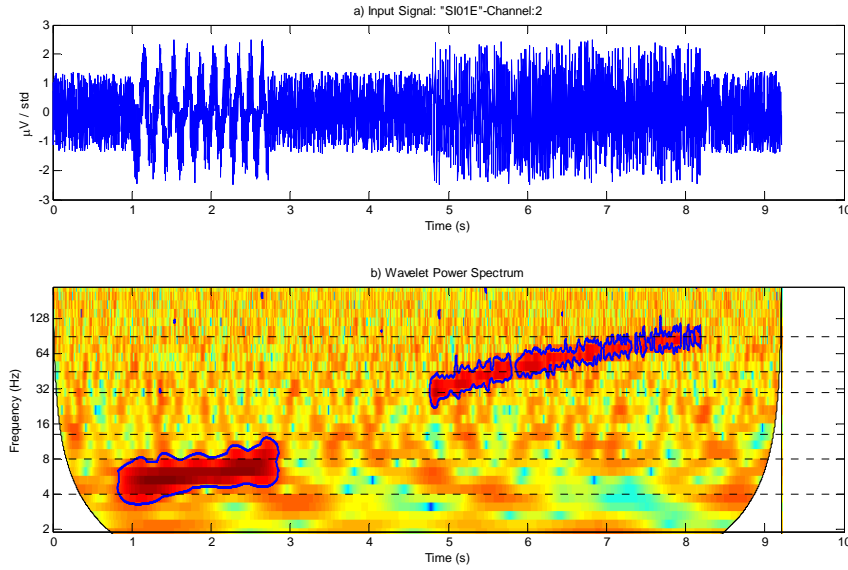
Figure 4.4: *a*) *The simulated Channel 2 consists of a time-varying (among different participants) theta linearly modulated signal (length ~ 2 s) occurring at a fixed latency and a gamma linearly modulated signal (length ~ 3 s) mixed with quasi-white noise. Quasi-white noise also covers the interval between the modulated signals. (**b**) The wavelet PS time-frequency representation picture. The significant regions over the time-frequency transform are indicated by the contours. The significant signal segments (contours) are successfully discriminated from the white noise background.*

Channel 2 consists of a time-varying theta EEG signal occurring at a fixed latency, linearly modulated (5-7 Hz) and varying in length randomly between 512 to 1024 samples among subjects and a gamma EEG signal, linearly modulated (30-90 Hz) and varying in length randomly between 1024-2048 samples among subjects, all mixed with quasi-white noise. In a similar manner, channel 5 consists of an alpha band linearly modulated signal (9-12 Hz) varying in length randomly (768-1536 samples) and a gamma linearly modulated signal (30-90 Hz) varying in length randomly between 512-1024 samples, mixed with quasi-white noise. Quasi-white noise covers the interval between the modulated signals. Such a generated signal (channel 2) together with the wavelet time-frequency representation is depicted in figure 4.4. Theta and gamma bands are apparent at different latencies. The tabulated channels in Table 4.II are the significant ones extracted with the proposed approach from the six frequency bands under investigation. The channels listed on the first column are the selected ones after the first statistical test (2nd step), whereas the channels listed on the second column are the refined ones after the second statistical selection (4th step).

TABLE 4.II
STATISTICAL FEATURE - CHANNEL SELECTION RESULTS

Band	Channel (2nd step)	Channel (4th step)	Target
Delta (δ)	2	-	-
Theta (θ)	2, 5	2	2
Alpha (α)	2, 5	5	5
Beta (β)	-	-	-
Gamma1 (γ1)	2, 5	2, 5	2, 5
Gamma2 (γ2)	2, 5	2, 5	2, 5

Although the first stage can identify both channels (2 & 5) with the pre-specified frequency content, it is not able to discriminate correctly the activated frequency bands because of leakage effects between bands, as illustrated in figure 4.4. In contrast, the second stage focuses on the significant regions and is able to detect and correctly account for the energy content of the selected regions.

Actual data Results

Based on previous clinically oriented study (Micheloyannis et al., 2005) using both linear Fourier power spectrum analysis and non-linear synchronization measures, task complexity is associated with systematic changes in EEG measures. The output of the proposed algorithm is summarized in Table 4.III. The tabulated lobes are the significant ones extracted from the six frequency bands under investigation. The lobes indicated are the selected ones after the first statistical test (2nd step), which are those used as input features for steps 3 and 4. The lobes indicated in bold are the refined ones after the second statistical selection (4th step), which are those used as input for the classification step 5 (Fig. 4.2). The symbol "↑" and "↓" denotes power increase and decrease, respectively.

Increased Theta activity is observed on both frontal lobes. More prominent

TABLE 4.III
STATISTICAL FEATURE - LOBE SELECTION RESULTS

Band	Lobe
Theta (θ)	**FL** ↑ FR ↑
Alpha1 (α1)	FL ↑ PL ↓
Alpha2 (α2)	-
Beta (β)	-
Gamma1 (γ1)	FL ↑
Gamma2 (γ2)	FL ↑ **CL** ↑

TABLE 4.IV
CROSS VALIDATION (LEAVE-ONE-OUT) SUCCESS RATES USING THE BAYES - QUADRATIC
CLASSIFIER FOR VARIOUS FEATURES' COMBINATIONS

Feature Type	Success Rate (%)
Energy (traditional Fourier)	73
Significant Energy	82

activity for the Theta bands is found on the FL lobe. Alpha1 band increase is found on the FL lobe, whereas decrease is found on the parietal left (PL) lobe. Related to the Gamma1 and Gamma2 bands, reactivity is detected on the FL lobe but more prominently around the central left (CL) region for the Gamma2 band.

To further validate the performance of the proposed methodology using wavelets vs. the traditional Fourier methods, a simple classification process is applied on the same dataset. The success rates using the Fourier based PS features calculated by the Fourier periodogram method on the same dataset as described in our previous study (Micheloyannis et al., 2005), as well as the success rates of the proposed Significant PS features are indicated in Table 4.IV. The improved performance indicates with increased confidence that the lobes selected indicate brain regions truly responsible for the mechanisms involved in the task considered (mathematical reasoning).

4.1.3 Discussion

Using the wavelet transform method on EEG signals, we evaluated cortical activation during a difficult mathematical task and compared it with a rest condition. This method, in contrast to traditional spectral ones, can estimate changes between EEG signals without being bounded to the stationarity assumption and can provide information for the entire time evolution of the signal. The results derived actually verify the "prospective" hypothesis that the complex multiplication task engages in a significantly different way certain lobes when compared to a control task. While in the simulation mode, we were able to derive the channels and frequency bands where this difference was mostly evident, whereas in the actual data the results were further validated by a classification step.

The simulation test and the results presented justify the suggestion that relevant characteristics are temporally localized in the most significant regions

(contours in the WT scalogram), rather than in the entire segment length of the EEGs. The *Global PS* only partially encapsulates the significant information, since there is significant frequency leakage between the bands, due to the transient response of the time-frequency filter in different frequencies. Using such features, both channels 2 and 5 in the simulated case induce activity in almost every band. However, the proposed methodology with its second statistical feature selection scheme can efficiently isolate the channels and the correct band activations. Traditional FT spectral analysis methods pose intrinsic limitations on encapsulating the time variation of the signal. Beyond traditional spectral analysis, the WT enables the consideration of time specific significant regions as in the 3rd step of the proposed methodology. WT is proved to be a useful measure to detect time-varying spectral power and performs better than traditional time-frequency methods in identifying activity, especially on a shorter temporal scale in high frequencies, which could indicate neuronal synchronous activation in some cortical regions. This is an advantage to previous methodologies, since high frequency bands are weak and difficult to evaluate using spectral methods.

A qualitative reasoning arising from the application of this methodology to the actual data is discussed next. There are numerous brain mapping studies related to mathematical thinking (Barth et al., 2006; Delazer et al., 2004; Lee and Kang, 2002). Most of them were performed using fMRI, PET or electrophysiological signals. Most findings in these studies are in accordance with previous anatomical studies. Based on these methods, local findings related to different kinds of mathematical thinking are detected mainly on frontal and central-parietal lobes. Frontal regions are constituents, among others, of frontal-subcortical, frontal-parietal and frontal-temporal circuits. These circuits have been proposed to activate memory while solving complex problems, and play an essential role in the regulation of behavior. Their fronto-executive function is important in mathematical thinking.

The cortical activation, as identified during the complex and difficult visually-presented multiplication task, was detected in our study mostly frontal and expressed mainly by the theta and gamma bands. In addition, prominent CL activation on the left side, expressed by the gamma2 frequency band, was detected by the proposed refinement step (Fig. 4.2, Step 4). These activations of the frontal

lobes with prominent left activation, the left central activation as well as the desynchronization of alpha1 band on the left parietal lobe (which means activation), are in accordance with the literature and previous findings using Fourier spectral methods (Micheloyannis et al., 2005). However, using the present wavelet analysis method makes it possible to accentuate task differences during mathematical thinking beyond the traditional spectral analysis on the same material. In this sense, more prominent reactivity for the Theta and Gamma2 bands was found on the FL and CL lobe, respectively. Hence, the proposed method is more sensitive in evaluating differences during cortical activations as shown by our results and the differentiation of the two hemispheres, which cannot be found by traditional spectral methods (Micheloyannis et al., 2005). Alpha band decrease (i.e., desynchronization) was evident on the left parietal lobe. These differences on theta, alpha1 and gamma2 bands are indicative of more prominent activation on the left hemisphere. Hemispheric differences in mathematical thinking were previously found mostly on simpler, language related mathematical processes (Barth et al., 2006; Zhang et al., 2005). Our findings are indicative of left prominent activation during difficult mathematical thinking as well.

Beta band activity was not identified by either the Fourier or the WT technique. In a previous spectral study (Micheloyannis et al., 2005), PL desynchronization in Alpha2 band was found, whereas WT indicates Alpha1 desynchronization in this region. This is explained as a result of spectral leakage in the mapping between WT scales and frequency bands. More specifically, the narrow Alpha1 and Alpha2 bands are not clearly discriminated through the discrete scale mapping (Table 4.III), causing the localization mismatch of these bands observed in the results of Fourier and WT techniques. Further refinement on scale resolution of the WT can resolve such issues.

Comparing spectral methods with the WT in terms of their discriminating power, the corresponding spectral features (i.e., spectral power at specific channels and bands) achieve a classification rate of 73%, whereas the features proposed in this paper based on the WT (Table 4.IV) enable an increased rate of 82%. Both, the WT method and the traditional Fourier technique are able to indicate with 95% confidence the task related lobes, but the WT method apart from achieving higher

classification rate it can reveal additional signal characteristics, since it captures not only its average power but also the time-localized activation of the signal.

4.1.4 Conclusion & Future work

The proposed algorithmic approach emphasizes the idea of selecting EEG features based on their statistical significance and further supports the use of time-scale WT domain in order to select significant EEG segments capable of describing the most prominent task related changes.

Results suggest that the proposed methodology is capable of identifying regions of cerebral activity during the specified task, even in complex cognitive tests. The entire process is automated in the sense that different feature types can be adaptively (according to the data profile) extracted and further refined in a way "transparent" to the user. Such processes may be easily transferred to a clinical environment if the methods prove to be valuable for the diagnosis of certain pathologies by comparing any routine EEG against a database of pathological ones.

Furthermore, the added value of this approach over other classical Fourier-based methods lies in its ability to further utilize time-domain characteristics of the WT in a way comparable to the evoked potential applications, without making any compromise in the statistical validity of the results.

Future work can proceed in several directions:

Input Data: The methodology presented can be readily applied to a variety of classification problems adapted to the nature of the input dataset; many different types of evolving biosignals seem to be perfect candidates for such classification processes. There is a plan to experiment with larger EEG datasets (more participants in various pathologies), in order to be able to use part of the data as the training subset and the remaining as the testing in a cross-validation scheme, for validating the classification potential and its performance in clinical diagnosis.

Feature Selection: There are numerous different statistical schemes capable of modeling in the best possible way the dataset being tested. One is free to make the right choice that will better fit the data profile and achieve more statistical power, which will lead to more representative features.

Classification: More classifiers, like several variations of Support Vector Machines (SVM) or combination of classifiers should be tested to better fit the data

under examination towards effectively understanding operations of the human brain. Furthermore, the proposed approach can be easily expanded and tested for the classification of multiple tasks.

4.2 Application to Schizophrenia

Among the various frameworks in which Electroencephalographic (EEG) signal synchronization has been traditionally formulated, the most widely studied and used is the coherence that is entirely based on frequency analysis. However, at present time it is possible to capture information about the temporal profile of coherence, which is particularly helpful in studying non-stationary time-varying brain dynamics, like the Wavelet Coherence (WC). In this section we propose a new approach of studying brain synchronization dynamics by extending the use of WC to include certain statistically significant (in terms of signal coherence) time segments, to study and characterize any disturbances present in the functional connectivity network of schizophrenia patients. Graph theoretical measures and visualization provide the tools to study the "disconnection syndrome" as proposed for schizophrenia. Specifically, we analyzed multichannel EEG data from twenty stabilized patients with schizophrenia and controls in an experiment of working memory (WM) using the gamma band (i.e., the EEG frequency of ca. 40 Hz), which is activated during the connecting activity (i.e., the "binding" of the neurons). Especially, higher frequency bands like gamma are characterized by brief low amplitude waves. Hence, one should use a method able to detect short but significant interdependencies, without making any stationarity assumptions, such as WC. Results are in accordance with the disturbance of connections between the neurons giving additional information related to the localization of most prominent disconnection.

4.2.1 Materials and Methods

Data Acquisition

The EEG signals in both groups (20 controls and 20 stabilized patients with schizophrenia) were recorded from 30 cap electrodes, according to the 10/20 international system, referred to linked A1+A2 electrodes (Fig. 4.6). The signals were digitized at 500 Hz.

Experimental setting and Test Description

Continuous EEGs were recorded in an electrically shielded, sound and light attenuated, room while participants sat in a reclined chair. EEG data were visually inspected for artifacts and epochs of 8 s were chosen for analysis. We analyzed epochs at rest i.e., while each individual had the eyes fixed on a small point on the computer screen and during a two-back WM test using capital Greek letters.

Methodology Overview

In this study apart from the traditionally formulated coherence, wavelet and significant wavelet coherence are applied, as discussed in sections 3.2.5 and 3.2.6, respectively. Visualization and statistics are performed using graph theoretic measures.

Hence, we are able to gain confidence in causal relationships of the coherence findings by estimating the statistical level of significance against a background spectrum using Monte Carlo methods (Grinsted et al., 2004). The background spectrum is defined as the mean time-averaged wavelet power spectrum over all healthy subjects performing the control task. A large set of surrogates (1000 datasets) was generated for each channel pair from the average WC of the healthy subjects and used to estimate the significance level for each
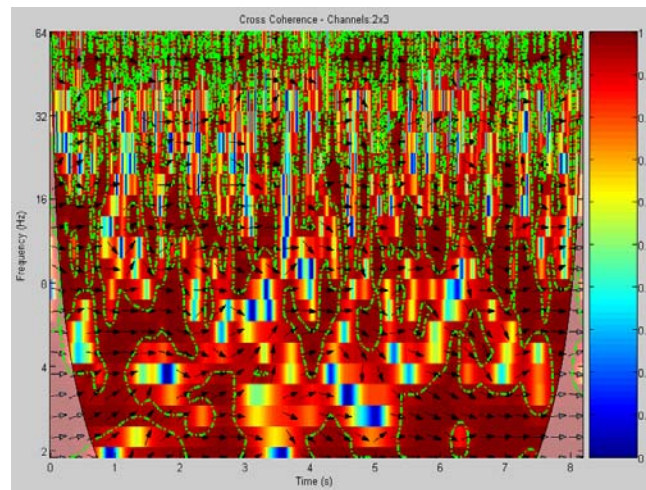
Figure 4.5: *The squared WC time-frequency transformed scalogram. The 5% significant regions over the time-scale transform are indicated by the contours (green dashed outline). The outer elliptical region at the edges of the second graph indicates the cone of influence in which errors (edge effects) may be apparent due to the transformation of a finite-length series EEG signal (Torrence and Compo, 1998). The relative phase relationship is shown as arrows (with in-phase pointing right, anti-phase pointing left).*

107

scale. Our aim is to map the WC scalogram (Fig. 4.5) into a feature vector that best characterizes each channel pair coupling. One may think of this step as an attempt to crop up the most significant (in terms of coherence) regions out of the bulk initial signal. Fig. 4.5 depicts the WC scalogram of two EEG channel signals of a schizophrenic patient. The significant regions (over the time-frequency transformed domain) that are strongly coupled while the subject is performing the WM task against the background spectrum are indicated by closed contours. Hence, one is able to form *Significant Coherency* features, which encapsulate the time and "band-scaled" coherence information, over those time regions where apparent significant differentiation is indicated (contours in Fig. 4.5). More detailed discussion on this approach is presented on section 3.2.6. Such features are constructed for each channel pair in both tasks and populations. As a result a 30x30 coherence matrix (CM) with elements ranging from 0 to 1 is formulated per task and subject.

In order to obtain a graph from a CM we need to convert it into an *NxN* binary adjacency matrix, *A*. To achieve that we define a variable called *threshold*
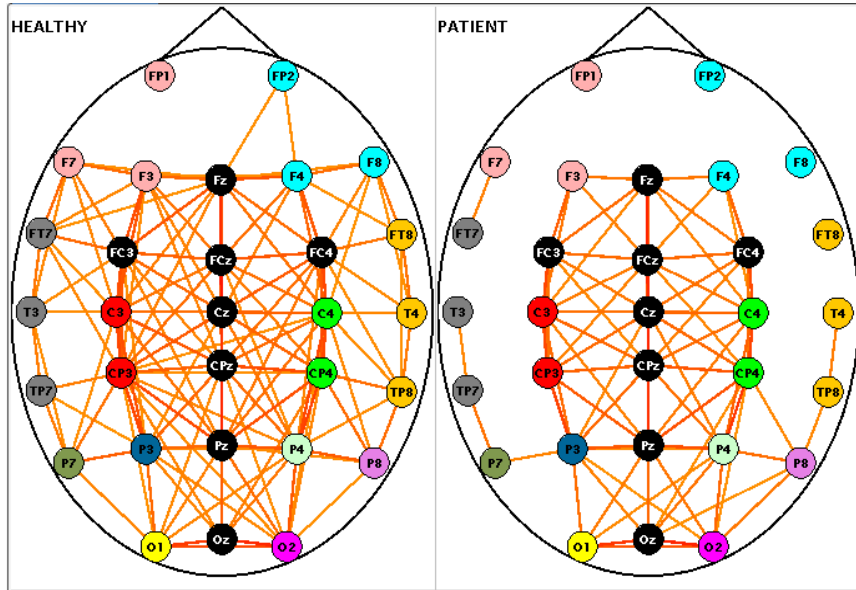
Figure 4.6: *A "healthy" network (left graph) (during a working memory task and selected threshold T) appears to have higher average degree K, clustering coefficient C and lower average shortest path length L values compared to the "schizophrenic" one (right graph). These disturbances are more prominent for the connections of the frontal lobes as well as the temporal lobes. Gamma1 band is depicted. Increased thickness of edges denotes stronger interdependence between adjacent pairs of nodes. Those channels belonging to the same lobe are painted with the same color, whereas the ones belonging to two lobes (i.e., P3 belongs to both (C7, P3) and (P3, O1), as well as P4 belongs to (P4, P8) and (P4, O2)) are colored using a mixture of both lobes' shades.*

T, such that $T \in [0,1]$. The value $A(i,j)$ is either 1 or 0, indicating the presence or absence of an edge between nodes i and j, respectively. Namely, $A(i,j)=1$ if $C(i,j) \geq T$, otherwise $A(i,j)=0$. Thus we define a graph for each value of T. For the purposes of our work, we defined 1000 such graphs, one for every thousandth of T. After constructing A, we compute various properties of the resulting graph, as discussed in section 3.6. For consistency the main measures used in this study are mentioned briefly.

These include the average degree K, the clustering coefficient C and the average shortest path length L of our graph. We define a graph in terms of a set of n nodes $V=v_1,v_2,..,v_n$ and a set of edges E, where e_{ij} denotes an edge between nodes v_i and v_j. The neighborhood N_i of a node v_i is defined as the set of vertices that have an edge to v_i, namely $N_i = \{v_j\} : e_{ij} \in E$.

The degree k_i of a node is the number of vertices in its neighborhood, i.e., $|N_i|$. The average degree of a graph is the average of the degrees of all nodes, i.e.,

$$K = \sum_{i \in V} k_i / n .$$

The clustering coefficient C_i of a node v_i is the fraction of the existing edges between the nodes in v_i's neighborhood over the number of all possible edges between them. For an undirected graph, if a node v_i has k_i neighbors, then $k_i(k_i-1)/2$ is the number of all possible edges in its neighborhood. Thus, $C_i = 2|\{e_{jk}\}| / k_i(k_i-1) : v_j,v_k \in N_i$. This measure is 1 if every neighbor connected to v_i is also connected to every other node within the neighborhood, and 0 if no node connected to v_i connects to any other node connected to v_i. The clustering coefficient for the whole graph is the average of C_i for each node, $C = \sum_{i=1}^{n} C_i / n$, and is a measure of the tendency of graph nodes to form local clusters (Watts and Strogatz, 1998).

The shortest path (distance) d_{ij} between two nodes v_i and v_j is the minimum number of edges we need to traverse in order to go from node v_i to node v_j. The average shortest path length $L = \sum_{i,j \in V, i \neq j} d_{ij} / n(n-1)$ is a measure of interconnectedness of the graph. Note that, in our experiments, the absence of a path between v_i and v_j implies $d_{ij} = 1000$.

Based on these properties one is able to form *K, C* and *L* feature vectors of size 40 (20 controls and 20 schizophrenics), for each subject and threshold in the gamma frequency band of interest. These vector indices were found to be normally distributed. Further statistical analysis comparing both populations was performed using t-tests.

4.2.2 Results

Our study focuses on gamma band coherence analysis. Significant coherent time-regions are transformed to the aforementioned binary matrix *A* served as input to the graph analysis algorithm. The values of *K, C* and *L* during *WM* were computed for both the healthy and schizophrenic groups. Their graphs along with the significant regions of apparent population differences are drawn in Figure 4.7.

Three selected threshold values are tabulated in tables 4.V and 4.VI along with the mean and standard error of the mean of each group. We concentrated in those values of *T,* where the values of *K* and *C* of schizophrenic patients were comparable (not significantly different) to control ones. For these values of *T,* the respective values of *L* for patients were significantly greater than those for controls, as tabulated in Table 4.VII using Bonferonni corrected t-test analysis. A detailed view of the network topology is depicted in Fig. 4.6.
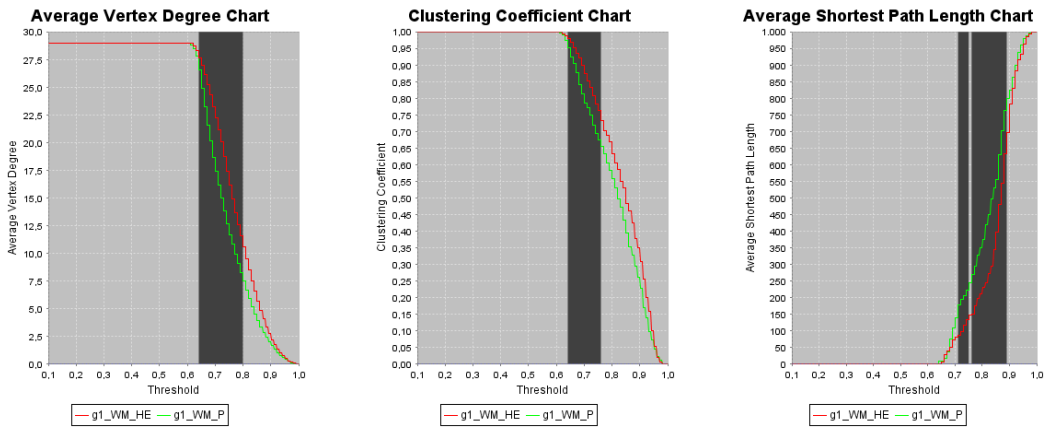

Figure 4.7: *The distribution of K (left graph), C (middle graph) and L (right graph) during WM for both the healthy (red line) and schizophrenic (green line) groups are drawn. The significant differences identified using t-tests (set at confidence level of p < 0.05) are indicated in the dark regions of the canvas.*

TABLE 4.V
SELECTED VALUES OF THRESHOLD ALONG WITH RESPECTIVE **K**, **C**, **L** VALUES FOR THE CONTROL POPULATION
K AND **C** WAS ELECTED TO BE COMPARABLE

	HEALTHY (Controls)		
T	**K** (mean ± S.E.)	**C** (mean ± S.E.)	**L** (mean ± S.E.)
0.791	11.56 ± 1.22	0.67 ± 0.03	210.75 ± 32.57
0.801	10.54 ± 1.19	0.63 ± 0.03	230.08 ± 35.12
0.831	7.46 ± 1.00	0.55 ± 0.03	294.93 ± 40.91

TABLE 4.VI
SELECTED VALUES OF THRESHOLD ALONG WITH RESPECTIVE **K**, **C**, **L** VALUES FOR THE SCHIZOPHRENIC POPULATION
K AND **C** WAS ELECTED TO BE COMPARABLE

	PATIENT (Schizophrenics)		
T	**K** (mean ± S.E.)	**C** (mean ± S.E.)	**L** (mean ± S.E.)
0.781	9.09 ± 1.04	0.61 ± 0.03	327.30 ± 45.81
0.791	8.25 ± 1.00	0.58 ± 0.03	349.62 ± 45.45
0.811	6.66 ± 0.91	0.53 ± 0.03	418.53 ± 45.09

TABLE 4.VII
STATISTICAL COMPARISON BETWEEN NEIGHBORING THRESHOLDS (PREVIOUSLY SELECTED)
RESULT: SIGNIFICANTLY DIFFERENT **K** AND **C**, BUT NON-SIGNIFICANT **L** VALUES

	PATIENT (Schizophrenics)			
$T_{HEALTHY}$	$T_{PATIENT}$	**K** (p-value)	**C** (p-value)	**L** (p-value)
0.791	0.781	0.13	0.15	0.05
0.801	0.791	0.15	0.26	0.04
0.831	0.811	0.56	0.68	0.05

4.2.3 Discussion

The proposed wavelet coherence analysis in combination with the graph analysis methodology indicated significant task differentiation in gamma band more prominent in frontal, frontal-central and temporal regions.

Such disturbances of integration of brain function in schizophrenic processes have been suspected from the first detailed descriptions of the disease and are

reinforced by clinical findings. Anatomical, biochemical brain mapping and electrophysiological findings support this hypothesis. Such clinical methods, using gamma band evaluation, further support the "disconnection" hypothesis i.e., the disturbance of the integrative processes. Various alternative studies relating gamma band and schizophrenia indicate that there is an overall reduction of the amount of the connected nodes and synchronization strength of this frequency band in schizophrenics. Additionally, there are differences between the gamma activity on the left and right hemispheres among patients and controls, as well as indices of less frontal integration as expressed by this band (Gallinat et al., 2004; Hong et al., 2004; Lee et al., 2003).

The three graph measures K, C, L actually represent an overall signature of the graph topology. Our experiments indicated that K, C and L are getting lower while moving from healthy to schizophrenics (in the whole threshold range). But instead of studying each measure independently, we attempt to quantify their interaction. Towards this direction we determined in three different values of T (Table 4.V), where the values of K and C of patients are equal to those of healthy. The physical meaning of this maneuver addresses the following question: Assuming both healthy and schizophrenic populations have the same average degree and clustering coefficient, is the network proportionally efficient? According to Table V the answer is no, which means that for the above values of T the respective values of L of the patients are much greater than those of healthy. This is also evident by observing figure 4.6. Alternative visualization schemes may also be proposed (Oikonomou et al., 2006). The latter syllogism leads to the suggestion that schizophrenic patients need significantly more direct node (channel) connections in order to perform the same WM task.

4.2.4 Conclusion

The algorithmic approach presented illustrates the idea of using statistically-based feature vectors in the time-scale WT domain in order to select the most significant time segments capable of revealing the most prominent task changes out of the background signal. Results suggest that the proposed methodology is capable of identifying regions of cerebral synchrony during the specified tasks.

Using the graph theoretical analysis we found that the integration, as expressed by the high frequency gamma band, related to the "binding" phenomenon i.e., the integration on neuronal activity, and the related parameters is overall reduced in schizophrenics. This is evident at rest but more prominent during a cognitive task, the WM. Additionally, these disturbances are more prominent for the connections of the frontal lobes as well as the temporal lobes.

4.3 Application to controlled Epilepsy

Epilepsy is one of the most common brain disorders and may result in brain dysfunction and cognitive disturbances. Epileptic seizures usually begin in childhood without being accommodated by brain damage and many drugs produce no brain dysfunction. In this study cognitive function in controlled epilepsy cases is evaluated where children with seizures are compared to controls i.e., children with epileptic seizures, without brain damage and under drug control. Two different cognitive tasks were designed and performed by both the epileptic and healthy children: i) a relatively difficult math task and ii) Fractal observation. Since there is no obvious differentiation between the groups under study, except from the clinical diagnosis and history of each subject, there is no way to prejudge which spectral estimation and synchronization method will perform better. Under this prism, we investigate both linear and nonlinear measures of quantifying synchronous oscillatory activity based on different underlying assumptions. Namely, in this section the most widely used coherence, a robust phase coupling measure known as PLV (Phase Locking Value), a reliable way of assessing generalized synchronization also in state-space and the unbiased alternative called Synchronization likelihood. Assessment was performed in three stages; initially the methods were validated on coupled nonlinear oscillators, secondly surrogate data testing was performed to assess the possible nonlinear nature of the acquired EEGs and finally synchronization on the actual data was measured. The results on the actual data suggest higher frequency band gamma2 was mostly apparent in occipital-parietal lobes during fractal tests.

4.3.1 Materials and Methods

Test signals & real data acquisition

To study the different properties of each of the proposed methods, we consider two classical coupled chaotic dynamical systems. The first model uses two coupled Rössler oscillators, whereas the second uses a Lorenz system nonlinearly driven by a Rössler oscillator with such coupling coefficient that

ensures GS (Hramov and Koronovskii, 2005a; Hramov and Koronovskii, 2005b), as described in section 3.4.2.

The studied population consisted of twenty mild epileptic subjects and twenty controls. The EEG signals in both groups (controls and controlled epileptics) were recorded from 30 cap electrodes (FP1, FP2, F7, F3, FZ, F4, F8, FT7, FC3, FCZ, FC4, FT8, T3, C3, CZ, C4, T4, TP7, CP3, CPZ, CP4, TP8, P3, PZ, P4, PO7, PO8, O1, OZ and O2), according to the 10/20 international system, referred to linked A1+A2 electrodes. The signals were amplified using a set of Contact Precision Instrument amplifiers, filtered on-line with a band pass between 0.1 and 200 Hz, and digitized at 400 Hz. Off-line, the recorded data were carefully reviewed for technical and biogenic artifacts, so that only artifact free epochs of eight seconds duration are investigated. The procedures used in the study had been previously approved by the University of Crete Institutional Review Board and all subjects signed a consent form after the nature of the procedures involved had been explained to them.

Test description

Continuous EEGs were recorded in an electrically shielded, sound and light attenuated, room while participants sat in a reclined chair. EEG data were visually inspected for artifacts and epochs of 8 sec were chosen for analysis. We analyzed epochs at rest i.e., while each individual had the eyes fixed on a small point on the computer screen and during the two cognitive tasks. The first includes two digits number subtractions or two digits minus one digit, which is thought to be a relatively difficult mathematical task and the second consist of Fractal observation. Stimuli were presented on an LCD screen located in front of the participants. Vertical and horizontal eye movements and blinks were monitored through a bipolar montage from the supraorbital ridge and the lateral canthus.

Methodology overview

The interdependence measures used in this study are directly applied as discussed in the previous sections 3.1.4 (mean squared coherence - MSC), 3.3 (Phase Locking Value - PLV) and 3.4.4 (reliable way of assessing generalized synchronization also in state-space - RSS-GL and synchronization likelihood - SL).

4.3.2 Results

Testing using artificially generated data using chaotic oscillators under variable noise

To demonstrate that the nonlinear synchronization methods addressed in this study are sensitive to nonlinear structures in the signals under investigation we consider two classical coupled chaotic dynamical systems. The first model uses two coupled Rössler oscillators (Hramov and Koronovskii, 2005b) (Fig. 4.8), whereas the second uses a Lorenz system (Hramov and Koronovskii, 2005a) nonlinearly driven by a Rössler oscillator with coupling coefficient that ensures GS (Fig. 4.9). The synchronization indexes vs. additive noise are plotted in the following figures.

Nonlinear coupling detection ability: Testing using surrogates

To demonstrate that the synchronization methods addressed in this study are sensitive to nonlinear structures in the real EEG signals (and thus reliable) under investigation bivariate surrogate data testing was used. The surrogating procedure used preserves both the autocorrelation of the signal and their linear cross-correlation, but the nonlinear individual structure of the individual signals, as well
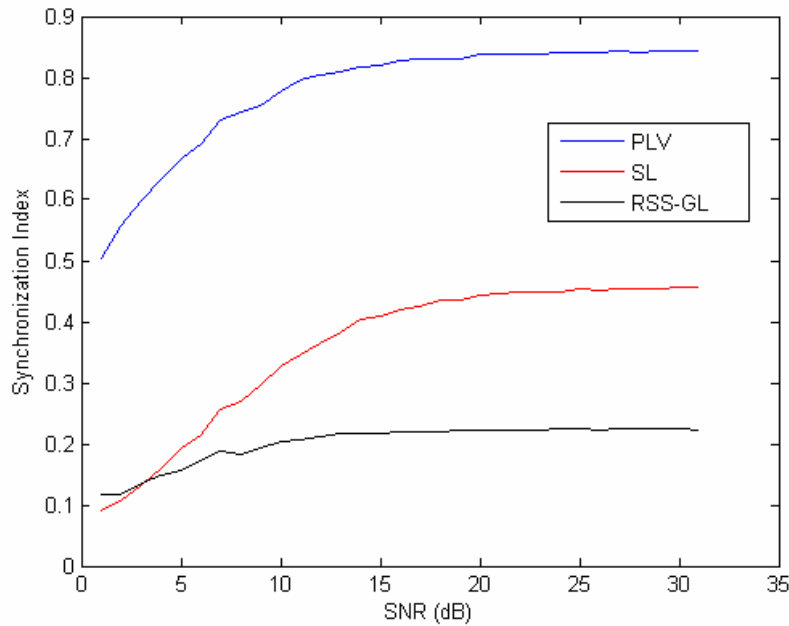

Figure 4.8: *Synchronization indexes applied on two coupled Rössler oscillators, configured to have phase synchronization. Obviously PLV performs best.*
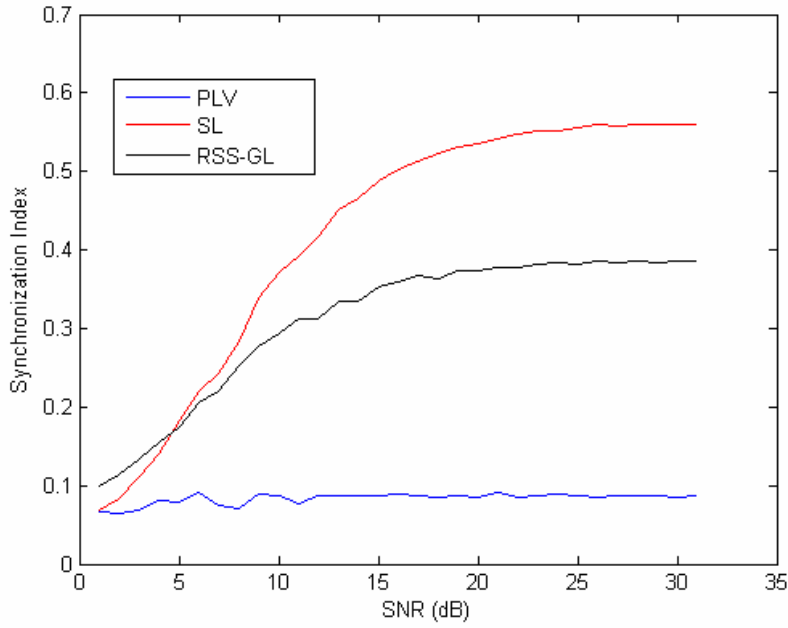
116

Figure 4.9: *Synchronization indexes applied on a Lorenz system nonlinearly driven by a Rössler oscillator. The coupling coefficient used is set for generalized synchronization (GS). Obviously PLV is not designed to detect GS, thus failing to do so. Both SL and RSS-GL perform better.*

as their nonlinear interdependence, if any, is destroyed (Andrzejak et al., 2003). One mild-epileptic and one normal signal of a single representative subject was selected to be the generator of the surrogates and the testing was performed focusing on channels O2 and PO8 located on the occipital-parietal brain lobe.

To reject the hypothesis (H_0) that the mean values of the original and the set of surrogate time series are equal, the Z-score is calculated. H_0 is rejected at the 95% level of confidence if $Z>1.96$ (one-sided test). The results obtained are tabulated in table 4.VIII. PLV is the only method that scored more than 1.96, hence the one able to detect possible nonlinear interdependences in our dataset. Bold values are

TABLE 4.VIII
SYNCHRONIZATION Z-SCORES (ORIGINAL VS. SURROGATE DATASETS)

Linear (Alpha1 band, 8-10 Hz)		Nonlinear	
Method	**Z-score**	**Method**	**Z-score**
COHERENCE	0.50	PLV	**3.85**
		SL	1.09
		RSS-GL	1.32

TABLE 4.VIII
ACTUAL EEG DATA: LOBE-BAND SELECTION

Method	Test1	Test2	Test3
WS	α: F7, FT7(N<E) β: FP1(N<E) γ1: FP1(N<E)	α: FP2, FP1, F3, C3, Fz, FC3(N<E) β: FP2, FP1, Fz(N<E) γ1: FP1(N<E) γ2: FP2, FP1(N<E)	β: FP2, FP1(N<E) γ1: FP2, FP1(N<E) γ2: FP2, FP1(N<E)
COHERENCE	γ1: OPR(N>E)	-	-
PLV	-	-	γ2: OPL, OPR(N>E)
RSS-GL	-	-	γ2: OPL, OPR(N>E)

the ones capable of identifying the nonlinearities of the signal. Coherence obviously was not successful in identifying significant differences as compared to the surrogates, since it is unable to detect nonlinearities.

Table 4.VIII tabulates the significant brain regions (lobes) as identified using the wavelet spectral (WS) estimation method and three synchronization measures; a linear one (coherence) and two nonlinear ones, one optimized for Phase Synchronization (PLV) and another for Generalized Synchronization (RSS-GL).

Actual EEG data

Testing using surrogates suggested that further testing on the real data is prospective using only the linear and the *PLV* method, as discussed in the next section. However, recalling that RSS-GL method actually tests for generalized synchronization (GS) and not phase synchronization (PS) and since the RSS-GL measure achieved a rather high Z-value, although lower than 1.96, we included this method in the results Table 4.VIII. The latter synchronization measures are performed on both normals and mild-epileptic band-filtered data. Averages over all possible channel couplings in each brain lobe and band are calculated, as described in section 3.5.2. Beside synchronization measures, Table 4.VIII includes also power spectrum significant differences using the wavelet spectral (WS) estimation method, as described in section 3.2.2.

The data were then subjected to a series of two-way repeated-measures multivariate analysis of variance (ANOVA) using the Greenhouse-Geisser method, when appropriate, to address potential problems of inhomogeneity of variance across data cells. Pairwise contrasts were examined with t-tests, using the

Bonferonni method to maintain the family-wise Type I error rate to $p =.05$. In addition, WS data were normalized using a log10 transformation. The first fixed within subject factor was the task, with three levels (two main experimental tasks and one control task). The second repeated measures within-subject factor was the Scalp Region (lobe) with 5 levels (frontal, temporal, fronto-temporal, central parietal, and parieto-occipital)[*], or channel in the case of WS (with 30 levels)[†].

Only those bands/lobes that achieved significant differentiation are tabulated. α, β, γ_1 and γ_2 denote alpha (8-13 Hz), Beta (13-30 Hz), Gamma1 (30-40 Hz) and Gamma2 (40-90 Hz) bands, respectively. The identified lobes are: OPR (O2-P4, O2-PO8, P4-P8) and OPL (O1-P3, O1-PO7, PO7-P3), while $N>E$ denotes that synchronization in normals was greater than in epileptics. The power spectrum values identified specific channels according to the 10-20 International System. Mostly the frontal regions are apparent, as opposed to the occipital synchronization estimations, while the mean power is found to be greater in epileptics than normals.

4.3.3 Discussion

The PLV method is designed to detect Phase Synchronization; hence when applied on phase synchronized oscillators obviously performs better (Fig.4.8) than the others, which are optimized for detecting Generalized Synchronization. However, SL and RSS-GL estimators were also able to identify the coupling, but underestimated it. RSS-GL found to be less susceptible to noise. However on the second paradigm using the generally synchronized oscillators, all methods were able to perform well, except the PLV as expected (Fig. 4.9). SL and RSS-GL were the best. SL and RSS-GL different responses are due to normalization factors and do not imply that one outperforms the other. Here again RSS-GL is more robust compared to SL, which seems to be rather prone to noise. As a conclusion in a real case scenario one should use both a PS measure (i.e., PLV) and one of the proposed GS measures (preferably RSS-GL or SL), as well as linear tools since

---

[*] More detailed information is given in section 3.5.2.

[†] More detailed information is given in section 3.5.1.

their underlined assumptions are different. In addition, power spectrum estimation methods are also useful, since they are identifying activations/ deactivations using single channels or lobes and not interactions among channels.

The testing using surrogate datasets testifies that there is strong statistical evidence that the interdependence in the real EEG data can be described by a linear model, but it is also evident that there also exists nonlinear coupling apparent in PS measures (PLV) only. In other words, since all GS methods were unable to discriminate the actual EEG from the surrogates (linear representations), lead to the conclusion that either the actual EEG does not contain strong nonlinear GS couplings or the measure used is not strong enough to detect them. But since we tested them on nonlinear models we conclude that the first assumption is right. However, PLV was able to detect differences. Hence, we used PLV and the linear methods proposed on the real EEG data. RSS-GL was also used to check whether a GS measure is also able to detect interdependencies.

The results indicated that the PLV method accentuates gamma2 reactivity on the parietal and occipital brain lobes during the Fractal simulation test. RSS-GL method also confirms these findings. The coherence linear synchronization estimator even if it does not identify the same brain regions in gamma2 band, it mostly supports activations around the parieto-occipital region in gamma1 band, during the control task. Such an increase in gamma band activity (Erimaki et al., 2006) is also found during observation of figures with illusory contours, and this finding was interpreted as an evidence of a bottom-up binding of coherent visual features (Tallon-Baudry et al., 2001). At the same time, there is evidence that gamma band oscillations subserve the modulation of visual processes by the perceiver's internal representations and cognitive context, in a top-down approach (Goffaux et al., 2004).

Bibliography

Andrzejak RG, Kraskov A, Stogbauer H, Mormann F, Kreuz T. Bivariate surrogate techniques: necessity, strengths, and caveats. Phys. Rev. E 2003; 68: 066202.

Barth H, La Mont K, Lipton J, Dehaene S, Kanwisher N, Spelke E. Non-symbolic arithmetic in adults and young children. Cognition 2006; 98: 199-222.

Delazer M, Domahs F, Lochy A, Karner E, Benke T, Poewe W. Number processing and basal ganglia dysfunction: a single case study. Neuropsychologia 2004; 42: 1050-62.

Erimaki S, Kanatsouli K, Karakonstandaki E, Vourkas M, Sakkalis V, Micheloyannis S. EEG Responses To Complex Fractal Stimuli. 2nd International Nonlinear Science Conference. Heraklion, Crete, Greece, 2006.

Gallinat J, Winterer G, Herrmann CS, Senkowski D. Reduced oscillatory gamma-band responses in unmedicated schizophrenic patients indicate impaired frontal network processing. Clin Neurophysiol 2004; 115: 1863-74.

Goffaux V, Mouraux A, Desmet S, Rossion B. Human non-phase-locked gamma oscillations in experience-based perception of visual scenes. Neurosci Lett 2004; 354: 14-7.

Grinsted A, Moore JC, Jevrejeva S. Application of the cross wavelet transform and wavelet coherence to geophysical time series. Nonlinear Processes in Geophysics 2004; 11: 561-566.

Hastie T, Tibshirani R, Friedman JH. The elements of statistical learning : data mining, inference, and prediction. New York: Springer, 2001.

Hong LE, Summerfelt A, McMahon R, Adami H, Francis G, Elliott A, et al. Evoked gamma band synchronization and the liability for schizophrenia. Schizophr Res 2004; 70: 293-302.

Hramov A, Koronovskii A. Generalized synchronization: a modified system approach. Physical Review E 2005a; 71: 067201.

Hramov A, Koronovskii A. Intermittent generalized synchronization in unidirectionally coupled chaotic oscillators. Europhysics Letters 2005b; 70: 169-175.

Lee KH, Williams LM, Breakspear M, Gordon E. Synchronous gamma activity: a review and contribution to an integrative neuroscience model of schizophrenia. Brain Res Brain Res Rev 2003; 41: 57-78.

Lee KM, Kang SY. Arithmetic operation and working memory: differential suppression in dual tasks. Cognition 2002; 83: B63-8.

Micheloyannis S, Sakkalis V, Vourkas M, Stam CJ, Simos PG. Neural networks involved in mathematical thinking: evidence from linear and non-linear analysis of electroencephalographic activity. Neurosci Lett 2005; 373: 212-7.

Oikonomou T, Sakkalis V, Tollis I, Micheloyannis S. Searching and Visualizing Brain Networks in Schizophrenia. Lecture Notes in Computer Science, Biological and Medical Data Analysis, 7th International Symposium, ISBMDA 2006, Thessaloniki, Greece, December 7-8 2006; 4345: 172-182.

Sakkalis V, Oikonomou T, Pachou E, Tollis I, Micheloyannis S, Zervakis M. Time-significant Wavelet Coherence for the Evaluation of Schizophrenic

Brain Activity using a Graph theory approach. Engineering in Medicine and Biology Society (EMBC 2006). New York, USA, 2006a.

Sakkalis V, Zervakis M, Bigan C, Cassar T, Camilleri KP, Fabri SG, et al. EEG feature extraction and selection methods using wavelets and ARMA model for classifying mild epileptic signal patterns. Joint Workshop On BIOPATTERN Analysis In Brain Diseases. Goteborg, Sweden, 2006b.

Sakkalis V, Zervakis M, Bigan C, Cassar T, Camilleri KP, Fabri SG, et al. Validation of time-frequency and ARMA feature extraction methods in classification of mild epileptic signal patterns. Information Technology Applications in Biomedicine (IEEE-ITAB 2006). Ioannina - Epirus, Greece, 2006c.

Sakkalis V, Zervakis M, Micheloyannis S. Significant EEG Features Involved in Mathematical Reasoning: Evidence from Wavelet Analysis. Brain Topography 2006d; 19: 53-60.

Simos PG, Papanikolaou E, Sakkalis E, Micheloyannis S. Modulation of gamma-band spectral power by cognitive task complexity. Brain Topogr 2002; 14: 191-6.

Tallon-Baudry C, Bertrand O, Fischer C. Oscillatory synchrony between human extrastriate areas during visual short-term memory maintenance. J Neurosci 2001; 21: RC177.

Torrence C, Compo G. A practical Guide to Wavelet Analysis. Bull. Am. Meteorol. Soc. 1998; 79: 61-78.

Watts DJ, Strogatz SH. Collective dynamics of 'small-world' networks. Nature 1998; 393: 440-2.

Zar JH. Biostatistical analysis. Upper Saddle River, N.J.: Prentice Hall, 1999.

Zhang YT, Zhang Q, Zhang J, Li W. Laterality of brain areas associated with arithmetic calculations revealed by functional magnetic resonance imaging. Chin Med J (Engl) 2005; 118: 633-8.

People do not like to think. If one thinks, one must reach conclusions.

Conclusions are not always pleasant.

—. *Helen Keller*

5

GENERAL DISCUSSION & CONCLUSION

This chapter validates the algorithms and methods discussed in the previous chapters. In many cases comparisons of the proposed methodologies with widely used alternative methods is performed in simulated signals and previous will. Concluding remarks and suggestions for future work will be addressed.

5.1 Comparison of Power spectral-based analysis methods

After getting acquainted with the different frequency and time-frequency spectral-based analysis methods, one might be tempted to favor some against others. But such a decision is highly subjective and application dependent. Instead, this section summarizes the pros and cons of different methods as presented throughout this thesis.

Fourier Transform (**§ 3.1**) gives the decomposition of the signal into complex sinusoids that extend through the entire time domain. It reveals significant frequency information and allows the identification of periodicities, otherwise difficult to observe from the EEG raw data itself, especially when certain rhythms occur simultaneously. Such periodicities are grouped together to form frequency bands related to certain cognitive functions or pathologies. Unfortunately, there is no information concerning the temporal evolution of those periodicities. Hence, any transients localized in time actually affect the whole spectrum estimation, (this is why stationarity is assumed) since there is no direct way to exclude them. Artifacts form such case scenario. Considering also the non stationary nature of EEG signals one should be cautious when using this method. In practice the most common way of partially resolving this situation is to visually select small representative artifact free segments of data and perform averaging on these, as addressed by the averaged modified periodogram estimation methods (**§ 3.1**).

When one is interested in analyzing or utilizing the time evolution of the EEG frequencies, the Short time Fourier Transform (**§ 3.2.1)** comes initially in mind. Here the problem of stationarity is partially resolved by taking short time windows. In practice, this approach performs better in estimating large scale frequency variations, of the order of tens of seconds and more. The most difficult question to answer is the size of the time window, since the Uncertainty Principle states that the narrower the window, the poorer the frequency resolution, whereas if the window is wide enough, the time localization will become less precise. Hence, slow processes favor wider windows, while faster processes call for narrow windows to increase time resolution. This discrimination occurs naturally in Wavelet Transform (**§ 3.2.2**). The latter actually uses adaptive window sizes according to the frequency being examined. Due to this inherent property of the Wavelet Transform the requirement for stationarity is more relaxed. Moreover, this method may be extended to include statistical significance tests and provide the most significant brain regions in terms of activation or deactivation patterns existence (**§ 3.2.3**).

5.2 Comparison of Interdependence estimation methods

Throughout this thesis both linear and nonlinear interdependence measures are discussed. Even if the complex nature of EEG signals justify the use of nonlinear methods there is no evidence to support and prejudge that such methods are superior to linear ones. On the contrary, the information provided by nonlinear analysis does not necessarily coincide with that of the linear methods. In fact, both approaches should be regarded as complementary in the sense that they are able to assess different properties of interdependence between the signals. In addition the linear ones most of the times appear to be robust against noise, whereas nonlinear measures are found to be rather unstable. Stationarity is again a main concern, since it is a prerequisite which is not satisfied in practice.

Under this prism the following diagrams may prove to be really useful in assessing the ability and robustness of different -in terms of "nature"- methods to capture "known" couplings generated by established nonlinear coupled oscillators. Hence, two unidirectionally coupled chaotic Hénon maps (Schiff et al., 1996), a Lorenz system nonlinearly driven by a Rössler system and a Rössler system nonlinearly driven by Rössler (Hramov and Koronovskii, 2005a; Hramov and Koronovskii, 2005b) are used. The strength of the coupling between the two systems is given by the coupling parameter, which calibrates the x-axis of each diagram. It varies between 0 (uncoupled systems) heading towards higher values as coupling increases till complete coupling is reached.

The main points stressed by the following illustrations are:

1)   to check whether the coupling measuring method increases when the coupling strength between the oscillator systems increases,

2)   to check whether the coupling measuring method is able to detect nonlinear coupling,

3)   to check how robust the coupling measures are in noisy environments.

The first point is self explanatory. To check the second one and demonstrate that our measures are sensitive to nonlinear structure in the coupled oscillators, bivariate surrogate datasets were used. The surrogating procedure used preserves

both the autocorrelation of the signal and their linear cross-correlation, but the nonlinear individual structure of each signal, as well as their nonlinear interdependence, if any, is destroyed (Andrzejak et al., 2003). For more information and technical details on surrogate testing refer to section 3.4.5. Finally, the third point is addressed through the final set of illustrations which include Gaussian noise.

Oscillators and parameters used in the following illustrations

For each of the oscillator generator the following parameters are used:

Hénon maps

The dynamical system is a discrete time system, which can be decomposed into two subsystems. The evolution of the second subsystem depends on the state of the first subsystem. The system can be described by the difference equations:

$$
\begin{aligned}
x_{i+1} &= 1.4 - x_i^2 + 0.3u_i \\
u_{i+1} &= x_i
\end{aligned}
\qquad \text{(1}^{\text{st}}\text{ subsystem, driver)}
$$

$$
\begin{aligned}
y_{i+1} &= 1.4 - \left(\varepsilon x_i + (1-\varepsilon)y_i\right)y_i + \beta v_i \\
v_{i+1} &= y_i
\end{aligned}
\qquad \text{(2}^{\text{nd}}\text{ subsystem, response)}
$$

where $\varepsilon \in [0,1]$ denotes the coupling parameter and $\beta = 0.1$ which states that both dynamical systems are not identical.

Lorenz driven by Rössler

The continuous time system is described by the differential equations:

$$
\begin{aligned}
\dot{x}_d &= -6\left(y_d + z_d\right) \\
\dot{y}_d &= 6\left(x_d + 0.2y_d\right) \\
\dot{z}_d &= 6\left(0.2 + z_d\left(x_d - 5.7\right)\right)
\end{aligned}
\qquad \text{(driver)}
$$

$$
\begin{aligned}
\dot{x}_r &= 10\left(y_r - x_r\right) \\
\dot{y}_d &= 28x_r - y_r - x_r z_r + \varepsilon y_d \\
\dot{z}_d &= -\frac{8}{3}z_r + x_r y_r
\end{aligned}
\qquad \text{(response)}
$$

where ε is the coupling parameter.

Rössler driven by Rössler

$$\dot{x}_d = -\omega_d y_d - z_d$$
$$\dot{y}_d = \omega_d x_d + 0.15 y_d \qquad \qquad \text{(driver)}$$
$$\dot{z}_d = 0.2 + z_d (x_d - 10)$$

$$\dot{x}_r = -\omega_r y_r - z_r + \varepsilon (x_d - x_r)$$
$$\dot{y}_r = \omega_r x_r + 0.15 y_r \qquad \qquad \text{(response)}$$
$$\dot{z}_r = 0.2 + z_r (x_r - 10)$$

The time series consist of 4096 samples, where the first 1000 iterations of the oscillator generator have been discarded. The continuous systems were integrated with the Runge Kutta (4, 5) method. Since we want to take measurements of the chaotic attractors of the systems, a large number of initial iterations that correspond to a transient trajectory are ignored. Next we take 4096 samples from the x_d and x_r observables. (x,y observables in Hénon map). The sampling period is in general higher than the integration timestep.

In the next illustrations *Coherence* serves as a linear reference method (assuming it will miss any nonlinearities introduced by the nonlinear oscillators), whereas *Synchronization Likelihood* and the *Robust state-space synchronization* are the Generalized Synchronization methods evaluated in this thesis. Ideally, the next illustrations should reflect the following behavior:

- the coupling index (y axis) should increase when the coupling strength between the oscillator systems increases,

- the coupling curve of each method should be well out of the linear surrogate counterparts in order to justify its ability to detect nonlinear coupling,

- each method's coupling curve should remain robust and retain its characteristic profile even in noisy environments.
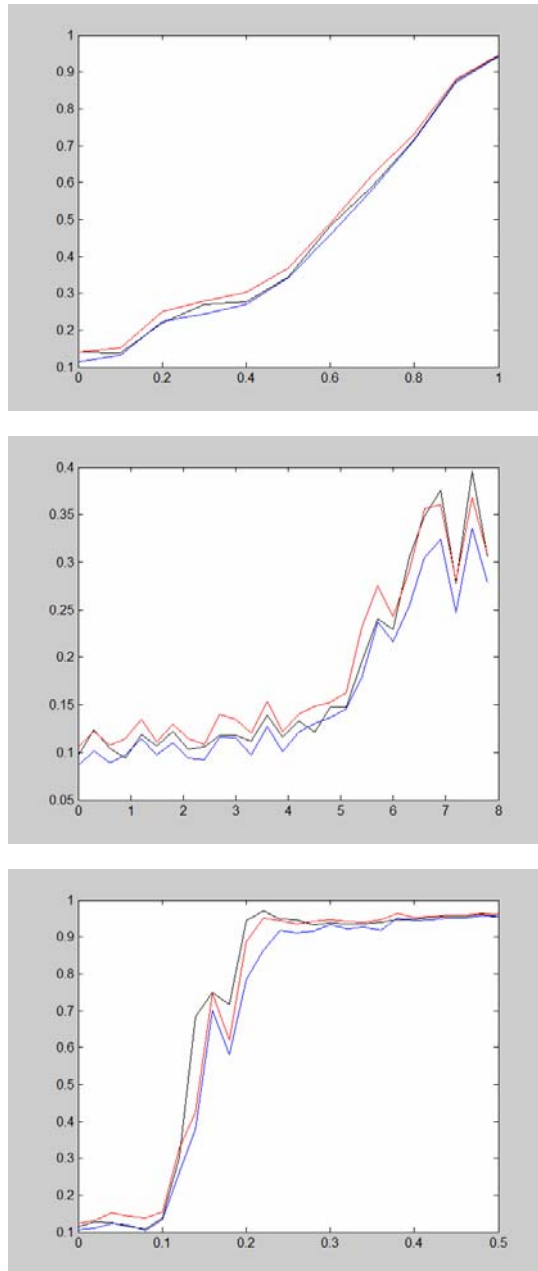
Coherence

Figure 5.1: *The black curve represents the coherence as identified between the original tested signals. The red and blue curves represent only the maximal and minimal coupling values, between 20 surrogate sets.*

*Three different oscillators are used to generate the signals: (**a**) Hénon maps, (**b**) Lorenz system nonlinearly driven by a Rössler system and (**c**) a Rössler system nonlinearly driven by Rössler.*

The synchronization for the original data is always inside the distribution of the surrogate's counterpart, indicating that coherence is not able to detect significant nonlinear coupling.
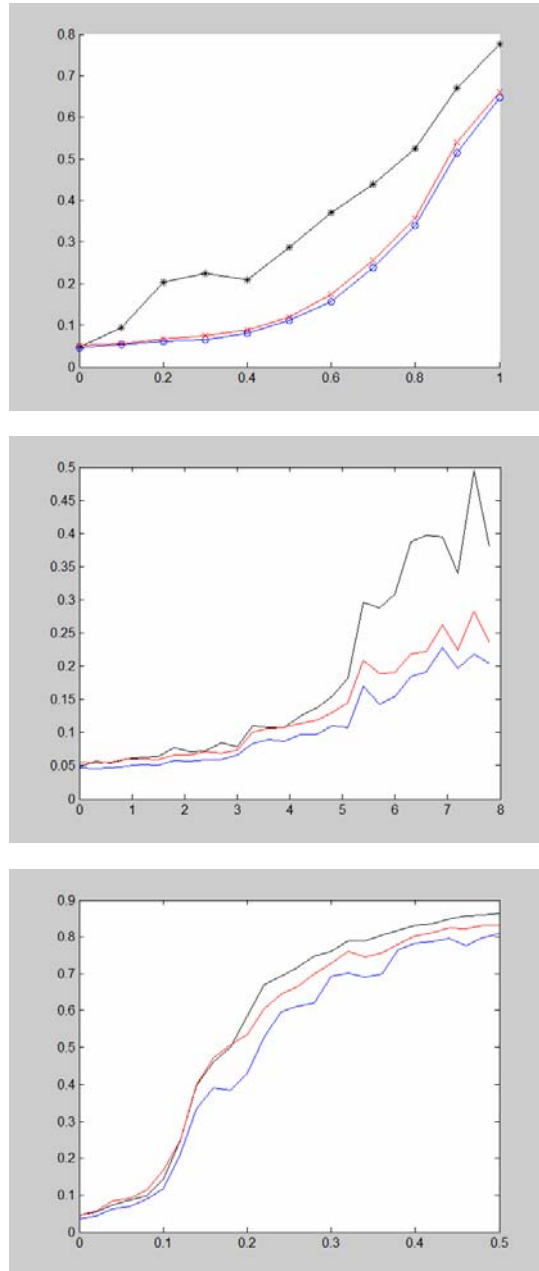
Synchronization Likelihood

Figure 5.2: *The black curve represents the synchronization likelihood as identified between the original tested signals. The red and blue curves represent only the maximal and minimal coupling values, between 20 surrogate sets.*

*Three different oscillators are used to generate the signals: (**a**) Hénon maps, (**b**) Lorenz system nonlinearly driven by a Rössler system and (**c**) a Rössler system nonlinearly driven by Rössler.*

The synchronization for the original data is always well outside the distribution of the surrogates counterpart, indicating that this method is able to detect significant nonlinear coupling.

(Parameters used: In all analyses the following fixed embedding parameters were used: lag l = 10; embedding dimension m = 10; w1 = 100; w2 = 400. pref was set equal to 0.05). w1 corresponds to Theiler correction for autocorrelation effects (§ 3.4.4).

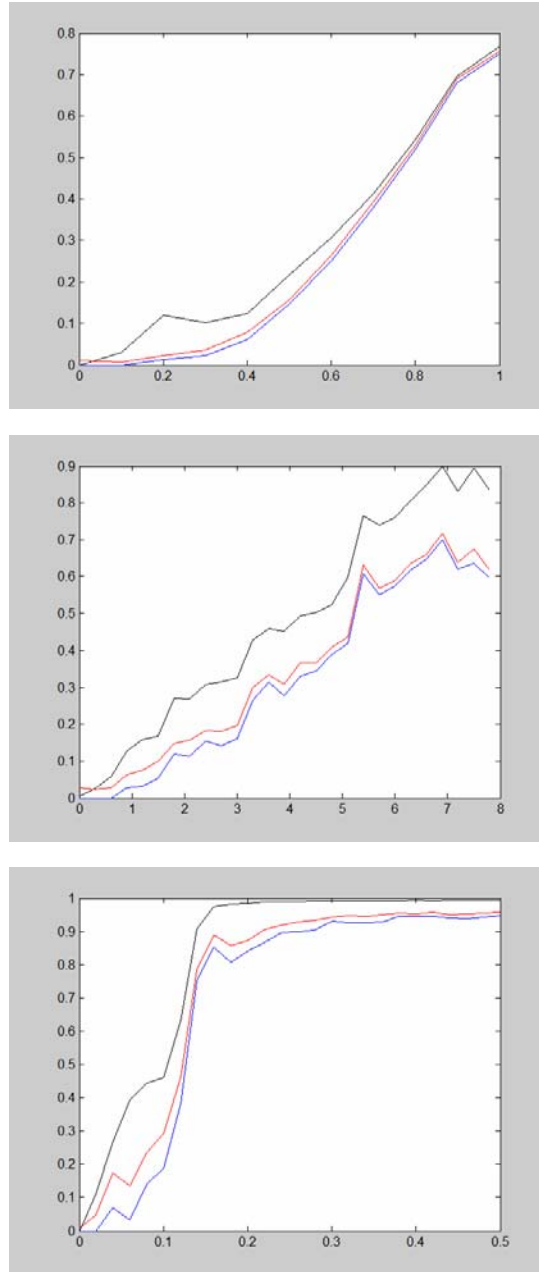Robust state-space generalized synchronization measure synchronization

Figure 5.3: *The black curve represents the robust state-space generalized synchronization measure as identified between the original tested signals. The red and blue curves represent only the maximal and minimal coupling values, between 20 surrogate sets.*

*Three different oscillators are used to generate the signals: (**a**) Hénon maps, (**b**) Lorenz system nonlinearly driven by a Rössler system and (**c**) a Rössler system nonlinearly driven by Rössler.*

The synchronization for the original data remains outside the distribution of the surrogates' counterpart, indicating that this method is able to detect significant nonlinear coupling.

(Parameters used: In all analyses the following fixed embedding parameters were used: lag $l = 10$; embedding dimension $m = 10$; $w1 = 100$; $NN = 10$). NN denotes the nearest neighbors and $w1$ is the Theiler correction.
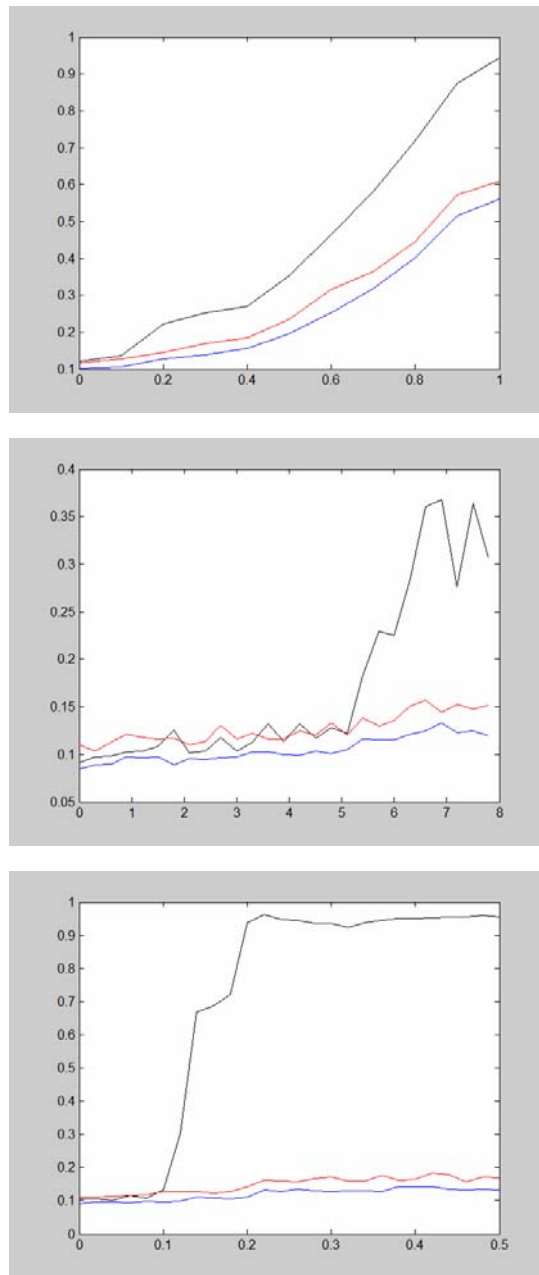
Coherence *(Additive Gaussian noise with SNR = 5)*

Figure 5.4: *The black curve represents the coherence, as identified in the previous illustrations, between the original tested signals. The red and blue curves represent only the maximal and minimal coupling values with added Gaussian noise (average of 10 examples).*

Three different oscillators are used to generate the signals: (a) Hénon maps, (b) Lorenz system nonlinearly driven by a Rössler system and (c) a Rössler system nonlinearly driven by Rössler.

Especially the latter two oscillators indicate that coherence is not able to detect significant nonlinear coupling when noise is added.

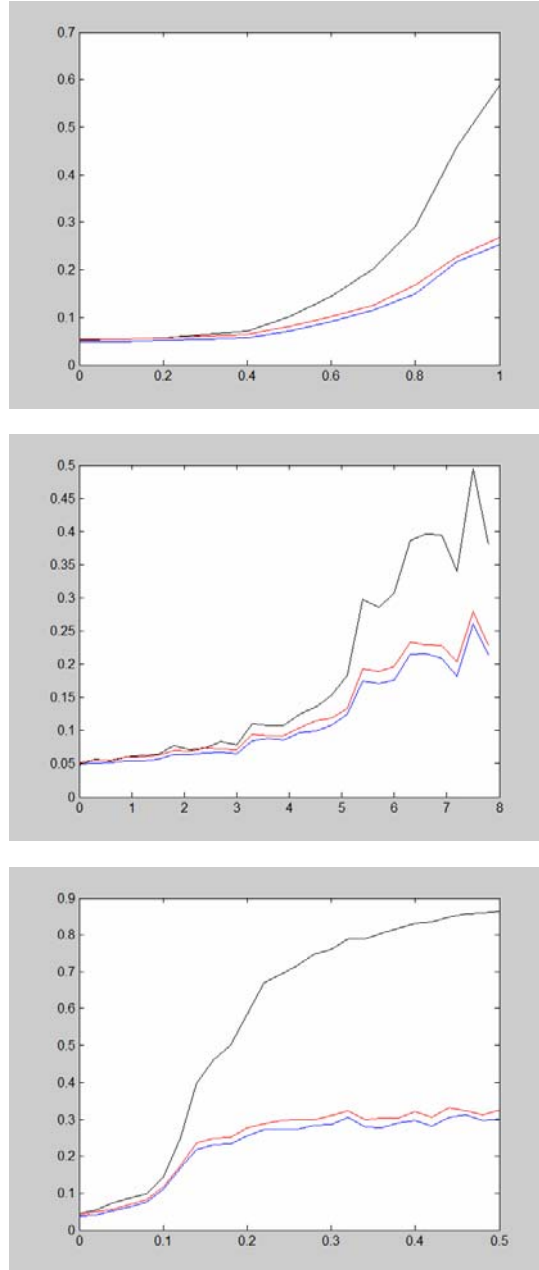Synchronization Likelihood *(Additive Gaussian noise with SNR = 5)*

Figure 5.5: *The black curve represents the coherence, as identified in the previous illustrations, between the original tested signals. The red and blue curves represent only the maximal and minimal coupling values with added Gaussian noise (average of 10 examples).*

*Three different oscillators are used to generate the signals: (**a**) Hénon maps, (**b**) Lorenz system nonlinearly driven by a Rössler system and (**c**) a Rössler system nonlinearly driven by Rössler.*

There is decay when in noisy signals. However, this method is still able to detect nonlinear coupling, even in noisy signals.

(Parameters used: In all analyses the following fixed embedding parameters were used: lag $l = 10$; embedding dimension $m = 10$; $w1 = 100$; $w2 = 400$. pref was set equal to 0.05).
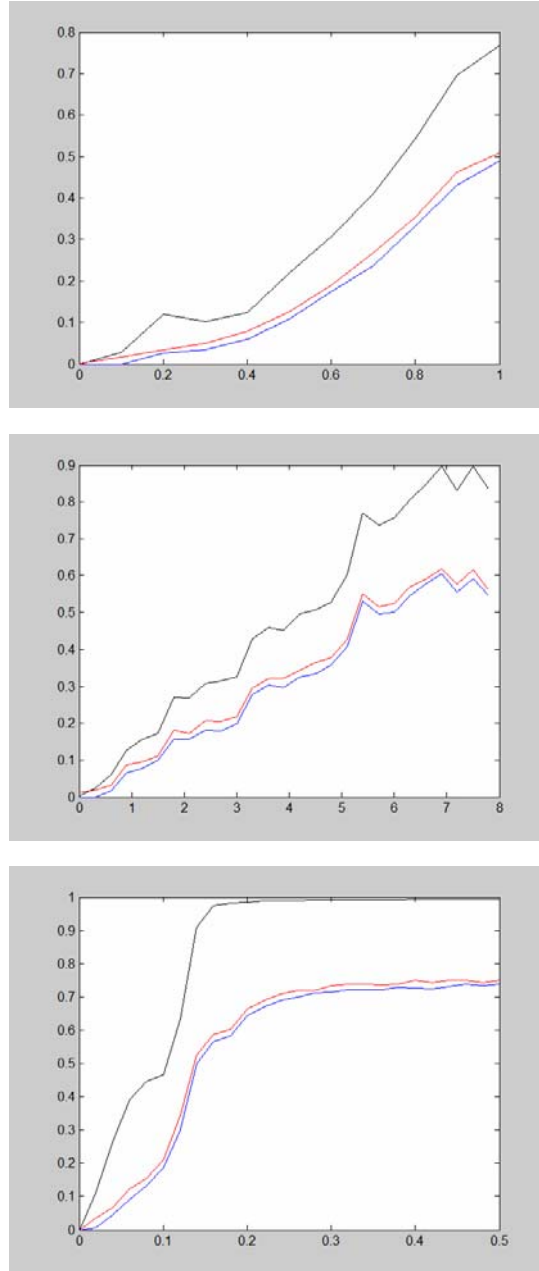
Robust state-space synchronization *(Additive Gaussian noise with SNR=5)*

Figure 5.6: *The black curve represents the coherence, as identified in the previous illustrations, between the original tested signals. The red and blue curves represent only the maximal and minimal coupling values with added Gaussian noise (average of 10 examples).*

*Three different oscillators are used to generate the signals: (**a**) Hénon maps, (**b**) Lorenz system nonlinearly driven by a Rössler system and (**c**) a Rössler system nonlinearly driven by Rössler.*

There is no significant decay when in noisy signals, indicating that this method remains robust and is able to detect significant nonlinear coupling, even in noisy signals. (Parameters used: In all analyses the following fixed embedding parameters were used: lag l = 10; embedding dimension m = 10; w1 = 100; NN = 10).

Interdependence concluding remarks

In principle I would like to state once more that there is no best method for quantitative analysis of EEG signals in general. The selection of an adequate method will depend on the type of signal to be studied and on the questions expected to be answered.

Hence, mean squared coherence (**§ 3.1.4**) is a straightforward linear measure of interdependence able to identify strong linear trends even in noisy environments, as shown from the previous signals.

When using the synchronization likelihood (SL) algorithm (**§ 3.4.4**) one should be aware that it may identify nonlinearities but is also strongly influenced by the linear trends as well. This becomes obvious in both oscillators except from Hénon where it demonstrates excellent behavior. When noise is involved the performance worsens drastically. In general, generalized synchronization (GS) is much more susceptible to noise than any other synchronization method. On the contrary, the GS measure introduced by Arnhold et al. (1999) (**§ 3.4.4**) seems to be a clearly nonlinear measure, robust in noisy environments and equally efficient in any oscillator generator. Clearly, the latter seems to be the most effective GS nonlinear interdependence estimator.

One should also bear in mind that all nonlinear methods presented require stationary signals. If this is not the case, one is better off using a linear alternative like wavelet coherence (**§ 3.2.5**), due to its inherent adaptive windowing scaling. Another alternative is phase synchronization (**§ 3.3**) calculation, PLV method in specific, which requires neither stationarity nor increases with amplitude covariance like coherence. In addition, since phase-locking on its own is adequate to indicate brain lobe interactions, PLV is superior because it is only based on the phase and does not consider the amplitude of the signals. However, an interesting extension in identifying the most significant regions, in terms of increased coherence, as compared to background signals is possible using the significant wavelet coherence (**§ 3.2.6**).

5.3 Visualization methods

As a conclusion of this thesis, the neurophysiologist should be interested in both the power estimation and interdependence of different brain lobes. The latter may be assessed using one linear and a couple of nonlinear ones (accessing PS and GS). Visual ways to illustrate the results and possibly fuse them together are the topographic maps and graphs. Topographic color maps (**§ 3.1.3**) maybe used in visualizing the power spectral-based estimations, where different colorings reflect altering brain activity. In addition, interdependencies may be illustrated using graph visualizations (**§ 3.6**), where channel pairwise coupling is visualized using lines (called edges) of increasing thickness with respect to increasing coupling strength.

5.4 Conclusion

Just before the main conclusion, probably a main remark should be made concerning the dynamically evolving research field of EEG. There is a need to advance and properly utilize the available analysis methods. Deterministic Chaos theory is a living proof of this, since the newly developed methods show how many systems in former times considered noise have in fact a deterministic chaotic nature.

In addition, the EEG signal itself is dynamic. In real EEG signals even if there are some really reproducible situations, i.e. EEG alpha oscillations are blockade with eyes opening, epileptic ictal activity; this is not always the case. Cognitive impairments and higher brain functions in general are hard to resolve, i.e., it is very difficult to design and maintain a psychological test under the exact similar conditions that could ensure the same subject responses and EEG measurements.

As the final conclusion of this thesis one should try to design experiments which will indicate reproducible signal patterns, but be able at the same time to choose and restrict the analysis using only the ideally suited methodologies. Hence, the discussion of the possibilities of these methods is of equal importance to a discussion about the nature of the EEG signal and the experimental setup. Hopefully, this thesis helps elucidating on the various available methodologies
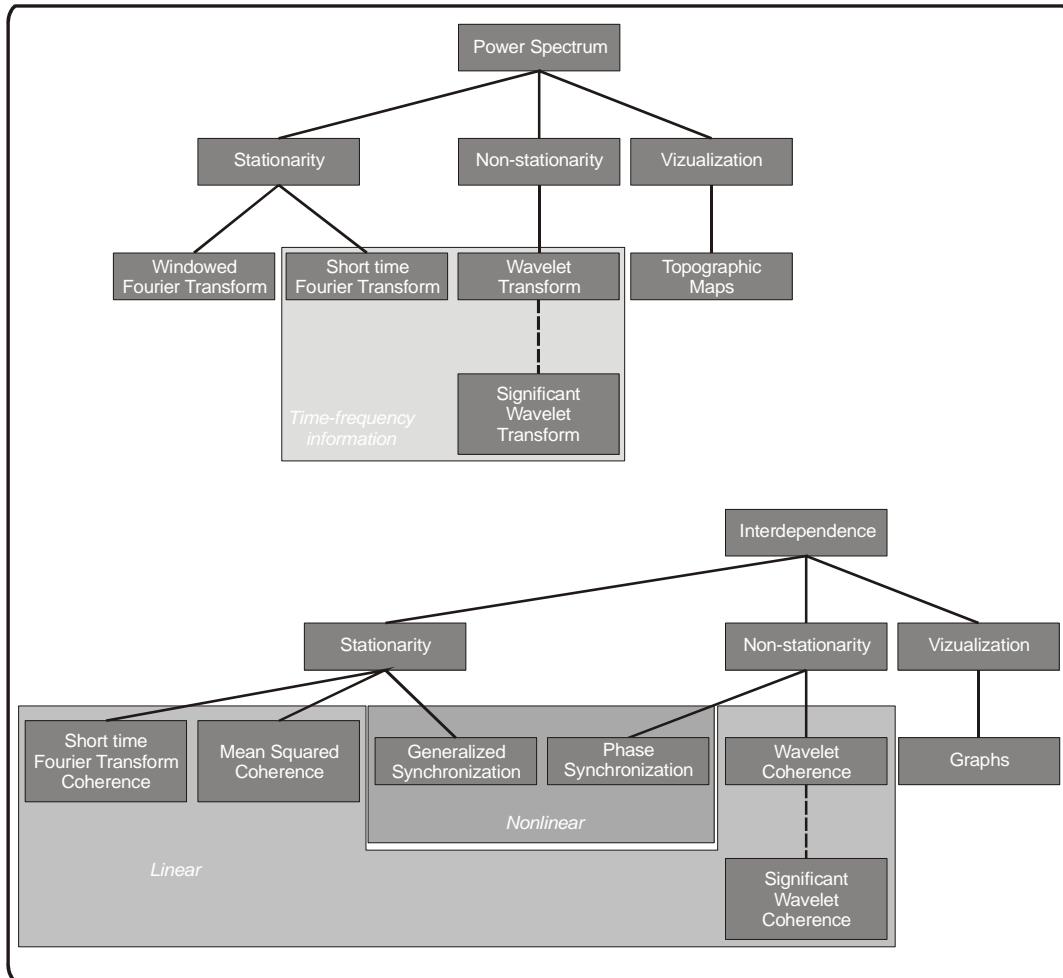
Figure 5.7: *Quick decision scheme for the presented methodologies. The main criteria for choosing the right approach may be summarized in the stationarity and possible linearity or nonlinearity of the process under investigation.*

presented along with the proposed extensions to form significant wavelet power and coherence estimation to better suit neurophysiologic data analysis. Of course there are certain alternatives in every methodology, which are also addressed throughout this thesis. The main criteria for choosing the right approach may be summarized in the stationarity and possible linearity or nonlinearity of the process under investigation. Figure 5.7 draws a quick decision scheme for the presented methodologies.

In this context, different methods have been applied to both cognitive brain functions, as well as certain pathologies.

The significant wavelet analysis was able to extract more precise information from the cortex reactions during mathematical reasoning. Activations were found mostly at frontal and central regions.

Traditional linear and nonlinear analysis methods were also applied on various brain regions to provide information regarding patterns of local and coordinated activity during performance of arithmetic tasks. Results indicated regionally increased neuronal signaling as a function of task complexity at frontal, temporal and parietal brain regions, although more robust task-related changes in EEG-indices of activation were derived over the left hemisphere. Both linear and non-linear indices of synchronization among EEG signals recorded from over different brain regions were consistent with the notion of more "local" processing in a number comparison task. Conversely, multiplication tasks were associated with a widespread pattern of distant signal synchronizations, which could potentially indicate increased demands for neural networks cooperation during performance of tasks that involve a greater number of cognitive operations.

Traditional spectral and coherence measures were also evaluated as indices of regional cerebral activation during performance of visuo-semantic analysis tasks (designed to tap into increasingly more complex operations regularly involved in the recognition of living animate objects) in neurologically intact adult volunteers. Results showed a significant linear increase in absolute power in the gamma band with increasing task complexity over left hemisphere frontal and occipital regions, and over right temporo-parietal regions.

Different measures of quantifying synchronous oscillatory activity based on different underlying assumptions were used to evaluate cognitive function (math and visual tasks) in controlled epilepsy cases, where children with controlled seizures are compared to controls. The results on the actual data suggested that higher frequency band gamma2 was mostly apparent in occipital-parietal lobes during visual tests.

Finally, the proposed significant wavelet coherence methodology was used to capture information about the temporal profile of synchronization disturbances present in the functional connectivity network of schizophrenia patients. Graph theoretical measures and visualization was capable of confirming the "disconnection syndrome" as proposed in the literature for schizophrenia.

All these results may contribute in elucidating brain dynamics. However, discovering and elucidating the way brain organizes itself seem to require a close partnership between theoretical and applied science. Fortunately, several

important research communities, worldwide, are currently working on similar or alternative methodological approaches, which will contribute in a certain practical value and will help to further elucidate not only brain pathologies, but also the functional "working brain". The great extent of related multidisciplinary approaches and interplay proves by itself the attractiveness of decoding brain and mind.

5.5   Future work and Recommendations

As noted throughout this thesis most of the methods presented, traditional linear or nonlinear, must assume some kind of stationarity. Therefore, changes in the dynamics during the measurement period usually constitute an undesired complication of the analysis, which in EEG may represent the most interesting structure in identifying dynamical changes in the state of the brain. Hence, a fundamental topic for further research should be the formation of a powerful test for stationarity able to indicate and reject, with increased certainty, the sections of the EEG raw signal that experience stationary behavior.

Another future research direction should focus on extending current interdependence analysis from bivariate to multivariate signals. This is important since pairwise analysis is likely to find plasmatic correlations in special cases where one driver drives two responses. In this case both responses may found to have a common driver component, even if the responses might be fully independent.

Finally, apart from the significant advances that have been achieved and applied in EEG analysis from a computational point of view, it becomes obvious that there is a large gap in effectively correlating diverse information sources towards the facilitation of reasoning and improved decision making. This gap is also enhanced by the fact that there are no clear protocols used when applying new not widely established analysis methods, such as the nonlinear ones. A consistent and expertise-independent fashion would be a valuable accomplishment. Probably neurophysiology should take also advantage of the multimodal integration (fusion), which will play a key role in the future of human brain research._

Bibliography

Andrzejak RG, Kraskov A, Stogbauer H, Mormann F, Kreuz T. Bivariate surrogate techniques: necessity, strengths, and caveats. Phys. Rev. E 2003; 68: 066202.

Arnhold J, Lehnertz K, Grassberger P, Elger CE. A robust method for detecting interdependences: Application to intracranially recorded EEG. Physica D 1999; 134: 419.

Hramov A, Koronovskii A. Generalized synchronization: a modified system approach. Physical Review E 2005a; 71: 067201.

Hramov A, Koronovskii A. Intermittent generalized synchronization in unidirectionally coupled chaotic oscillators. Europhysics Letters 2005b; 70: 169-175.

Schiff SJ, So P, Chang T, Burke RE, Sauer T. Detecting dynamical interdependence and generalized synchrony through mutual prediction in a neural ensemble. Physical Review E 1996; 54: 6708.
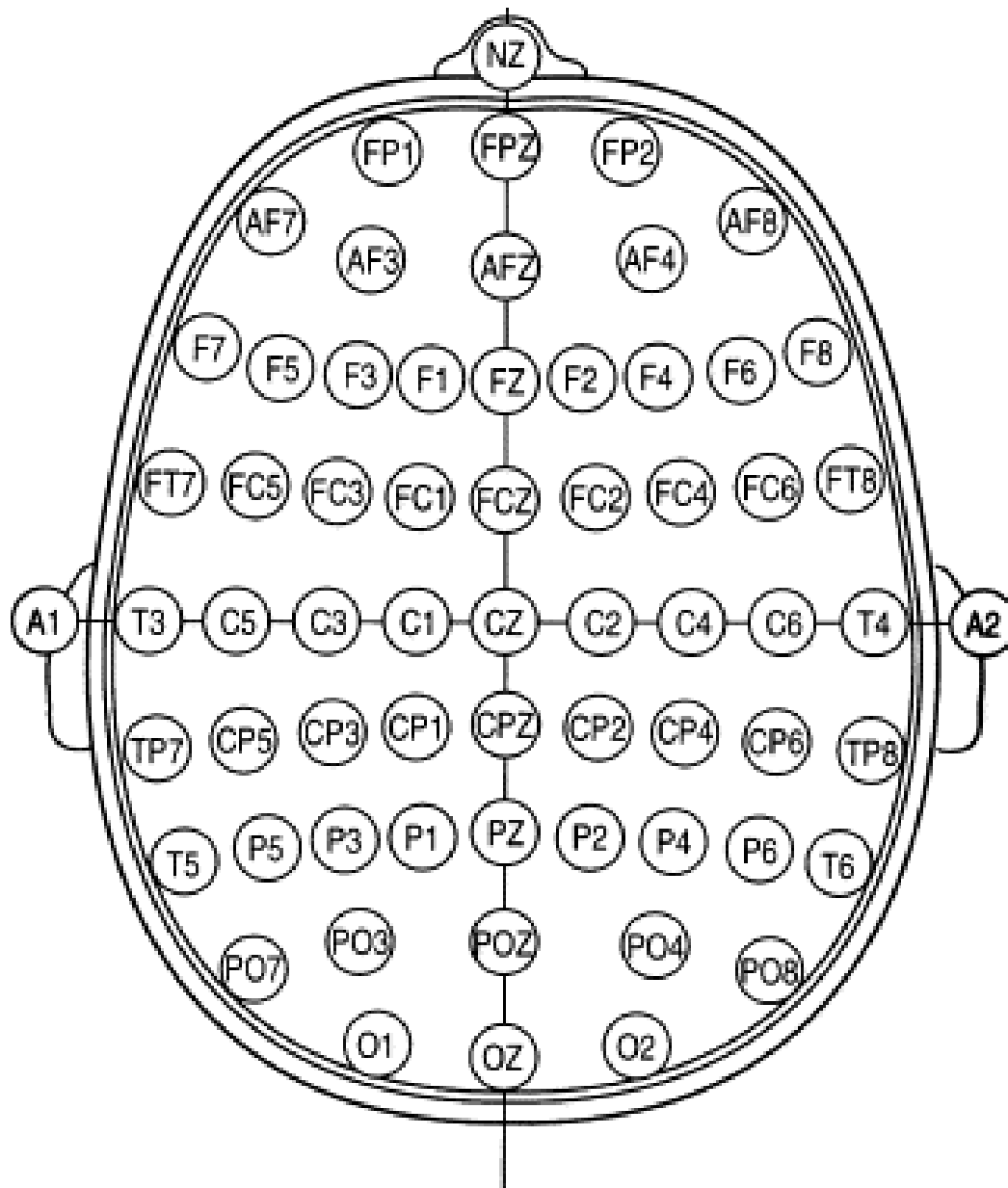
APPENDIX A

Figure A: *The modified 10-20 International System used throughout this thesis' experiments.*

APPENDIX B

B.1 The origins and physiology of the signals

The origin of the electrical potentials and currents lies in the neurons of the brain.

Neuron Structure

Neurons can have a variety of shapes, but a representative one that can be found in the Central Nervous System (CNS) is the multipolar neuron that has only one axon but multiple dendrites. Figure B.1 depicts the different types of neurons. The structural components of a neuron are the soma, the dendrites, the axon and the synapse. The soma contains a relatively large round nucleus with a prominent nucleolus. A variable number of dendrites, which are highly branched, extend out of the soma. The axon is a long cytoplasmic process capable of propagating an action potential. It can be myelinated or unmyelinated, as it will be discussed later on. Finally, a synapse is a specialized site of intercellular communication. There are two cells at every synapse, the pre- and postsynaptic cell, which transmits or receives a message, respectively.
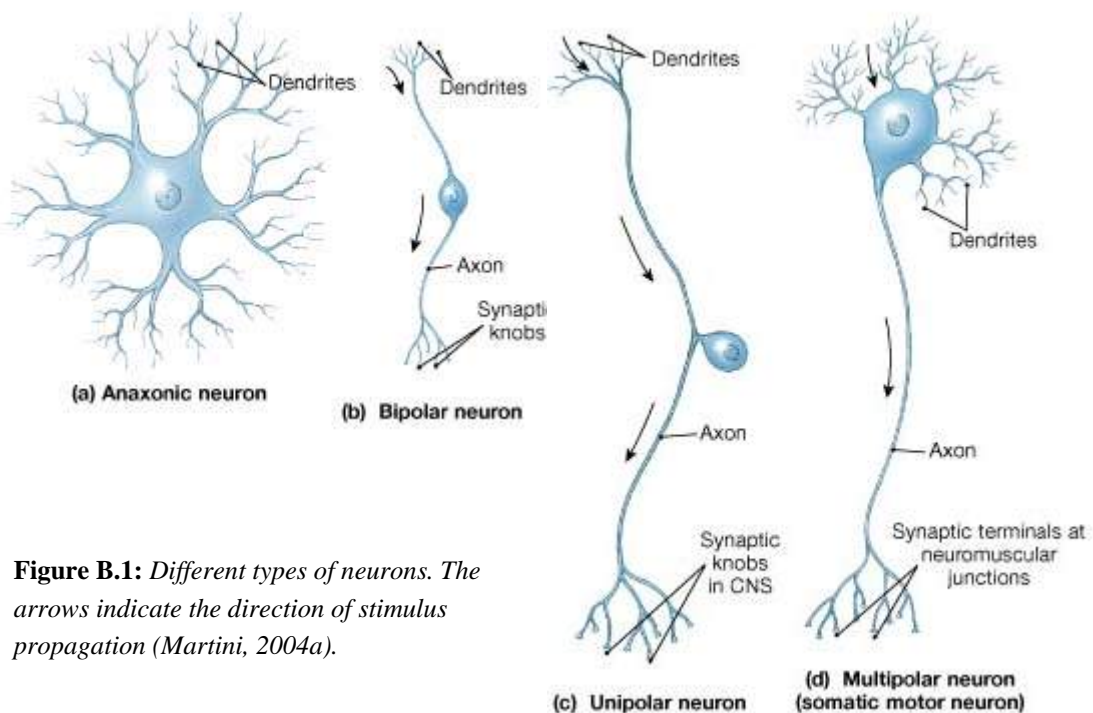

Figure B.1: *Different types of neurons. The arrows indicate the direction of stimulus propagation (Martini, 2004a).*

Neurons (like all cells) are bounded by the cell membrane (plasma membrane). Except from the structural support it offers, it acts as a physical barrier that separates the inside of the cell from the surrounding extracellular fluid. It regulates the exchange with the environment by controlling the entry of ions and nutrients and eliminating the wastes. Thus, it can be said that the cell membrane is selectively permeable. This membrane function of selectively permitting the ions to cross its membrane is crucial since it generates an unequal charge distribution and thus a potential difference known as the transmembrane potential. The inside of the cell membrane has a slight negative charge with respect to the outside, because there is a slight excess of positive charged ions outside the cell membrane and a slight excess of negatively charged ions inside the cell membrane. More specifically the extracellular fluid contains high concentration of sodium ions (Na^+) and chloride ions (Cl^-), whereas the intracellular fluid (cytosol) contains high concentrations of potassium ions (K^+) and negatively charged proteins (Pr^-). These ions can enter or leave the cell through different kinds of membrane channels, each with its own properties. There are also active mechanisms that move specific ions into or out of the cell. The passive channels are always open, whereas the active channels open –or close in response to specific chemical stimuli. These passive and active mechanisms do not ensure equal distribution of positive and negative charges across the cell membrane, since membrane permeability varies from one ion to another. This inner surface excess of negative charges with respect to the outer surface is resulting in a potential of approximately −70 mV, the so-called neuron *resting potential*, which is determined chiefly by the membrane permeability to potassium ions (Martini, 2004b).

Most gated channels are closed at the resting potential. The rate of ion movement across the cell membrane is regulated according to the opening of the gated channels resulting in transmembrane potential altering. The result may be a *graded potential* or an *action potential.*

Graded Potentials

When sodium ions enter the cell, thus arriving positive charges, shifts the transmembrane potential away from resting levels towards 0 mV or above. This effect is called *depolarization*. The movement of sodium ions across the cell membrane at one location causes the depolarization of the surrounding membrane.

Sodium ions entering the cell spread along the inner surface, attracted by the excess of negative charges. The arrival of these positive ions reduces the imbalance between negative and positive charges on the inside of the membrane and at the same time, extracellular sodium ions move toward the open channels, replacing those that enter the cell. This ion movement parallel to the inner and outer surfaces of a membrane produces a local current (Figure B.2) (Martini, 2004b). The depolarization effect degrades with distance (this is why these local potentials often called graded potentials) because the spread of the ions is not oriented to a certain direction but they just spread into cytosol. According to the same idea when a potassium channel opens, the outflow of potassium ions will lead the inside of the cell to the loss of positive ions; thus *hyperpolarization* is produced. In this case there is a potential shift towards −80 mV or less and again a local current is generated. Both depolarisation and hyperpolarization effects can be described as a current dipole, which in turn gives rise to currents in the surrounding tissues, the so-called volume currents (Karp, 1981; Plonsey, 1981).

Though, graded potentials may occur in the membranes of many different cell types, the dendrites, soma and presynaptic surfaces of a typical neuron support only graded potentials. Graded potentials are effective only in those neurons that commit short processes, like the anaxonic neurons and bipolar neurons in the eye. In this case a graded potential on a dendrite or soma can affect the transmembrane potential at the synaptic knobs and change the rate of neurotransmitter release. However, in other neurons the graded potentials on the dendrites and cell bodies are too far from the synaptic terminals to have any effect there. Hence another mechanism is needed that would provide the link between graded potentials at the
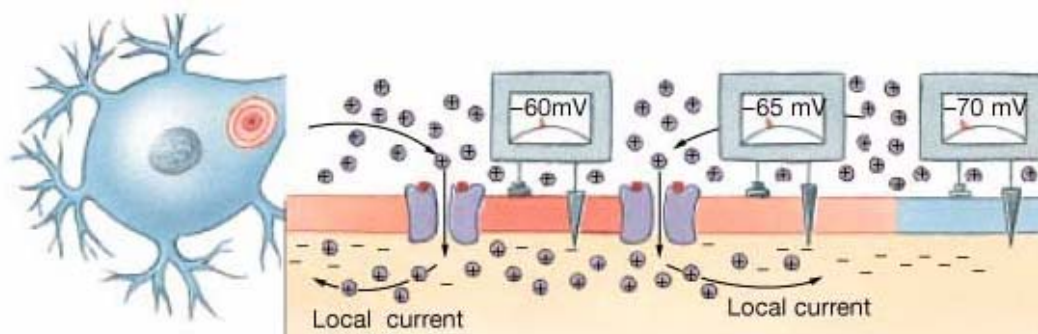

Figure B.2: *When the sodium channels open, the sudden influx of positive charges depolarizes the cell membrane (the potential changes towards −65 mV) and local currents develop as sodium ions spread along the inner surface of the membrane (Martini, 2004a).*
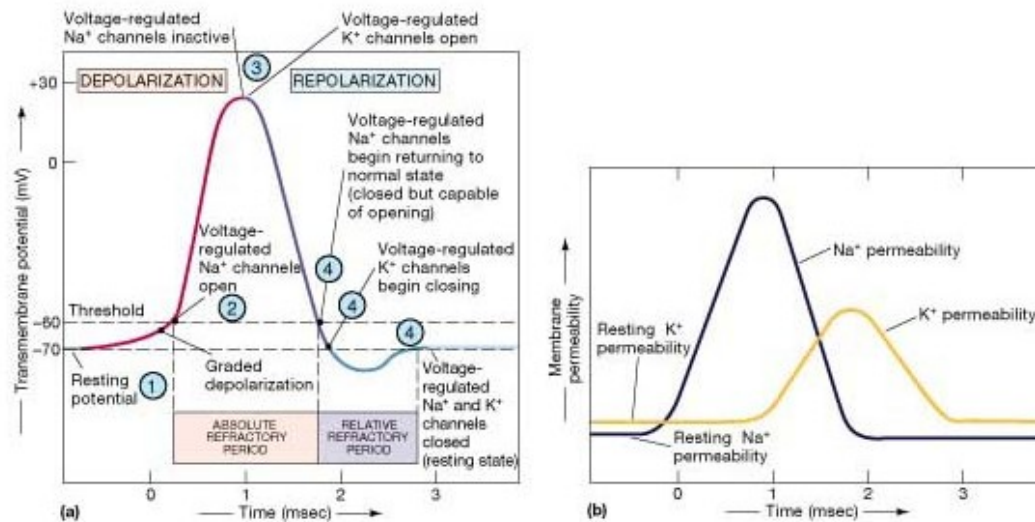
143

Figure B.3: *How the transmembrane potential* **(a)** *and permeability* **(b)** *change with respect to the steps involved in the generation of an action potential (Martini, 2004a).*

dendrites or soma and the synaptic terminals. *Action potentials,* which are generated only in the areas of excitable membrane that contain voltage-regulated channels, play this role, since they propagate along the axon.

Action Potentials

An action potential is initiated when a depolarization large enough to open voltage-regulated sodium channels occurs. Sodium channels open at a transmembrane potential typically between –60 mV and –55 mV, the so-called *threshold*. If the depolarization effect shifted the membrane potential from –70 mV to –62 or less, instead of an action potential, a graded potential would occur.

Briefly, the steps involved in producing an action potential, are the following:

1) Local currents associated with a graded depolarization of the soma depolarize the initial segment to –60 mV.

2) Na^+ channels are activated and a rapid depolarization drives the membrane potential to +30 mV.

3) Sodium channels are inactivated, whereas potassium gates open and potassium ions leave the cell, resulting in the initiation of the repolarization phase.

4) Return to normal membrane permeability (threshold). Na^+ channels return to resting position and K^+ channels begin closing. The membrane potential drops until all K^+ channels have closed.

The sequence described above (depicted in Figure B.3) takes place in a relatively small portion of the cell membrane. However, an action potential is stronger than a graded one and can affect the adjacent portions of the cell membrane. Each time a local current develops; the action potential moves forward and as a result continuous propagation occurs (the speed of which is about 1 m/sec). This can be easily explained if one imagines the cell membrane as a series of adjacent segments, as shown in figure B.4.

It should be noted that the former progression mechanism is met mostly on neural cells that form the gray matter of the brain. The axon of those neurons is unmyelinated, because a multilayered membrane that is called myelin does not wrap it. On the contrary, regions dominated by myelinated axons constitute the white matter of the brain. The latter have the ability of carrying the nerve impulses (the action potentials that travel along the axon) five to seven times faster that the previous unmyelinated ones. This is possible because the action potential appears to leap from node to node, skipping the intervening membrane surface. This more rapid propagation is named saltatory propagation.

Synaptic Transmission

In order for an impulse to travel from one neuron to another through a synapse, an electrical (with direct physical contact between cells) or chemical (involving a *neurotransmitter*) mechanism is needed. Electrical synapses are extremely rare; they can be found in some centers of the brain, like the vestibular nuclei. In this case the presynaptic and postsynaptic membranes are locked together, whereas in the case of chemical synapses there is no direct contact. The neurotransmitter (chemical release) may or may not be enough to pass an arriving impulse to the next cell. Hence, chemical synapses are far more dynamic and can be tuned by a variety of factors. The most common and studied neurotransmitter is the acetylcholine (ACh). Depending on their effects, neurotransmitters are classified as *excitatory* or *inhibitory*.

Excitatory neurotransmitters cause depolarization and promote the action potential generation, whereas inhibitory neurotransmitters cause hyperpolarization and depress action potential generation. Both neurotransmitter types can act on a synapse and the net result is the one that will regulate the postsynaptic transmembrane potential. *Postsynaptic potentials* are graded potentials (they affect only the area immediately surrounding the synapse) and can be *excitatory* (EPSP) or *inhibitory* (IPSP) on the basis of the type of neurotransmitter they develop.
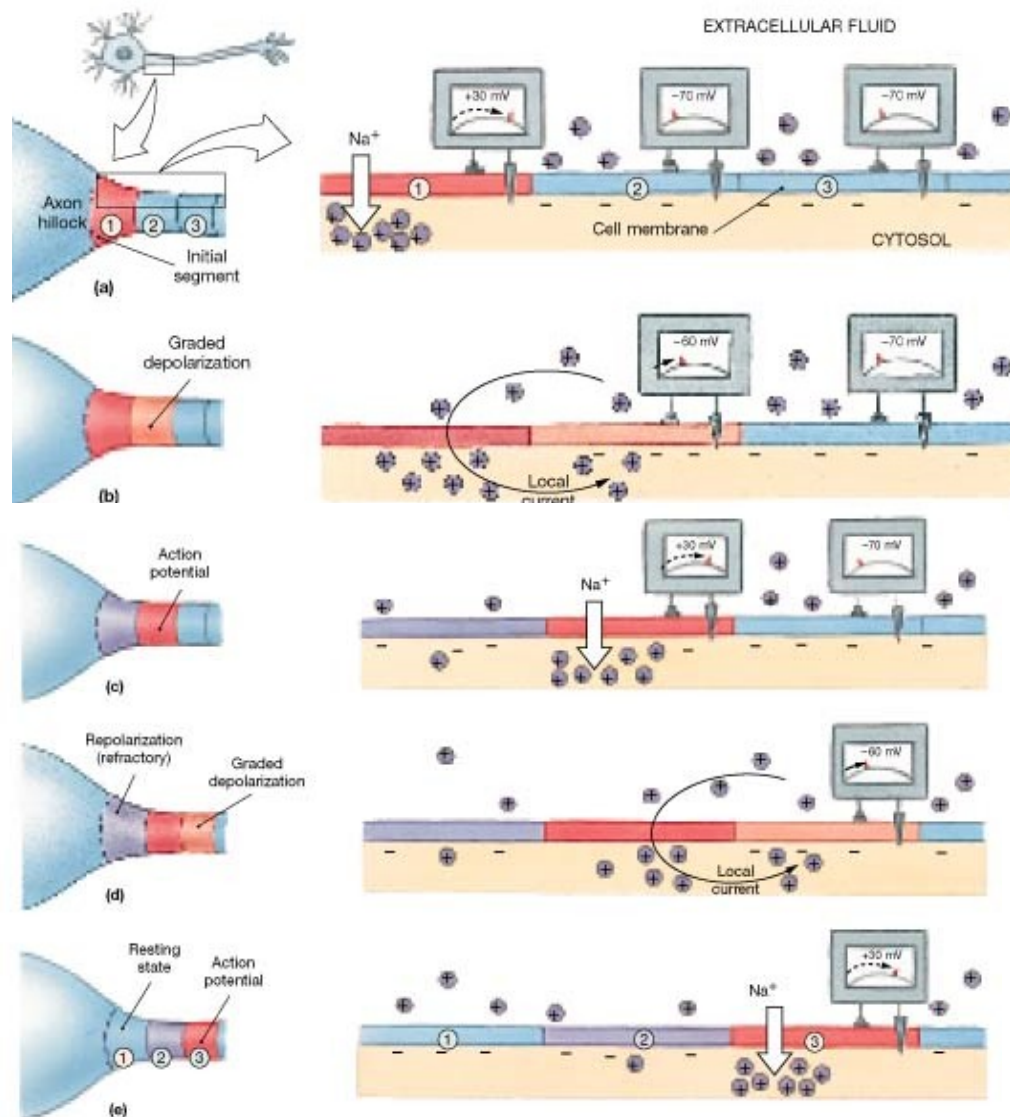
Figure B.4: a) *The transmembrane potential depolarizes to +30 mV as an action potential develops in the initial segment.* **b)** *A local current depolarizes the adjacent position of the membrane to threshold and* **(c)** *then an action potential develops there.* **d)** *A local current depolarizes the next segment of the axon and another action potential develops at the affected region of the membrane and the chain process proceeds to the next segment.* **e)** *It should be pointed out that the action potential proceeds away from the site of generation and cannot reverse direction because the previous segment is still in the absolute refractive period (Martini, 2004a).*

Individual EPSPs and IPSPs can be integrated and combined through the *summation* mechanism. Summation can be temporal (occurring at a single synapse when a second EPSP arrives before the effects of the first have decayed) or spatial (resulting from the cumulative effects of multiple synapses at various locations) as shown in figure B.5.

From a technical point of view a postsynaptic potential can be seen as a current dipole that exists only for several tens of milliseconds, whereas an action potential can be described by a quadrupole (Wikswo, 1983). Consequently, the EEG mainly registers the summation of the cortex pre- and postsynaptic potentials that last for about 10-250 msec (Niedermeyer and van Rotterdam, 1999), but not all of the cortical activity (Mitzdorf, 1988). The accumulation of charge outside the dendrite generates electric currents that flow through the surrounding media, causing the resulting current to change the electrical potential measured from the skin electrodes, because of the electrical resistance of the tissue (Ohm's law). Not only the type of neural cells, but the orientation and depth, play a significant role in the measured potential. Thus, the cortex and neural structure need to be studied.

The cortex is organized in layers parallel to the surface with each layer containing different types of neurons. Six layers (I-VI) can be discriminated, with
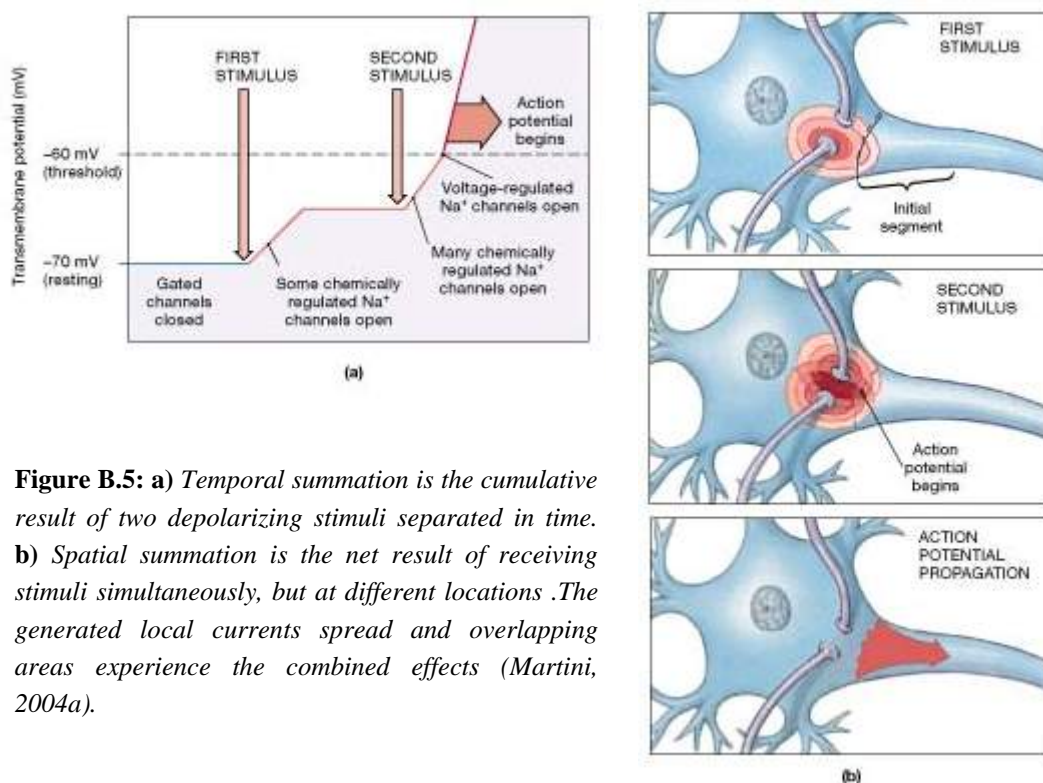

Figure B.5: a) *Temporal summation is the cumulative result of two depolarizing stimuli separated in time.* **b)** *Spatial summation is the net result of receiving stimuli simultaneously, but at different locations .The generated local currents spread and overlapping areas experience the combined effects (Martini, 2004a).*

layer I being the superficial one. The layers are:

I.   Molecular Layer

II.   External Granular Layer

III.   External Pyramidal Layer

IV.   Internal Granular Layer

V.   Internal Pyramidal Layer

VI.   Fusiform Layer

The cortical neurons are interconnected mainly in a direction perpendicular to the surface of the cortex. More specifically, layers II, IV and VI are populated with the so-called stellate cells, which have a star shaped form and do not generate significant electric field, whereas layers III and V consist mostly from pyramidal cells, which have a linear structure with dendrites arranged parallel to each other, resulting in electric field generation (Bear et al., 2007). Due to this symmetry the summation effect is much stronger in the pyramidal cells; hence their impact on the EEG is the strongest.

It should be noted that the ability of the EEG to acquire the electrical activity of the radially oriented pyramidal cells covers approximately 30 percent of the whole cortical activity. Unfortunately, the laterally oriented discharges are being invisible from the EEG, but may be inferred by measuring the coherence and phase of the EEG recordings. The latter is possible because of the covariance effect of distant or adjacent areas.

B.2 Measuring the EEG

Electrodes

The *electrodes* play a significant role in the proper and accurate data acquisition. The metal cap sitting at the end of the electrode wire can be made from a variety of materials. Gold disks are expensive, work well but must be disposed when their surface is scratched. Electrode scratches introduce artifacts. Plated chloride on silver is a very stable electrode but surface scratches again degrade their performance, whereas the more modern silver-silver chloride pellets of

amalgamates small pieces avoids this problem. Attention must be paid on the proper skin contact and preparation. Electrode-skin contact below 10 kΩ is essential. Skin preparation may be done with numerous commercial surface cleaners. In everyday practice, cap systems are used. These provide small holes to apply conductivity gel through. Moist gel application helps skin hydration and avoids skin damage. Finally one must ensure the stability of the electrodes, because every movement changes the conductivity and produces unreliable results.

Amplifiers and Filters

The potentials measured on the skin surface are in the order of a microvolt. Hence amplification is needed in order for the signals to be scaled and drawn in the display. A certain electrode is used as a reference, like the Cz electrode or maybe a montage of electrode mountings that mostly include the linked ears or even more complex electrode formations that use all available or adjacent electrodes. Amplifier inputs are shielded with impedance values capable of diminishing direct or static currents contacted from the patient. However, high impedance settings increase the sensitivity to field effects.

Moreover, the *amplifiers* need to filter out those frequencies that are higher or lower from the EEG spectrum (0 to over 1000 Hz). *High* and *low pass filters* combined (band pass filters) take care of this requirement. More specifically, a *notch filter* is applied, in order to remove the 50 Hz electrical interference frequency. This filter is a band pass filter with a notch at the specified frequency.

Analog to Digital conversion (ADC)

An *analog to digital converter* is the device needed to convert the continuous-time EEG signal (analog) to discrete (digital), which can be further processed in computers and microprocessors. The digital signal consists of a number of equally spaced samples. The resolution of the ADC specifies the accuracy of the conversion. However, a continuous signal can be exactly recoverable from the samples under the conditions specified by the sampling theorem (Shannon, 1949). This theorem assume that a signal can be reconstructed exactly, if the signal to be sampled is band limited and the sampling frequency is greater than twice the highest frequency in the signal to be sampled (Nyquist

principle). If the sampling theorem is not fulfilled the reconstructed signal is distorted. This effect is referred as *aliasing* (Oppenheim et al., 1997).

B.3 Sources and treatment of artifacts

Although EEG is designed to record cerebral activity, it also records electrical activities arising from sites other than the brain. An EEG artifact can be defined as the activity that even though registered in the EEG, does not reflect cortical activity. EEG artifacts can be classified in three broad categories; those arising from physiological processes, the exogenous ones and those coming from the Analog to Digital conversion (ADC). Physiological artifacts include eye blink and movement, as well as muscle, pulse, cardioballistic and electrodermal artifacts. The exogenous artifacts are introduced from movement, electrodes, electrical interference, field effect and instrument related artifacts. Finally, the artifacts coming from the ADC include quantum noise, non-linearity of the converter and thermal noise. In addition one should add the spectral leakage or Gibbs's artifact that is introduced when a Fast Fourier Transform (FFT) is attempted. The latter is discussed in the fore coming sections.

Physiological artifacts

Eye movements

Eye movement and blinking (Fig. B.8) introduces signal artifacts, because it involves the rotation of the electrical field of the eye. Eye movements are observed on all EEGs and are useful in identifying sleep stages. The fluids filling the front (aqueous) and back (vitreous) of the eye are separated by a membrane with a potential of approximately 100 mV. Hence, the eyeball acts as a dipole with a positive pole oriented anteriorly (cornea) and a negative pole oriented posteriorly (retina). When the globe rotates about its axis, it generates a large-amplitude alternate current field, which is detectable by any electrodes near the eye.

Vertical eye movements typically are observed with blinks, where the globes turn slightly upwards (Bell's phenomenon). A blink causes the positive pole (i.e., cornea) to move closer to frontopolar (FP1-FP2) electrodes, producing symmetric downward deflections. During downward eye movement the positive pole (i.e.,
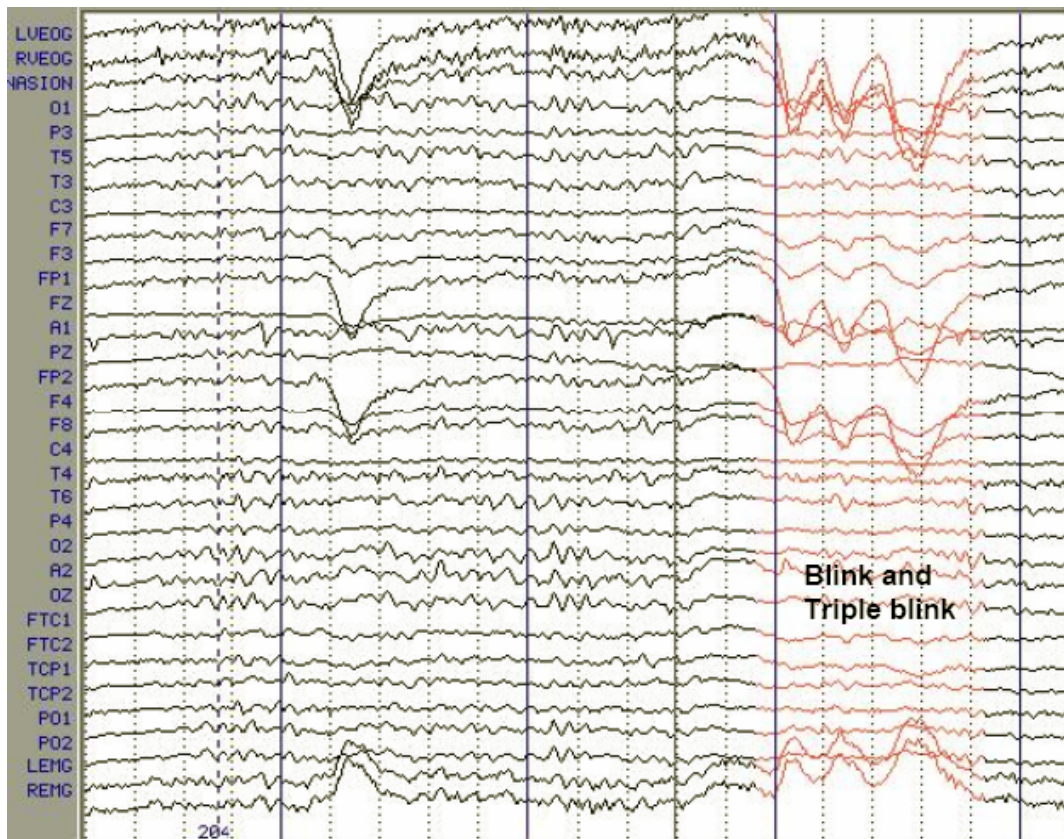
Figure B.6: *Eye blinking introduces signal artifacts, because it involves the rotation of the electrical field of the eye. Single and triple blink artifacts are obvious.*

cornea) of the globe moves away from frontopolar electrodes, producing an upward deflection.

Lateral eye movements most affect lateral frontal electrodes F7 and F8. During a left lateral eye movement, the positive pole of the globe moves toward F7 and away from F8. Using a bipolar longitudinal montage, maximum positivity in electrode F7 and maximum negativity in electrode F8 is recorded. With right lateral eye movement, the opposite occurs. Note also that very rapid spike potentials may occur during lateral eye movements of the lateral rectus muscles known as lateral rectus spikes.

The remedy entails the placing of slight pressure from fingertips on the surface of the eyelids in order to restrict the generated pulses from passing through. More often, off-line post processing regression techniques and adaptive filtering are applied.

151

Muscle activity

Myogenic potentials are the most common artifacts (Fig. B.7). Frontalis and temporalis muscles (i.e., clenching of jaw muscles) are common causes. Muscular discharges during contraction-tension of a muscle introduce biphasic high frequency short duration spikes. Though apparent in some extent even in low frequencies (10 Hz), their spectral power is also apparent at frequencies up to and exceeding 70 Hz. This artifact can be reduced by relaxation of the subjects. Particular patterns of *electromyogram* (EMG) artifacts can occur in some movement disorders. Essential tremor and Parkinson disease can produce rhythmic 4 to 6-Hz sinusoidal artifacts that may mimic cerebral activity. Hemifacial spasm is another disorder that can produce repetitive muscle artifacts due to a special type of EMG artifact that occurs during intermittent photic stimulation (flash), known as the photomyoclonic response. Some subjects contract the frontalis and orbicularis muscles approximately 50-60 milliseconds after each flash. They disappear after eye opening and use of paralyzers. They are located mostly frontally, and have no concomitant EEG changes.
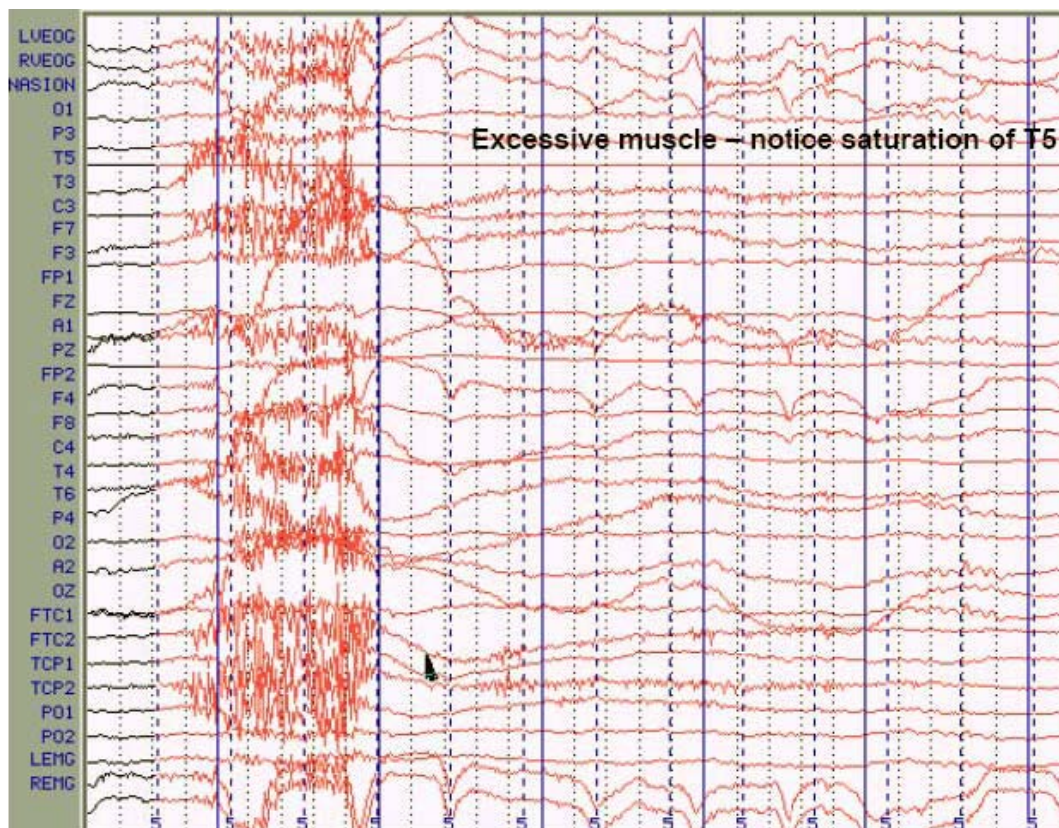

Figure B.7: *High frequency myogenic artifacts are the most common artifacts.*

Pulse & Cardioballistic artifacts

Pulse artifacts are due to the movement of the electrode-skin contact when an EEG electrode is placed over a pulsating vessel i.e., .due to a pressure wave from a heartbeat. These pulses arrive with a slight phase delay (200-300 ms) from the electrical pulses of the heart. Thus, an *electrocardiogram* (ECG) and the QRS complex (electrical component of the heart contraction) can be used to identify these pulses.

Cardioballistic artifacts are the sharp waves associated with the ECG, but also registered in the EEG. These can be reduced with linking of ears or using a complex electrode montage rather than a referential one (as noted in previous section).

Skin artifacts

Electrodermal effects can be seen when sweat (sympathetic nervous system signal) is excreted and the impedance is altered. The electrolytic salty solution of the sweat causes a direct current introduction to the EEG baseline. They can also be observed when a collection (i.e., subgaleal hematoma) is under or in the skin that produces asymmetry. In the latter case, the amplitude of the background rhythm is reduced in derivations from electrodes overlying the hematoma. Skull defects also can be the source of asymmetry. In this situation, amplitudes are greater in derivations from electrodes overlying or adjacent to skull defects.

Thermally induced sweating can be overcome using air conditioning, but emotionally induced sweating can be pharmaceutically treated by an injection of atropine, which is a sympathetic blocking agent.

Glossokinetic artifact

The tongue may also function as a dipole (similarly to the eyeball case), with the tip being the negative pole with respect to the base. The tip of the tongue is the more mobile part and can produce a broad potential field that drops from frontal to occipital areas, although it is less steep than that produced by eye movement artifacts. The amplitude of the potentials is greater inferiorly than in parasagittal regions, while the frequency is variable but usually in the delta range and occurs synchronously when the patient says "Lah-lah-lah-lah" or "Lilt-lilt-lilt-lilt," which can be verified by the technologist. Chewing and sucking can produce similar

artifacts. Such artifacts are commonly observed in young uncooperative subjects or in patients with dementia.

Respiration artifacts

Respiration can mainly produce two kinds of artifacts. One type is in the form of slow and rhythmic activity, synchronous with the body movements of respiration and mechanically affecting the impedance of (usually) one electrode. The other type can be slow or sharp waves that occur synchronously with inhalation or exhalation and involve those electrodes on which the patient is lying. Several commercially available devices to monitor respiration can be coupled to the EEG machine. The simplest way to monitor respiration is by the EEG technician making notations with a pencil (i.e., upward movement of the pencil for inhalations, downward return for exhalations).

Exogenous artifacts

Subject movement or generic movements in the environment

The first of the exogenous artifacts is the movement by the patient. It can generate in the muscular and pulse artifacts described above, which can be treated as mentioned above. Movement of other persons around the patient can generate artifacts, usually of capacitive or electrostatic origin.

Electrode artifacts

Electrode artifacts can be caused, if mismatched electrode metals are used, resulting in polarization of the amplifier's input stages. In the case of bad or damaged electrodes, intermittent spiking is apparent and imbalances in the amplifier's input are possible. The only solution is the regular checking of the electrodes. Electrode locomotion or popping can produce single or multiple sharp waveforms due to abrupt impedance change. It is identified easily by its abrupt vertical transient that does not modify the usual background activity of the distribution, which is limited to a single electrode. At other times, the impedance change is not so abrupt, and the artifact may mimic a low-voltage arrhythmic delta wave.

Alternating current artifact

Finally, mains interference (50 or 60 Hz depending on the country location) and the field effect artifact can be seen when electrical sources are close to the

patient or when the electrode impedances are unbalanced. 50-Hz artifact is diminished when a notch filter is used (as described in earlier section). The problem arises when the impedance of one of the active electrodes becomes significantly large between the electrodes and the ground of the amplifier. In this situation, the ground becomes an active electrode that produces the 50-Hz artifact. Practically, adequate grounding on the patient has almost eliminated this type of artifact from power lines.

Interference from high-frequency radiation from radio, TV, hospital paging systems and other electronic devices can overload EEG amplifiers. Shielding against external sources may prevent field effect artifacts. This is why EEG is usually recorded within a Faraday cage. One should also check the electrode impedances for imbalances.

Analog to Digital conversion artifacts

During the ADC process mainly three sources of artifacts (noise) degrade the quality of the signal[1]; quantum noise, converter's non-linearity and thermal noise.

Noise is a fundamental property of all physical systems that operate at finite temperatures. More specifically, quantum level noise power is given by the formula:

$$P_n = \frac{1}{q} \int_{-q/2}^{q/2} e^2 de = \frac{q^2}{12} \tag{B.1}$$

where q is the quantum step and depends on quantization's resolution. This type of noise is uniformly distributed.

Converter's non-linearity noise experiences the same statistical behavior as quantum noise. As a result the previous equation is multiplied by a factor of two squared, in the case of power calculation. Hence, (B.1) becomes:

$$P_n = \frac{q^2}{3} \tag{B.2}$$

---

[1] Signal to noise ratio (SNR) is a measure of signal strength relative to background noise. The measurement unit is the decibel (dB) and is expressed by the formula:

$$SNR = 10 \log (P_s / P_n)$$

where P_s and P_n is the power of the signal and noise, respectively.

Finally, thermal noise is the noise generated by thermal agitation of electrons in any conductor. The thermal noise is considered as random noise, which means that it consists from a large number of transient disturbances with a statistically random time distribution. It complies with the normal distribution and its power is given by:

$$P_n = kT\Delta f \tag{B.3}$$

where k is Boltzman's constant and Δf is the bandwidth. If added in equation (B.2) the result is again noise doubling. Thus, the power of the noise summed is:

$$P_n = \frac{2q^2}{3} \tag{B.4}$$

Assuming a full-scale sinusoidal signal of amplitude $2^{N-1}q$, one may calculate the power as:

$$P_s = \left[\frac{1}{\sqrt{2}} \left(2^{N-1} q \right) \right]^2 = 2^{2N-3} q^2 \tag{B.5}$$

and the signal to noise ratio will be:

$$SNR = 10\log\frac{P_s}{P_n} = 10\log\left(\frac{2^{2N-3}q^2}{2q^2/3}\right) = 10\log\left(\frac{2^{2N-4}q^2}{3}\right) = 6N - 7.3dB \tag{B.6}$$

This is the theoretical upper limit but in practice is not found to be above *5N*.

A simple, at least in theory, way of reducing noise artifacts is to lower as much as possible the temperature at which the electrical devices operate.

Conclusion

In everyday practice it is utopia to assert that the data will not contain artifacts, even if all of the above remedies are applied. In our study an extra step is included that ensures the rejection of the affected data, visual inspection from an expert neurologist. This manual process of checking and carefully selecting epochs increases the credibility and accuracy of the results gathered from EEG further analysis.

Bibliography

Bear FM, Connors BW, Paradiso MA. Structure of the Nervous System. In: Bear MF, Connors BW and Paradiso MA, editors. Neuroscience : exploring the brain. Philadelphia, PA: Lippincott Williams & Wilkins, 2007.

Karp P. Cardiomagnetism. In: Erné SN, Hahlbohm HD and Lübbig H, editors. Biomagnetism : proceedings, third International Workshop on Biomagnetism, Berlin (West), May 1980. Berlin ; New York: de Gruyter, 1981: 219-258.

Martini F. Fundamentals of anatomy & physiology. San Francisco: Benjamin Cummings, 2004a.

Martini F. Neural Tissue. In: Martini F, editor. Fundamentals of anatomy & physiology. San Francisco: Benjamin Cummings, 2004b.

Mitzdorf U. Evoked potentials and their physiological causes: an access to delocalised cortical activity. In: Basar E and Melnechuk T, editors. Dynamics of sensory and cognitive processing by the brain : integrative aspects of neural networks, electroencephalography, event-related potentials, contingent negative variation, magnetoencephalography, and clinical applications. Berlin ; New York: Springer-Verlag, 1988: xiii, 406 p.

Niedermeyer E, van Rotterdam A. Biophysical aspects of EEG and MEG generation. In: Niedermeyer E and Lopes da Silva FH, editors. Electroencephalography : basic principles, clinical applications, and related fields. Baltimore: Williams & Wilkins, 1999: 15-26.

Oppenheim AV, Willsky AS, Nawab SH. Signals & systems. Upper Saddle River, N.J.: Prentice Hall, 1997.

Plonsey R. Generation of magnetic fields by the human body (theory). In: Erné SN, Hahlbohm HD and Lübbig H, editors. Biomagnetism : proceedings, third International Workshop on Biomagnetism, Berlin (West), May 1980. Berlin ; New York: de Gruyter, 1981: 177-200.

Shannon CE. Communication in the Presence of Noise. Proc. of the IRE 1949: 10-21.

Wikswo JP, Jr. Cellular action currents. In: Williamson SJ, Romani G-L, L. K and I. M, editors. Biomagnetism : an interdisciplinary approach. New York: Plenum Press, 1983: 173-207.

CONTRIBUTING PAPERS

Significant EEG Features Involved in Mathematical Reasoning: Evidence from Wavelet Analysis

Vangelis Sakkalis*,†, Michalis Zervakis*, and Sifis Micheloyannis‡

Summary: Using electroencephalographic (EEG) signals and a novel methodology based on wavelet measures in the time-scale domain, we evaluated cortex reactions during mathematical thinking. Our purpose was to extract more precise information from the cortex reactions during this cognitive task. Initially, the brain areas (lobes) of significant activation during the task are extracted using time-averaged wavelet power spectrum estimation. Then, a refinement step makes use of statistical significance-based criteria for comparing wavelet power spectra between the task and the rest condition. EEG signals are recorded from 15 young normal volunteers using 30 scalp electrodes as participants performed one difficult arithmetic task and the results are compared with a rest situation. The results are in accordance with similar previous studies, showing activations of frontal and central regions. Compared with the alternative spectral-based techniques, the method we propose achieves higher task discrimination on the same dataset and provides additional detail-signal information to evaluate cortical reactivity during local cortical activation.

Key words: EEG; Wavelet analysis; Mathematical thinking; Brain activation; Significance tests.

Introduction

The analysis of EEG signals using linear (Dumermuth and Molinari 1987), as well as non-linear (Breakspear et al. 2003; Dahaene et al. 1999; Stam et al. 2002; Stam 2005) analysis methods derives valuable information regarding patterns of local and coordinated activity during the performance of cognitive tasks (Stam et al. 2003). Mathematical thinking as a cognitive process activates local but also more spatially distributed cortical networks depending upon task specificity and complexity (Micheloyannis et al. 2005). It is also strongly correlated with working memory capacity, language function and general intelligence. Simpler arithmetic tasks such as additions, subtractions, simple multiplication and divisions are correlated to language and long-term explicit semantic memory (Dahaene et al. 2004). Comparisons between quantities activate mostly the bilateral intraparietal sulcus (Delazer et al. 2006; Barth et al. 2006). Frontal and parietal regions are

---

*Department of Electronic and Computer Engineering, Technical University of Crete, Greece.

†Institute of Computer Science, Foundation for Research and Technology, Heraklion 71110, Greece.

‡Clinical Neurophysiology Laboratory (L. Widen), Faculty of Medicine, University of Crete, Heraklion, Greece

Accepted for publication: August 21, 2006; Published Online: September 19 2006.

Correspondence and reprint requests should be addressed to Vangelis Sakkalis, Institute of Computer Science, Foundation for Research and Technology, Heraklion 71110, Greece.

E-mail: sakkalis@ics.forth.gr.

the most referred in the literature related to mathematical thinking (Barnea-Goraly et al. 2005; Rivera et al. 2005; Dehaene et al. 2003). An asymmetry between left and right hemispheres with predominance of the left hemisphere in simple arithmetic calculations is often mentioned in the literature (Zhang et al. 2005; Rivera et al. 2005).

EEG signal analysis provides the advantage of high time resolution and thus it can deduce information related to both local and widespread neuronal activations in short time periods, as well as their time evolution. The Fourier transform (FT) and its windowed power spectral density function, known as periodogram (Stoica and Moses 1997), forms the most commonly used analytical tool for spectral representation and evaluation of activity on different EEG frequency bands (Dumermuth and Molinari 1987; Simos et al. 2002). However, this approach considers the EEG signal as a stationary process, which assumption is not satisfied in practice, thus restricting the actual confidence on results. An improved methodology is based on the time-varying spectral analysis that takes into account the non-stationary dynamics of the neuronal processes (Bianchi et al. 2000). The short-time Fourier (STFT) and the wavelet transforms are the most prevalent analysis frameworks of this class. The first approach uses a sliding time window, whereas the second one forms the projection of the signal onto several oscillatory kernel-based wavelets matching different frequency bands. The aforementioned time-varying methods have been applied in event-related potential (ERP) data, where distinct waveforms are associated

with an event related to some brain function (Bressler 2002). Under certain assumptions, both techniques are in fact mathematically equivalent, since they both use generic window functions that can take the same form and thus provide the same results (Bruns 2004). The reason why these approaches are often regarded as different relies in the way they are used and implemented. STFT uses a fixed window length, which leads to the dilemma of resolution; a narrow window leads to poor frequency resolution, whereas a wide window leads to poor time resolution, so that according to Gabor time-frequency uncertainty principle (Feichtinger and Strohmer 2002) one cannot accurately discriminate frequencies in small time intervals. The WT can overcome the resolution problem by providing actual multiresolution analysis. The signal may be analyzed at different frequencies with different resolutions achieving good time resolution but poor frequency resolution at high frequencies and good frequency resolution but poor time resolution at low frequencies. Such a setting is suitable for short duration of higher frequency and longer duration of lower frequency components of the EEG bands.

In this study we attempt to extract additional information (as compared to traditional spectral and wavelet analysis methods) by making use of the time profile of the EEG signal during the difficult mathematical test. For this test, more regions of the cortex are activated since the demands for a neural efficiency are increased and additional functions are implemented, not only from the regions responsible for mathematical reasoning but also from other tasks such as language. (Micheloyannis et al. 2005). Thus, these cognitive processes necessitate the extraction of information from different cortical regions. The motivation for this work stems from the fact that the WT method is able to extract not only the spectral activations but also the time segments in which they occur. It constitutes the cornerstone of our feature extraction scheme and is used in analyzing task-related or control EEG signals, by effectively capturing the significant increase or decrease of the power of the power spectrum (PS) of each band and channel. In particular, it encodes the activation differences between the mental states of interest. The proposed feature selection steps apply test statistics on the extracted "time-averaged" PS features. In addition, our approach introduces an extra refinement step that makes further use of the time profile provided by the WT, as to derive and encode the truly activated brain lobes and bands.

Methods

Subjects

The studied population consisted of fifteen right-handed volunteers (9 females and 6 males) of age range 21–26 years, mean age 23 years, who were medical school students at the University of Crete. They had normal or corrected-to-normal vision, and reported no history of brain injury or verbal/non-verbal learning disability. The procedures used in the study had been previously approved by the University of Crete Institutional Review Board and all subjects signed a consent form after the nature of the procedures had been explained to them.

EEG Recording and Test Description

We recorded the EEG signals in an electrical and sound attenuated room while the participants were seated comfortably on an armchair. First we recorded EEG for the control situation i.e., during a passive viewing condition when the participants simply focused at the centre of the computer screen on a small star. We inspected the recorded EEG on a PC screen and we stopped the recording when we had artifact free pieces of proper length, at least 8 s without artifacts. Subsequently, we repeat the process for an arithmetic task comprised of two-digit multiplication (e.g. 34 × 23, 49 × 32). Stimuli were presented on an LCD screen located in front of the participants at a distance of approximately 80 cm, subtending 2–4° of horizontal and 2–3° of vertical visual angle. The continuous EEG signals reported here were recorded from 30 scalp locations using an electrode cap (FP1, FP2, F7, F3, FZ, F4, F8, FT7, FC3, FCZ, FC4, FT8, T3, C3, CZ, C4, T4, TP7, CP3, CPZ, CP4, TP8, P3, PZ, P4, PO7, PO8, O1, OZ and O2, referenced to linked earlobe electrodes). Vertical and horizontal eye movements and blinks were monitored through a bipolar montage from the supraorbital ridge and the lateral canthus. The signals were amplified using a set of Contact Precision Instruments amplifiers (Cambridge, MA, USA—http://www.psylab.com), filtered on-line (band pass) between 0.1 and 200 Hz, and digitized at 512 Hz and 12 Bits. The recorded data were again carefully reviewed offline for technical and biogenic artifacts, so that only artifact free segments of eight seconds duration are further investigated. Each EEG channel segment involves 4096 data points and is analyzed as four non-overlapping epochs of 1024 samples. The frequency analysis bands are the "classical" ones: Theta (4–8 Hz), Alpha1 (8–10 Hz), Alpha2 (10–13 Hz), Beta (13–30 Hz), Gamma1 (30–45 Hz) and Gamma2 (45–90 Hz).

Data Analysis and Statistics

A generic overview of the methodology emphasizing the lobe selection and refinement blocks matching our data characteristics is presented in Figure 1. Over the past decade the WT has developed into an important tool for analysis of time series that contain non-stationary power at many different frequencies (such as the EEG signal), as well as a powerful feature extraction method
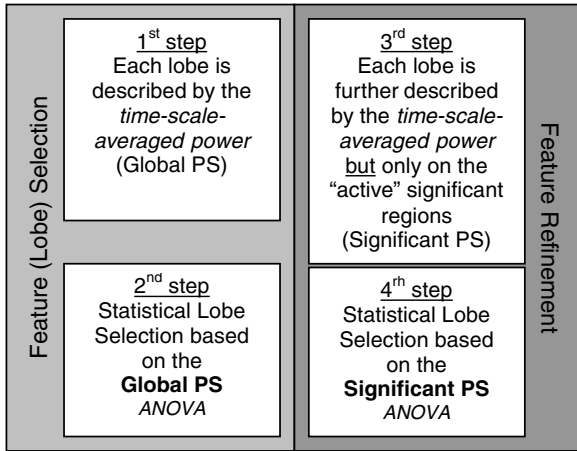
Figure 1. The diagram of the proposed algorithmic transitions, heading towards derivation of significant activity lobes and bands.

(Daubechies 1990; Kalayci and Ozdamar 1995). There are several types of wavelet transforms, namely the discrete (DWT) and the continuous (CWT), which involve the use of orthogonal bases or even non-orthogonal wavelet functions, respectively (Farge 1992). CWT is preferred in this work, so that the time and scale parameters can be considered as continuous variables. The WT employs the notion of scale s as an alternative to frequency, leading to the so-called time-scale representation domain. Details of the methodology applied and its mathematical rationale are provided in Appendix A.

Power spectra are projected onto six sequential frequency bands that are coarsely mapped to wavelet scales (Appendix A, Table A.I). The first step of the lobe selection method is based on capturing the time-averaged power spectrum $\overline{W}_t^2$ for each electrode and scale (Appendix A, equation. (A.2)). Furthermore, for the frequency bands of interest *the scale-averaged power spectrum* $\overline{W}_s^2$ is computed (Appendix A, equation. (A.3)).

Once the scale-averaged PS for each of the six EEG bands is calculated for each EEG channel and task, we have a total of 180 (6 × 30) feature vectors per task representing each subject, which is actually the time-scale averaged PS (Global PS - Figure 1—1st step). In order to reduce the degrees of freedom in the parametric analysis of PS and since entire cortical regions are assumed to function in a similar manner, data from adjacent electrode sites are averaged together to form four right and four left lobes: Frontal left (FL): FP1, F3, F7, FC3, FT7 Frontal right (FR): FP2, F4, F8, FC4, FT8, Temporal left (TL): FT7, T3, TP7, Temporal right (TR): FT8, T4, TP8, Central left (CL): FC3, C3, CP3, Central right (CR): FC4, C4, CP4, Parietal-occipital left (PL): P3, P7, O1, and Parietal-occipital right (PR): P4, P8, O2. Hence, the arithmetic

energy means for each subject, task, band and lobe are computed and entered into the next step for further statistical analysis.

The second step (Figure 1—2nd step) involves the statistical test selection, which depends upon the feature-vector properties and the experimental design. Normality of the log-transformed PS is tested using the D' Agostino-Pearson test (Zar 1999); no significant departure from normal distribution was found. Afterwards, analysis of variance (ANOVA) is employed for statistical hypotheses testing, with a critical level $p = 0.05$ for rejection of the respective null hypothesis, which may be stated as there are no differences between the "resting" and "mathematical reasoning" states. A related study design (the same subjects perform each task) using repeated-measures ANOVA (Zar 1999) is applied with common measures factors being the two Tasks and the eight Lobes. Greenhouse-Geisser-corrected degrees of freedom are used on data that do not meet the sphericity assumption. For those bands where the significance criterion is fulfilled, follow-up post-hoc tests for each lobe are performed to accentuate the most significant lobes.

The aforementioned steps indicate only a significant lobe subset, based on task differentiation confidence intervals using Global PS measures. Either synchronization or de-synchronization may be detected compared to the control task. To further refine the lobe/band selection step, we propose to isolate only those time segments of the EEG signal where notable activity differences occur from the control to the arithmetic task. The aim is to further map the EEG signal into a feature vector that best characterizes the EEG pattern of activity for the arithmetic task, in terms of significant temporal and spectral content. The fundamental idea here is to consider EEG energy differences between the mathematics and control tasks not over the entire duration of the signal but only over those time intervals where significant activation-deviations are recorded. As we are interested in ongoing EEG activity within various tasks, the time-localized activity differences of EEG events over the control task are of particular interest. Thus, we may describe the next step as an attempt to crop up the most significantly different regions from control to mathematics activity out of the bulk initial signal (may be either significant power increase or decrease while performing the requested task compared to the control condition). In fact, this study proposes a way to achieve "crucial" EEG time-segment selection, by testing for significance in the wavelet-time domain the "active" task over the "control" task (Significant PS—Figure 1—3rd step). Figure 2 depicts one subject's initial normalized EEG signal (Figure 2a) together with its WT (Figure 2b). The significant regions over the time-scale transformed domain that differentiate the two tasks are indicated by closed contours. Having derived
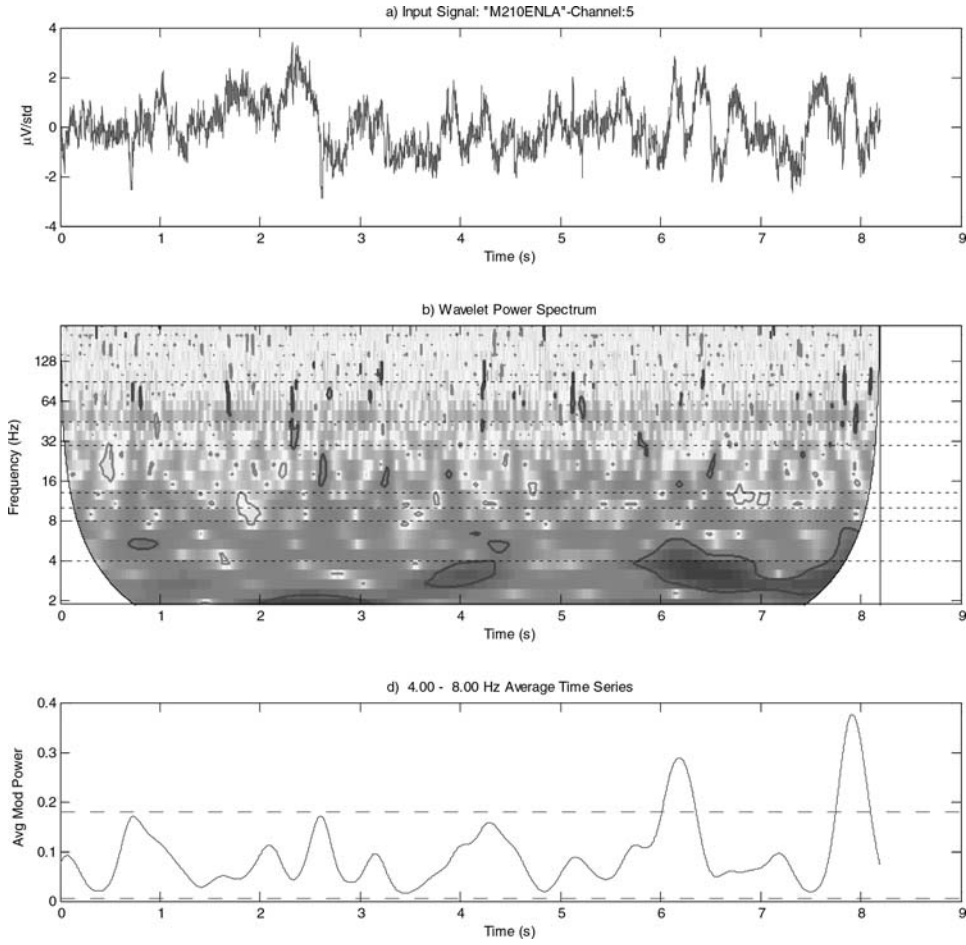
Figure 2. (a) A typical normalized EEG signal acquired from a single electrode. (b) The wavelet power spectrum presented as a color-coded picture. Mapped scales to frequencies are calibrated on the y-axis, with the horizontal dashed lines indicating the different frequency bands. The significant regions over the time-scale transform are indicated by the contours. Power increase and decrease is bounded by thick and thin contours, respectively. The outer elliptical region at the edges of the second graph indicates the cone of influence in which errors (edge effects) may be apparent due to the transformation of a finite-length series EEG signal (Torrence and Compo 1998). (c) The scalogram of a selected averaged band (Theta 4–8 Hz). The significance levels are indicated by the horizontal dashed lines. PS values greater above the upper dashed-line indicate increase, whereas PS values below the lower dashed-line indicates decrease.

this significant information, we are now able to form the so-called Significant Energy (Significant PS) features (Appendix A, equation. (A.4)), which form the time and band-scaled power levels over those time regions where apparent significant differentiation is indicated (within contours in Figure 2b). More details on the rationale and implementation of this refinement step are provided in Appendix A.

Finally, the last step (Figure 1—4th step) of the proposed feature selection methodology is actually a repetition of the testing in the second step on the new feature set. ANOVA statistics (as described previously) is used in order to further filter out the best lobes in terms of task discriminating power.

It should be noted that the proposed methodology is initially tested on simulated data, where there exist well defined spatiotemporal differences in frequency content between the target and control tasks (Appendix B). Successful task discrimination and lobe selection was achieved. Further application on the actual experimental dataset is presented in the following sections.

Results

The outcome of the proposed algorithm on the experimental dataset is summarized in Table I. The tabulated brain lobes are the significant ones extracted from the six frequency bands under investigation. The lobes indicated are the selected ones after the first statistical test (2nd step), which are those used as input for steps 3 and 4. The lobes indicated in bold are the refined ones

Table I. Statistical feature loss selection results

Band	Lobe (wavelet anaysis)
Theta (θ)	FL ↑ FL ↑
Alpha1 ($\alpha1$)	FL ↑ PL ↓
Alpha2 ($\alpha2$)	–
Beta (β)	–
Gammma1 ($\gamma1$)	FL ↑
Gammma2 ($\gamma2$)	FL ↑ CL ↑

Note. The tabulated brain lobes are the significant ones extracted from the six frequency bands under investigation. The lobes indicated are the selected ones after the first statistical test (2nd step), which are those used as input for steps 3 and 4. The lobes indicated in bold are the refined ones after the second statistical selection (4th step in Figure 1). The symbol "↑" and "↓" denotes power increase and decrease, respectively.

after the second statistical selection (4th step in Figure 1). The symbol "↑" and "↓" denotes power increase and decrease, respectively.

Increased Theta activity is observed on both frontal lobes. More prominent activity for the Theta bands is found on the FL lobe. Alpha1 band increase is found on the FL lobe, whereas decrease is found on the parietal left (PL) lobe. Related to the Gamma1 and Gamma2 bands, reactivity is detected on the FL lobe but more prominently around the central left (CL) region for the Gamma2 band.

To further validate the performance of the proposed methodology using wavelets vs. the traditional Fourier methods, a simple classification process is applied on the same dataset. The success rates using the Fourier based PS features calculated by the Fourier periodogram method on the same dataset, as described in our previous study (Micheloyannis et al. 2005), as well as the success rates of the proposed Significant PS features are indicated in Table II. The improved performance indicates with increased confidence that the lobes and features selected by the proposed methodology indicate brain regions truly responsible for the mechanisms involved in the task considered (mathematical thinking).

Table II. Cross validation of the actual data

Feature type	Success rate (%)
Energy (traditional fourier)	73
Significant energy	82

Note. Cross Validation (Leave-One-Out) Success Rates Using the Bayes—Quadratic Classifier For Various Features' Combinations. Classification scores denote the ability of the extracted features to encapsulate relevant information about the task so that they enable more accurate classification of each sample tested.

Discussion and Conclusions

Using the wavelet transform method on EEG signals, we evaluated cortical activation during a difficult mathematical task and compared it with a rest condition. This method, in contrast to traditional spectral ones, can estimate changes between EEG signals without being bounded to the stationarity assumption and can provide information for the entire time evolution of the signal. Traditional FT spectral analysis methods pose intrinsic limitations on encapsulating the time variation of the signal. Beyond traditional spectral analysis, the WT enables the consideration of time specific significant regions as in the 3rd step of the proposed methodology. WT is proved to be a useful measure to detect time-varying spectral power deviations from the control state and performs better than traditional time-frequency methods in identifying activity, especially on a shorter temporal scale in high frequencies, which could indicate neuronal synchronous activation in some cortical regions. This feature is very useful for estimating cortical activation of one or more lobes simultaneously, as usually required in neuropsychological studies. These activations are expressed, among others, with changes in high frequency, gamma bands (binding phenomenon) (Katsumi et al. 2003). This is an added advantage, since high frequency bands are weak in power and difficult to evaluate using spectral methods.

Numerous brain mapping studies exist that are related to mathematical thinking. Most of them were performed using fMRI, PET or electrophysiological signals. Most findings in these studies are in accordance with previous anatomical studies. Using these methods, local findings related to different kinds of mathematical thinking are detected mainly on frontal and central-parietal lobes. Frontal regions are constituents, among others, of frontal-subcortical, frontal-parietal and frontal-temporal circuits. These circuits have been proposed to activate memory while solving complex problems and play an essential role in the regulation of behavior. Their fronto-executive function is important in mathematical thinking (Lee and Kang 2002; Delazer et al. 2004; Barth et al. 2006). Parietal lobes are activated simultaneously with prefrontal and cingulated areas during mental arithmetic. However, bilateral intraparietal sulcus activations seem to play a central role in basic quantity representation and manipulation (Dehaene et al. 2004). Language areas are co activated during mental calculations especially simple arithmetic facts (Dehaene et al. 2004; Fernández et al. 1995; Van Harskamp et al. 2002). Since difficult mental calculation activates more cortical regions, the use of such a task engages more information from the cortex during the task and thus it is appropriate for comparing methodologies for characterization of brain activity.

The cortical activation, as derived in this study during the complex and difficult visually-presented multiplication task, was detected mostly frontal and expressed mainly by the theta and gamma bands. In addition, prominent CL activation on the left side, expressed by the gamma2 frequency band, was detected by the proposed refinement step (Figure 1, Step 4). This power increase of the frontal lobes with prominent left activation, the left central activation as well as the desynchronization of alpha1 band on the left parietal lobe (power decrease), are in accordance with the literature and our previous findings using Fourier spectral methods (Micheloyannis et al. 2005). The contamination with muscle activity is not present on the occipital regions and the frontal asymmetry cannot be explained as a result of EMG signal. Our previous work using nonlinear synchronization measures (synchronization likelihood) showed also differences in the gamma range that can not be due to muscle activity since it is not rhythmical in contrast to the gamma activity. However, using the present wavelet analysis method makes it possible to accentuate task differences during mathematical thinking beyond the traditional spectral analysis on the same material. In this sense, more prominent reactivity for the Theta and Gamma2 bands were found on the FL and CL lobe, respectively. Hence, the proposed method appears to be more sensitive in evaluating differences during cortical activations as shown by our results and the differentiation of the two hemispheres, which cannot be found by the traditional spectral method. Alpha band decrease (i.e., desynchronization) was evident on the left parietal lobe. The differences on theta, alpha1 and gamma2 bands are indicative of more prominent activation on the left hemisphere. Hemispheric differences in mathematical thinking were previously found mostly on simpler, language related mathematical processes (Zhang et al. 2005; Barth et al. 2006). Our findings are indicative of left prominent activation during difficult mathematical thinking as well. The prominent involvement of the left hemisphere during this difficult mathematical cognitive task is indicative of the activation of language areas, as was found with other methods during simpler mathematical tasks. This finding, in combination with the other activations of different lobes found, as well as the more clear results of reactivity of the gamma frequency bands, are of particular importance towards accurately addressing the cognitive processes involved in mathematical thinking.

Beta band activity was not identified by either the Fourier or the WT technique. In the previous spectral study (Micheloyannis et al. 2005), PL desynchronization in Alpha2 band was found, whereas WT indicates Alpha1 desynchronization in this region. This is explained as a result of the spectral leakage effect in the mapping between WT scales and frequency bands. More specifically, the narrow Alpha1 and Alpha2 bands are not clearly discriminated through the discrete scale mapping (Table A.I, Appendix A), causing the localization mismatch of these bands observed in the results of Fourier and WT techniques. Increased scale resolution could eliminate this mismatch.

The comparison of spectral methods to the WT show that the corresponding spectral features (i.e., spectral power at specific channels and bands) achieve a classification rate of 73%, whereas the features proposed in this paper (Table II) enable an increased rate of 82% (12 out of 15 subjects were classified correctly). Both, the WT method and the traditional Fourier technique are able to indicate with 95% confidence the task related lobes, but the WT method apart from achieving higher classification rate it can reveal additional signal characteristics, since it captures not only its average power but also the time variation of the signal.

Appendix A

In our application, we employ the normalized complex Morlet wavelet (Mallat 1997; Burrus et al. 1998) denoted as $|W_n(s)|^2$, where n denotes the discretized-time (sample) number and s indicates the scale. There exists a concrete relationship between each scale and an equivalent set of Fourier frequencies, often known as pseudo-frequencies (Mayers et al. 1993). This relation in our formulation is provided in Table A.I.

The control-task spectrum is defined as the mean time-averaged wavelet power spectrum over all subjects performing the control task.

$$\overline{W}_n(s) = (1/P) \sum_{p=1}^{P} \left| W_n^p(s) \right|^2 \qquad (A.1)$$

where p is the subject index and $W_n^p(s)$ is calculated for each subject and P is the total number of participants. It should be noted that all EEG signals are normalized to zero mean and identity variance. Further rescaling and comparisons are performed using each subject's actual

Table A.1. Frequency bands-scale set mapping

Band	Frequency Hz	Scale
Theta (θ)	4–8	21, 22, 23, 24
Alpha1 (α1)	8–10	20
Alpha2 (α2)	10–13	18, 19
Beta (β)	13–30	14, 15, 16, 17
Gammma1 (γ1)	30–45	11, 12, 13
Gammma2 (γ2)	45–90	7, 8, 9, 10

Note. Power spectra are projected onto six sequential frequency bands that are coarsely mapped to wavelet scales.

signal variance, in order to include subject-specific information. The control task spectrum in equation (A.1) is used as the baseline for detecting significantly different synchronization (or de-synchronization) during the mathematical thinking task, as depicted in Figure 2.

The time-averaged power spectrum $\overline{W}_t^2$ for each electrode and scale for each participant is computed by averaging the power spectrum $|W_n(s)|^2$ over time: (we drop the superscript p for notation convenience)

$$\overline{W}_t^2(s) = (1/N) \sum_{n=0}^{N-1} |W_n(s)|^2 \qquad (A.2)$$

Further averaging in scale is performed, in order to construct the frequency bands of interest. Thus, the scale-averaged power spectrum $\overline{W}_s^2$ is defined as the weighted sum of the wavelet power spectrum $|W_n(s)|^2$ over scales s_{j_1} to s_{j_2}:

$$\overline{W}_s^2 = (1/N) \sum_{n=0}^{N-1} |\overline{W}_{s,n}|^2 \qquad (A.3)$$

where

$$\overline{W}_{s,n}^2 = (\delta j \delta t / C_\delta) \sum_{j=j_1}^{j_2} \left(|W_n(s_j)|^2 / s_j \right)$$

where C_δ is a constant, scale independent factor used for the exact reconstruction of a delta $\delta(.)$ function from its wavelet transform (for the Morlet wavelet that was used, it equals to 0.776) (Torrence and Compo 1998).

Significant power increase is calculated using the 95% confidence level at each scale by multiplying the control task spectrum in equation (A.1) by the 95th percentile value for the chi-squared distributed variable χ^2 with two degrees of freedom (*DOF*) χ_2^2. This is justified because the wavelet power spectrum uses the Morlet wavelet in a complex product with the signal, so that both the squares of the real and imaginary parts of the result are being χ^2 distributed with one *DOF* each (Torrence and Compo 1998; Chatfield 1989). In a similar manner, significant power decrease is measured using as upper power limit the 5% confidence level at each scale by multiplying the control task spectrum in equation (A.1) by the 5th percentile value for the chi-squared distributed variable χ^2 with two degrees of freedom (*DOF*) χ_2^2. Figure 2 depicts one subject's initial normalized EEG signal (Figure 2a) together with the WT (Figure 2b). The significant regions over the time-scale transformed domain that differentiate the two tasks are indicated by the closed contours (thick and thin contours for significant power increase and decrease, respectively). Figure 2c illustrates another view of the scalogram focusing on a selected averaged band i.e., (Beta 13–30 Hz). The signif-

icance levels in this case are indicated by the horizontal dashed lines.

The proposed Significant Power Spectral features are obtained from the signal energy over those time- and band-localized regions, where apparent significant differentiation is indicated (contours in Figure 2b). For the computation of these features, equation (A.3) is adapted as:

$$\overline{W}_{st}^2(s) = (1/m) \sum_{m=m_i}^{m_{i+1}} |W_m(s)|^2, i = 1 \ldots I \qquad (A.4)$$

where m is the total number of time points delimited between the boundaries m_i and m_{i+1} of all significant regions I denoted by each contour in Figure 2b and i is the index of each significant region.

Appendix B

The two different tasks under investigation (rest and mathematical thinking) were simulated by two different groups of signals. The first group (control task) comprised of ten simulated signals, where each one was further divided into 5 channels. The idea is to reflect ten participants virtually registered with a 5 channel EEG system. Every channel, resembling the control task, comprised of randomly generated quasi-white noise signals, approximately 9 s long (500 Hz sampling rate—4608 samples). The second group (target task) comprised of three channels (channel 1, 3, 4) filled with quasi-white noise and two channels (channel 2, 5) with frequency modulated signals mixed again with quasi-white noise signals. Channel 2 consists of a time-varying theta EEG signal, linearly modulated (5–7 Hz) varying in length randomly between 512 to 1024 samples among subjects, occurring at a fixed latency, and a gamma EEG signal, linearly modulated (30–90 Hz) varying in length randomly between 1024–2048 samples among subjects, mixed with quasi-white noise. In a similar manner, channel 5 consists of an alpha band linearly modulated signal (9–12 Hz) varying in length randomly (768–1536 samples) and a gamma linearly modulated signal (30–90 Hz) varying in length randomly (512–1024 samples). Quasi-white noise covers the interval between the modulated signals. The performance of the algorithm was 100% successful in discriminating the different tasks and in providing information on the certain channels and bands that were significantly different than the control state.

Acknowledgments

References

Barnea-Goraly, N., Eliez, S., Menon, V., Bammer, R. and Reiss, A.L. Arithmetic ability and parietal alterations: A diffusion tensor imaging study in velocardiofacial syndrome. Brain. Res. Cogn. Brain. Res., 2005, 25: 735–740.

Barth, H., La Mont, K., Lipton, J., Dehaene, S., Kanwisher, N. and Spelke, E. Non-symbolic arithmetic in adults and young children. Cognition, 2006, 98: 199–222.

Bianchi, A.M., Mainardi, L.T. and Cerutti, S. Time-frequency analysis of biomedical signals. Trans. Inst. Measur. Controls, 2000, 22: 321–336.

Breakspear, M., Terry, J.R., Friston, K.J., Harris, A.W.F., Williams, L.M., Brown, K., Brennan, J. and Gordon E. A disturbance of nonlinear interdependence in scalp EEG of subjects with first episode schizophrenia. NeuroImage, 2003, 20: 466–478.

Bressler, S.L. The Handbook of Brain Theory and Neural Networks. In: M.A. Arbib (Ed.) MIT Press, Cambridge, MA, 2002: 412–415.

Bruns, A. Fourier-, Hilbert- and wavelet-based signal analysis: Are they really different approaches? J. Neurosci. Methods, 2004, 137(2): 321–332.

Burrus, S., Gopinoth, R. and Haitao, G. Introduction to wavelets and Wavelet transforms. Prentice Hall Inc., 1998.

Chatfield, C. The analysis of time series: An introduction, In: Chapman and Hall 4th edn. 1989: 241.

Daubechies, I. The Wavelet transform time-frequency localization and signal analysis. IEEE Trans. Inform. Theory, 1990, 36: 961–1004.

Dehaene, S., Molko, N., Cohen, L. and Wilson, A.J. Arithmetic and the brain. Curr. Opin. Neurobiol., 2004, 14: 218–224.

Deheane, S., Piazza, M., Pinel, P. and Cohen, L. Three parietal circuits for number processing. Cogn. Neuropsychol., 2003, 20: 487–506.

Dahaene, S., Spelke E., Pinel P., Stanescu R. and Tsivkin S. Sources of mathematical thinking: Behavioral and brain-imaging evidence. Science, 1999, 284: 970–974.

Delazer, M., Domahs, F., Lochy, A., Karner, E., Benke, T. and Poewe, W. Number processing and basal ganglia dysfunction: a single case study. Neuropsychol., 2004, 42: 1050–1062.

Delazer, M., Karner, E., Zamarian, L., Donnemiler, E. and Benke T. Number processing in posterior cortical atrophy — A neuropsychological case study. Neuropsychol., 2006, 44: 36–51.

Dumermuth, G. and Molinari, L. Spectral analysis of the EEG. Some fundamentals revisited and some open problems. Neuropsychobiol, 1987, 17: 85–99.

Farge, M. Wavelet transforms and their applications to turbulence. Annu. Rev. Fluid. Mech., 1992, 24: 395–457.

Feichtinger, H.G. and Strohmer, T. Advances in Gabor Analysis, In: Birkhäuser Boston (Ed.), 2002.

Fernández, T., Harmony, T., Rodríguez, M., Bernal, J., Silva, J., Reyes, A. and Marosi, E. EEG activation patterns during the performance of tasks involving different components of mental calculation. Electroenceph. Clin. Neurophys., 1995: 175–182.

Kalayci, T. and Ozdamar, O. Wavelet preprocessing for automated neural network detection of EEG spikes. IEEE Eng. Med. Biol. Mag., 1995, 14: 160–166.

Katsumi, U., Etsuro, H., Eiichi, T., Hiromasa, T., Keiichi, M., Taketoshi, O. and Hisao, N. Gamma-band EEGs predict autonomic responces during mental arithmetic. Neuroreport, 2003, 14: 477–480.

Lee K-M. and Kang S.Y. Arithmetic operation and working memory: Differential suppression in dual tasks. Cognition, 2002, 83: B63–B68.

Mallat, S. A wavelet tour of signal processing. Academic Press, 1997.

Micheloyannis, S., Sakkalis, V., Vourkas, M., Stam, C.J. and Simos, P.G. Neural networks involved in mathematical thinking: Evidence from linear and non-linear analysis of electroencephalographic activity. Neurosci. Lett., 2005, 373: 212–217.

Rivera, S.M., Reiss, A.L., Eckert, M.A. and Menon, V. Developmental changes in mental arithmetic: Evidence for increased functional specialization in the left inferior parietal cortex. Cereb. Cortex, 2005, 15: 1779–1790.

Simos, P.G., Papanikolaou, E., Sakkalis, E. and Micheloyannis, S. Modulation of gamma-band spectral power by cognitive task complexity. Brain Topogr., 2002, 14: 191–196.

Stam, C.J. Nonlinear dynamical analysis of EEG and MEG: Review of an emerging field. Clinical. Neurophysiol., 2005, 116: 2266–2301.

Stam, C.J., Breakspear, M., van Cappellen, A.-M. and van Dijk, B.W. Nonlinear synchronization in EEG and whole-head MEG recordings of healthy subjects. Hum. Brain Mapp., 2003, 19: 63–78.

Stam, C.J. and Dijk, B.W. Synchronization likelihood: An unbiased measure of generalized synchronization in multiple data sets. Physica D, 2002, 163: 236–251.

Stoica, P. and Moses, R.L. Introduction to Spectral Analysis. Prentice-Hall, 1997: 24–26.

Torrence, C. and Compo, G.P. A practical Guide to Wavelet Analysis. Bull. Am. Meteorol. Soc., 1998, 79: 61–78.

Van Harskamp, N.J., Rudge, P. and Cipoliti, L. Are multiplication facts imlemented by the left supramarginal and angular gyri? Neuropsychol, 2002, 1403: 1–8.

Zar, J.H. Biostatistical analysis. Prentice Hall Upper, Saddle River, New Jersey, 1999.

Zhang, Y.T., Zhang, Q., Zhang, J. and Li, W. Laterality of brain areas associated with arithmetic calculations revealed by functional magnetic resonance imaging. Chin. Med. J. (Engl.), 2005, 118: 633–638.

ELSEVIER

Neural networks involved in mathematical thinking: evidence from linear and non-linear analysis of electroencephalographic activity

Sifis Micheloyannis[a,*], Vagelis Sakkalis[a], Michalis Vourkas[a],
Cornelis J. Stam[b], Panagiotis G. Simos[c]

[a] *Medical Division (Laboratory L.Widén), University of Crete, 71409 Iraklion/Crete, Greece*
[b] *Department of Clinical Neurophysiology, VU University Medical Center, P.O. Box 7057, 1007 MB Amsterdam, The Netherlands*
[c] *Department of Psychology, University of Crete, Rethymno, Crete, Greece*

Abstract

Using linear and non-linear methods, electroencephalographic (EEG) signals were measured at various brain regions to provide information regarding patterns of local and coordinated activity during performance of three arithmetic tasks (number comparison, single-digit multiplication, and two-digit multiplication) and two control tasks that did not require arithmetic operations. It was hypothesized that these measures would reveal the engagement of local and increasingly complex cortical networks as a function of task specificity and complexity.

Results indicated regionally increased neuronal signalling as a function of task complexity at frontal, temporal and parietal brain regions, although more robust task-related changes in EEG-indices of activation were derived over the left hemisphere. Both linear and non-linear indices of synchronization among EEG signals recorded from over different brain regions were consistent with the notion of more "local" processing for the number comparison task. Conversely, multiplication tasks were associated with a widespread pattern of distant signal synchronizations, which could potentially indicate increased demands for neural networks cooperation during performance of tasks that involve a greater number of cognitive operations.
© 2004 Elsevier Ireland Ltd. All rights reserved.

Keywords: Mathematics; Electroencephalography; Power spectrum; Coherence; Non-linear synchronization

Mathematics plays an increasingly important role in our civilization, which is based to a great extent on advanced technology [3,4,12]. Some aspects of number processing such as reading, writing, and mentally manipulating numerical symbols rely heavily on general verbal abilities. Moreover, number facts (such as the multiplication table) are the subject of rote learning and are subsequently retrieved while performing more complex computations via automatic verbal associations [6]. More complex computations require, in addition to math fact retrieval, knowledge and fluent use of mathematical procedures. Performance on related tasks

is also strongly correlated with working memory capacity and general intelligence. Finally, a core process underlying general mathematical ability involves the number concept: an implicit understanding of the numerical quantities which is in turn based on serial or spatial representations. The number concept ability is required during performance of number comparison tasks [10].

Brain imaging studies show activation of a small region in the horizontal intraparietal sulcus during number comparisons [5,18]. Conversely, performance of complex calculations is often associated with activity in inferior frontal regions, while temporal lobe activity is typically found in tasks that require fact retrieval [6]. Hemodynamic brain imaging techniques, however, lack the temporal resolution necessary to reveal rapidly changing patterns of local neurophysiological responses and functional connections

* Corresponding author. Tel.: +30 693 243 1138.
E-mail addresses: mixelogj@med.uoc.gr (S. Micheloyannis), sakkalis@ics.forth.gr (V. Sakkalis), vourkas@physics.uoc.gr (M. Vourkas), cj.stam@vumc.nl (C.J. Stam), psimos@psy.soc.uoc.gr (P.G. Simos).

between brain areas that are part of the brain mechanism that supports performance of a particular cognitive task.

Neuronal signalling between specialized brain regions has been intensively studied in the last decade. Edelman, Tononi, Friston, Breakspear, and Stam are among the researchers who studied local and widespread interactions associated with cognitive function [1,2,13,21,22]. Local reactivity can be studied, among others, using spectral analysis such as the power spectrum (PS) of different EEG frequency bands [8,15,17,20]. Interactions among areas can be assessed using linear (like coherence [8,26]) and non-linear indices of synchronization among recording sites located above and near functionally interconnected neuronal networks (including a newly developed method, synchronization likelihood (SL) [23]). The question addressed in the present study is whether arithmetic tasks, which involve distinct mathematical operations, are associated with different patterns of local reactivity and distal connectivity. Specifically, it was hypothesized that power spectrum and coherence measures computed at and between areas located above different lobes would differ as a function to the nature of cognitive operations necessary to perform arithmetic tasks varying in complexity. Further, it was hypothesized that performance of these tasks would be associated with varying patterns of regional interactions reflecting task-specific cortico-cortical connectivity patterns.

For that purpose we recorded ongoing electroencephalographic (EEG) activity from 18 right-handed volunteers (9 females; aged: 21–26 years, mean 23 years, who were Medical School students in the University of Crete) during performance of arithmetic tasks differing in nature and level of complexity. All participants signed an informed consent form after the nature of the procedures were explained to them, had normal or corrected-to-normal vision, and reported no history of verbal or non-verbal learning disability (all medical students in Greece go through a rigorous national testing processes that includes advanced math and written composition). Stimuli were presented on an LCD screen located in front of the participants at a distance of approximately 80 cm, subtending 2–3° and 2–4° of horizontal and vertical visual angle, respectively.

Continuous EEG was recorded during performance of three arithmetic and two control tasks: (1) Four-digit number comparison (e.g., 5467 versus 6689; numbers in "different pairs" differed by less than 20%). The position of the larger number varied randomly, and participants had to raise their left index finger if the number on top was greater and their right finger if the lower was greater; (2) Single digit multiplication (e.g., 1×2, 2×3, 3×4, . . ., 5×6); (3) Two-digit multiplication (e.g., 34×23, 49×32). Participants were allowed 10 s from the time the number stimuli were presented on the screen until either a fixation spot was presented (in the number comparison task) or a number was briefly flashed on the screen (in the multiplication tasks) and participants were asked to say if the result was correct or not. Baseline EEG was recorded during a passive viewing condition (participants simply fixated at the centre of the computer screen,

on a small star), whereas a task involving passive viewing of single-digit numbers served as a second (visual) control condition. Stimulus presentation was always 1.5 s with an ISI of 0.5 s, during which a fixation star was presented.

The EEG signals reported here were recorded from 24 scalp locations using an electrode cap (FP1, F3, C3, P3, O1, F7, T3, P7, FC3, FT7, CP3, TP7, FP2, F4, C4, P4, O2, F8, T4, P8, FC4, FT8, CP4, TP8, referenced to linked earlobes). Vertical and horizontal eye movements and blinks were monitored through a bipolar montage from the supraorbital ridge and the lateral canthus. The signals were amplified using a set of Contact Precision Instrument amplifiers, filtered online with a band pass between 0.1 and 200 Hz, and digitized at 500 Hz. Data were visually inspected in order to identify biogenic artefacts, and an 8-s long artefact-free epoch was randomly selected for analysis for each task. In that way each epoch contained 4000 data points for each EEG channel. Given that the total average time that subjects were engaged in each task was in the order of 40 s, the length of the selected EEG epoch (8 s) was a representative sample of brain activity during task performance [20]. This was proper for the non-linear analysis since small number of data points is more likely to give spurious results.

PS and coherence analysis was performed using MATLAB (FFT, Hamming window, averaging the raw autospectra over four successive epochs of 2 s, averaging the coherence spectra for four 2-s data segments to compute coherence estimates for each EEG band). The absolute PS as well as coherence in the theta (4–8 Hz), alpha 1 (8–10 Hz), alpha 2 (10–13 Hz), beta (13–30 Hz), gamma 1 (30–45 Hz) and gamma 2 (45–90 Hz) bands were computed. In addition to coherence, a linear estimate of phase synchronicity among time series, we employed a complementary measure, synchronization likelihood, of the dynamical interdependencies between EEG segments recorded at different brain regions. SL is an estimate of the linear and non-linear synchronization of the EEG signal recorded at a given electrode site, in relation to other electrodes. In contrast to coherence, synchronization likelihood measures linear as well as non-linear interdependencies and it can do so as a function of time, making it suitable for non-stationary time series [23]. There is mounting evidence for weak but significant non-linearity in the EEG [22,23]. Nevertheless, using the SL parameter, we did not test for non-linearity with surrogates since our approach was to compare the differences between the tasks using, additionally, coherence estimates. Linear, in combination with non-linear methods have been used in several studies during the last years for better evaluation of brain function [14], since EEG signals have both stochastic (non-stationary) and deterministic (stationary) properties. It is assumed that high synchronization (measured by coherence and SL), especially for the slow spectral bands, between one or more adjacent electrode sites and other sets of electrodes indicates neural networks interactions that take place during performance of a particular cognitive task. For instance, local desynchronization in the range of the alpha bands is indicative of local activation

and can be accompanied by lower local coherence with other regions since the neurons in this region are locally closely functional interconnected during this activation [26]. Different patterns of oscillatory activity are believed to reflect distinct dynamic properties of neuronal assemblies in underlying neuronal networks that participate in different functions. Results from several research groups clearly demonstrate that it is not possible to assign a single function to a given type of oscillatory activity. Additionally, these oscillations have multifold functions and act as universal operators or codes of brain functional activity. Nevertheless, knowledge has been accumulated concerning the relation of some basic functional properties of different frequency bands [16,19,24,25].

In this study, we first computed SL for the range of EEG signals where most of the signal power is found (i.e., between 0.5 and 30 Hz) to evaluate a wide range of potential functional components represented in different frequencies as well as more complex patterns of interdependencies that were not frequency-specific [9,22,23]. In order to identify the EEG bands that contribute more prominently to the broadband SL results, SL values were subsequently computed for each EEG frequency band separately. In order to reduce the degrees of freedom in the parametric analyses of PS and SL, data from adjacent electrode sites were averaged together to form four areas over each hemisphere: Frontal (FP1, F3, F7, FC3, FT7 or FP2, F4, F8, FC4, FT8), Temporal (FT7, T3, TP7 or FT8, T4, TP8), Central (FC3, C3, CP3 or FC4, C4, CP4), and Parietal (P3, P7, O1 or P4, P8, O2). The (absolute) PS values were computed for each frequency band and each electrode. The SL parameters were first computed between each individual electrode and the remaining 23 electrode sites. Electrode-specific PS or SL values for each condition were then averaged across the three or five electrodes that were grouped together according to their location with respect to lobes. Coherence values were extracted between groups of electrodes representative of the five brain regions in each hemisphere: Frontal (FP1-F7, FP1-F3, F7-F3, FP1-FT7, FP1-FC3, or FP2-F8, FP2-F4, F8-F4, FP2-FT8, FP2-FC4), Temporal (FT7-T3, T3-TP7, FT7-TP7 or FT8-T4, T4-TP8, FT8-TP8), Central (C3-CP3, CP3-P3, TP7-CP3, P3-P7, or C4-CP4, CP4-P4, TP8-CP4, P4-P8) and Parietal (P3-O1, P7-P3, P7-O1, or P4-O2, P8-P4, P8-O2) representing local coherence measures, and Frontal–Temporal (FP1-CP3, FP1-P3, F3-CP3, F3-P3, FC3-P3 or FP2-CP4, FP2-P4, F4-CP4, F4-P4, FC4-P4), representing distant coherence. Local and distant coherence data were analyzed separately in order to deal with scaling issues (local coherence values can be more accurate than distant estimates). PS, SL, and coherence data were analyzed separately using SPSS 12.0. Common repeated measures factors in all ANOVAs were Task (5) and Hemisphere (2). For Ps, SL and local coherence data the third within-subjects factor included in the ANOVAs was region (Frontal, Temporal, Central, and Parietal). Distant coherence data (estimated coherence values between frontal and temporal sites) were submitted to a two-way, repeated measures ANOVA with Task (5) and

Hemisphere (2). In order to evaluate task-related trends associated with operational complexity (and difficulty), tasks were entered in the ANOVAs in the following order: Simple fixation, viewing numbers, number comparison, single-digit multiplication, two-digit multiplication. Greenhouse–Guyser-corrected degrees of freedom are reported below for tests performed on data that did not meet the sphericity assumption.

We begin presentation of results from a well-established measure of local neuronal synchronization, the absolute power of rhythmic activity in successive frequency bands. As expected on the basis of task complexity and difficulty, spectral power of fast rhythmic activity (gamma 1–2) increased linearly across tasks. This trend although present bilaterally reached statistical significance (at the $0.05/3 = 0.0125$ level) over the left hemisphere (Frontal: $F(1,17) = 13.96$, $p < 0.002$, Temporal: $F(1,17) = 12.45$, $p < 0.003$, Central: $F(1,17) = 10.61$, $p < 0.005$, Parietal: $F(1,17) = 11.77$, $p < 0.003$). Fig. 1 displays representative data for the frontal and parietal regions which clearly suggest that the task-specific trends found did not reflect spurious changes in high-frequency rhythmic activity due to myogenic artefacts (if that were true task effects would be restricted to frontal sites where these artefacts are more prominent). The opposite trend was found for power in the alpha 2 band. This increasing local desynchronization (i.e., reduction in alpha power) was statistically significant only at Central (right hemisphere: $F(1,17) = 12.87$, $p < 0.002$) and Parietal areas, bilaterally (left: $F(1,17) = 9.93$, $p < 0.006$ and right: $F(1,17) = 11.11$, $p < 0.004$). Both data sets are shown in Fig. 1 for comparison. Another interesting finding concerned the linear increase in power in the theta band that was restricted to frontal sites, bilaterally (left: $F(1,17) = 10.59$, $p < 0.005$ and right: $F(1,17) = 8.31$, $p < 0.01$). There were no significant hemispheric asymmetries for any of the tasks.

In general, task-related variation for local coherence estimates paralleled systematic changes in corresponding PS data: coherence in (slow) alpha 2 band decreased with task complexity/difficulty. Fig. 2 graphically displays a significant linear trend for coherence in the alpha 2 band computed among frontal sites over the left hemisphere, $F(1,17) = 10.99$, $p < 0.004$. Systematic reduction in phase synchrony (coherence) in the alpha band, among adjacent electrodes, may reflect a similar phenomenon, i.e., desynchronization among neuronal populations in the left frontal lobe as they become increasingly more engaged in the complex arithmetic tasks.

Inspection of mean SL values computed over the entire range of EEG frequencies, indicated notable changes in the degree of long-distance neuroelectrical synchronization across tasks. Representative trends for each of the four recording regions are shown in the upper panels of Fig. 3. Specifically, SL values were lowest for the number comparison task, higher for the single-digit multiplication task, and highest during performance of the more difficult, two-digit multiplication task. The profiles of task-related changes in SL were somewhat different at more posterior sites: SL
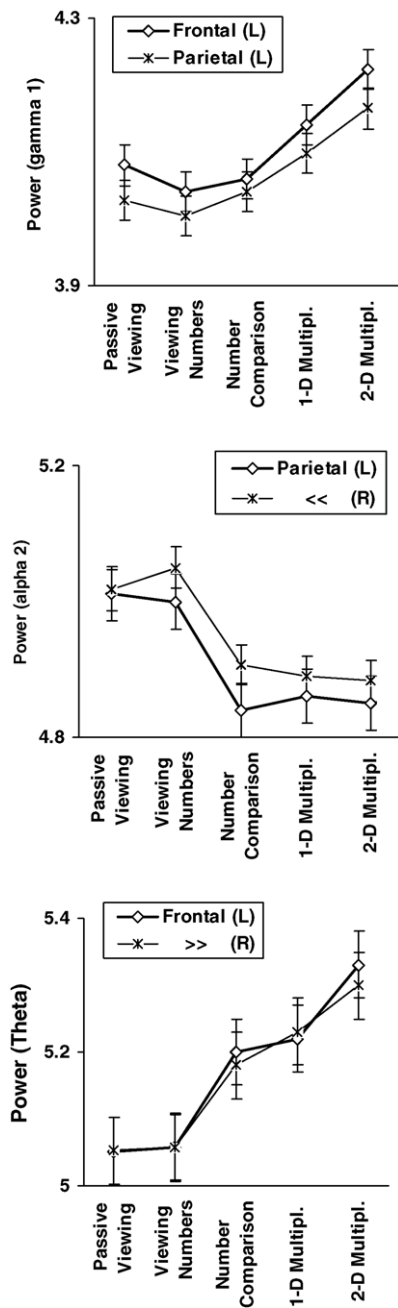
Fig. 1. Power in the gamma 1, alpha 2, and theta bands at frontal and parietal sites. Systematic change in power (PS) in three EEG bands (top: gamma 1, middle: alpha 2, bottom: theta) as a function of task. Significant linear trends were found in all cases. Vertical bars represent standard error values.
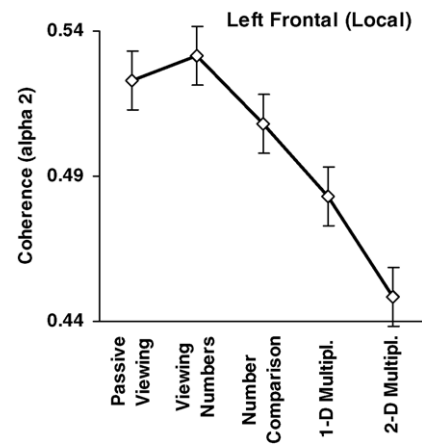

Fig. 2. Coherence in the alpha 2 band at left frontal sites. Linear trend of coherence estimates computed between left frontal electrode sites as a function of task. Standard error in vertical bars.

signal synchronization between parietal and central areas and the rest of the brain regions, during performance of the most difficult arithmetic task as compared to the number comparison task (see Table 1). A similar increase in SL was noted between both frontal and temporal areas and the remaining of the brain regions, but this time during performance of either
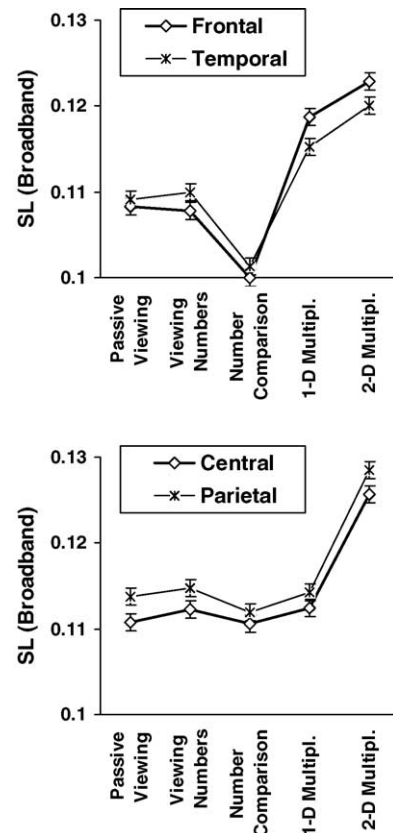
Fig. 3. SL values for broadband EEG signals and for slow frequency bands. Plots of significant trends involving task for the synchronization likelihood parameter, computed over a range of key EEG frequencies (0.5–30 Hz; upper panels) and, separately, for two frequency bands (theta: lower left, and alpha 2: lower right panels).

values were similar for the two control tasks, the number comparison and the single-digit multiplication arithmetic tasks and notably higher during performance of the two-digit multiplication task. These observations were confirmed by the presence of significant main effects of task at Frontal, $F(4,68) = 5.43$, $p < 0.001$, Temporal, $F(4,68) = 5.43$, $p < 0.0001$, Central, $F(2.63,44.63) = 4.35$, $p < 0.012$, and Parietal areas, $F(2.66,45.24) = 4.89$, $p < 0.012$.

Finally, analyses on the broadband SL data indicated significant or marginally significant increases in the amount of

Fig. 3. (*Continued*).

Fig. 4. Coherence in the theta band between frontal and temporal sites. Non-significant trends for coherence data in the theta band. Vertical bars represent standard error values.

calculation task as compared to the number comparison task that does not require arithmetic calculations.

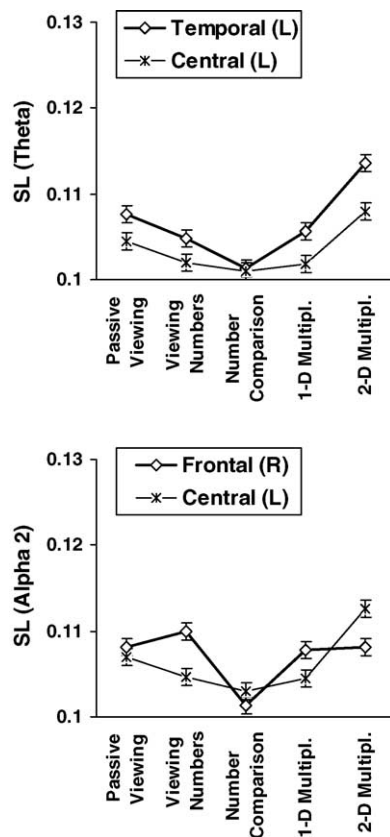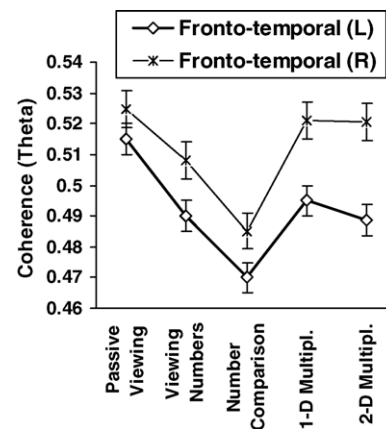Further analyses on SL data computed separately for each band indicate that the pattern of task-related variation observed in the broadband data, was primarily due to changes in linear and non-linear synchronization in the "slow" bands, mainly alpha 2 and theta. Significant task main effects and quadratic trends were found for theta at right Temporal $F(1,17) = 14.43$, $p < 0.001$, and left Central sites, $F(1,17) = 13.46$, $p < 0.002$, and for data in the alpha 2 band at right Frontal, $F(1,17) = 10.56$, $p < 0.004$, and left Parietal sites, $F(1,17) = 11.11$, $p < 0.003$. SL results, providing estimates of primarily distant neural networks interactions parallel, in part, the coherence data, where task-related changes in distant coherence were restricted to the alpha 2 band (see Fig. 3). Again, there were no significant effects involving hemisphere for any of the SL measures.

Distant coherence estimates computed between frontal and temporal sites were used as complementary measures

to the SL data. Although, task effects did not reach statistical significance there were notable similarities across measures in the shape of task-related trends, especially for coherence in the theta band as shown in Fig. 4.

Two key findings in the present data are to notice. First, performance of the number comparison task was associated with minimal signal interdependencies across recording sites. This result was apparent in both linear and non-linear analyses (distant coherence and SL), and may reflect reduced cortico-cortical interactions for this task. It has been suggested that number comparison depends largely upon a core system responsible for numerical representations [10]. Although the neural basis of this system is not yet clear, there is growing evidence from functional imaging studies that a key component can be found within the horizontal segment of the intraparietal sulcus, bilaterally [5,18]. It should be noted, however, that indices of regional neurophysiological activation (power spectrum and local coherence estimates) did not lend direct support to this notion without contradicting it either, since this area is a small region of the sulcus [5]. Thus, the lack of significant differences among the number comparison and the two multiplication tasks at parietal sites may simply reflect the fact that the putative "number concept" core area in the parietal lobe is also routinely engaged in calculation tasks as well, as one of the (many) components of the brain mechanism responsible for the functions exemplified by these tasks.

Performance of the two calculation tasks was associated with: (a) increased power in the gamma bands, primarily over the left hemisphere, (b) reduced power in the alpha 2 band

Table 1
Significant main effects, pair wise comparisons, and linear trends for the three arithmetic tasks using broadband SL estimations (number comparison, single- and two-digit multiplication)

Region	F(d.f.), p	Pairwise contrasts (p)	Trends: F(d.f.), p
Frontal	10.47 (2,34), 0.0001	Number comparison < single-digit multiplication (0.003), Two-digit multiplication (0.004)	14.92 (1,17), 0.001
Temporal	12.23 (2,34), 0.0001	Number comparison < single-digit multiplication (0.002), Two-digit multiplication (0.001)	23.03 (1,17), 0.0001
Central	5.25 (1.46,24.80), 0.012	Number comparison < two-digit multiplication (0.06)	6.61 (1,17), 0.02
Parietal	5.95 (2,34), 0.006	Number comparison < two-digit multiplication (0.03)	8.41 (1,17), 0.01

at central and parietal areas, (c) reduced local coherence in that frequency band at left frontal areas, and (d) increased power in the theta band at frontal locations bilaterally. Taken together these findings provide indirect, yet convincing evidence of increased levels of neuronal signalling within a distributed set of neuronal networks, primarily in left frontal and parietal areas, but also in the right fronto-parietal area. Both tasks require retrieval of simple mathematical facts (multiplication table), which are typically stored in the form of verbal representations. Two-digit multiplication requires retrieval of simple mathematical facts and, in addition, adherence to a series of mental calculation procedures that exemplify higher order mathematical thinking [11]. These processes are expected to engage a network of areas responsible for language functions, including long-term (consolidated) verbal memory [6,7] as well as verbal working memory. There is ample evidence that these functions depend largely upon neurophysiological processes located in left hemisphere frontal, posterior temporal and inferior parietal areas. Our data are at least partially consistent with this notion, given that the most robust task effects were found at left hemisphere locations. Signal desynchronization was also found at right hemisphere areas, which could reflect the engagement of additional operations that are specific to math functions.

While findings presented thus far essentially confirm prior notions regarding the outline of the brain mechanism that supports math functions, the temporal resolution of EEG and a relatively new analysis method (SL) provided additional clues regarding the said mechanism. The present findings further suggest that increasing the complexity of arithmetic tasks by increasing the demand for additional operations (such working memory, retrieval, and implementation of procedural knowledge in the case of the two-digit-multiplication task) is associated with a pattern of widespread synchronizations involving all four lobes of the brain. In turn, increased linear and non-linear interdependencies between signals recorded at remote areas may indicate increased neuronal networks interactions, a phenomenon that is expected to take place when diverse brain areas hosting specialized neurophysiological operations are required to work together to ensure successful task performance.

Acknowledgments

References

[1] M. Breakspear, J.R. Terry, K.J. Friston, A.W.F. Harris, L.M. Williams, K. Brown, J. Brennan, E. Gordon, A disturbance of nonlinear interdependence in scalp EEG of subjects with first episode schizophrenia, NeuroImage 20 (2003) 466–478.

[2] S.L. Bressler, J.A.S. Kelso, Cortical coordination dynamics and cognition, Trends Cogn. Sci. 5 (2001) 26–36.

[3] S. Dehaene, G. Dehaene-Lambertz, L. Cohen, Abstract representations of numbers in the animal and human brain, Trends Neurosci. 21 (1998) 355–361.

[4] S. Dehaene, N. Molko, L. Cohen, A.J. Wilson, Arithmetic and the brain, Curr. Opin. Neurobiol. 14 (2004) 218–224.

[5] S. Dehaene, M. Piazza, P. Pinel, L. Cohen, Three parietal circuits for number processing, Cogn. Neuropsychol. 20 (2003) 487–506.

[6] H. Dehaene, E. Spelke, P. Pinel, R. Stanescu, S. Tsivkin, Sources of mathematical thinking: behavioral and brain-imaging evidence, Science 284 (1999) 970–974.

[7] M. Delazer, F. Domahs, L. Bartha, C. Breneis, A. Lochy, T. Trieb, T. Benke, Learning complex arithmetic—an fMRI study, Cogn. Brain Res. 18 (2003) 76–88.

[8] G. Dumermuth, L. Molinari, Spectral analysis of the EEG. Some fundamentals revisited and some open problems, Neuropsychobiology 17 (1987) 85–99.

[9] M. Dumont, F. Jurysta, J.-P. Lanqart, P.-F. Migeotte, P. van de Borne, P. Linkowski, Interdependency between heart rate variability and sleep EEG: linear/non-linear? Clin. Neurophysiol. 115 (1994) 2031–2040.

[10] L. Fegenson, S. Dehaene, E. Spelke, Core systems of number, Trends Cogn. Sci. 215 (2004).

[11] O. Gruber, P. Indefrey, H. Steinmetz, A. Kleinschmidt, Dissociating neural correlates of cognitive components in mental calculation, Cereb. Cortex 11 (2001) 350–359.

[12] T. Kobayashi, K. Hiraki, R. Mugitani, T. Hasegawa, Baby arithmetic: one object plus one tone, Cognition 91 (2004) B23–B34.

[13] L. Lee, L.M. Harrison, A. Mechelli, A report of the functional connectivity workshop, Dusseldorf 2002, NeuroImage 19 (2003) 457–465.

[14] S. Micheloyannis, N. Flitzanis, E. Papanikolaou, M. Bourkas, D. Terzakis, S. Arvanitis, C.J. Stam, Usefulness of non-linear EEG analysis, Acta Neurol. Scand. 97 (1998) 13–19.

[15] S. Micheloyannis, M.M. Tzenaki, M. Bamboukas, M. Giachnakis, N. Paritsis, M. Prokopakis, L. Molinari, Electroencephalographic evaluation of children without neuropsychiatric distrurbances but with poor school performance, J. Child Neurol. 11 (1996) 309–312.

[16] H. Mizuhama, L.-Q. Wang, K. Kobayashi, Y. Yamguchi, A long-range cortical network emerging with theta oscillation in a mental task, NeuroReport 15 (2004) 1233–1238.

[17] G. Pfurtscheller, Induced oscillations in the alpha band: functional meaning, Epilepsia 44 (Suppl. 12) (2003) 2–8.

[18] P. Pinel, S. Dehaene, D. Riviere, D. LeBihan, Modulation of parietal activation by semantic distance in a number comparison task, NeuroImage 14 (2001) 1013–1026.

[19] B. Schack, N. Vath, H. Petsche, H.-G. Geissler, E. Moeller, Phase-coupling of theta-gamma EEG rhythms during short-term memory processing, Int. J. Psychophysiol. 44 (2002) 143–163.

[20] P.G. Simos, E. Papanikolaou, E. Sakkalis, S. Micheloyannis, Modulation of gamma-band spectral power by cognitive task complexity, Brain Topogr. 14 (2002) 191–196.

[21] O. Sporns, G. Tononi, G.M. Edelman, Theoretical neuroanatomy and the connectivity of the cerebral cortex, Behav. Brain Res. 135 (2002) 69–74.

[22] C.J. Stam, M. Breakspesr, A.-M. van Cappellen, B.W. van Dijk, Nonlinear synchronization in EEG and whole-head MEG recordings of healthy subjects, Hum. Brain Mapp. 19 (2003) 63–78.

[23] C.J. Stam, B.W. Dijk, Synchronization likelihood: an unbiased measure of generalized synchronization in multiple data sets, Physica D 163 (2002) 236–251.

[24] A. von Stein, J. Sarntheim, Different frequencies for different scales of cortical integration: from local gamma to long range alpha/theta synchronization, Int. J. Psychophysiol. 38 (2000) 301–313.

[25] L.M. Ward, Synchronous neural oscillations and cognitive processes, Trends Cogn. Sci. 7 (2003) 553–559.

[26] S. Weiss, H.M. Mueller, The contribution of EEG coherence to the investigation of language, Brain Lang. 85 (2003) 325–343.

Modulation of Gamma-Band Spectral Power by Cognitive Task Complexity

Panagiotis G. Simos*, Elias Papanikolaou+, Evangelos Sakkalis+, and Sifis Micheloyannis+

Summary: This study evaluated the utility of electroencephalographic (EEG) measures as indices of regional cerebral activation during performance of visuo-semantic analysis tasks in neurologically intact adult volunteers. EEG was recorded from 28 scalp locations as participants performed three visual discrimination tasks designed to tap into increasingly more complex operations regularly involved in the recognition of living animate objects. In addition, data from a control task involving the same stimuli, but requiring no cognitive decision or response, was included. EEG records were quantified using power spectrum measures in five frequency bands (delta, theta, alpha, beta, and gamma). Results showed a significant linear increase in absolute power in the gamma band with increasing task complexity over left hemisphere frontal and occipital regions, and over right temporoparietal regions.

Key words: EEG; Power Spectrum; Gamma band; Cognition; Pictures; Visual analysis; Figural analysis.

Introduction

Electroencephalographic (EEG) measures have been used successfully in the past as indices of cerebral engagement in cognitive tasks. The majority of investigations have searched for systematic, task-related changes in the energy in the alpha band (8-13 Hz). There is evidence, however, that changes in spectral energy in higher (Krausse et al. 1998; Pulvermüller et al. 1997; Papanicolaou et al. 1986) frequency bands (such as beta -- 14 to 30 Hz -- and gamma bands - 30 to 60 Hz) are very sensitive as indices of task-related cerebral activation.

Briefly, EEG studies have shown alpha suppression (e.g., Makino 1986) and/or beta enhancement over the left hemisphere during verbal tasks (Bizas et al. 1999; Papanicolaou et al. 1986; Pulvermüller et al. 1997). Changes in gamma activity have been reported in a variety of perceptual/cognitive tasks (Keil et al. 1999; Pulvermüller et al. 1996; Krausse et al. 1998; Rodriguez et al. 1999). Specifically, activity in the gamma band has been reported in the context of face recognition tasks (Rodriguez et al. 1999), in tasks in-

volving mental search of internal object representations (Tallon-Baudry et al. 1999), and in other complex visuo-perceptual tasks (Keil et al. 1999). The interest in non-invasive recordings of high-frequency electrical activity in humans has grown considerably in recent years, after reports of similar high-frequency oscillations recorded invasively from large neuronal aggregates in animals (Gray and Singer 1989). The wide scalp distribution of task-related variations in gamma power and phase-locking raise the possibility that high frequency EEG activity reflects synchronized oscillations in the human brain that form the basis of the engagement of neuronal populations in a particular function (Basar et al. 2000).

In order to show, however, that variations in EEG spectral energy reflect engagement of neurophysiological processes specialized for particular cognitive operations, one must first demonstrate that power spectrum measures vary systematically with the degree of complexity of the cognitive decisions required by the experimental task. Unfortunately, only a few studies have been designed along those lines (Bizas et al. 1999; Papanicolaou et al. 1986; Krausse et al. 1998).

In the present study we explored the sensitivity of EEG-derived measures as indices of cerebral activation in areas involved in visuo-perceptual operations. In order to engage component operations that are critical for the decisions that require such operations, we manipulated the number of dimensions along which subjects were asked to make discriminatory decisions, while maintaining overall degree of visual complexity of the stimuli roughly constant across tasks.

* Department of Neurosurgery, The University of Texas, Health Science Center, Houston, Texas, USA.

+ Clinical Neurophysiology Laboratory (L.Widen), Faculty of Medicine, University of Crete, Iraklion, Greece.

Accepted for publication: October 12, 2001.

Correspondence and reprint requests should be addressed to Dr. P.G. Simos, Department of Neurosurgery, The University of Texas Medical School, 6431 Fannin Suite 7.154, Houston, Texas, 77030, USA.

Fax: (713) 500-0655   E-mail: psimos@uth.tmc.edu

Methods

Subjects

Sixteen right-handed male volunteers (aged 20-26 years) who were medical students at the University of Crete served as subjects. They had no history of brain injury or learning disability. All subjects had normal or corrected-to-normal vision. The procedures used in the study had been approved by The University of Crete Institutional Review Board and all subjects signed a consent form after the nature of the procedures involved had been explained to them.

Materials and Procedures

Continuous EEG recordings were obtained in the context of four continuous target detection tasks. The stimuli were 40 drawings of animals (black on white background). A common pool of drawings were used to select stimuli for each task. In Task 1, they were instructed to pay attention to the drawings in order to report, after the end of the recording session, the presence of a single target item (either a dog or a cat) within a particular block. In Tasks 2-4, subjects were asked to raise their left index finger to indicate the detection of target stimuli. In Task 2, target stimuli consisted of pictures of four-legged animals (e.g., goat, tiger, crocodile, frog) and distractors were pictures of two-legged animals, insects, snakes, and marine animals. In Task 3, targets were pictures of four-legged animals larger than a (mature) sheep (e.g., tiger, lion, and crocodile). Pictures of two-legged animals, insects, snakes, marine animals, as well as of four-legged animals smaller than a sheep, served as distractors. Finally, pictures of four-legged herbivores larger than a cat (e.g., goat, elephant, camel) served as targets in Task 4. Pictures of a variety of animal species not meeting the aforementioned specifications were included as distractors (e.g., tiger, chicken, mouse). No other response or decision was required during the recordings. In all tasks the stimuli were presented in blocks of 20 items at a rate of one stimulus every 2 sec. The order of tasks was counterbalanced across subjects.

Recording and Analysis Procedures

EEG signals were recorded, according to the modified 10-20 International System, from F3-4, F7-8, C3-4, FC3-4, FT7-8, P3-4, CP3-4, T3-4, T5-6, TP7-8, O1-2, Fz, Cz, Pz, FCz, CPz, and Oz (28 electrodes), with a linked earlobe electrode reference. The amplifier bandwidth was set between 0.1 and 200 Hz. Using a 12-bit Analog to Digital converter and a sample frequency of 500 Hz, signals were input to a PC and monitored online on the PC screen. Subjects were lying comfortable in a dimly illuminated, sound

attenuated, and electrically shielded room. Signals were visually inspected offline in order to identify biogenic artifacts, and a 8-sec long artifact-free epoch was randomly selected for analysis for each task. In that way each epoch contained 4,000 data points for each EEG channel. Given that the average time that subjects were engaged in each task was in the order of 80 sec, the length of the selected EEG epoch was a representative sample of brain activity during task performance (Dumermuth and Molinari 1987). Absolute power spectrum estimation in the delta (1-3.5 Hz), theta (3.5-7.5 Hz), alpha (7.5-12.5 Hz), beta (13-30 Hz), gamma bands (30-45 Hz), at each electrode site using the software developed by one of the authors (E.P.) (for more details see Micheloyannis et al. 1996).

Given the large number of electrode locations used in the study, it was felt that the omnibus Analysis of Variance with Task (4), and Electrode Site (28) as the within-subjects factors would not have adequate power to reveal systematic task effects, if these effects were restricted to the data from only a few electrode locations. In a similar manner, task differences restricted to only a handful of electrode locations would likely be missed by a Task (4) by Electrode Site (11: excluding six midline sites) by Hemisphere (2) ANOVA. Therefore, to accommodate our main hypothesis, which predicts regional systematic variation in spectral power with increasing task complexity, we employed trend analyses, performed separately on data combined across adjacent electrode locations within each hemisphere (the relative locations of the recording sites are shown in figure 1). These tests were computed for frontocentral (F3, F7, FC3, FT7, and C3 over the left hemisphere and F4, F8, FC4, FT8, and C4 over the right hemisphere), and temporoparietal sites (T3, TP7, CP3, P3, and T5 over the left hemisphere and T4, TP8, CP4, P4, and T6 over the right hemisphere). In addition, data from the left (O1) and right occipital leads (O2) were examined separately. The Bonferroni method was used to maintain experiment-wise Type I error rate below the .05 level. Given that a total of 30 tests were performed across all five spectral bands, a nominal alpha level of .05/30 = 0.0017 was used for each test. In addition, linear trends were computed for individual electrode sites by adopting a less stringent approach whereby the Bonferroni method was used to maintain amily-wise Type I error rate (for each set of 28 tests performed on data from a given spectral band) at a nominal alpha level of .05/28 = 0.0018.

Results

All participants were successful at identifying every target stimulus in all four tasks. Visual inspection of mean spectral power values across tasks revealed a quasi-linear increase in power especially in the gamma
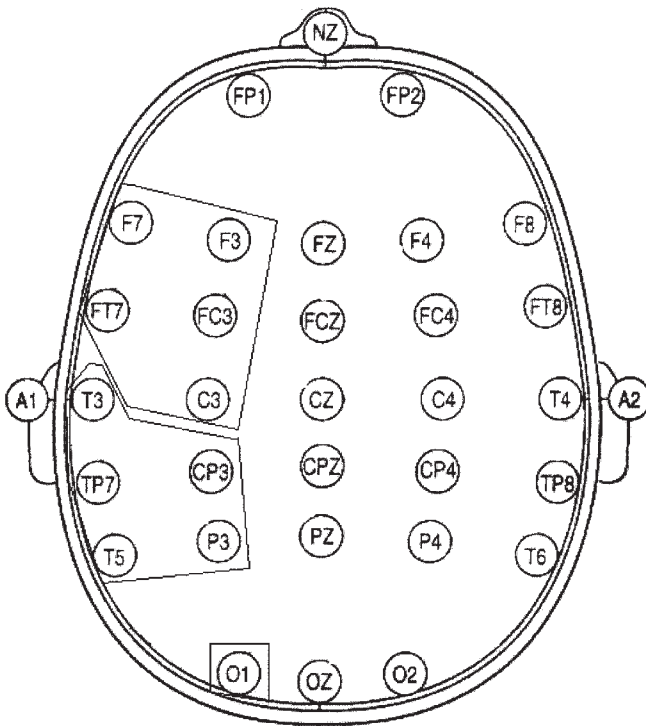
Figure 1. The topographical relationship among the 28 recording locations showing the three regions of interest in the left half of the electrode array (data from three mirror regions on the right side were also included in the analyses).

band at left frontocentral, $F(1,15) = 15.29$, $p < .001$, and occipital scalp locations, $F(1,15) = 27.95$, $p < .0001$, and at right temporoparietal locations, $F(1,15) = 19.07$, $p < .001$, as shown in figure 2. Although such trends were observed in the data recorded from several recording sites (in addition to O1), significant linear contrasts were found at the following sites: F3, $F(1,15) = 21.67$, $p < .0001$, F7, $F(1,15) = 24.61$, $p < .0001$, P4, $F(1,15) = 16.29$, $p < .001$, and CPz, $F(1,15) = 16.76$, $p < .001$. Although, as illustrated in figure 2, the increase in gamma power was substantial across Tasks 2-4 (especially at F3 and F7), the linear trends were not significant when data from only these tasks were analyzed. Task effects, involving power in any other band, did not reach statistical significance.

Discussion

Establishing the relevance of any measure of brain activity, recorded from the scalp, for the mechanism responsible for performing a particular function is contingent upon three pieces of information: (1) where in the

brain is the underlying activity generated, (2) what is the temporal course of this activity with respect to the presentation of task-relevant stimuli, and (3) how does the measured activity change across tasks that are valid representations of that function. The present study was designed to address (3) and it can also provide limited information regarding (1). In the data presented here, spectral EEG power in the gamma band varied systematically with increasing complexity of the cognitive task performed by the participants. The three discrimination tasks used in the present study (tasks 2-4) were matched on a number of important aspects such as the type of decision and response required. They varied, however, on the number of dimensions or visuo-semantic stimulus attributes on which the subjects' decision was based. Task 2 involved focusing on only one attribute: number of extremities of the depicted animals (two or four). Performance of this task required, at a minimum, visual analysis of the drawings. Identification of the depicted animals with respect to a subordinate class (i.e., dog) with subsequent, automatic, access to the main visuo-semantic attributes of that particular class (i.e., four legs, fur, approximate size etc.) is also possible, but not required. On the other hand, access to a stored representation that specifies visuo-semantic information regarding the class of the depicted animal was required during Tasks 3 and 4. In Task 3, the real-life size of the depicted animal was also relevant (in addition to the number of extremities). During Task 4 subjects were required to process each stimulus on the basis of three attributes, namely, number of extremities (two or four), real-life size (in relation to a cat), and dietary habits (herbivore or carnivore). Task 1 served as a control as it entailed no overt decision or motor response, but required visual recognition of the same stimuli used in Tasks 2-4.

It is unlikely that visual stimulus complexity per se was responsible for the systematic increase in gamma power across tasks, given that stimuli were selected from a common pool of pictures. In fact, whenever possible, the same pictures were used in all tasks. On the other hand, changes in gamma power in the data presented here were contingent upon the requirement for an overt cognitive decision, response selection, motor programming and execution of a motor response. Thus, the increase in gamma power was significant only when Task 1 (which did not involve any overt decision/response) was included in the trend analysis. It appears, however, that differences in gamma power between Task 1 and Tasks 2-4 were is not likely the result of increased cortical activity associated with the motor response per se. Such activity would be maximal in posterior frontal cortices contralateral to the responding hand (Selenius et al. 1996). In the present study, the effects on gamma power were observed at electrodes located over the left frontal lobe, i.e., ipsilateral to
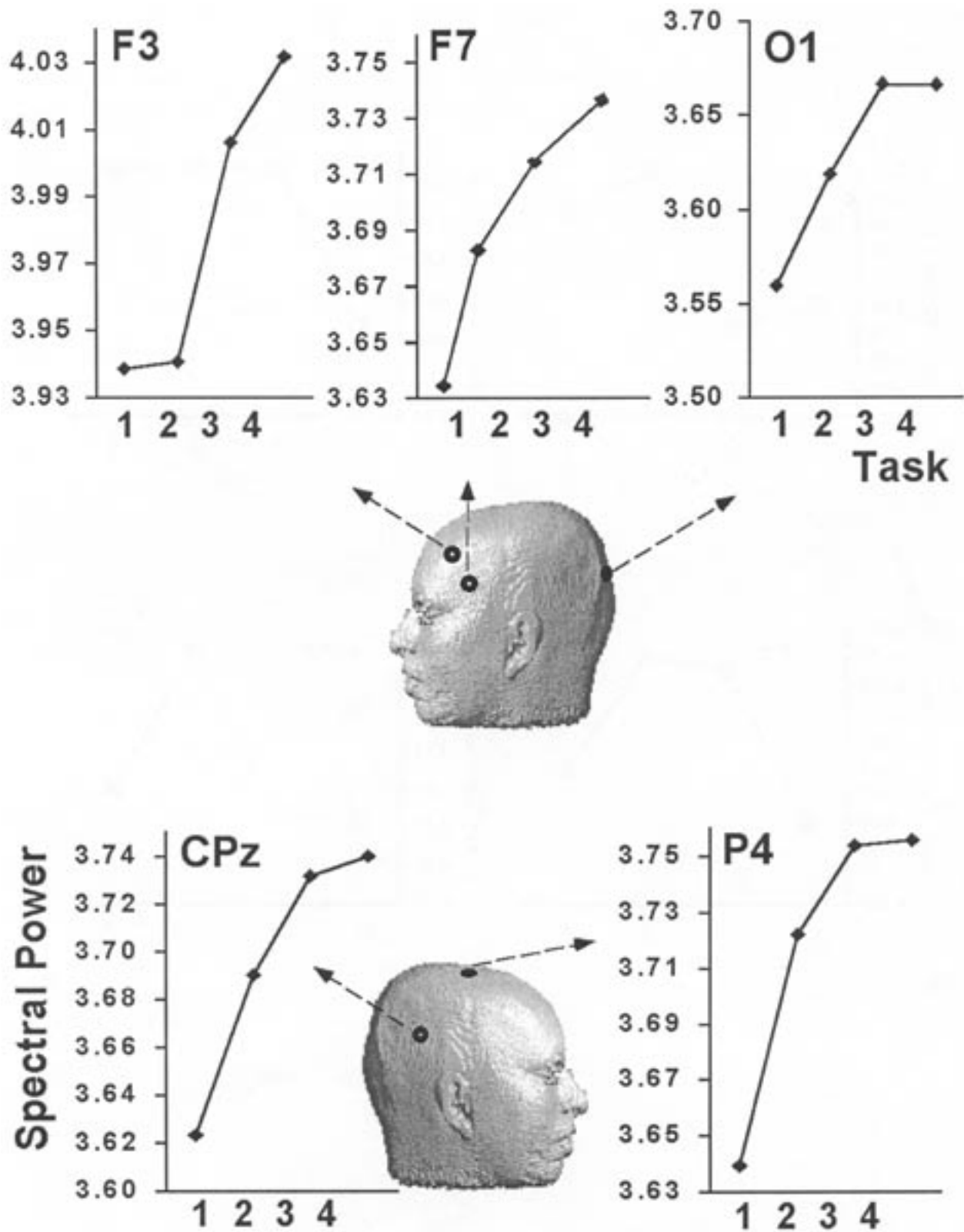
Figure 2. Mean power in the gamma band detected in EEG segments recorded at left frontal and occipital sites (top) and at posterior midline and right parietal sites (bottom) during each of the four experimental tasks (labeled 1 through 4 on the x axis). The approximate locations of each recording electrode is shown on the head model. The graphs illustrate the significant quasi-linear increase in gamma power with increasing task complexity.
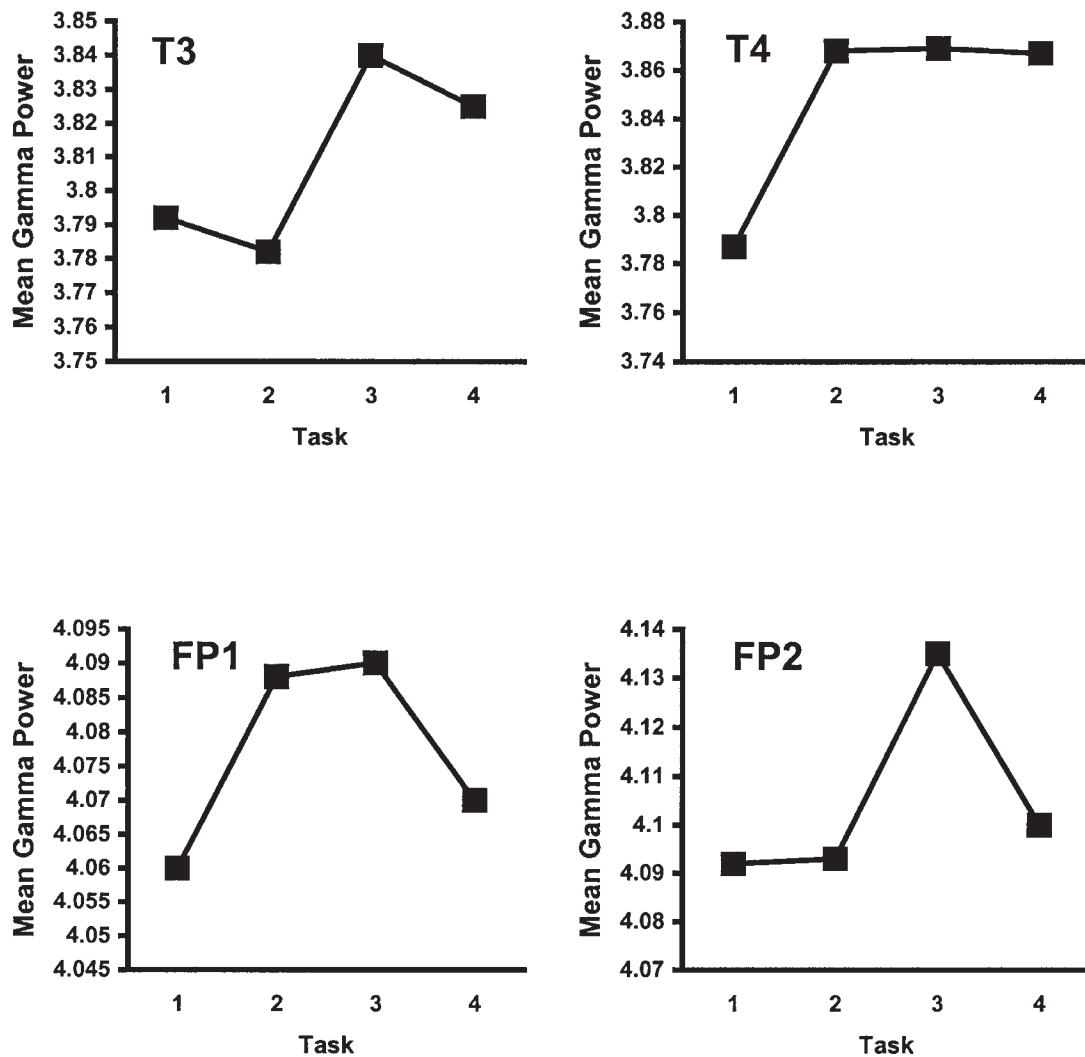
Figure 3. Mean gamma band power recorded at four sites located over the frontalis (Fp1/2) and temporalis muscles (T3/4) sensitive to EMG activity. Notice that the quasi-linear task-related changes in power are not evident, an indication that the task effects observed at other frontal and temporoparietal sites were not an artifact of systematic changes in ongoing muscle activity.

the responding hand. No task-related change in gamma power was observed over the right frontal lobe.

Another issue that merits special care in studies reporting task-related effects in the gamma band is the risk of contamination of the data by myogenic artifacts. Although in the present study EMG was not recorded through separate electrodes, the magnitude of myogenic contamination was assessed indirectly. Thus, if systematic changes in EMG activity associated with increasing task difficulty were present, they would have been more prominent at electrodes located near the frontalis and temporalis muscles. However, as is clearly evident in the plots presented in figure 3, there was no indication of a linear trend in gamma-band power at such sites (i.e., at

FP1/2, or T3/4). In contrast, task-related changes in gamma-band power were found at selective sites (including occipital and centroparietal leads that are further away from all likely sources of myogenic activity), and showed hemisphere asymmetries, which would not be expected in the case of systematic EMG contamination.

Given the wide range of tasks during which increases in gamma power have been observed across different studies, it is likely that such high frequency oscillations are not specific to a particular cognitive function but, rather represent a universal correlate of neuronal signaling (Basar et al. 2000). Naturally, the rate of signaling becomes accelerated when diverse cortical regions participate conjointly in the execution of a cognitive function. In this

framework, this activity might be interpreted as reflecting the engagement of a network of left hemisphere brain regions involved in visuo-semantic analysis. Occipital gamma may reflect the late phase-locked component that occurs at approximately 300 ms after stimulus onset, given that the early (100 ms) component is typically not affected by cognitive task demands (Karakas and Basar 1999). Whether the changes in gamma power observed in our study reflected neuronal oscillations in modality-specific (i.e., visual) cortex remains to be seen.

References

Basar, E., Basar-Eroglu, C., Karakas, S. and Schurmann, M. Brain oscillations in perception and memory. Int. J. Psychophysiol., 2000, 35: 95-124.

Bizas, E., Simos, P.G., Stam, C.J., Arvanitis, S., Terzakis, D. and Micheloyannis, S. EEG correlates of cerebral engagement in reading tasks. Brain Topogr., 1999, 12: 99-105.

Dumermuth, G. and Molinari, L. Spectral analysis of the EEG. Some fundamentals revisited and some open problems. Neuropsychobiology, 1987, 17: 85-99.

Gray, C.M. and Singer, W. Stimulus-specific neuronal oscillations in orientation columns of cat visual cortex. Proc. Natl. Acad. Sci. USA 1989, 86: 1698-1702.

Keil, A., Muller, M.M., Ray, W.J., Gruber, T. and Elbert, T. Human gamma band activity and perception of a gestalt. J. Neurosci., 1999, 19: 7152-7161.

Krausse, C., Korpilahti, P., Pörn, B., Jantti, J. and Lang, H.A. Automatic auditory word perception as measured by 40 Hz EEG responses. Electroencephal. clin. Neurophysiol., 1998, 107: 84-87.

Makino, A. Topographic EEG analysis in relation to higher brain function. J. Exp. Med., 1986, 33: 59-68.

Micheloyannis, S., Tzenaki, M.M., Bamboukas, M., Giachnakis, M., Paritsis, N., Prokopakis, M. and Molinari, L. Electroencephalographic evaluation of children without neuropsychiatric disturbances but with poor school performance. J. Child Neurol., 1996, 11: 309-312.

Papanicolaou, A.C., Loring, D., Deutsch, G. and Eisenberg, H.M. Task-related EEG asymmetries: a comparison of alpha blocking and beta enhancement. Int. J. Neurosci., 1986, 30: 81-85.

Pulvermüller, F., Eulitz, C., Pantev, C., Mohr, B., Feige, B., Lutzenberger, W., Elbert, T. and Birbaumer, N. High-frequency cortical responses reflect lexical processing: an MEG study. Electroencephal. clin. Neurophysiol., 1996, 98: 76-85.

Pulvermüller, F., Birbaumer, N., Lutzenberger, W. and Mohr, B. High-frequency brain activity: its possible role in attention, perception and language processing. Progr. Neurobiol., 1997, 52: 427-445.

Rodriguez, E., George, N., Lachaux, J.P., Martinerie, J. Renault, B. and Varela, F.J. Perception's shadow: long-distance synchronization of human brain activity. Nature, 1999, 397: 430-433.

Salenius, S., Salmelin, R., Neuper, C., Pfurtscheller, G. and Hari, R. Human cortical 40 Hz rhythm is closely related to EMG rhythmicity. Neurosci. Lett., 1996, 213: 75-78.

Tallon-Baudry, C., Bertrand, O., Delpuech, C. and Pernier, J. Oscillatory gamma-band (30-70 Hz) activity induced by a visual search task in humans. J. Neurosci., 1997, 17: 722-734.

Assessment of linear and non-linear EEG synchronization measures for evaluating mild epileptic signal patterns

Vangelis Sakkalis, Ciprian Doru Giurcăneanu, Petros Xanthopoulos, Michalis Zervakis, Vassilis Tsiaras, Yinghua Yang, and Sifis Micheloyannis

Abstract—**Epilepsy is one of the most common brain disorders and may result in brain dysfunction and cognitive disturbances. Epileptic seizures usually begin in childhood without being accommodated by brain damage and many drugs produce no brain dysfunction. In this study cognitive function in mild epilepsy cases is evaluated where children with seizures are compared to controls i.e., children with epileptic seizures, without brain damage and under drug control. Two different cognitive tasks were designed and performed by both the epileptic and healthy children: i) a relatively difficult math task and ii) Fractal observation. Under this prism, we investigate seven measures of quantifying synchronous oscillatory activity based on different underlying assumptions. Namely, the most widely used coherence, a coding-based measure known as MDL (Minimum Description Length) and the Geweke alternative, a robust phase coupling measure known as PLV (Phase Locking Value), a cortical synchrony measure defined from the embedding dimension in state-space called S-estimator, a reliable way of assessing generalized synchronization also in state-space and an unbiased alternative called Synchronization likelihood. Assessment was performed in three stages; initially the methods were validated on coupled nonlinear oscillators, secondly surrogate data testing was performed to assess the possible nonlinear nature of the acquired EEGs and finally synchronization on the actual data was measured. The results on the actual data suggest higher frequency band gamma2 was mostly apparent in occipital-parietal lobes during fractal tests.**

V. Sakkalis is with the Department of Electronic and Computer Engineering, Technical University of Crete, Chania 73100 and the Institute of Computer Science, Foundation for Research and Technology, Heraklion 71110, Greece (+30-281-0391448; fax: +30-281-0391609; e-mail: sakkalis@ics.forth.gr).

C.D. Giurcăneanu and Y. Yang are with the Institute of Signal Processing, Tampere University of Technology, Tampere FIN-33101, Finland (e-mail: ciprian.giurcaneanu@tut.fi, yinghua yang @tut.fi).

P. Xanthopoulos and M. Zervakis are with the Department of Electronic and Computer Engineering, Technical University of Crete, Chania 73100, Greece (e-mail: petros@danai.systems.tuc.gr, michalis@systems.tuc.gr).

V. Tsiaras is with the Institute of Computer Science, Foundation for Research and Technology, Heraklion, Greece and the Department of Computer Science, University of Crete, Heraklion 71409, Greece (e-mail:tsiaras@ics.forth.gr).

S. Micheloyannis is with the Clinical Neurophysiology Laboratory (L. Widen), Faculty of Medicine, University of Crete, Heraklion 71409, Greece (e-mail: michelogj@med.uoc.gr).

I. INTRODUCTION

NEURONAL dynamics and synchronization phenomena have been increasingly recognized to be an important mechanism by which specialized cortical and sub-cortical regions integrate their activity to form distributed neuronal assemblies that function in a cooperative manner [1]. Synchronous oscillations of certain types of such assemblies in different frequency bands relate to different perceptual, motor or cognitive states and may be indicative of a wider range of cognitive functions or brain pathologies [2][3]. In general, low frequencies, like the theta band, are believed to reveal the coupling between distant brain regions, whereas high frequencies, like the gamma band, are thought to be more important for short range interactions [4].

The traditionally formulated but still the most common way of analyzing the functional coupling of cortical assemblies has been the *magnitude squared coherence (MSC)* or coherence. MSC is a normalized measure of linear dependence between two signals and is capable of identifying linear synchrony on certain frequency bands [5][6][7], but it is not able to give indications on the feedback that exists between the analyzed systems. The idea of measuring the causality between two time series can be traced back to the work of Granger [6] and Geweke [9]. The results of Geweke are especially important for neuroscience to evaluate neuronal interactions [10], because they give frequency decompositions for the time domain measures. The latter method relies on strong assumptions for the autoregressive representation of the analyzed signals, whereas the application of *Minimum Description Length principle (MDL)* relaxes these assumptions and new measures of feedback may also be introduced [11].

Since all the measures mentioned above are linear, we extend our investigations by considering also nonlinear measures. Phase Synchronization present a different approach in analyzing the possible nonlinear interdependencies of the EEG signal and focuses on the phases of the signals. The idea of studying the phase relationships of two neurophysiological signals is not new [12], but later studies has shown that even if the amplitudes of two coupled chaotic oscillators remain uncorrelated, their phases may synchronize [13]. A robust phase coupling measure is the *Phase Locking Value (PLV)* [14]. Finally,

another group of synchronization measures are based on the assumption that neurons are highly nonlinear devices, which in some cases show chaotic behavior [15]. Hence, the use of nonlinear measures derived from studying chaotic dynamical systems may be of interest in neurophysiology applications. Such measures belong to the Generalized Synchronization concept and are based on analyzing the interdependence between the amplitudes of the signals in a state-space reconstructed domain. In this study, we use three variants of this idea, the *S-estimator* [20], a robust measure proposed by [21][22] and the *synchronization likelihood* method [23].

The focus of this study is on investigating the differences in coupling of EEG channels in controls-normals versus children with mild epilepsy. We compare the capabilities of the proposed measures using chaotic noisy models and we investigate their use in real band-limited signals. We also compare the capabilities of both linear and nonlinear measures in revealing the coupling between EEG channels.

II. METHODS

A. Test Signals & Real Data Acquisition

To study the different properties of each of the proposed methods, we consider two classical coupled chaotic dynamical systems. The first model uses two coupled Rössler oscillators, whereas the second uses a Lorenz system nonlinearly driven by a Rössler oscillator with such coupling coefficient that ensures GS [26][27].

The studied population consisted of twenty mild epileptic subjects and twenty controls. The EEG signals in both groups (controls and mild epileptics) were recorded from 30 cap electrodes (FP1, FP2, F7, F3, FZ, F4, F8, FT7, FC3, FCZ, FC4, FT8, T3, C3, CZ, C4, T4, TP7, CP3, CPZ, CP4, TP8, P3, PZ, P4, PO7, PO8, O1, OZ and O2), according to the 10/20 international system, referred to linked A1+A2 electrodes. The signals were amplified using a set of Contact Precision Instrument amplifiers, filtered on-line with a band pass between 0.1 and 200 Hz, and digitized at 400 Hz. Off-line, the recorded data were carefully reviewed for technical and biogenic artifacts, so that only artifact free epochs of eight seconds duration are investigated. The procedures used in the study had been previously approved by the University of Crete Institutional Review Board and all subjects signed a consent form after the nature of the procedures involved had been explained to them.

B. Test Description

Continuous EEGs were recorded in an electrically shielded, sound and light attenuated, room while participants sat in a reclined chair. EEG data were visually inspected for artifacts and epochs of 8 sec were chosen for analysis. We analyzed epochs at rest i.e., while each individual had the eyes fixed on a small point on the computer screen and during the two cognitive tasks. The first includes two digits number subtractions or two digits minus one digit, which is

thought to be a relatively difficult mathematical task and the second consist of Fractal observation. Stimuli were presented on an LCD screen located in front of the participants. Vertical and horizontal eye movements and blinks were monitored through a bipolar montage from the supraorbital ridge and the lateral canthus.

C. Mean Squared Coherence (MSC)

Let us suppose we have two simultaneously measured discrete time series x_n and y_n, $n=1\ldots N$. The most commonly used linear synchronization method is the cross-correlation function (C_{xy}) defined as:

$$C_{xy}(\tau) = \frac{1}{N-\tau} \sum_{i=1}^{N-\tau} \left(\frac{x_i - \overline{x}}{\sigma_x} \right) \left(\frac{y_{i+\tau} - \overline{y}}{\sigma_y} \right) \qquad (1)$$

where $\overline{x}$ and σ_x denote mean and variance, while τ is the time lag. MSC or simply coherence is the cross spectral density function S_{xy}, which is simply derived via the FFT of (1), normalized by their individual autospectral density functions. However, due to finite size of neural data one is able to actually estimate the true spectrum, known as periodogram, using smoothing techniques (e.g. Welch's method). Thus, MSC is calculated as:

$$\gamma_{xy}(f) = \frac{\left| \langle S_{xy}(f) \rangle \right|^2}{\left| \langle S_{xx}(f) \rangle \right| \left| \langle S_{yy}(f) \rangle \right|} \qquad (2)$$

Where $\langle \cdot \rangle$ indicates window averaging in the case of Welch's method. The estimated MSC for a given frequency f ranges between 0 (no coupling) and 1 (maximum linear interdependence).

D. Geweke feedback measure

In [9] it is defined $f_{x \to y}(\omega)$, a linear measure of feedback at frequency ω from an arbitrary time series x to another time series y. We note that x and y are assumed to be wide-sense stationary and purely nondeterministic. The interested reader can find in [9] more details on this definition and on the relationship between $f_{x \to y}(\omega)$ and the MSC.

Since the analysis of coupling between EEG channels is mainly performed in frequency bands that have a well-known biomedical significance, we use the following formula for computing the coupling in $[\omega_{inf}, \omega_{sup}] \subseteq [-\pi, \pi]$:

$$F_{x,y} = \frac{1}{2\pi} \int_{\omega_{inf}}^{\omega_{sup}} \left[f_{x \to y}(\omega) + f_{y \to x}(\omega) \right] d\omega. \qquad (3)$$

We consider next the steps to be followed when evaluating the expression above. Given the measurements x^n and y^n, we can resort to well-known algorithms for fitting a bivariate autoregressive model. The optimal model order $\hat{p}$ can be chosen from the pre-defined set $\{p_{min}, \ldots, p_{max}\}$ by applying the MDL criterion $\hat{p} = \mathrm{argmin}\left[\ln|\hat{\Sigma}_p| + 4p\frac{\ln N}{N} \right]$, where

$\hat{\Sigma}_p$ is the covariance matrix for the vector of residuals. The algorithm Whittle-Wiggins-Robinson (W^2R) [16] has the advantage that the stability of the estimated AR model is guaranteed. In our experiments, we have used both the W^2R algorithm and the ARFIT algorithm [17][29]. In our settings $p_{max}=50$, and we observed experimentally that the results produced by W^2R and ARFIT for the same data set were similar in terms of the calculated coupling values. The integral in (3) can be computed with Monte Carlo methods. More precisely, we resorted to the use of the Matlab implementation for Sobol sequences available at [30], and the number of integration points for each frequency band was 100000.

E. An MDL measure for inter-channel coupling

The dependence between time series is recast to reflect the predictability of each of the two time series from the other, and the method can be applied for measuring the coupling between band-limited signals. We are interested on evaluating the coupling between $\tilde{x}$ and $\tilde{y}$, where $\tilde{x}$ and $\tilde{y}$ are obtained after filtering x and y with a bandpass filter whose frequency range is $[\omega_{inf},\omega_{sup}]$. *MDL* principle claims the best model to be the one which leads to the shortest possible code length for the available measurements. In the hypothesis that $\tilde{y}_1^n$ must be transmitted from an encoder to a decoder, we apply the following methodology based on the results from [11].

First coding scenario: For an arbitrary prediction order $k \in \{0,..,k_{max}\}$, we compute the predicted value $\hat{y}_t$ for $\tilde{y}_t$ based on the past samples $\tilde{y}_1^{t-1}$: $\hat{y}_t = \sum_{i=1}^{k} f_i \tilde{y}_{t-i}$. Let $\varepsilon_t = \tilde{y}_t - \hat{y}_t$ be the prediction error and $E[\varepsilon_t^2] = \varsigma_k^2$. The parameters f_i are chosen such that to minimize ς_k^2, and after quantization they are sent to the decoder as side information. Then the prediction errors ε_t, $1 \leq t \leq n$, are also sent to the decoder. The expression of the code length for y_1^n is asymptotically given by $\frac{n}{2}\ln\varsigma_k^2 + \frac{k+1}{2}\ln n$. We choose the prediction order $k^* \in \{0,..,k_{max}\}$ that minimizes the code length, and the expression of the "average code length per sample" becomes $L(\tilde{y}_t|\tilde{y}_1^{t-1}) = \frac{1}{2}\ln\varsigma_{k^*}^2 + \frac{k^*+1}{2}\frac{\ln n}{n}$ [11].

Second coding scenario: Assuming that the decoder has complete knowledge on the past and the present of $\tilde{x}$, the current value of $\tilde{y}$ can be predicted as

$$\hat{y}_t = \sum_{i=1}^{k^*} g_i \tilde{y}_{t-i} + \sum_{i=0}^{\ell} h_i \tilde{x}_{t-i}, \text{ where } \ell \in \{0,..,k^*-1\}.$$ Remark that the number of samples from the past of the $\tilde{y}$ process used in the linear regression is given by k^* determined in the previous step, and also the number of $\tilde{x}$ samples used in the linear regression is limited by k^*. For each possible value of ℓ, the parameters g_i and h_i are estimated from the available measurements such that to minimize the variance $\varsigma_{k^*,\ell}^2$ of the prediction errors, and then the structure parameter ℓ^* is chosen to minimize the asymptotic code length. The expression of the code length is given by

$$L(\tilde{y}_t|\tilde{y}_1^{t-1},\tilde{x}_1^t) = \frac{1}{2}\ln\varsigma_{k^*,\ell^*}^2 + \frac{k^*+\ell^*+1}{2}\frac{\ln n}{n} \text{ [11]}.$$

The savings in code length of $\tilde{y}_1^n$ due to the knowledge on $\tilde{x}_1^n$ it is a measure of dependence between the two processes that it is grounded in the MDL principle. Based on this observation, we define $\mu_{\tilde{x}\to\tilde{y}} = L(\tilde{y}_t|\tilde{y}_1^{t-1}) - L(\tilde{y}_t|\tilde{y}_1^{t-1},\tilde{x}_1^t)$, and similarly $\mu_{\tilde{y}\to\tilde{x}} = L(\tilde{x}_t|\tilde{x}_1^{t-1}) - L(\tilde{x}_t|\tilde{x}_1^{t-1},\tilde{y}_1^t)$. We further define the *MDL* coupling measure: $\mu_{\tilde{x},\tilde{y}} = (\mu_{\tilde{x}\to\tilde{y}} + \mu_{\tilde{y}\to\tilde{x}})/2$.

Solving the estimation problem in the first coding scenario is equivalent with estimating the coefficients of an AR model, and we apply the celebrated Levinson-Durbin algorithm [18]. In our implementation, the maximum prediction order depends on the frequency band, and it takes values between 2 and 48. The second coding scenario relies on estimating the coefficients of an ARX model for which we employ the *arx* Matlab function.

F. Phase Locking Value (PLV)

One of the mostly used phase synchronization measures is the PLV approach. It assumes that two dynamic systems may have their phases synchronized even if their amplitudes are zero correlated [19]. The PS is defined as the locking of the phases associated to each signal, such as:

$$\left| n\phi_x(t) - m\phi_y(t) \right| = const \tag{5}$$

However, in this case the phase locking ratio of $n{:}m=1{:}1$, since both signals arise from the same physiological system (i.e., the brain).

In order to estimate the instantaneous phase of our signal, we transform it using the Hilbert transform (HT), whereby the analytical signal *H(t)* is computed as:

$$H(t) = x(t) + i\tilde{x}(t) \tag{6}$$

where $\tilde{x}(t)$ is the HT of *x(t)*, defined as:

$$\tilde{x}(t) = \frac{1}{\pi} PV \int_{-\infty}^{\infty} \frac{x(t')}{t-t'} dt' \tag{7}$$

where *PV* denotes the Gauchy principal value.

The analytical signal phase is defined as:

$$\phi(t) = \arctan\frac{\tilde{x}(t)}{x(t)} \tag{8}$$

Therefore for the two signals *x(t)*, *y(t)* of equal time length

with instantaneous phases $\phi_x(t), \phi_y(t)$ respectively the PLV bivariate metric is defined given by:

$$PLV = \left| \frac{1}{N} \sum_{j=0}^{N-1} e^{i(\phi_x(j\Delta t) - \phi_y(j\Delta t))} \right| \quad (9)$$

where Δt is the sampling period and N is the sample number of each signal. PLV takes values within the [0,1] space, where 1 indicates perfect phase synchronization and 0 indicates lack of synchronization.

G. S-estimator

An alternative measure for synchronization which can be applied in both bivariate and multivariate data is the S-estimator [20]. First we perform PCA meaning that we eigendecompose the covariance matrix of the data:

$$R_{FF} = E\left\{ F \cdot F^T \right\} = L\Lambda L^T \quad (10)$$

where Λ is a diagonal eigenvalue matrix and L is the corresponding eigenvector matrix. From the diagonal elements λ_i of the eigenvalue matrix Λ we compute the normalized eigenvalues λ_i' as follows:

$$\lambda_i' = \frac{\lambda_i}{tr(\Lambda)} \quad (11)$$

From the K normalized eigenvalues we compute the S-estimator:

$$S = 1 + \frac{\sum_{i=1}^{K} \lambda_i' \log(\lambda_i')}{\log(K)} \quad (12)$$

We can see from (12) that when all eigenvalues are equal to $1/K$ then S become zero, whereas if only one strong eigenvelue exist then S becomes maximum and equal to 1. The number of eigenvalues indicates the number of uncorrelated signals within data matrix F. In brief, when the EEG channels are combinations of many uncorrelated signals no synchronization exists. On the contrary when we have small number of uncorrelated signals all brain sources are synchronized according to these signals.

H. Robust state-space GS method (RSS-GS)

Alternatively, one may measure how neighborhoods (i.e., recurrences) in one attractor maps into the other. This idea turned out to be the most robust and reliable way of assessing the extent of GS [21][22]. First, we reconstruct delay vectors [23] out of our time series; $x_n = (x_n, ..., x_{n-(m-1)\tau})$ and $y_n = (y_n, ..., y_{n-(m-1)\tau})$, where $n=1...N$, and m, τ are the embedding dimension and time lag, respectively. Let $r_{n,j}$ and $s_{n,j}$, $j=1,...,k$, denote the time indices of the k nearest neighbors of x_n and y_n, respectively. For each x_n the squared mean Euclidean distance to its k neighbors is defined as:

$$R_n^{(k)}(X) = \frac{1}{k} \sum_{j=1}^{k} (x_n - x_{r_{n,j}})^2 \quad (13)$$

And the Y-conditioned squared mean Euclidean distance

$R_n^{(k)}(X|Y)$ is defined by replacing the nearest neighbors by the equal time partners of the closest neighbors of y_n.

If the set of reconstructed vectors (point cloud x_n) has an average squared radius $R(X) = (1/N) \sum_{n=1}^{N} R_n^{(N-1)}(X)$, then $R_n^{(k)}(X|Y) \approx R_n^{(k)}(X) \ll R(X)$ if the systems are strongly correlated, while $R_n^{(k)}(X|Y) \approx R(X) \gg R_n^{(k)}(X)$ if they are independent. Hence, an interdependence measure is defined as [21]:

$$S^{(k)}(X|Y) = \frac{1}{N} \sum_{n=1}^{N} \frac{R_n^{(k)}(X)}{R_n^{(k)}(X|Y)} \quad (14)$$

Since $R_n^{(k)}(X|Y) \gg R_n^{(k)}(X)$ by construction, it is clear that S ranges between 0 (indicating independence) and 1 (indicating maximum synchronization). Another normalized and more robust version of S maybe defined as [22] and is the one actually used in this study:

$$N^{(k)}(X|Y) = \frac{1}{N} \sum_{n=1}^{N} \frac{R_n(X) - R_n^{(k)}(X|Y)}{R_n(X)} \quad (15)$$

I. Synchronization Likelihood (SL)

Finally, the last measure (SL) used is an unbiased normalized synchronization estimator, closely related to the previous idea and to represent a normalized version of mutual information [24].

Supposing that x_n, x_v and y_n, y_v be the time delay vectors, SL actually expresses the chance that if the distance between x_n and x_v is very small, the distance between the corresponding vectors y_n and y_v in the state space will also be very small. For this, we need a small critical distance ε_x, such that when the distance between x_n and x_v is smaller than ε_x, x will be considered to be in the same state at times n and v. ε_x is chosen such that the likelihood of two randomly chosen vectors from x (or y) will be closer than ε_x (or ε_y) equals a small fixed number p_{ref}. p_{ref} is the same for x and y, but ε_x need not be equal to ε_y. Now SL between x and y at time n is defined as follows:

$$SL_n = \frac{1}{N'} \sum_{\substack{v=1 \\ w_1 < |n-v| < w_2}}^{N} \theta(\varepsilon_{y,n} - |y_n - y_v|)\theta(\varepsilon_{x,n} - |x_n - x_v|) \quad (16)$$

Here, $N'=2(w_2-w_1-1)P_{ref}$, $|\cdot|$ is the Euclidean distance and θ is the Heaviside step function, $\theta(x)=0$ if $x \leq 0$ and $\theta(x)=1$ otherwise. The value of w_1 is window equal to the Theiler correction for autocorrelation effects and w_2 is a window that sharpens the time resolution of the synchronization measure and is chosen such that $w_1 \ll w_2 \ll N$ [25]. When no synchronization exists between x and y, SL_n will be equal to the likelihood that random vectors y_n and y_v are closer than ε_y; thus $SL_n=p_{ref}$. In the case of complete synchronization $SL_n=1$. Intermediate coupling is reflected by $p_{ref} < SL_n < 1$. Finally, SL is defined as the time average of the SL_n values.

In the present study, SL was computed with the following

parameter settings: $\tau=10$; $m=10$; $w_1=100$ samples; $w_2=400$ samples; $p_{ref}=0.05$.

III. RESULTS

A. Testing using artificially generated data using chaotic oscillators under variable noise

To demonstrate that the nonlinear synchronization methods addressed in this study are sensitive to nonlinear structures in the signals under investigation we consider two classical coupled chaotic dynamical systems. The first model uses two coupled Rössler oscillators [26], whereas the second uses a Lorenz system [27] nonlinearly driven by a Rössler oscillator with coupling coefficient that ensures GS. The synchronization indexes vs. additive noise are plotted in the following figures.
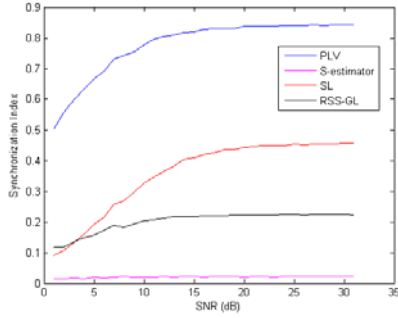

Fig. 1: Synchronization indexes applied on two coupled Rössler oscillators, configured to have phase synchronization.
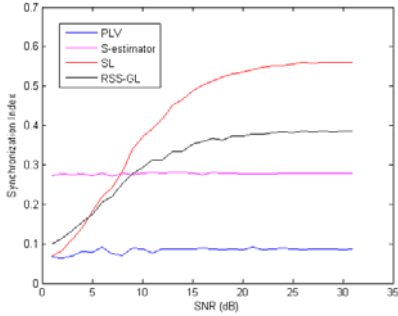

Fig. 2: Synchronization indexes applied on a Lorenz system nonlinearly driven by a Rössler oscillator. The coupling coefficient used is set for general synchronization.

B. Nonlinear coupling detection ability: Testing using surrogates

To demonstrate that the synchronization methods addressed in this study are sensitive to nonlinear structures in the real EEG signals (and thus reliable) under investigation bivariate surrogate data testing was used. The surrogating procedure used preserves both the autocorrelation of the signal and their linear cross-correlation, but the nonlinear individual structure of the individual signals, as well as their nonlinear interdependence, if any, is destroyed [28]. One mild-epileptic and one normal signal of a single representative subject was selected to be the generator of the surrogates

TABLE I
SYNCHRONIZATION Z-SCORES (ORIGINAL VS. SURROGATE DATASETS)

Linear (Alpha1 band, 8-10 Hz)		Nonlinear	
Method	Z-score	Method	Z-score
COHERENCE	0.50	PLV	**3.85**
GEWEKE	0.11	S-estimator	0.25
MDL	0.51	SL	1.09
		RSS-GL	1.32

and the testing was performed focusing on channels O2 and PO8 located on the occipital-parietal brain lobe. To reject the hypothesis (H_0) that the mean values of the original and the set of surrogate time series are equal different the Z-score is calculated. H_0 is rejected at the 95% level of confidence if $Z>1.96$ (one-sided test). The results obtained are tabulated below. Bold values are the ones capable of identifying the nonlinearities of the signal.

C. Actual EEG data

Testing using surrogates suggested that further testing on the real data is prospective using only the linear and the *PLV* method, as discussed in the next section. The latter synchronization measures are performed on both normals and mild-epileptic band-filtered data. Averages over all possible channel couplings in each brain lobe and band are calculated (Table II). Only those bands/lobes that achieved significant differentiation using ANOVA (p=0.05) statistics

TABLE II
ACTUAL EEG DATA: LOBE-BAND SELECTION

Method	Test1	Test2	Test3
COHERENCE	α_1: OPR$^{(N>E)}$	-	-
GEWEKE	-	-	γ_2: FL$^{(N<E)}$
MDL	-	-	β: OPR$^{(N>E)}$ γ_2: OPR$^{(N>E)}$ γ_2: TL$^{(N>E)}$
PLV	-	-	γ_2: CPL$^{(N>E)}$ γ_2: OPL$^{(N>E)}$ γ_2: OPR$^{(N>E)}$

are tabulated. α_1, α_2, β and γ_2 denote alpha1 (8-10 Hz), alpha2 (10-13 Hz), Beta (13-30 Hz) and Gamma2 (40-90 Hz) bands, respectively. The identified lobes are: OPR (O2-P4, O2-PO8, P4-P8), OPL (O1-P3, O1-PO7, PO7-P3) and CPL (C3-CP3, CP3-P3, P3-PO7), TL (FT7-T3, T3-TP7, FT7-TP7), FL (FP1-F7, FP1-F3, F7-F3), while *N>E* denotes that synchronization in normals was greater than in epileptics.

IV. DISCUSSION

The *PLV* method applied on phase synchronized oscillators obviously was the one performed better (Fig.1). *SL* and *RSS-GL* estimators were also able to identify the coupling, but underestimated it. *S-estimator* could not identify any PS. However on the second paradigm using the generally synchronized oscillators, all methods were able to perform well, except the *PLV* as expected (Fig. 2). *SL* and *RSS-GL* were the best, but S-estimator was very stable and

robust even in a really noisy environment. *SL* and *RSS-GL* difference responses are due to normalization factors and do not imply that one outperforms the other. As a conclusion in a real case scenario one should use both a PS measure (i.e., *PLV*) and one of the proposed GS measures (preferably *RSS-GS* or *SL*), as well as linear tools since their underlined assumptions are different.

The testing using surrogate datasets testifies that there is strong statistical evidence that the interdependence in the real EEG data can be described by a linear model, but it is also evident that there also exists nonlinear coupling apparent in PS measures (*PLV*) only. In other words, since all GS methods were unable to discriminate the actual EEG from the surrogates (linear representations), lead to the conclusion that either the actual EEG does not contain strong nonlinear GS couplings or the measure used is not strong enough to detect them. But since we tested them on nonlinear models we conclude that the first assumption is right. However, *PLV* was able to detect differences. Hence, we used *PLV* and the linear methods proposed on the real EEG data.

The results indicated that the *PLV* method accentuates gamma2 reactivity on the central and occipital brain lobes during the Fractal simulation test. Linear synchronization estimators even if they identify some additional significant brain regions, they mostly support activations around the occipital regions in gamma2 band. Such an increase in gamma band activity [33] is also found during observation of figures with illusory contours, and this finding was interpreted as an evidence of a bottom-up binding of coherent visual features [31]. At the same time, there is evidence that gamma band oscillations subserve the modulation of visual processes by the perceiver's internal representations and cognitive context, in a top-down approach [32].

REFERENCES

[1] W. Singer, "Consciousness and the binding problem," *Ann NY Acad. Sci.*, Vol. 929, pp. 123-146, 2001.

[2] E. Basar, C. Basar-Eroglu, S. Karakas, and M. Schurmann, "Gamma, alpha, delta, and theta oscillations govern cognitive processes," *Int. J. Psychophysiol*, Vol. 39, pp. 241-248, 2001.

[3] A.P. Anokhin, W. Lutzenberger, and N. Birbaumer, "Spatiotemporal organization of brain dynamics and intelligence: an EEG study in adolescents," *Int. J. Psychophysiology*, Vol. 33, pp. 259-273, 1999.

[4] A. von Stein, J. Sarnthein, "Different frequencies for different scales of cortical integration: from local gamma to long range alpha theta synchronization," *Int. J. Psychophysiol* vol. 38, pp. 301- 313, 2000.

[5] M. Ford, J. Goethe, D. Dekker, "EEG coherence and power changes during a continuous movement task," *Int. J. Psychophysiol*, vol. 4, pp. 99–110, 1986.

[6] D. Kiper, M. Knyazeva, L. Tettoni, G. Innocenti, "Visual stimulus dependent changes in interhemispheric EEG coherence in ferrets," *J. Neurophysiol*, vol. 82, issue 6, pp. 3082– 3094, 1999.

[7] S. Micheloyannis, V. Sakkalis, M. Vourkas, C.J. Stam, and P.G. Simos, "Cortical networks involved in mathematical thinking: Evidence from linear and non-linear cortical synchronization of electrical activity", *Neuroscience Letters*, Vol. 373, pp. 212-217, 2005.

[8] C.W.J. Granger, "Investigating causal relations by econometric models

and cross-spectral methods," *Econometrica*, vol. 37, issue 3, pp. 424–438, 1969.

[9] J. Geweke, "Measurement of linear dependence and feedback between multiple time series," *J. of the American Statistical Association*, vol. 77, no. 378, pp. 304–313, 1982.

[10] A. Brovelli, M. Ding, A. Ledberg, Y. Chen, R. Nakamura, and S.L. Bressler, "Beta oscillations in a large-scale sensorimotor cortical network: directional influences revealed by Granger causality," *Proc. Natl. Acad. Sci. USA*, vol. 101, no. 26, pp. 9849–9854, 2004.

[11] J. Rissanen and M. Wax, "Measures of mutual and causal dependence between two time series," *IEEE Trans. on Information Theory*, vol. 33, issue 4, pp. 598–601, 1987.

[12] S.R. Butler, A. Glass, "Asymmetries in the electroencephalogram associated with cerebral dominance," *Electroencephalogr. Clin. Neurophysiol* vol. 36, issue 5, pp. 481–491, 1974.

[13] A. Pikovsky, M. Rosenblum, J. Kurths, "Synchronization: a Universal Concept in Nonlinear Science," *Cambridge University Press*, Cambridge 2001.

[14] J. Lachaux, E. Rodriguez, J. Martinerie, F. Varela, "Measuring phase synchrony in brain signals," *Hum. Brain Mapp.* vol. 8, pp. 194–208, 1999.

[15] K. Matsumoto, I. Tsuda, "Calculation of information flow rate from mutual information," *J. Phys. A,* vol. 21, pp. 1405–1414, 1988.

[16] R. Wiggins and E. Robinson, "Recursive solution to the multichannel filtering problem," *J. Geophysical Research*, vol. 70, pp. 1885-1891, 1966.

[17] T. Schneider and A. Neumaier, "Algorithm 808: ARFIT - a Matlab package for the estimation of parameters and eigenmodes of multivariate autotegressive models," *ACM Tr. Mathematical Software*, vol. 27, issue 1, pp. 58-65, 2001.

[18] P. Stoica and R.L. Moses, "Introduction to spectral analysis," *Prentice Hall, Inc.*, 1997.

[19] F. Mormann, K. Lehnertz, P. David, C. Elger, "Mean phase coherence as a measure for phase synchronization and its application to the EEG of epilepsy patients," *Physica D*, vol. 144, pp. 358–369, 2000.

[20] C. Carmeli, M. G. Knyazeva, G. M. Innocenti, and O. De Feo "Assessment of EEG synchronization based on state-space analysis," NeuroImage, vol. 25, issue 2, pp. 339-354, 2005.

[21] J. Arnhold, P. Grassberger, K. Lehnertz, C.E. Elger, "A robust method for detecting interdependencies: application to intracranially recorded EEG," *Physica D,* vol. 134 pp. 419-430, 1999.

[22] R. Quian Quiroga, A. Kraskov, T. Kreuz, P. Grassberger, "Performance of different synchronization measures in real data: a case study on electroencephalographic signals," *Phys. Rev. E,* vol. 65, no. 041903, 2002.

[23] F. Takens, D.A. Rand, L.S. Young, "Detecting strange attractors in turbulence," *Dynamical systems and Turbulence, Lecture Notes in Mathematics*, vol. 898, pp. 366–381, 1981.

[24] C.J. Stam, B.W. van Dijk, "Synchronization likelihood: an unbiased measure of generalized synchronization in multivariate data sets," *Physica D,* vol. 163, pp. 236–251, 2002.

[25] J. Theiler, "Spurious dimension from correlation algorithms applied to limited time-series data," *Phys. Rev. A,* vol. 34, no. 2427, 1986.

[26] A. Hramov, and A. Koronovskii "Intermittent generalized synchronization in unidirectionally coupled chaotic oscillators," *Europhysics Letters,* vol. 70, issue 2, pp. 169-175, 2005.

[27] A. Hramov and A. Koronovskii "Generalized synchronization: a modified system approach," *Physical Review E,* vol. 71, no. 067201, 2005.

[28] R.G. Andrzejak, A. Kraskov, H. Stogbauer, F. Mormann, T. Kreuz, "Bivariate surrogate techniques: necessity, strengths, and caveats," *Phys. Rev. E,* vol. 68, issue 6, no. 066202, 2003.

[29] http://www.gps.caltech.edu/~tapio/arfit/.

[30] http://www2.math.uic.edu/hanson/mcs507/cp4f04.html.

[31] C. Tallon-Baudry and O. Bertrand "Oscillatory gamma activity in humans and its role in object representation," *Trends in Cognitive Sciences*, Vol.3, pp. 151-162, 1999.

[32] V. Goffaux, A. Mouraux, S. Desmet, and B. Rossion "Human non-phase-locked gamma oscillations in experience-based perception of visual scenes," *Neuroscience Letters,* Vol. 354, pp. 14-17, 2004.

[33] S. Erimaki, et al. "EEG responses to complex fractal stimuli," *2nd International Nonlinear Sciences Conference*, Heraklion Crete, 2006.

Time-significant Wavelet Coherence for the Evaluation of Schizophrenic Brain Activity using a Graph theory approach

Vangelis Sakkalis, Theofanis Oikonomou, Ellie Pachou, Ioannis Tollis, Sifis Micheloyannis, and Michalis Zervakis, *member IEEE*

Abstract—Among the various frameworks in which Electroencephalographic (EEG) signal synchronization has been traditionally formulated, the most widely studied and used is the coherence that is entirely based on frequency analysis. However, at present time it is possible to capture information about the temporal profile of coherence, which is particularly helpful in studying non-stationary time-varying brain dynamics, like the Wavelet Coherence (WC). In this paper we propose a new approach of studying brain synchronization dynamics by extending the use of WC to include certain statistically significant (in terms of signal coherence) time segments, to study and characterize any disturbances present in the functional connectivity network of schizophrenia patients. Graph theoretical measures and visualization provide the tools to study the "disconnection syndrome" as proposed for schizophrenia. Specifically, we analyzed multichannel EEG data from twenty stabilized patients with schizophrenia and controls in an experiment of working memory (WM) using the gamma band (i.e., the EEG frequency of ca. 40 Hz), which is activated during the connecting activity (i.e., the "binding" of the neurons). The results are in accordance with the disturbance of connections between the neurons giving additional information related to the localization of most prominent disconnection.

I. INTRODUCTION

ELECTROENCEPHALOGRAPHIC (EEG) coherence measures have been successfully used in the past as indices of cerebral engagement in cognitive tasks using linear [1] and non-linear [2] methods.

Coherence has been a well-established and traditionally used tool to investigate the linear relation between two signals or EEG channels, by means of examining

V. Sakkalis is with the Department of Electronic and Computer Engineering, Technical University of Crete, Chania 73100 and the Institute of Computer Science, Foundation for Research and Technology, Heraklion 71110, Greece (+30-281-0391448; fax: +30-281-0391609; e-mail: sakkalis@ics.forth.gr).

T. Oikonomou and I. Tollis are with the Institute of Computer Science, Foundation for Research and Technology, Heraklion, Greece and the Department of Computer Science, University of Crete, Heraklion 71409, Greece (e-mail:thoikon@ics.forth.gr , tollis@ics.forth.gr).

M. Zervakis is with the Department of Electronic and Computer Engineering, Technical University of Crete, Chania 73100, Greece (e-mail: michalis@systems.tuc.gr).

E. Pachou and S. Micheloyannis are with the Clinical Neurophysiology Laboratory (L. Widen), Faculty of Medicine, University of Crete, Heraklion 71409, Greece (e-mail: michelogj@med.uoc.gr).

periodicities in frequency domain using classical Fourier analysis. This method actually neglects time resolution for the sake of perfect frequency resolution (Heisenberg uncertainty principle) and assumes stationary processes in the time domain. However, EEG signals reflect the underlying brain dynamics and in principle convey information on dynamically evolving channel interdependencies. Thus, measuring the dynamic behavior of EEG channels coupling, while different cognitive tasks are happening, is possible only if temporal resolution is conserved. Towards the latter direction, several Fourier-based adaptations [3] have been attempted, but still require stationarity within each window for which coherence is calculated.

In this study the aforementioned limitations are addressed by adopting the Continuous Wavelet Transform (CWT). The CWT is able to examine whether regions in time frequency space with large common power have a consistent phase relationship and therefore are suggestive of causality between EEG channels. In addition, CWT makes use of complex basis functions (wavelets) that are able to capture the amplitude and phase information from the analyzed EEG signals, as well as time information [4]. Using the CWT is possible to compute the WC, which has already been successfully used in EEG analysis [5]. Motivated by the additional "time profile" information gained from the use of CWT, this paper proceeds one step further and utilizes statistics to identify only those EEG signal time segments where significant coherence occurs.

In this study two different situations are considered: the control (rest) and the cognitive activation during working memory (WM), testing both control subjects and schizophrenia patients. The testing hypothesis suggests that WM task requires considerable mental effort and the disconnection on neuronal assemblies in patients could be visible by reduced "binding" expressed by the gamma band (30-45 Hz). The disconnection hypothesis [6] and WM deficits [10][11] are well established in the literature on schizophrenia.

Both local and long distance functional connectivity in complex networks is evaluated using measures and visualizations derived from graph theory. Special interest in using graph theory to study neural networks has been in focus recently, since it offers a unique perspective of

studying local and distributed brain interactions [12][13].

The paper proceeds as follows. Section II provides a brief background of the proposed methods. Section III presents the results obtained followed by a discussion of the findings (Section IV). Finally, Section V concludes this paper.

II. METHODS

A. Data Acquisition

The EEG signals in both groups (20 controls and 20 stabilized patients with schizophrenia) were recorded from 30 cap electrodes, according to the 10/20 international system, referred to linked A1+A2 electrodes (Fig. 2). The signals were digitized at 500 Hz.

B. Experimental setting and Test Description

Continuous EEGs were recorded in an electrically shielded, sound and light attenuated, room while participants sat in a reclined chair. EEG data were visually inspected for artifacts and epochs of 8 sec were chosen for analysis. We analyzed epochs at rest i.e., while each individual had the eyes fixed on a small point on the computer screen and during a two-back WM test using capital Greek letters.

C. The Continuous Wavelet Transform (CWT)

Over the past decade, the WT has been developed into an important tool for time series analysis that contains non-stationary power (such as the EEG signal) at many different frequencies [14]. The CWT of a discrete sequence x_n with time spacing δt and N data points ($n = 0 \ldots N-1$) is defined as the convolution of x_n with consecutive scaled and translated versions of the wavelet function $\psi_0(\eta)$:
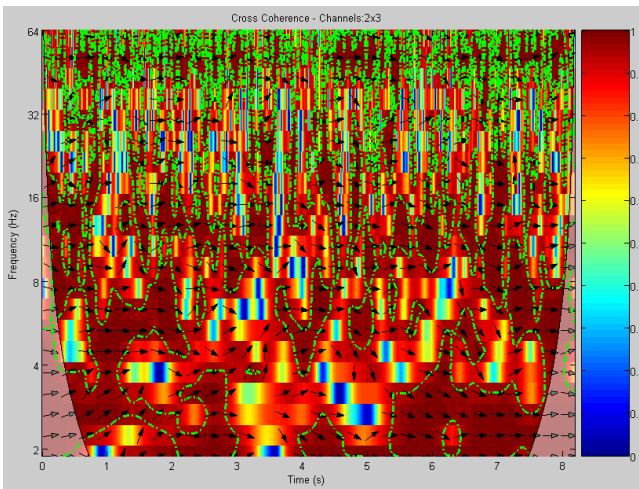

Fig. 1: The squared WC time-frequency transformed scalogram. The 5% significant regions over the time-scale transform are indicated by the contours (green dashed outline). The outer elliptical region at the edges of the second graph indicates the cone of influence in which errors (edge effects) may be apparent due to the transformation of a finite-length series EEG signal [4]. The relative phase relationship is shown as arrows (with in-phase pointing right, anti-phase pointing left).

$$W_n^X(s) = \sqrt{\delta t/s} \sum_{n'=0}^{N-1} x_{n'} \psi_0 * \left[(n'-n)\delta t/s \right] \quad (1)$$

$$\psi_0(\eta) = \pi^{-1/4} e^{i\omega_0 \eta} e^{-\eta^2/2} \quad (2)$$

where η and $\omega_0 = 6$ is a non-dimensional "time" parameter and frequency, respectively. $\psi_0(\eta)$ describes the most commonly used wavelet type for spectral analyses: the *normalized complex Morlet wavelet* (2). The *power spectrum* of the WT is defined by the square of coefficients (1) of the wavelet series as $\left| W_n^X(s) \right|^2$. The notion of scale s is introduced as an alternative to frequency [14]. Thus, we may define frequency bands of interest, such as *gamma* band, capable of encapsulating the different functional frequencies of the brain.

D. Wavelet Coherence

Assuming two ergodic and stationary signals x and y, then the traditional *coherence* γ_{xy}^2 is defined as follows:

$$\gamma_{xy}^2(f) = \frac{\left| S_{xy}(f) \right|^2}{S_{xx}(f) \cdot S_{yy}(f)} \quad (3)$$

where S_{xx}, S_{yy} denote the Fourier transform of the respective autocorrelation function and S_{xy} the Fourier transform of the cross-correlation function. In a similar way, given two time series X and Y, with wavelet transforms $W_n^X(s)$ and $W_n^Y(s)$, one can initially define the *cross-wavelet spectrum* as $W_n^{XY}(s) = W_n^X(s) W_n^{Y*}(s)$, where * denotes the complex conjugate. The cross-wavelet power is given by $\left| W_n^{XY}(s) \right|$. If one closely resembles (3) then the WC R_n^2 of two signals may be defined as:

$$R_n^2(s) = \frac{\left| S(s^{-1} W_n^{XY}(s)) \right|^2}{S \left(s^{-1} \left| W_n^X(s) \right|^2 \right) \cdot S \left(s^{-1} \left| W_n^Y(s) \right|^2 \right)} \quad (4)$$

where S is a smoothing operator in time S_t and scale S_s such as $S(W) = S_s(S_t(W_n(s)))$ which for the Morlet wavelet is given by a Gaussian and a boxcar filter of width equal to 0.6, (the scale-decorrelation length) respectively [4][15]:

$$S_t(W,s) = \left(W_n(s) * c_1^{-t^2/2s^2} \right) \quad (5)$$

$$S_s(W,n) = \left(W_n(s) * c_2 \prod (0.6s) \right) \quad (6)$$

where c_1 and c_2 are normalization constants and $\prod$ is the rectangle function. The squared WC time-frequency transformed scalogram is depicted in Fig.1.

Additionally, we are able to gain confidence in causal relationships of the coherence findings by estimating the statistical level of significance against a background spectrum using Monte Carlo methods [15]. The background spectrum is defined as the mean time-averaged wavelet power spectrum over all healthy subjects performing the

control task. A large set of surrogates (1000 datasets) was generated for each channel pair from the average WC of the healthy subjects and used to estimate the significance level for each scale. Our aim is to map the WC scalogram (Fig. 1) into a feature vector that best characterizes each channel pair coupling. One may think of this step as an attempt to crop up the most significant (in terms of coherence) regions out of the bulk initial signal. Fig. 1 depicts the WC scalogram of two EEG channel signals of a schizophrenic patient. The significant regions (over the time-frequency transformed domain) that are strongly coupled while the subject is performing the WM task against the background spectrum are indicated by closed contours. Hence, one is able to form *Significant Coherency* features, which encapsulate the time and "band-scaled" coherence information, over those time regions where apparent significant differentiation is indicated (contours in Fig. 1). Such features are constructed for each channel pair in both tasks and populations. As a result a 30x30 coherence matrix (CM) with elements ranging from 0 to 1 is formulated per task and subject.

E. Measures & Signatures of Graph Topology

In order to obtain a graph from a CM we need to convert it into an NxN binary adjacency matrix, A. To achieve that we define a variable called *threshold T*, such that $T \in [0,1]$. The value $A(i,j)$ is either 1 or 0, indicating the presence or absence of an edge between nodes i and j, respectively. Namely, $A(i,j)=1$ if $C(i,j) \geq T$, otherwise $A(i,j)=0$. Thus we define a graph for each value of T. For the purposes of our work, we defined 1000 such graphs, one for every thousandth of T. After constructing A, we compute various properties of the resulting graph. These include the average degree K, the clustering coefficient C and the average shortest path length L of our graph. For statistical analysis we compared the graph properties using t-tests. The significant results (according to *p*-value) are concentrated in the region of $0.75 \leq T \leq 0.85$ (with step 0.001 and $0.001 \leq p \leq 0.02$). We define a graph in terms of a set of n nodes $V=v_1,v_2,..,v_n$ and a set of edges E, where e_{ij} denotes an edge between nodes v_i and v_j. The neighborhood N_i of a node v_i is defined as the set of vertices that have an edge to v_i, namely $N_i = \{v_j\} : e_{ij} \in E$.

The degree k_i of a node is the number of vertices in its neighborhood, i.e., $|N_i|$. The average degree of a graph is the average of the degrees of all nodes, i.e., $K = \sum_{i \in V} k_i / n$.

The clustering coefficient C_i of a node v_i is the fraction of the existing edges between the nodes in v_i's neighborhood over the number of all possible edges between them. For an undirected graph, if a node v_i has k_i neighbors, then $k_i(k_i-1)/2$ is the number of all possible edges in its
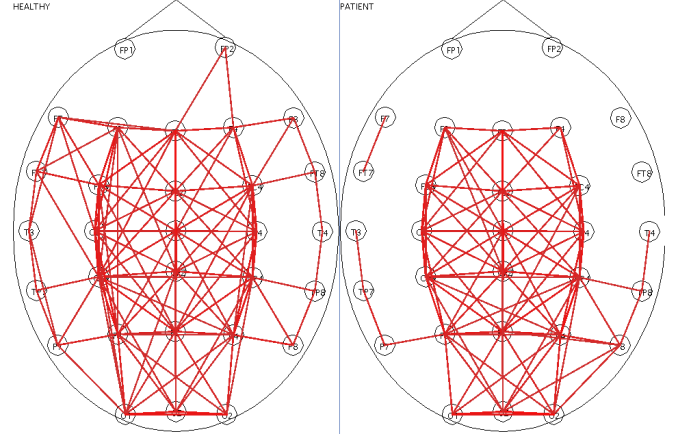

Fig. 2: A "healthy" network (left graph) (WM task and selected threshold) appears to have higher K, C values and lower L values compared to the "schizophrenic" one (right graph). These disturbances are more prominent for the connections of the frontal lobes as well as the temporal lobes.

neighborhood. Thus, $C_i = 2|\{e_{jk}\}| / k_i(k_i-1) : v_j, v_k \in N_i$. This measure is 1 if every neighbor connected to v_i is also connected to every other node within the neighborhood, and 0 if no node connected to v_i connects to any other node connected to v_i. The clustering coefficient for the whole graph is the average of C_i for each node, $C = \sum_{i=1}^{n} C_i / n$, and is a measure of the tendency of graph nodes to form local clusters [16].

The shortest path (distance) d_{ij} between two nodes v_i and v_j is the minimum number of edges we need to traverse in order to go from node v_i to node v_j. The average shortest path length $L = \sum_{i,j \in V, i \neq j} d_{ij} / n(n-1)$ is a measure of interconnectedness of the graph. Note that, in our experiments, the absence of a path between v_i and v_j implies $d_{ij} = 1000$.

III. RESULTS

Our study focuses on gamma band coherence analysis. Significant coherent time-regions are transformed to the aforementioned binary matrix A served as input to the graph analysis algorithm. The average values of K, C and L for

TABLE I

HEALTHY				PATIENTS			
T	K	C	L	T	K	C	L
0.8	11.03	0.71	100.95	0.755	11.35	0.7	163.55
0.805	10.2	0.68	100.99	0.765	10.05	0.64	163.71
0.84	5.11	0.43	224.78	0.815	5.08	0.43	383.99

$0.75 \leq T \leq 0.85$ with step 0.005 during WM were computed (three selected values shown in Table I). We concentrated in different values of T, where the values of K and C of schizophrenic patients were equal to those of control subjects. For the above values of T, the respective values of L for patients were much greater than those for controls. A

detailed view of the network topology is depicted in Fig. 2.

IV. DISCUSSION

The proposed wavelet coherence analysis in combination with the graph analysis methodology indicated significant task differentiation in gamma band more prominent in frontal, frontal-central and temporal regions. Such disturbances of integration of brain function in schizophrenic processes have been suspected from the first detailed descriptions of the disease and are reinforced by clinical findings. Anatomical, biochemical brain mapping and electrophysiological findings support this hypothesis. Such clinical methods, using gamma band evaluation, further support the "disconnection" hypothesis i.e., the disturbance of the integrative processes. Various alternative studies relating gamma band and schizophrenia indicate that there is an overall reduction of the amount of the connected nodes and synchronization strength of this frequency band in schizophrenics. Additionally, there are differences between the gamma activity on the left and right hemispheres among patients and controls, as well as indices of less frontal integration as expressed by this band [6][7][8].

The three graph measures K, C, L actually represent an overall signature of the graph topology. Our experiments indicated that K, C and L are getting lower while moving from healthy to schizophrenics (in the whole threshold range). But instead of studying each measure independently, we attempt to quantify their interaction. Towards this direction we determined in three different values of T (Table I), where the values of K and C of patients are equal to those of healthy. The physical meaning of this maneuver addresses the following question: Assuming both healthy and schizophrenic populations have the same average degree and clustering coefficient, is the network proportionally efficient? According to Table I the answer is no, which means that for the above values of T the respective values of L of the patients are much greater than those of healthy. This is also evident by observing Fig. 2. The latter syllogism leads to the suggestion that schizophrenic patients need significantly more direct node (channel) connections in order to perform the same WM task.

V. CONCLUSION

The algorithmic approach presented illustrates the idea of using statistically-based feature vectors in the time-scale WT domain in order to select the most significant time segments capable of revealing the most prominent task changes out of the background signal. Results suggest that the proposed methodology is capable of identifying regions of cerebral synchrony during the specified tasks. Using the graph theoretical analysis we found that the integration, as expressed by the high frequency gamma band, related to the

"binding" phenomenon i.e., the integration on neuronal activity, and the related parameters is overall reduced in schizophrenics. This is evident at rest but more prominent during a cognitive task, the WM. Additionally, these disturbances are more prominent for the connections of the frontal lobes as well as the temporal lobes.

REFERENCES

[1] G. Dumermuth, and L. Molinari, "Spectral analysis of the EEG. Some fundamentals revisited and some open problems," *Neuropsychobiology,* vol. 17, pp. 85–99, 1987.

[2] S. Micheloyannis, V. Sakkalis, M. Vourkas, C.J. Stam, and P.G. Simos, "Neural networks involved in mathematical thinking: evidence from linear and non-linear analysis of electroencephalographic activity," *Neuroscience Letters*, vol. 373, pp. 212–217, 2005.

[3] Y. Xu, S. Haykin, and R.J. Racine, "Multiple window time-frequency distribution and coherence of eeg using slepian and hermite functions," *IEEE Trans. Biomed. Eng.,* vol. 46, no. 7, pp. 861–866, 1999.

[4] C. Torrence, and G.P. Compo, "A practical Guide to Wavelet Analysis," *Bull. Am. Meteorol. Soc.*, vol. 79, pp. 61-78, 1998.

[5] J.P. Lachaux, et al., "Estimating the time-course of coherence between single-trial brain signals: an introduction to wavelet coherence," *Neurophysiol. Clin,* vol. 32, no. 3, pp. 157–174, 2002.

[6] K.H. Lee, L.M. Williams, M. Breakspear, and E. Gordon, "Synchronous gamma activity: a review and contribution to an integrative neuroscience model of schizophrenia," *Brain Res. Brain Res. Rev.*, vol. 41, pp. 57-78, 2003.

[7] L.E. Hong, et al., "Evoked gamma band synchronization and the liability for schizophrenia," *Schizophr. Res.,* Vol. 70, No. 2-3, pp. 293-302, 2004.

[8] J. Gallinat, G. Winterer, C.S. Herrmann, and D. Senkowski, "Reduced oscillatory gamma-band responses in unmedicated schizophrenic patients indicate impaired frontal network processing", *Clin. Neurophysiol.*, Vol. 115, No. 8, pp. 1863-1874, 2004.

[9] K.J. Friston, "Schizophrenia and the disconnection hypothesis," *Acta Psychiatr Scand Suppl,* vol. 395, pp. 68-79, 1999.

[10] H.M. Conklin, C.E. Curtis, M.E. Calkins, and W.G. Iacomo, "Working memory functioning in schizophrenia patients and their first-degree relatives: cognitive functioning shedding light on aetiology," *Neuropsychologia*, vol. 43, pp. 930-942, 2005.

[11] H. Silver, P. Feldman, W. Bilker, and R.C. Gur, "Working memory deficit as a core neuropsychological dysfunction in schizophrenia," *Am. J. Psychiatry*, vol. 160, pp. 1809-1816, 2003.

[12] F. Varela, J.P. Lachaux, E. Rodriguez, and J. Martinerie, "The brainweb: phase synchronization and large-scale integration," *Nat. Rev. Neurosci.*, vol. 2, pp. 229-239, 2001.

[13] A.A. Fingelkurts and S. Kähkönen, "Functional connectivity in the brain—is it an elusive concept?," *Neurosci. Biobehav. Reviews*, vol. 28, pp. 827-836, 2004.

[14] I. Daubechies, "The Wavelet transform time-frequency localization and signal analysis," *IEEE Trans. Inform. Theory*, vol. 36, pp.961-1004, 1990.

[15] A. Grinsted, J.C. Moore, and S. Jevrejeva, "Application of the cross wavelet transform and wavelet coherence to geophysical time series," *Nonlinear Processes in Geophysics,* vol. 11, pp. 561–566, 2004.

[16] D.J. Watts and S.H. Strogatz, "Collective dynamics of 'small-world' networks," *Nature*, Vol. 393, pp. 440-442, 1998.

EVANGELOS SAKKALIS

Date of Birth :   11.05.1975

EDUCATION

2000 – today   **PhD** in **"Statistical Quantitative EEG analysis based on Time-frequency and Nonlinear Synchronization methods during Altered States of Consciousness"**

Technical University of Crete – Department of Electronic and Software Engineers

1998 – 1999   **MSc** in **"Engineering and Physical Science in Medicine"** Imperial **College** of Science, Technology and Medicine – London – UK

1994 – 1998   **University of Crete** - Department of Physics **(Majoring in Atomic – Molecular Physics and Laser)**

1997 *(7 July - 7 August)*   **9th** – **10th** Summer School of the _**Advanced Physics**_, **1998** *(6 July – 31 July)* which is organized by Foundation for Research and Technology, Hellas (FORTH) – Institute of Electronic Structure and Laser (IESL).

Professional/ Research Experience

December 1999 - today

ITE (FORTH) – Institute of Computer Science (ICS)
Biomedical Informatics lab

March 1998 – August 1998

Heraklion University Hospital (PEPAGNI) – School of Medicine, University of Crete
Vardinoyannion Eye Institute of Crete (VEIC) – EPEAEK European Framework

190

January 1996 – December 1997

> **University of Crete - Department of Physics**
> **Multimedia Lab**

June 1996 – August 1996

> **ITE (FORTH) – Microelectronics Laboratory**
> **Summer Scholarship**

October 1995 – December 1995

> **University of Crete - Department of Physics**
> **Multimedia Lab**

1st Degree Thesis

At the end of the academic session 1997 - 1998, I presented my thesis on **«Study on the propagation of ultra short laser pulses in human tissue (breast biopsy samples) using diffusion theory»**, under the supervision of Dr. Papazoglou and Prof. Fotakis, which took place at Institute of Electronic Structure and Lasers IESL - FORTH. The data used in this thesis was acquired from both artificial and <u>human tissue</u>; mainly breast tissue, testing for tumor malignancy. More specifically, we used optical tomography techniques based on ***non-ionizing*** laser radiation.

MSc Thesis

In September 1999, my MSc thesis on **"PC based detection of abnormal ventricular wall motion using Echocardiography",** under the supervision of Dr. Cashman and Dr. Bignall, was submitted. It took place at the Visualization Lab - Bagrit Centre in Imperial College of Science, Technology & Medicine, in collaboration with the St. Mary's Hospital in London. More specifically, a specialized in image processing software was developed, aiming towards a fully automated method of estimating the left ventricular cavity cross sectional area.

Journal Papers

- *V. Sakkalis*, M. Zervakis, and S. Micheloyannis, "Significant EEG Feature Selection for the Evaluation of Cognitive Task Complexity Functions", Brain Topography, Vol. 19, No.1-2, pp. 53-60, 2006.

- S. Micheloyannis, *V. Sakkalis*, M. Vourkas, C.J. Stam, and P.G. Simos, "Cortical networks involved in mathematical thinking: Evidence from linear and non-linear cortico-cortical synchronization of electrical activity", Neuroscience Letters, Vol. 373, pp. 212-217, 2005.

- P. G. Simos, E. Papanikolaou, *E. Sakkalis*, and S. Micheloyannis, "Modulation of Gamma-Band Spectral Power by Cognitive Task Complexity", Brain Topography, Vol. 14, No. 3, pp. 191-196, Spring 2002.

- G. Zacharakis, A. Zolindaki, *V. Sakkalis*, G. Filippidis,, E. Koumantakis, and T.G. Papazoglou, "Non-parametric characterization of human breast tissue by the Laguerre expansion of the

kernels technique applied on propagating femtosecond laser pulses through biopsy samples", Appl. Phys. Lett., Vol. 74, No. 5, pp. 771-772, 1999.

Conferences

♦ T. Oikonomou, *V. Sakkalis*, I. Tollis, and S. Micheloyannis, "Searching and Visualizing Brain Networks in Schizophrenia", Lecture Notes in Computer Science, 7th International Symposium on Biological and Medical Data Analysis (ISBMDA 2006), Thessaloniki, Greece, December 7-8, 2006.

♦ *V. Sakkalis*, T. Oikonomou, E. Pachou, I. Tollis, S. Micheloyannis, and M. Zervakis, "Time-significant Wavelet Coherence for the Evaluation of Schizophrenic Brain Activity using a Graph theory approach", Engineering in Medicine and Biology Society (EMBC 2006), New York, USA, August 30-Sept. 3, 2006.

♦ P. Xanthopoulos, S. Golemati, *V. Sakkalis*, P.Y. Ktonas, M. Zervakis, and and C.R. Soldatos, "Modeling the time-varying microstructure of simulated sleep EEG spindles using time-frequency analysis methods", Engineering in Medicine and Biology Society (EMBC 2006), New York, USA, August 30-Sept. 3, 2006.

♦ *V. Sakkalis*, M. Zervakis, C. Bigan, T. Cassar, K.P. Camilleri, S.G. Fabri, and Sifis Micheloyannis, "Validation of time-frequency and ARMA feature extraction methods in classification of mild epileptic signal patterns", Information Technology Applications in Biomedicine (IEEE-ITAB 2006), Ioannina - Epirus, Greece, October 26-28, 2006.

♦ *V. Sakkalis*, C.D.Giurcăneanu, P. Xanthopoulos, M. Zervakis, Y. Yang, and S. Micheloyannis, "Assessment of linear and non-linear EEG synchronization measures for evaluating mild epileptic signal patterns", Information Technology Applications in Biomedicine (ITAB 2006), Ioannina - Epirus, Greece, October 26-28, 2006.

♦ P. Xanthopoulos, S. Golemati, *V. Sakkalis*, P.Y. Ktonas, M.D. Ortigueira, M. Zervakis, T. Paparrigopoulos, X.Tsekou, and C.R. Soldatos, "Comparative analysis of time-frequency methods estimating the time-varying microstructure of sleep EEG spindles", Information Technology Applications in Biomedicine (ITAB 2006), Ioannina - Epirus, Greece, October 26-28, 2006.

♦ A. Kouroubali, *V. Sakkalis*, C. Chronaki, and M. Tsiknakis, "eChallenges in the Implementation of eHealth Services over a Hybrid Network Architecture", eChallenges e-2006, Barcelona, Spain, 25-27 October, 2006.

♦ Α. Κουρούμπαλη, Δ. Βουρβαχάκης, *Β. Σακκαλής*, Β. Κοντογιάννης, Μ. Μυτάρας, Ν. Αγγουράκης, Κ. Χρονάκη, «Μαθήματα τηλε-εκπαίδευσης στην επείγουσα προνοσοκομειακή ιατρική: εμπειρία και προοπτικές», περίληψη για το 9ο Συνέδριο Αναισθησιολογίας και Εντατικής Ιατρικής, Χαλκιδική, 7-10 Σεπτεμβρίου 2006.

♦ C. Bigan, M. Besleaga, M. Zervakis, *V. Sakkalis*, K. Michalopoulos, M. Woolfson, M. Ortigueira, A. Batista, R. Rato, M. Righi, U. Barcaro, A. Starita, K.P. Camilleri, S.G. Fabri, J. Muscat, R. Grech, and T. Cassar, " EEG signal pre-processing for segmentation into significant regions, major artefacts removal, and uncertainty reduction in epileptic seizure characterization", Joint Workshop On BIOPATTERN Analysis In Brain Diseases, Goteborg, Sweden, May 18-19, 2006.

♦ P. Xanthopoulos, S. Golemati, *V. Sakkalis*, P.Y. Ktonas, M.D. Ortigueira, M. Zervakis, T. Paparrigopoulos, X. Tsekou, and C.R. Soldatos, "Modeling the time-varying microstructure of

sleep EEG spindles using time-frequency analysis methods", Joint Workshop On BIOPATTERN Analysis In Brain Diseases, Goteborg, Sweden, May 18-19, 2006.

♦ *V. Sakkalis*, M. Zervakis, C. Bigan, T. Cassar, K.P. Camilleri, S.G. Fabri, and S. Micheloyannis, "EEG feature extraction and selection methods using wavelets and ARMA model for classifying mild epileptic signal patterns", Joint Workshop On BIOPATTERN Analysis In Brain Diseases, Goteborg, Sweden, May 18-19, 2006.

♦ S. Erimaki, K. Kanatsouli, E. Karakonstandaki, M. Vourkas, *V. Sakkalis*, and S. Micheloyannis, "EEG Responses To Complex Fractal Stimuli", 2nd International Nonlinear Science Conference, Heraklion, Crete, Greece March 10-12, 2006.

♦ *V. Sakkalis*, M. Zervakis, S. Erimaki, and S. Micheloyannis, "Evaluation of Electroencephalographic Activity involved in Mathematical thinking using Wavelet Analysis and Significance-Based Features", 2nd International Conference on Computational Intelligence in Medicine and Healthcare (CIMED), Lisbon, PORTUGAL, June 2005.

♦ *V. Sakkalis*, M. Zervakis, and S. Micheloyannis, "Biopattern Initiative: towards the Development and Integration of Next-Generation Information Fusion Approaches", 26th IEEE-EMBS - Annual International Conference of the IEEE Engineering in Medicine and Biology Society, San Fransisco, CA, USA, September 2004.

♦ *V. Sakkalis*, M. Zervakis, and S. Micheloyannis, "Evaluation of EEG Power Spectrum Measures using Fourier and Wavelet based Transformation Techniques as a Function of Task Complexity ", EWADB 2004 - 1st European Workshop on the Assessment of Diagnostic Performance, Milan, ITALY, July 2004.

♦ *V. Sakkalis*, F. Chiarugi, S. Kostomanolakis, C.E. Chronaki, M. Tsiknakis and S.C. Orphanoudakis, "A Gateway between the SCP-ECG and the DICOM 3.0 Supplement 30 Waveform Standards", Computers in Cardiology, Chalkidiki, GREECE, September 2003.

♦ G. Zacharakis, A. Zolindaki, *V. Sakkalis*, G. Filippidis, T.G. Papazoglou, D.D. Tsiftsis, E. Koumantakis, "In vitro optical characterization and discrimination of female breast tissue during near infrared femtosecond laser pulses propagation", Journal of Biomed. Opt., Vol. 6, No. 4, pp. 446-449, October 2001.

♦ Kostomanolakis, S; Kavlentakis, G.; *Sakkalis, V.*; Chronaki, C.E.; Tsikankis, S.C.;Orphanoudakis, S.; "Seamless Integration of Healthcare Processes related to Image Management and Communication in Primary Healthcare Centers", Proceedings of the 18th international Conference EuroPACS 2000, Graz, Austria books@ocg.at BAND 144 pp. 126-132 (2000).

♦ G. Zacharakis, *V. Sakkalis*, G. Filippidis, A. Zolindaki, E. Koumantakis, T.G. Papazoglou, "In vitro optical characterization of female breast tissue with near infrared fsec laser pulses" Series of the International Society on Optics Within Life Science (OWLS) Volume V Springer - Verlag, Berlin, Heidelberg pp. 294-296 (2000).

♦ Κ. Γεωργίου, Ν. Δαλαμάγκας, Π. Καραβίτη, *Β. Σακκαλής*. Ε. Τριανταφύλλου, Γ. Νεοφώτιστος, "Πειραματισμός με τη χρήση του Παγκοσμίου ιστού στα πλαίσια του μαθήματος 'Διαφορικές Εξισώσεις Ι' του Φυσικού Τμήματος του Πανεπιστημίου Κρήτης", Πρακτικά της 1ης Παγκρήτιας Ημερίδας Καθηγητών Πληροφορικής "Η Πληροφορική στην Εκπαίδευση", Ηράκλειο 1996.